

2015

# I. Synthesis of Ascarosides for Biological Evaluation and II. Development of Visible Light-Promoted Selenofunctionalization and Grafting of Aryl Iodides

Elizabeth Susan Conner Balapitiya

*Louisiana State University and Agricultural and Mechanical College*

Follow this and additional works at: [https://digitalcommons.lsu.edu/gradschool\\_dissertations](https://digitalcommons.lsu.edu/gradschool_dissertations)



Part of the [Chemistry Commons](#)

---

## Recommended Citation

Balapitiya, Elizabeth Susan Conner, "I. Synthesis of Ascarosides for Biological Evaluation and II. Development of Visible Light-Promoted Selenofunctionalization and Grafting of Aryl Iodides" (2015). *LSU Doctoral Dissertations*. 637.  
[https://digitalcommons.lsu.edu/gradschool\\_dissertations/637](https://digitalcommons.lsu.edu/gradschool_dissertations/637)

This Dissertation is brought to you for free and open access by the Graduate School at LSU Digital Commons. It has been accepted for inclusion in LSU Doctoral Dissertations by an authorized graduate school editor of LSU Digital Commons. For more information, please contact [gradetd@lsu.edu](mailto:gradetd@lsu.edu).

I. SYNTHESIS OF ASCAROSIDES FOR BIOLOGICAL EVALUATION AND II.  
DEVELOPMENT OF VISIBLE LIGHT-PROMOTED SELENOFUNCTIONALIZATION  
AND GRAFTING OF ARYL IODIDES

A Dissertation

Submitted to the Graduate Faculty of the  
Louisiana State University and  
Agricultural and Mechanical College  
in partial fulfillment of the  
requirements for the degree of  
Doctor of Philosophy

in

The Department of Chemistry

by  
Elizabeth Susan Conner Balapitiya  
B.A., Baylor University, 2010  
May 2015

*Dedicated to my  
family for all of their love  
and encouragement*

## ACKNOWLEDGMENTS

On the way to obtaining my Ph.D., I have been blessed with the help and encouragement of so many people. First, I am extremely grateful to Professor Justin R. Ragains for his guidance and mentorship throughout my graduate career. I have always had the comfort of knowing that I could go to him with any problem, whether it was big or small. I look forward to following his career and the great discoveries that will inevitably come from his lab.

I extend a special thank you to my committee members, Professors Rendy Kartika, Carol Taylor and Rui Lu for their advice and encouragement along the way. In addition, I would like to thank the LSU faculty and staff that have been an integral part of obtaining my Ph.D., especially Drs. Connie David, Frank Fronzcek, Thomas Weldeghioghis and Dale Treleaven. Our collaborators, Drs. Rebecca Butcher, Jayne Garno and Xianlin Zhai, have also been so generous with their time and resources. Their expertise in analysis of samples was extremely valuable.

I would also like to show my appreciation for my amazing group members (Kyle Hollister, Mark Spell, Xiaoping Wang, Kristina Deveaux, Rashanique Quarels and John Crafton) for their support and humor. Thanks for making lab fun. In addition, I owe so much gratitude to my undergraduate Katie Crocker and my high school student Marika Buchholz. They were a true joy to work with.

Most importantly, I would like to recognize my family, especially my amazing husband Nuwan. He has always been a source of constancy and love in the times where I needed it most. His positive attitude and humor are invaluable. My parents, Tim and Mary Conner, should also take so much credit for obtaining my Ph.D. There are no words to express how deeply I appreciate everything they have done for me. To my sister Katherine and my brother Charles, thank you for bringing so much fun and joy to my life. It has been an honor living life with you.

## TABLE OF CONTENTS

ACKNOWLEDGMENTS.....	iii
LIST OF TABLES.....	vi
LIST OF FIGURES.....	vii
LIST OF SCHEMES.....	ix
LIST OF ABBREVIATIONS.....	xi
ABSTRACT.....	xiv
CHAPTER 1: SYNTHESIS AND BIOLOGICAL EVALUATION OF ASCAROSIDE ANALOGS FOR BETTER UNDERSTANDING OF DAUER FORMATION IN <i>CAENORHABDITIS ELEGANS</i> .....	1
1.1 Introduction.....	1
1.1.1 Life Cycle.....	2
1.1.2 The Dauer Pheromone.....	3
1.1.3 Biosynthesis of Dauer Ascarosides.....	7
1.2 Results and Discussion.....	9
1.2.1 Synthesis of Ascaroside Analogs.....	9
1.2.2 Biological Evaluation of Ascaroside Analogs.....	14
1.3 Conclusions.....	16
1.4 Experimental.....	17
1.4.1 General Methods.....	17
1.4.2 Procedures and Characterization.....	18
1.5 References.....	25
CHAPTER 2: SYNTHESIS AND BIOLOGICAL EVALUATION OF THE INFECTIVE JUVENILE HORMONE OF <i>HETERORHABDITIS BACTERIOPHORA</i> .....	29
2.1 Introduction.....	29
2.1.1 Life Cycle.....	29
2.1.2 Symbiosis and <i>Photorhabdus luminescens</i> .....	31
2.1.3 Regulation of Processes in <i>H. bacteriophora</i> Using Chemical Cues.....	31
2.2 Results and Discussion.....	33
2.2.1 Synthesis of Infective Juvenile Hormone.....	33
2.2.2 Biological Evaluation of IJ hormone and asc-C11.....	39
2.3 Conclusions.....	40
2.4 Experimental.....	42
2.4.1 Procedures and Characterization.....	42
2.5 References.....	47

CHAPTER 3: DEVELOPMENT OF NOVEL VISIBLE LIGHT-PROMOTED METHOD FOR SELENO-AND TELLUROFUNCTIONALIZATION AND SYNTHESIS OF $\gamma$ -LYCORANE.....	49
3.1 Introduction.....	49
3.2 Results and Discussion.....	52
3.3 Conclusions.....	65
3.4 Experimental.....	66
3.4.1 General Methods.....	66
3.4.2 Experimental Setup.....	66
3.4.3 Procedures and Characterization.....	67
3.4.4 Computational Methods.....	78
3.4.5 Crystal Structures.....	79
3.5 References.....	79
 CHAPTER 4: DEVELOPMENT OF VISIBLE LIGHT PHOTOCATALYTIC METHOD FOR ORGANIC THIN FILM FORMATION ON GOLD USING ARYL IODIDES.....	82
4.1 Introduction.....	82
4.1.1 History and Significance of Organic Thin Films.....	82
4.1.2 Methods for Thin Film Formation.....	83
4.1.3 Photocatalytic Generation of Aryl Radicals from Aryl Iodides.....	86
4.1.4 Brief Overview of Atomic Force Microscopy.....	88
4.2 Results and Discussion.....	90
4.3 Future Work.....	96
4.4 Conclusions.....	97
4.5 Experimental.....	97
4.5.1 General Methods.....	97
4.5.2 Synthesis of $[\text{Ir}(\text{dtbbpy})(\text{ppy})_2][\text{PF}_6]$ .....	98
4.5.3 Procedure for Immersion Particle Lithography.....	98
4.5.4 Cleaning of Large Au (111) Slides.....	98
4.5.5 Experimental Setup.....	99
4.5.6 Photografting Procedure for AFM TSG Au Plates.....	100
4.5.7 Photografting Procedure for XPS Large Au Slides (0.1 M).....	100
4.5.8 Water Contact Angle Measurements on Large Au Slides.....	101
4.5.9 X-ray Photoelectron Spectroscopy (XPS).....	101
4.5.10 Atomic Force Microscopy (AFM).....	102
4.6 References.....	102
 APPENDIX A: COPYRIGHT RELEASES.....	105
 APPENDIX B: NMR SPECTRA OF COMPOUNDS FOUND IN CHAPTER 1.....	111
 APPENDIX C: NMR SPECTRA OF COMPOUNDS FOUND IN CHAPTER 2.....	142
 APPENDIX D: NMR SPECTRA OF COMPOUNDS FOUND IN CHAPTER 3.....	162
 VITA.....	200

## LIST OF TABLES

Table 1.1	Activity of dauer pheromone components and synthesized ascarosides.....	15
Table 3.1	Solvent screen for selenocyclization of 5-penten-1-ol.....	55
Table 3.2	Substrate scope for selenofunctionalization.....	58
Table 3.3	Visible light-promoted tellurofunctionalization.....	63
Table 3.4	Gaussian 2009 calculated enthalpies, entropies, and Gibbs free energies.....	78

## LIST OF FIGURES

Figure 1.1	Life cycle of <i>C. elegans</i> .....	2
Figure 1.2	Ascarosides in the dauer pheromone.....	4
Figure 1.3	General structure of dauer ascarosides.....	5
Figure 1.4	Targeted ascaroside analogs.....	10
Figure 2.1	Comparison of life cycles of <i>C. elegans</i> and <i>H. bacteriophora</i> .....	29
Figure 2.2	Isolation of crude IJ hormone.....	32
Figure 2.3	Structure of <b>asc-C11EA 25</b> .....	33
Figure 2.4	IJ recovery assay.....	39
Figure 3.1	Selenium-containing anti-cancer agents.....	51
Figure 3.2	<sup>77</sup> Se NMR Studies.....	53
Figure 3.3	(±)-γ-lycorane.....	59
Figure 3.4	Experimental setup.....	67
Figure 3.5	Crystal structure of telluride <b>69</b> .....	79
Figure 3.6	Crystal structure of <b>71</b> .....	79
Figure 4.1	Iridium catalysts.....	86
Figure 4.2	Basic experimental setup for AFM.....	89
Figure 4.3	Immersion particle lithography.....	90
Figure 4.4	AFM images of 4-anisyl on gold using Stephenson's conditions.....	91
Figure 4.5	AFM image of 4-anisyl on gold using Lee's conditions with a 4-iodoanisole concentration of 0.01 M.....	93
Figure 4.6	AFM image of 4-anisyl on gold using a 4-iodoanisole concentration of 0.1 M.....	94
Figure 4.7	Water contact angles of gold plate before and after grafting with idoanisole.....	94



Figure 4.8	XPS spectrum of anisole thin film on gold plate.....	95
Figure 4.9	Proposed substrate scope.....	96
Figure 4.10	Apparatus for cleaning of gold slides.....	99
Figure 4.11	Photografting experimental setup.....	99

## LIST OF SCHEMES

Scheme 1.1	Biosynthetic pathway for dauer pheromone ascarosides.....	8
Scheme 1.2	Glycosylation with ascarylose via neighboring group participation.....	11
Scheme 1.3	Optimization of cross metathesis.....	11
Scheme 1.4	Cross metathesis producing analogs with varying chain lengths.....	12
Scheme 1.5	Hydrogenation and oxidation of ascarosides.....	12
Scheme 1.6	Deprotection via methanolysis or hydrolysis .....	13
Scheme 2.1	Attempt at the synthesis of oxidized product <b>17</b> .....	34
Scheme 2.2	Synthesis of the saturated methyl ester <b>23</b> .....	35
Scheme 2.3	Attempts at aminolysis.....	36
Scheme 2.4	Successful synthesis of amide <b>asc-C11EA 25</b> .....	37
Scheme 2.5	Synthesis of amide <b>32</b> .....	38
Scheme 2.6	Synthesis of <b>asc-C11 24</b> .....	40
Scheme 3.1	Mechanism for selenocyclization.....	49
Scheme 3.2	C-Se bond homolysis.....	49
Scheme 3.3	Selenoxide elimination.....	50
Scheme 3.4	Pummerer rearrangement.....	50
Scheme 3.5	Pandey's light-promoted selenocyclization.....	51
Scheme 3.6	Attempted glycosylation using 4-peten-1-ol.....	52
Scheme 3.7	Attempted addition of PhSeBr across an alkene.....	54
Scheme 3.8	First attempt at the synthesis of ( $\pm$ )- $\gamma$ -lycorane.....	60
Scheme 3.9	Addition of TMS-protecting group.....	61
Scheme 3.10	TTMSS as radical initiator.....	62

Scheme 3.11	Mechanistic considerations.....	64
Scheme 4.1	Photografting of arenediazonium salts.....	85
Scheme 4.2	Proposed mechanism for aryl radical generation under the Stephenson conditions.....	87
Scheme 4.3	Proposed mechanism for aryl radical generation under the Lee conditions.....	88
Scheme 4.4	Synthesis of $[\text{Ir}(\text{dtbbpy})(\text{ppy})_2][\text{PF}_6]$ .....	92
Scheme 4.5	Monolayers resulting from removable blocking groups.....	97

## LIST OF ABBREVIATIONS

$^1\text{H}$	proton NMR
$^{13}\text{C}$	carbon NMR
$^{77}\text{Se}$	selenium NMR
AFM	atomic force microscopy
AIBN	azobisisobutyronitrile
$\text{CDCl}_3$	deuterated chloroform
$\text{CD}_3\text{OD}$	deuterated methanol
COSY	homonuclear correlation spectroscopy
DCM	dichloromethane
DCN	1,2-dicyanonaphthalene
dfq-COSY	double quantum filtered COSY
DIPEA	<i>N,N</i> -diisopropylethylamine
DMF	dimethylformamide
$\text{EC}_{50}$	half maximal effective concentration
EtOAc	ethyl acetate
EtOH	ethanol
GC-MS	gas chromatography-mass spectrometry
GPCR	G protein-coupled receptor
HMBC	heteronuclear multiple-bond correlation
HPLC	high performance liquid chromatography
HREELS	high resolution electron energy loss spectroscopy
HRMS	high-resolution mass spectrometry

HSQC.....	heteronuclear single-quantum coherence
IC.....	indole-3-carbonyl
IGF-1.....	insulin-like growth factor 1
IJ.....	infective juvenile
<i>i</i> PrOH.....	isopropanol
IRRAS.....	infrared reflection-absorption spectroscopy
LC <sub>50</sub> .....	median lethal concentration
LED.....	light-emitting diode
LiOH.....	lithium hydroxide
MeCN.....	acetonitrile
MeOH.....	methanol
MK.....	methyl ketone
NGM.....	nematode growth media
NMR.....	nuclear magnetic resonance
PABA.....	<i>para</i> -aminobenzoic acid
PCC.....	pyridinium chlorochromate
Pd/C.....	palladium on carbon
ROESY.....	rotating frame nuclear Overhauser effect spectroscopy
SCE.....	saturated calomel electrode
SET.....	single-electron transfer
TBTU.....	<i>O</i> -(benzotriazol-1-yl)- <i>N,N,N',N'</i> -tetramethyluronium tetrafluoroborate
<i>t</i> BuOH.....	<i>tert</i> -butyl alcohol
TFA.....	trifluoroacetic acid

TGF- $\beta$ .....transforming growth factor beta  
THF.....tetrahydrofuran  
TLC.....thin-layer chromatography  
TMS.....trimethyl silyl  
TTMSS.....tris(trimethylsilyl)silane  
UV.....ultraviolet  
VLCA.....very long chain ascaroside  
VLCFA.....very long chain fatty acid  
XPS.....X-ray photoelectron spectroscopy

## ABSTRACT

This dissertation focuses on analog synthesis for biological evaluation and visible light promoted method development. Chapter 1 centers upon the synthesis of *Caenorhabditis elegans* dauer pheromone analogs. *C. elegans* is a nematode which, in times of environmental stress, enters a dauer stage. Two highly conserved pathways, which play important roles in some diseases in higher organisms, monitor dauer formation: TGF- $\beta$  and IGF-1. Dauer formation is triggered by the nematode's chemosensation of the dauer pheromone, consisting of a group of previously-isolated ascarosides. These compounds differ in chain length, saturation, terminal functionality of side chain,  $\omega$  vs.  $\omega-1$  oxygenation and presence of an indole-3-carboxyl protecting group. The roles that these various functionalities play in dauer formation are poorly understood. Therefore, analogs containing these functionalities are targeted for synthesis and biological evaluation in dauer formation assays to determine their structure-activity relationships.

Chapter 2 concentrates on the synthesis of the infective juvenile (IJ) hormone of *Heterorhabditis bacteriophora*. This nematode exists in the soil as a robust infective juvenile, a “non-aging” and nonfeeding stage, homologous to the dauer stage of *C. elegans*. The hormone responsible for IJ formation and accumulation is isolated via bioassay-guided fractionation. This hormone's structure is then elucidated, synthesized and evaluated for IJ formation activity.

In Chapter 3 of this dissertation, a new method for seleno- and tellurofunctionalization is demonstrated. Selenocyclization has proven to be invaluable in the synthesis of complex natural products. However, it often involves the use of PhSeX (X = Br or Cl), which is a class of water-sensitive and toxic compounds. As a result, a visible light-promoted method is developed in which PhSeBr is generated in situ from the reaction of Ph<sub>2</sub>Se<sub>2</sub> and CBr<sub>4</sub>, as determined by <sup>77</sup>Se

NMR. Selenofunctionalizations using this novel method with an array of substrates, including the total synthesis of Amaryllidaceae alkaloid,  $\gamma$ -lycorane, is accomplished in excellent yields.

Chapter 4 describes the formation of an organic thin film using photocatalysis and aryl iodides. Most commonly, organic thin films are generated using thiol precursors. However, these thin films are often unstable to oxidation and thermal desorption. To circumvent these issues, a visible light photocatalytic method is developed where aryl radicals generated from aryl iodides are grafted to gold surfaces. The resulting thin films are extremely stable, due to the strength of the covalent carbon-gold bond. The multilayers were characterized using atomic force microscopy (AFM), X-ray photoelectron spectroscopy (XPS) and water contact angle measurements.



# CHAPTER 1: SYNTHESIS AND BIOLOGICAL EVALUATION OF ASCAROSIDE ANALOGS FOR BETTER UNDERSTANDING OF DAUER FORMATION IN *CAENORHABDITIS ELEGANS*

## 1.1 Introduction

Sydney Brenner pioneered the use of *C. elegans* as a model organism for biological study and won the Nobel Prize in 2002 for his efforts.<sup>1</sup> *C. elegans* is a soil-dwelling nematode of 1 mm length as an adult, whose transparency allows researchers to study every cell and many biological processes in action under a microscope.<sup>2</sup> It is an unsegmented roundworm, consisting of two tubes, an inner and an outer, and a pseudocoelom, which lies between the two.<sup>3</sup> The pseudocoelom serves as both an immune and circulatory system and facilitates intracellular signaling and nutrient dispersal.<sup>3-4</sup> The outer tube is comprised of the cuticle and its underlying hypodermis, excretory system, nervous system and muscles. The inner tube consists of the reproductive and the alimentary systems.

*C. elegans* serves as an excellent model organism for many reasons. The worm is widely used in part because of its short generation time and ease of manipulation in the laboratory. It is also relatively inexpensive, and it has an average lifespan of 17 days, provided that food is readily available and the temperature is held at 20°C.<sup>5</sup> The nematodes are of small size, both physically and genetically. Adult hermaphrodites have only 959 somatic cells and a genome size of only 100 Mb. In a laboratory environment, they can be easily grown on a diet of bacteria (usually *E. coli*) on agar plates or in a liquid medium. The diet of *C. elegans* in the wild is still under speculation.<sup>6</sup> It has been proposed that it feeds off of decaying organic matter, perhaps necromenically from the corpse of its host.

Despite the relative simplicity of its physiology, *C. elegans* exhibits higher behavioral processes such as response to sensory cues, learning and memory.<sup>3, 7</sup> The nematode also has

nearly as many genes as humans (20,000 in *C. elegans* versus 23,000 in humans).<sup>5</sup> Scientists have determined that 60-80% of *C. elegans*' genes are homologous to those of humans.<sup>8</sup>

### 1.1.1 Life Cycle

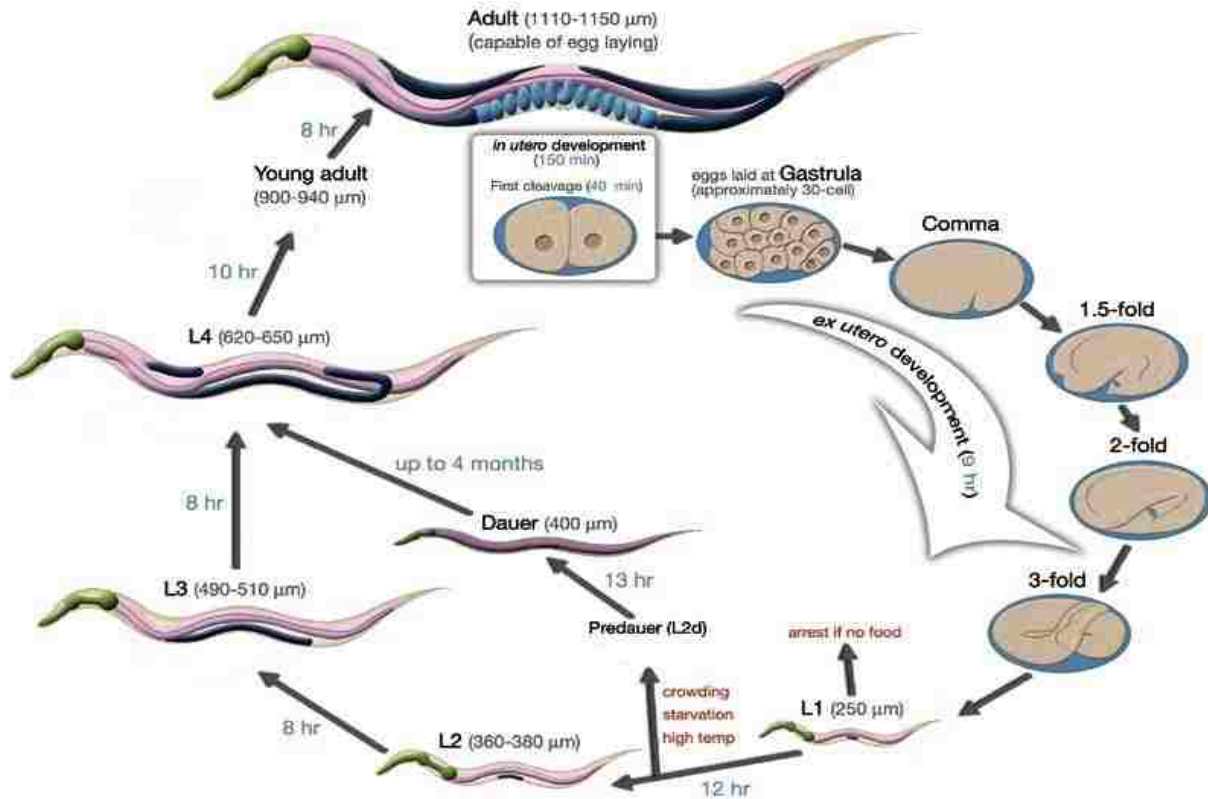


Figure 1.1 Life cycle of *C. elegans* (Adapted from *Wormatlas*)

The life cycle of *C. elegans* is similar to that of other nematodes (Figure 1.1).<sup>3</sup> The normal cycle starts with embryogenesis in the hermaphrodite uterus and then moves through the reproductive stages (L1-L4) to adulthood. The adult worm has an average lifespan of 2-3 weeks. However, if exposed to harsh conditions – insufficient food supply, high population density, or non-ideal temperature – *C. elegans* in the L1 larval stage can respond to chemical cues and enter the non-aging dauer phase.<sup>9</sup> In this stage, the nematode exhibits interesting behavioral and developmental traits. While in this dauer phase, *C. elegans* experiences increased longevity and

can live up to 4 months, approximately 5 times longer than the normal lifespan of the worm. The morphology of *C. elegans* is also modified in the dauer stage. For example, the worm develops a specialized tough cuticle that protects the dauer larva from environmental pressures.<sup>10</sup> It can also exhibit behavioral changes such as the cessation of feeding and relative immobility. When conditions once again become favorable, the nematode senses environmental chemical cues and can exit from the dauer stage to the L4 larva stage and continue on to adulthood.

### 1.1.2 The Dauer Pheromone

The dauer stage of *C. elegans* has become of increasing interest to the scientific community. This is due, in part, to the conservation of biological pathways between the nematode and higher organisms. Two highly conserved pathways regulate dauer formation in *C. elegans*: transforming growth factor beta (TGF- $\beta$ ) and insulin-like growth factor 1 (IGF-1).<sup>11</sup> In higher organisms, these pathways play an integral role in metabolism, aging and development as well as some diseases like Alzheimer's.<sup>12</sup> The study of these pathways in high organisms can often be difficult due to monetary, ethical or technical issues. Because *C. elegans* is easily manipulated, grown and observed in a laboratory setting, it is an ideal candidate for the study of these pathways. Studying these pathways in *C. elegans* may lead to therapeutics for human diseases.

Dauer formation is triggered by *C. elegans*' chemosensation of the "dauer pheromone," a secreted combination of ascarosides that are produced by the worm.<sup>13</sup> The ascaroside components of the dauer pheromone can be seen in Figure 1.2. The dauer pheromone includes five compounds: **asc-C6-MK**,<sup>12</sup> **asc- $\Delta$ C9**,<sup>12</sup> **asc- $\omega$ C3**,<sup>14</sup> **IC-asc-C5**<sup>15</sup> and **asc-C7-PABA**<sup>16</sup>. The first four compounds were isolated using bioassay-guided fractionation of extracts from high volume worm cultures, and the structure was elucidated using NMR spectroscopy and mass

spectrometry. These compounds demonstrate activity for dauer formation in the nM range and have EC<sub>50</sub> values corresponding to 120 nM, 370 nM, 240 nM and 5 nM. EC<sub>50</sub> values represent the concentration at which 50% dauer formation is observed. The last ascaroside was discovered after comparative metabolomics studies and NMR spectroscopy. The most potent of the compounds is **IC-asc-C5**, with an EC<sub>50</sub> value of 5 nM. However, this ascaroside is only effective up to a certain concentration. At high concentrations, it inhibits its own activity, and the percent dauer formation decreases drastically. One of the ascarosides, **asc- $\omega$ C3**, works synergistically with some of the other dauer pheromone components, **asc- $\Delta$ C9**, **asc-C6-MK**, and **IC-asc-C5**, to induce dauer formation.<sup>14</sup> **Asc- $\omega$ C3** is also the only compound of the dauer pheromone that is oxygenated at the  $\omega$  position of the fatty side chain.

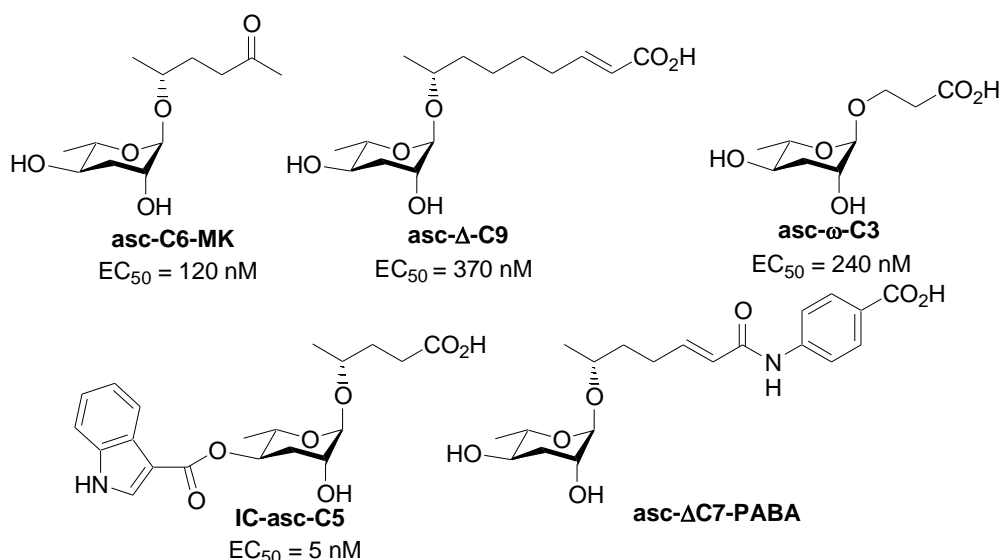


Figure 1.2 Ascarosides in the dauer pheromone

All of the ascarosides that compose the dauer pheromone adhere to a set of structural guidelines. The backbone of each compound is the ascarylose sugar moiety, seen in red in Figure 1.3. This building block can be functionalized in several ways. Firstly, there can be several head groups, of which the unprotected alcohol and the indole-3-carbonyl (IC) are the

most common. The fatty acid side chain can also be modified to include the presence of an alkene or an R group. When R = H, the compound is termed an  $\omega$ -ascaroside. However, when R=Me, the compound is defined as an ( $\omega$ -1)-ascaroside. The terminus of the side chain, seen in pink, may also be functionalized to include a simple carboxylic acid, methyl ketone (MK), or a *para*-aminobenzoic acid (PABA) group. As can be observed in Figure 1.2, small changes in structure can alter the dauer formation activity of the ascaroside.

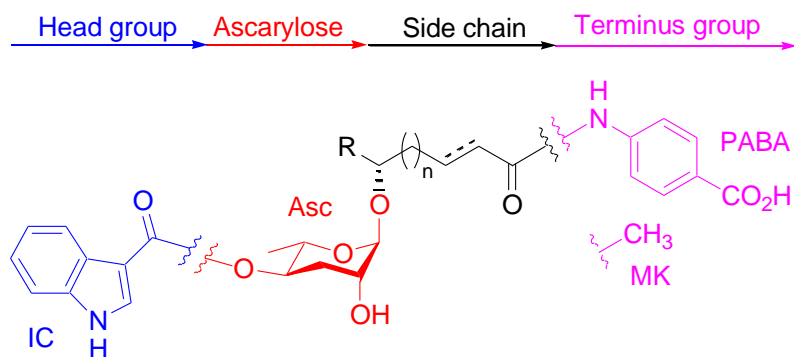


Figure 1.3 General structure of dauer ascarosides

As previously stated, *C. elegans* enters the dauer stage via chemosensation of the dauer pheromone. The dauer pheromone is secreted into the environment by the worm as a way to gather information about the population density in its immediate vicinity.<sup>17</sup> As a result, the greater the number of nematodes present at any given time, the higher the concentration of the dauer pheromone. The dauer pheromone promotes dauer formation and prevents recovery to its normal life cycle. In direct competition with the dauer pheromone is an, as yet, unknown “food signal,” which can give information about food availability in the environment. Whether *C. elegans* will enter the dauer stage and continue to stay in this stage of arrested development relies heavily upon the balance between these two chemical cues, the dauer pheromone and the “food signal.”<sup>13</sup>

The dauer pheromone is sensed by *C.elegans* using G protein-coupled receptors (GPCRs). Hundreds of GPCRs are expressed by chemosensory neurons located on the head of the worm.<sup>18</sup> Binding of the ascarosides by the GPCRs on the neurons and the resulting dauer formation was discovered through various experimental methods. For example, when two alpha subunits of GPCRs, *gpa-2* and *gpa-3*, were upregulated, dauer formation was induced.<sup>19</sup> When the same subunits were mutated, no dauer formation was observed. The main neurons associated with GPCR expression in *C.elegans* are ADF, ASG, ASI, ASJ and ASK. These neurons are responsible for the chemosensation of the dauer pheromone. The ASI and ASJ neurons are particularly important, because they regulate the IGF-1 and TGF- $\beta$  pathways.<sup>20</sup> When the dauer pheromone is detected, the neurons will downregulate the production of secondary messengers like TGF- $\beta$  and insulin-like peptides.<sup>20b</sup> The IGF-1 and TGF- $\beta$  pathways, as a result, are downregulated. As previously mentioned, the IGF-1 pathway is highly conserved throughout nature, remaining relatively unchanged from *C. elegans* to higher organisms, like humans. The IGF-1, in particular, plays an important role in the aging process. For example, when DAF-2, *C. elegans*'s sole IGF-1 receptor, is mutated, the worm's lifespan is doubled.<sup>21</sup> Mutations of genes related to the IGF-1 pathway in other, more complex organisms like *Drosophila melanogaster* and mice has also led to deceleration of the aging process.<sup>22</sup> IGF-1 is also associated with cancer. In studies where there is a presence of decreased IGF levels, the growth of existing cancer cells is also decreased.<sup>23</sup> Additionally, diets that have been demonstrated to downregulate IGF-1 pathways are also associated with a lower cancer risk.<sup>24</sup>

The TGF- $\beta$  pathway is also highly conserved between *C. elegans* and humans. This pathway is associated with various diseases as well. Studies have shown that TGF- $\beta$  plays different roles in cancer promotion and metastasis. Interestingly, the role can change

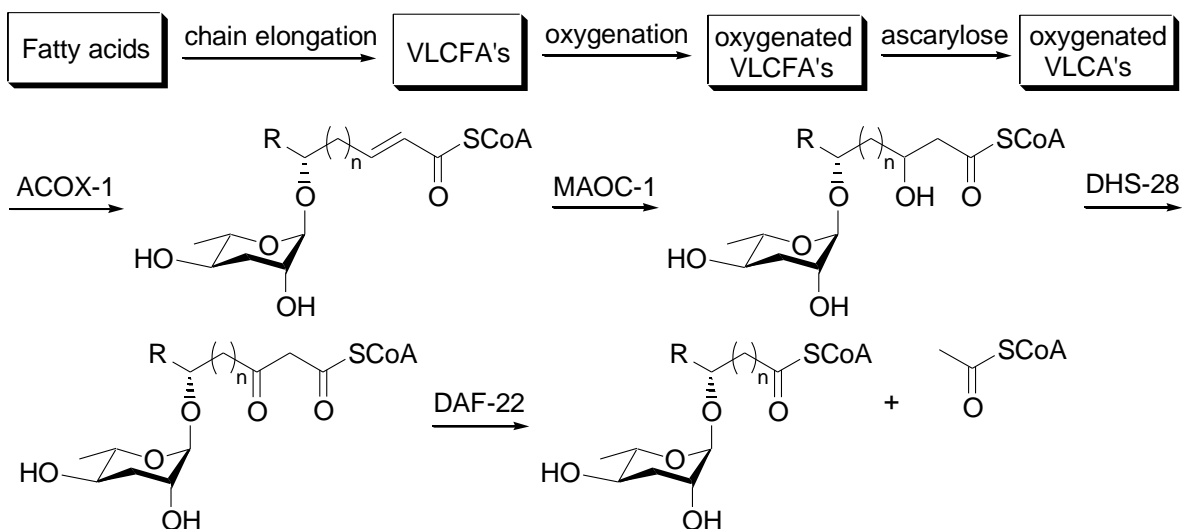
dramatically between the various types of cancer.<sup>25</sup> For example, in gastric and pancreatic cancers, the TGF- $\beta$  pathway is effectively shut down. However, the opposite is true for breast and skin cancer. In these types of cancer, the TGF- $\beta$  pathway is actually shown to be associated with tumor progression and is upregulated in some cases. This pathway, therefore, has a complex relationship with cancer and can act as both a cancer promoter and suppressor. In addition to cancer, there is also a correlation between the TGF- $\beta$  pathway and Alzheimer's disease. The blood and cerebral fluid of human patients with the disease exhibit higher concentrations of TGF- $\beta$ .<sup>26</sup> Therefore, the study of these two pathways is of great importance in order to get a better insight in the hopes of finding therapeutic treatments or even cures for various diseases.

### **1.1.3 Biosynthesis of Dauer Ascarosides**

The biosynthesis of the dauer pheromone ascarosides inside of the worm has been the subject of many studies, but many questions still remain. Less is known about the initial steps in the biosynthesis of the dauer pheromone ascarosides. However, it is suspected that the first step in the biosynthesis is the chain elongation of fatty acids (Scheme 1.1).<sup>27</sup> This could be accomplished using chain elongase homolog *elo 1-9*, which has been demonstrated to perform this function in other signaling pathways.<sup>28</sup> After elongation, the newly formed very long chain fatty acids (VLCFA's) would undergo oxygenation at either the  $\omega$  or  $\omega-1$  position and then glycosylation with 3,6-dideoxysugar ascarylose.<sup>27</sup> The oxygenated very long chain ascarosides (VLCA's) then enter the peroxisomal  $\beta$ -oxidation cascade, which consists of the enzymes *acox-1*, *maoc-1*, *dhs-28* and *daf-22*. It is also possible that ascarylose addition occurs after  $\beta$ -oxidation. However,  $\omega$  or  $\omega-1$  oxygenation is thought to occur prior to oxidation due to an

experiment which determined that the *acox-1* mutant affects  $\omega$  and  $\omega-1$  oxygenated ascarosides in different ways.

After glycosylation, the VLCA's enter the peroxisomal  $\beta$ -oxidation pathway, as seen in Scheme 1.1.<sup>27</sup> The first step of peroxisomal  $\beta$ -oxidation is the introduction of the alkene at the  $\alpha,\beta$  position. This is accomplished using the enzyme, acyl-CoA oxidase ACOX-1. The next step involved the hydration of the alkene using enoyl-CoA hydratase (MAOC-1). After hydration, the alcohol is oxidized to the ketone with (3*R*)-hydroxyacyl-CoA dehydrogenase (DHS-28). In higher organisms like some vertebrates and *Drosophila melanogaster*, these two steps (hydration and oxidation) are combined, and the transformation is performed by one protein, *e.g.* MFE-2. The last step in the peroxisomal  $\beta$ -oxidation pathway is the cleavage of the diketone intermediate by  $\beta$ -ketoacyl-CoA thiolase DAF-22. Usually, this entire process continues until the chain is between 6 and 12 carbons in length.<sup>29</sup> The indole group is added last, but the mechanism of addition is not known. However, this step is known to be highly specific.



Scheme 1.1 Biosynthetic pathway for dauer pheromone ascarosides



Although the biosynthesis of ascarylose in bacteria is well understood, less is known about the biosynthesis of ascarylose in *C. elegans*. Studies that demonstrated the presence of ascarosides in axenic cultures of *C. elegans* point to the endogenous synthesis of ascarylose.<sup>30</sup> Additionally, the *C. elegans* genome contains many homologs to genes that are a part of the synthetic pathway of ascarylose in bacteria, which deserves further investigation.

## 1.2 Results and Discussion

### 1.2.1 Synthesis of Ascaroside Analogs

The ascarosides that comprised the dauer pheromone are similar in many ways. For example, all contain the ascarylose backbone, with the anomeric carbon being in the  $\beta$  configuration. The majority of the pheromone components also have free alcohols. Despite these similarities, the molecules differ greatly in terminal functional groups (carboxylic acid, ketone, and amide), chain length, saturation and indolyl carboxyl protection of one of the free alcohols. In an effort to determine structure-activity relationships of the various functional groups present in the dauer pheromone ascarosides and to potentially discover a new ascaroside with high dauer-formation activity, multiple analogs were synthesized and biologically evaluated using dauer formation assays.<sup>31</sup> The synthesized analogs containing various functionalities were used to determine structure-activity relationships for side chain attributes and their dauer-inducing ability.

The analogs targeted for synthesis and biological evaluation contained a wide variety of moieties. The analogs synthesized by this researcher, ascarosides in the **OH/MK** series, differed in side-chain length and terminal functionality (alcohol vs. methyl ketone), as is demonstrated by the boxed region of Figure 1.4. The first step towards the synthesis of the selected analogs was glycosylation using dibenzoyl ascarylose **3** as glycosyl donor and alcohols **1** and **2** as glycosyl

acceptors (Scheme 1.2).<sup>32</sup> Dibenzoyl ascarylose was previously synthesized according to a known procedure.

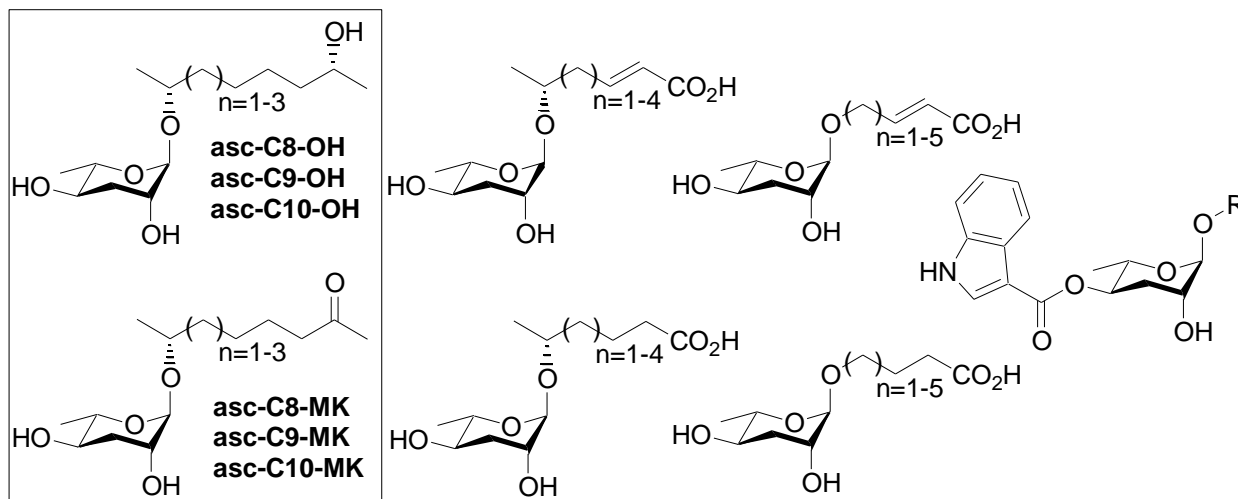
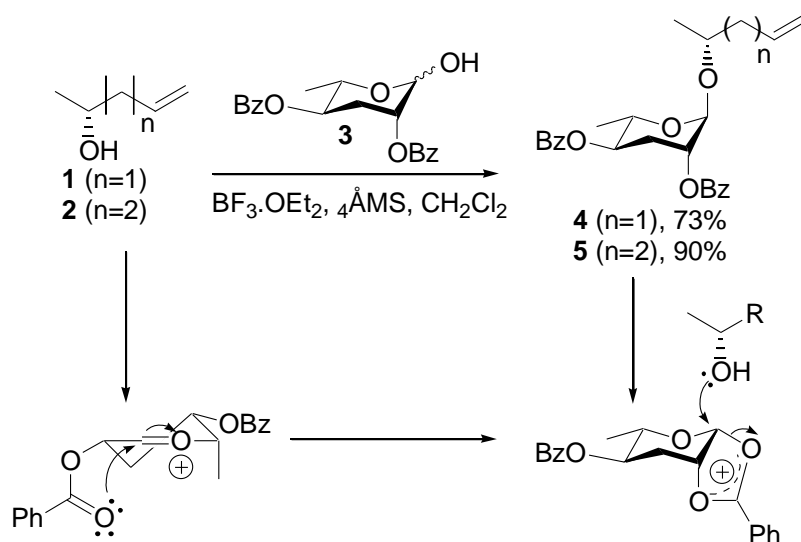


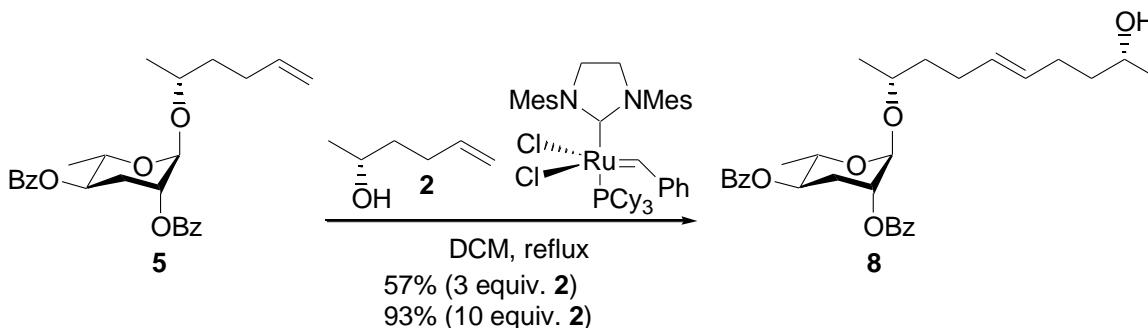
Figure 1.4 Targeted ascarylose analogs

$\text{BF}_3$  etherate, which coordinated to the anomeric alcohol of dibenzoyl ascarylose **3**, was used as a Lewis acid, rendering it a better leaving group. Sugars **4** and **5** were produced solely in the  $\beta$  configuration due to neighboring group participation from the adjacent benzoyl protecting groups. This phenomenon is shown in Scheme 1.2. After the lone pair from the ring oxygen donates into the  $\sigma^*$  orbital of the anomeric carbon-oxygen bond, promoting the loss of the alcohol, an oxonium intermediate is formed. The electron lone pair on the carbonyl oxygen on the benzoyl protecting group adjacent to the anomeric carbon attacks, effectively blocking the bottom face from addition of alcohols **1** or **2**. Using this method, glycosylation products **4** and **5** were successfully synthesized in 73% and 90%, respectively, in a short amount of time. Originally, reagent grade DCM was used, but dry DCM from a solvent system increased the glycosylation yields significantly. For example, glycosylation using alcohol **2** and dry DCM increased yields from 70% to 90%.



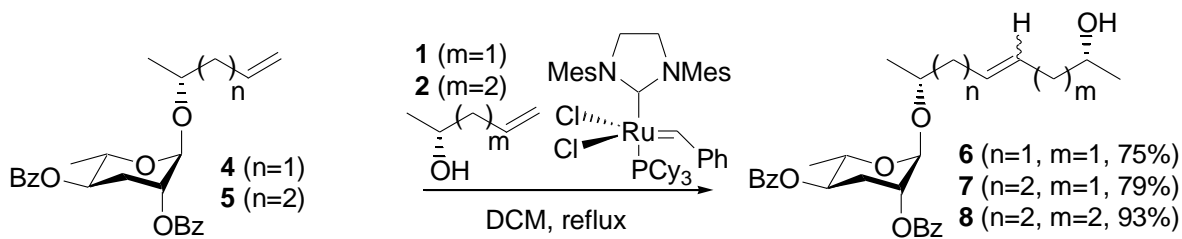
Scheme 1.2 Glycosylation with ascarlose via neighboring group participation

Next in the synthesis of the desired ascaroside analogs, olefin cross metathesis was performed using Grubbs 2<sup>nd</sup> generation ruthenium catalyst.<sup>33</sup> This catalyst was used as opposed to the Grubbs 1<sup>st</sup> generation catalyst due to its comparatively higher reactivity. Cross metathesis under these conditions gave alkenes **6-8** as a mixture of *E* and *Z* isomers. The mixture of *E/Z* isomers, however, did not pose any concern as the next step in the synthesis would negate any stereochemistry. Using 3 equivalents of Grubbs 2<sup>nd</sup> generation catalyst, ascaroside **5** was converted into the desired metathesis product **8** in a modest yield of 57%. In order to optimize this reaction, varying equivalents of alcohol were used (Scheme 1.3). Out of 3 and 10 equivalents, the reaction using 10 equivalents of alcohol provided the best yield of 93%.



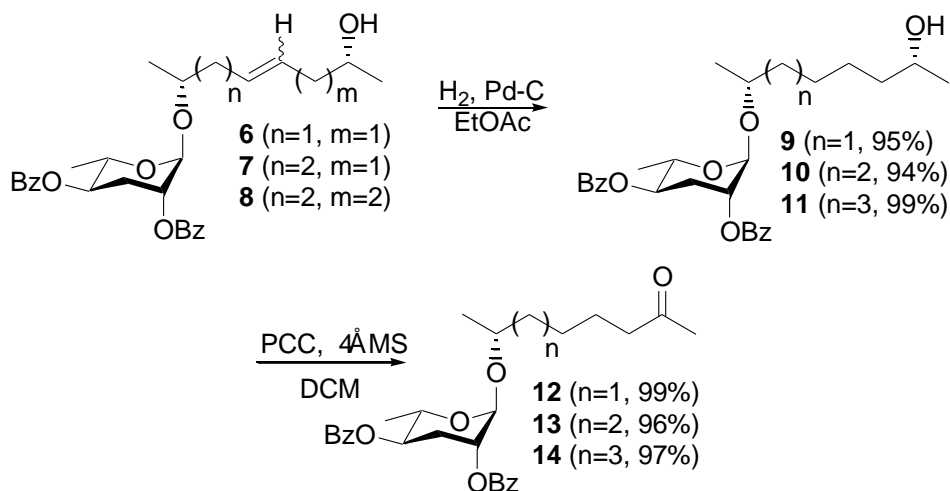
Scheme 1.3 Optimization of cross metathesis

After optimizing the reaction conditions, alcohol **1** was submitted to cross metathesis with the ascaroside **4**, and alcohol **2** was paired with ascaroside **4** (Scheme 1.4). Both reactions proceeded successfully, giving the 8 carbon chain alcohol **6** and 9 carbon chain alcohol **7** in 75% and 79% yields, respectively. Purification of all cross metathesis products was completed readily via column chromatography.



Scheme 1.4 Cross metathesis producing analogs with varying chain lengths

The next step in the synthesis of the ascaroside analogs was the hydrogenation of the alkene in the side chain to produce the saturated sugars **9-11**. This transformation was accomplished using 1atm H<sub>2</sub> (balloon) and 10% palladium on activated carbon. Purification proved to be simple, consisting only of filtration through a short Celite<sup>®</sup> plug. Yields were excellent, ranging from 94%-99% for saturated analogs **9-11** (Scheme 1.5).



Scheme 1.5 Hydrogenation and oxidation of ascarosides



In an attempt to provide a more basic environment which would increase reactivity of the system, 1M LiOH was used with methanol as solvent. This method was determined to be a much better method when coupled with purification via HPLC, improving yields dramatically. Yields of hydrolysis for **asc-C9-OH** and **asc-C10-OH** were increased to 89% and 94%, respectively. Hydrolysis using 1M LiOH and methanol was also successful for the **asc-MK** series, giving yields ranging from 77%-84%. Hydrolysis conditions were also attempted for the formation of **asc-C8-OH**. Purification of this reaction was difficult due to the similar polarities of the desired product and impurities. Therefore, for this transformation, methanolysis was considered the better synthetic route.

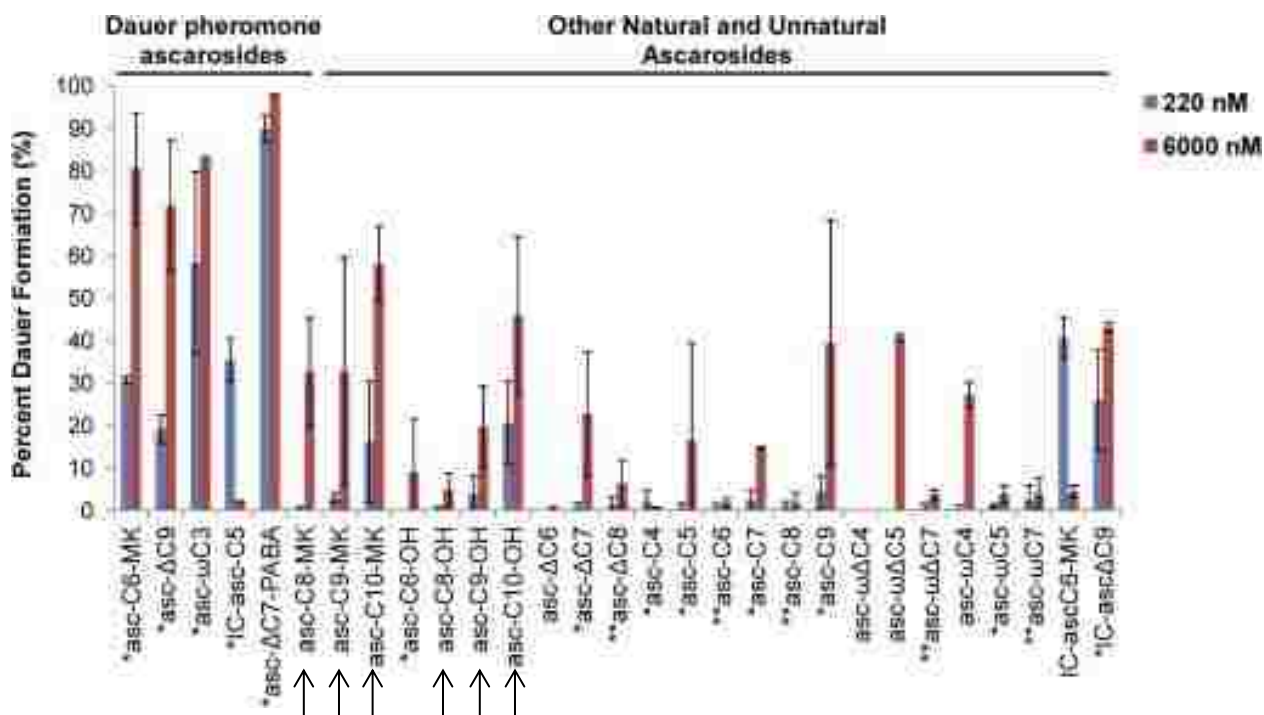
### 1.2.2 Biological Evaluation of Ascaroside Analogs

After synthesizing all of the ascaroside analogs, the research lab of Rebecca Butcher at University of Florida performed biological evaluations to determine the activity of each synthesized compound in promoting dauer formation.<sup>31</sup> These determinations were made by performing dauer formation assays. In these assays, the synthesized ascarosides at two concentrations, 220 nM and 6000 nM, were mixed with nematode growth media (NGM) agar and heat-killed *E. coli*, poured into plates and allowed to set. The concentrations of synthesized ascarosides were chosen for specific reasons. The lower concentration, 220 nM, was used because it is in the range of the EC<sub>50</sub> values for the dauer pheromone components. The higher concentration, 6000 nM, was chosen because any activity towards dauer formation would be observable at this concentration. The *C.elegans* nematodes were then allowed to lay eggs on the media and incubated for 68-72 hrs at 25°C. After the allotted incubation time, plates containing 50-100 worms were collected for analysis and dauers were recognized by small size and lack of

pharyngeal pumping. The percentage of dauers over the total population of worms in each experiment was then determined.

The activities of all of the synthesized compounds were compared to those of the ascarosides that comprise the dauer pheromone. The assay was performed at two concentrations, 220 nM and 6000 nM. Overall, the activities of each of the compounds were low compared to those of the known dauer pheromone ascarosides. There was a direct correlation present in chain length versus percent dauer formation. As the chain length increased, the activity towards dauer formation also increased. The most active of the OH/MK series consisted of a ten carbon side chain. The **asc-C10-MK** analog was slightly more active than the **asc-C10-OH** ascaroside. In general, the MK series was more active for dauer formation than the OH series. Predictably, the high concentration for almost all of the ascarosides led to a higher percent of dauer formation. However, in nature, the dauer pheromone is never present at either concentration.

Table 1.1 Activity of dauer pheromone components and synthesized ascarosides



None of the synthesized ascarosides exhibited activities near those of the known dauer pheromone components even though many only differed by one carbon or one functional group. For example, **asc-C8-MK** only differs from the naturally-occurring **asc-c6-MK** by two carbons. However, the percent dauer formation for the unnatural ascaroside was drastically lower than that of the dauer pheromone component, especially at the lower concentration. The performed biological studies indicate that the activity in promoting dauer formation is highly dependent on the structure of the ascarosides. The synthesized ascarosides and the dauer pheromone components are largely similar, containing an ascarylose moiety, and only differing in structural attributes like chain length, terminal functionality and degree of unsaturation. Yet all of the ascarosides exhibited drastically different activities. These results led to the conclusion that the G-coupled protein receptors that bind their respective cognate ascarosides are highly selective. Evolutionarily speaking, this selectivity could be due to the need to prohibit “cross talk” between similar species in the same environment. For example, *C.elegans* and *C.briggsae* occupy the same general environment and both use ascarosides for signaling purposes.<sup>35</sup> Each worm would need to have its own means of receiving chemical cues without interference from the other species.

### **1.3 Conclusions**

In conclusion, multiple analogs containing varying functionalities were synthesized in order to determine structure-activity relationships for side chain structural attributes and their dauer-inducing ability. The synthesized analogs differed in chain length and terminal functionality oxidation state, both alcohol and ketone. The general scheme for synthesizing the ascarosides began with the benzoyl ascarylose backbone. The glycosylation of this building block with various alkenols yielded the intermediates **4** and **5** in excellent yields, especially after



using dry solvents. The glyosylation products then underwent cross metathesis with other alkenols **6-8** using Grubbs 2<sup>nd</sup> generation catalyst. Interestingly, a mixture of *E/Z* isomers was produced. This lack of stereoselectivity was not a concern, however, because the next step was hydrogenation of the alkene to give the saturated ascarosides **9-11**. Ketones **12-14** were synthesized from the alcohol via oxidation by PCC. Lastly, the benzoate groups on the OH-MK series were removed using either methanolysis or hydrolysis to yield the desired ascaroside analogs.

Once synthesized, the ascaroside analogs were then analyzed in biological assays by collaborators at University of Florida to determine each compound's activity towards dauer formation in *C. elegans*. However, none of the analogs exhibited any relevant activity in the dauer formation, despite structural similarities between these analogs and the dauer pheromone components. This evidence points to the G protein-coupled receptors' high selectivity towards binding of their cognate ascarosides. The lack of promiscuity in receptor binding may have developed over time as a need to prevent "cross-talk" between various species, which occupy the same environment and use ascarosides for chemical signaling.

## **1.4 Experimental**

### **1.4.1 General Methods**

Flash column chromatography was performed using 60 Å silica gel. <sup>1</sup>H NMR and <sup>13</sup>C NMR spectroscopy were performed on a Bruker AV-400, DPX 400, DPX 250 or Varian 500 spectrometer. HPLC purifications were conducted with a Waters Breeze 2 system equipped with an XBridge C18 semi-preparative column (5 lm, 10 x 100 mm) with gradient runs of H<sub>2</sub>O in CH<sub>3</sub>CN. Mass spectra were obtained using an Agilent 6210 electrospray time-of-flight mass spectrometer. Optical rotation measurements were obtained using a JASCO P-2000 polarimeter. Unless otherwise noted, all materials were obtained from commercial suppliers and used without

further purification. Analytical TLC was conducted on aluminum sheets (Merck, silica gel 60, F254). Compounds were visualized by UV absorption (254 nm) and staining with anisaldehyde or KMnO<sub>4</sub>. All glassware (save for hydrolysis reactions) was flame-dried under vacuum and backfilled with dry nitrogen prior to use. Deuterated solvents were obtained from Cambridge Isotope Labs. All solvents were purified according to the method of Grubbs.<sup>36</sup>

#### 1.4.2 Procedures and Characterization

Representative procedure for glycosylation – synthesis of **5**:

A suspension of 1.0228 g (2.8701 mmol) dibenzoylascarylose **3**, 0.54 mL (4.5 mmol) alcohol **2** and 325.8 mg 4Å molecular sieves in 32 mL CH<sub>2</sub>Cl<sub>2</sub> was cooled to 0°C. To this suspension was added 1.54 mL (12.2 mmol) BF<sub>3</sub>·OEt<sub>2</sub> at once. The resulting suspension was stirred at 0°C for 7 h. 30 mL saturated NaHCO<sub>3</sub> solution was then added. Upon cessation of effervescence, the aqueous layer was separated from the organic layer and then extracted with 3x20mL CH<sub>2</sub>Cl<sub>2</sub>. The resulting organic extracts were dried over MgSO<sub>4</sub> and filtered to obtain 1.5492 mg of oil after evaporation of solvent. Silica gel column chromatography (35 g silica gel, gradient run from 50% hexanes in CH<sub>2</sub>Cl<sub>2</sub> to 30% hexanes in CH<sub>2</sub>Cl<sub>2</sub>) afforded 1.1364 g (90%) of a colorless syrup.  $[\alpha]_D^{25} = -15.0$ ,  $c$  1.74 (CH<sub>2</sub>Cl<sub>2</sub>); HRMS ( $m/z$ ): [M+Na]<sup>+</sup> calcd. for C<sub>26</sub>H<sub>30</sub>O<sub>6</sub>Na 461.1935, found 461.1946; <sup>1</sup>H NMR (250 MHz, CDCl<sub>3</sub>): δ 8.13 (d,  $J = 7.0$  Hz, 2H), 8.06 (d,  $J = 7.0$  Hz, 2H), 7.56 (m, 2H), 7.45 (m, 4H), 5.89 (ddt,  $J = 16.8, 10.2, 6.5$  Hz, 1H), 5.09 (m, 5H), 4.16 (dq,  $J = 9.8, 6.2$  Hz, 1H), 3.89 (m, 1H), 2.45 (dt,  $J = 13.5, 4.0$  Hz, 1H), 2.24 (m, 3H), 1.70 (m, 2H), 1.30 (d,  $J = 6.2$  Hz, 3H), 1.22 (d,  $J = 6.1$  Hz, 3H); <sup>13</sup>C NMR (62.5 MHz, CDCl<sub>3</sub>): δ 166.0; 165.9; 138.6; 133.43; 133.37; 130.2; 130.1; 129.8; 128.6; 115.0; 93.9; 72.2; 71.4; 70.8; 67.2; 36.5; 30.2; 29.9; 19.3; 18.1.

Synthesis of **4**:

Started with 1.027 g (2.884 mmol) dibenzoylascarylose **3**, 0.46 mL (4.5 mmol) alcohol **1**, 302.9 mg 4Å molecular sieves, and 1.54 mL (12.2 mmol) BF<sub>3</sub>·OEt<sub>2</sub> in 30 mL CH<sub>2</sub>Cl<sub>2</sub>. Purified to obtain 891.5 mg (73%) of a colorless oil.  $[\alpha]_D^{25} = -10.7$ ,  $c$  1.015 (CH<sub>2</sub>Cl<sub>2</sub>); HRMS ( $m/z$ ): [M+Na]<sup>+</sup>calcd. for C<sub>25</sub>H<sub>28</sub>O<sub>6</sub>Na 447.1778, found 447.1790; <sup>1</sup>H NMR (250 MHz, CDCl<sub>3</sub>): δ 8.12 (d,  $J = 7.6$  Hz, 2H), 8.05 (d,  $J = 7.9$  Hz, 2H), 7.57 (m, 2H), 7.47 (m, 4H), 5.89 (ddt,  $J = 17.3$ , 10.3, 7.1 Hz, 1H), 5.16 (m, 4H), 4.96 (s, 1H), 4.15 (dq,  $J = 12.7$ , 6.2 Hz, 1H), 3.92 (m, 1H), 2.32 (m, 4H), 1.28 (d,  $J = 6.2$  Hz, 3H), 1.21 (d,  $J = 6.0$  Hz, 3H); <sup>13</sup>C NMR (62.5 MHz, CDCl<sub>3</sub>): δ 165.8; 165.7; 135.0; 133.31; 133.25; 130.1; 129.9; 129.7; 128.5; 117.3; 94.0; 72.5; 71.3; 70.7; 70.0; 41.7; 29.8; 19.0; 17.9.

Representative procedure for cross metathesis – synthesis of **8**:

To a solution of 18.8 mg (0.0429 mmol) alkene **5** and 52 μL (0.43 mmol) alcohol **2** in 1.3 mL CH<sub>2</sub>Cl<sub>2</sub> at reflux was added 3.7 mg (0.0044 mmol) Grubbs 2<sup>nd</sup> generation ruthenium catalyst at once. The resulting solution was allowed to stir at reflux for 1 h and allowed to cool to 25°C. The reaction mixture was concentrated to 58.4 mg of brown oil. Silica gel column chromatography (silica gel, gradient run from 10% ethyl acetate in hexanes to 30% ethyl acetate in hexanes) afforded 20.4 mg (93%) of a yellow oil.  $[\alpha]_D^{25} = -23.7$ ,  $c$  0.76(CH<sub>2</sub>Cl<sub>2</sub>); HRMS ( $m/z$ ): [M+Na]<sup>+</sup>calcd. for C<sub>30</sub>H<sub>38</sub>O<sub>7</sub>Na 533.2510, found 533.2522; <sup>1</sup>H NMR (250 MHz, CDCl<sub>3</sub>): δ 8.12 (d,  $J = 7.2$  Hz, 2H), 8.05 (d,  $J = 7.0$  Hz, 2H), 7.59 (m, 2H), 7.47 (m, 4H), 5.53 (m, 2H), 5.16 (m, 2H), 4.96 (s, 1H), 4.12 (dq,  $J = 12.7$ , 6.2 Hz, 1H), 3.85 (m, 2H), 2.42 (dt,  $J = 13.4$ , 4.0 Hz, 1H), 2.21 (m, 5H), 1.55 (m, 5H), 1.28 (d,  $J = 6.2$  Hz, 3H), 1.20 (m, 6H).

Synthesis of **6**:

Started with 235.2 mg (0.5541 mmol) alkene **4**, 0.57 mL (5.5 mmol) alcohol **1**, and 47.0 mg (0.0553 mmol) Grubbs 2<sup>nd</sup> generation ruthenium catalyst in 17 mL CH<sub>2</sub>Cl<sub>2</sub>. Purified to obtain 223.6 mg (84%) of a yellow oil.  $[\alpha]_D^{25} = 24.5$ ,  $c$  0.965 (CH<sub>2</sub>Cl<sub>2</sub>); HRMS ( $m/z$ ): [M+Na]<sup>+</sup>calcd.

for  $C_{28}H_{34}O_7Na$  505.2197, found 505.2210;  $^1H$  NMR (250 MHz,  $CDCl_3$ ):  $\delta$  8.11 (d,  $J = 7.1$  Hz, 2H), 8.05 (d,  $J = 7.0$  Hz, 2H), 7.57 (m, 2H), 7.46 (m, 4H), 5.59 (m, 2H), 5.16 (m, 2H), 4.95 (s, 1H), 4.14 (dq,  $J = 9.9, 6.2$  Hz, 1H), 3.86 (m, 2H), 2.27 (m, 6H), 1.28 (d,  $J = 6.2$  Hz, 3H), 1.20 (d,  $J = 6.3$  Hz, 3H), 1.19 (d,  $J = 6.1$  Hz, 3H).

#### Synthesis of **7**:

Started with 1.1364 g (2.5915 mmol) alkene **4**, 2.67 mL (25.9 mmol) alcohol **2**, and 220.1 mg (0.2589 mmol) Grubbs 2<sup>nd</sup> generation ruthenium catalyst in 80 mL  $CH_2Cl_2$ . Purified to obtain 1.0211 g (79%) of a yellow oil.  $[\alpha]_D^{25} = -6.446$ ,  $c$  11.47 ( $CH_2Cl_2$ ); HRMS ( $m/z$ ):  $[M+Na]^+$  calcd. for  $C_{29}H_{36}O_7Na$  519.2353, found 519.2356;  $^1H$  NMR (400 MHz,  $CDCl_3$ ):  $\delta$  8.10 (d,  $J = 7.4$  Hz, 2H), 8.03 (d,  $J = 7.5$  Hz, 2H), 7.54 (m, 2H), 7.43 (m, 4H), 5.53 (m, 2H), 5.18 (m, 2H), 4.95 (s, 1H), 4.13 (dq,  $J = 12.1, 6.3$  Hz, 1H), 3.83 (m, 2H), 2.42 (dt,  $J = 13.0, 4.1$  Hz, 1H), 2.18 (m, 5H), 1.71 (m, 1H), 1.58 (m, 1H), 1.28 (d,  $J = 6.2$  Hz, 3H), 1.19 (d,  $J = 6.1$  Hz, 3H), 1.17 (d,  $J = 6.3$  Hz, 3H).

#### Representative procedure for hydrogenation – synthesis of **11**:

A suspension of 376.7 mg (0.7382 mmol) unsaturated alcohol **8** and 44.9 mg 10 % palladium on activated carbon in 41 mL EtOAc was vacuum purged and back filled with  $H_2$  from a balloon. The resulting suspension was allowed to stir at 23°C for 7 h. The reaction mixture was filtered through Celite<sup>®</sup> and concentrated to obtain 375.4 mg (99%) of colorless oil that required no further purification.  $[\alpha]_D^{25} = -36$ ,  $c$  0.12 ( $CH_2Cl_2$ ); HRMS ( $m/z$ ):  $[M+Na]^+$  calcd. for  $C_{30}H_{40}O_7Na$  535.2666, found 535.2654;  $^1H$  NMR (250 MHz,  $CDCl_3$ ):  $\delta$  8.11 (d,  $J = 7.7$  Hz, 2H), 8.04 (d,  $J = 7.7$  Hz, 2H), 7.59 (m, 2H), 7.47 (m, 4H), 5.18 (m, 2H), 4.95 (s, 1H), 4.12 (dq,  $J = 12.0, 6.1$  Hz, 1H), 3.83 (m, 2H), 2.42 (dt,  $J = 13.6, 4.1$  Hz, 1H), 2.19 (m, 1H), 1.46 (m, 13H), 1.28 (d,  $J = 6.2$  Hz, 3H), 1.19 (d,  $J = 6.0$  Hz, 6H);  $^{13}C$  NMR (100 MHz,  $CDCl_3$ ):  $\delta$  166.0; 165.9;

133.43; 133.39; 130.2; 130.1; 129.8; 128.6; 94.0; 72.9; 71.5; 70.9; 68.3; 67.2; 39.6; 37.3; 29.9; 29.84; 29.77; 26.0; 25.9; 23.7; 19.4; 18.1.

#### Synthesis of **9**:

Started with 168.7 mg (0.3496 mmol) unsaturated alcohol **6** and 25.8 mg 10 % palladium on activated carbon in 23 mL EtOAc. Obtained 160.1 mg (95%) of a pure colorless oil without further purification.  $[\alpha]_D^{25} = -27$ ,  $c$  0.18 (CH<sub>2</sub>Cl<sub>2</sub>); HRMS ( $m/z$ ): [M+Na]<sup>+</sup> calcd. for C<sub>28</sub>H<sub>36</sub>O<sub>7</sub>Na 507.2353, found 507.2348; <sup>1</sup>H NMR (400 MHz, CDCl<sub>3</sub>):  $\delta$  8.11 (m, 2H), 8.05 (m, 2H), 7.58 (m, 2H), 7.46 (td,  $J = 7.7, 3.5$  Hz, 4H), 5.17 (m, 2H), 4.95 (s, 1H), 4.12 (dq,  $J = 9.8, 6.2$  Hz, 1H), 3.85 (m, 2H), 2.42 (dt,  $J = 13.6, 4.0$  Hz, 1H), 2.21 (ddd,  $J = 13.9, 11.4, 3.2$  Hz, 1H), 1.50 (m, 8H), 1.28 (d,  $J = 6.2$  Hz, 3H), 1.21 (d,  $J = 6.2$  Hz, 3H); 1.19 (d,  $J = 6.2$  Hz, 3H); <sup>13</sup>C NMR (100 MHz, CDCl<sub>3</sub>):  $\delta$  166.0; 165.9; 133.5; 133.4; 130.2; 130.1; 129.8; 128.7; 94.0; 72.8; 71.5; 70.9; 68.3; 67.2; 39.5; 37.3; 29.9; 26.0 (2C); 23.8; 19.4; 18.1.

#### Synthesis of **10**:

Started with 786.6 mg (1.584 mmol) unsaturated alcohol **7** and 94.2 mg 10 % palladium on activated carbon in 88 mL EtOAc. Obtained 743.4 mg (94%) of a pure colorless oil without further purification.  $[\alpha]_D^{25} = 7.04$ ,  $c$  1.81 (CH<sub>2</sub>Cl<sub>2</sub>); HRMS ( $m/z$ ): [M+Na]<sup>+</sup> calcd. for C<sub>29</sub>H<sub>38</sub>O<sub>7</sub>Na 521.2510, found 521.2506; <sup>1</sup>H NMR (250 MHz, CDCl<sub>3</sub>)  $\delta$  8.11 (m, 2H), 8.04 (m, 2H), 7.58 (m, 2H), 7.42 (m, 4H), 5.18 (m, 2H), 4.95 (s, 1H), 4.12 (m, 1H), 3.84 (m, 2H), 2.42 (dt,  $J = 14.2, 3.9$  Hz, 1H), 2.24 (m, 1H), 1.49 (d,  $J = 46.5$  Hz, 10H), 1.28 (d,  $J = 6.3$  Hz, 3H), 1.21 (d,  $J = 2.6$  Hz, 3H), 1.18 (d,  $J = 2.5$  Hz, 3H); <sup>13</sup>C NMR (100 MHz, CDCl<sub>3</sub>):  $\delta$  166.0; 165.9; 133.41; 133.36; 130.2; 130.0; 129.8; 128.6; 94.0; 72.8; 71.4; 70.9; 68.3; 67.1; 39.5; 37.3; 29.9; 29.8; 25.9 (2C); 23.7; 19.3; 18.1.

Representative procedure for oxidation – synthesis of **12**:

To a suspension of 129.7 mg (0.6017 mmol) pyridinium chlorochromate and 111.2 mg 4Å molecular sieves in 21 mL CH<sub>2</sub>Cl<sub>2</sub> at 0°C was added 72.2 mg (0.149 mmol) saturated alcohol **9** at once. The resulting suspension was allowed to stir 0°C for 2 h. The reaction mixture was concentrated to 89.2 mg of dark red oil. Silica gel column chromatography (30.24 g silica gel, gradient run from 7.5% diethyl ether in CH<sub>2</sub>Cl<sub>2</sub> to 12% diethyl ether in CH<sub>2</sub>Cl<sub>2</sub>) afforded 71.3 mg (99%) of a colorless oil.  $[\alpha]_D^{25} = -66$ ,  $c$  0.065 (CH<sub>2</sub>Cl<sub>2</sub>); HRMS ( $m/z$ ): [M+Na]<sup>+</sup> calcd. for C<sub>28</sub>H<sub>34</sub>O<sub>7</sub>Na 505.2197, found 505.2181; <sup>1</sup>H NMR (400 MHz, CDCl<sub>3</sub>) δ 8.11 (d,  $J = 7.7$  Hz, 2H), 8.05 (d,  $J = 7.4$  Hz, 2H), 7.57 (t,  $J = 7.5$  Hz, 2H), 7.45 (m, 4H), 5.16 (m, 2H), 4.94 (s, 1H), 4.10 (dq,  $J = 12.3, 6.4$  Hz, 1H), 3.83 (m, 1H), 2.47 (t,  $J = 7.4$  Hz, 2H), 2.41 (dt,  $J = 13.7, 3.9$  Hz, 1H), 2.21 (m, 1H), 2.15 (s, 3H), 1.56 (m, 6H), 1.28 (d,  $J = 6.3$  Hz, 3H), 1.18 (d,  $J = 6.1$  Hz, 3H); <sup>13</sup>C NMR (100 MHz, CDCl<sub>3</sub>): δ 209.1; 166.0; 165.9; 133.5; 133.4; 130.2; 130.1; 129.8; 128.7; 94.0; 72.7; 71.4; 70.9; 67.2; 43.8; 37.1; 30.2; 29.9; 25.5; 24.0; 19.3; 18.1.

#### Synthesis of **13**:

Started with 605.7 mg (2.810 mmol) pyridinium chlorochromate, 328.3 mg (0.6584 mmol) saturated alcohol **10**, and 513.8 mg 4Å molecular sieves in 120 mL CH<sub>2</sub>Cl<sub>2</sub>. Purified to obtain 313.6 mg (96%) of a colorless oil.  $[\alpha]_D^{25} = 3.33$ ,  $c$  3.83 (CH<sub>2</sub>Cl<sub>2</sub>); HRMS ( $m/z$ ): [M+Na]<sup>+</sup> calcd. for C<sub>29</sub>H<sub>36</sub>O<sub>7</sub>Na 519.2353, found 519.2363; <sup>1</sup>H NMR (400 MHz, CDCl<sub>3</sub>): δ 8.11 (m, 2H), 8.05 (m, 2H), 7.58 (td,  $J = 7.3, 2.2$  Hz, 2H), 7.46 (td,  $J = 7.4, 2.9$  Hz, 4H), 5.16 (m, 2H), 4.95 (s, 1H), 4.11 (m, 1H), 3.84 (m, 1H), 2.44 (m, 3H), 2.15 (m, 4H), 1.50 (m, 8H), 1.29 (d,  $J = 6.1$  Hz, 3H), 1.19 (d,  $J = 6.1$  Hz, 3H); <sup>13</sup>C NMR (100 MHz, CDCl<sub>3</sub>): δ 209.2; 166.0; 165.9; 133.41; 133.37; 130.2; 130.0; 129.8; 128.6; 93.9; 72.7; 71.4; 70.8; 67.2; 43.9; 37.1; 30.1; 29.9; 29.4; 25.8; 23.9; 19.3; 18.1.

#### Synthesis of **14**:

Started with 123.4 mg (0.5725 mmol) pyridinium chlorochromate, 58.6 mg (0.114 mmol) saturated alcohol **11**, and 93.9 mg 4Å molecular sieves in 20 mL CH<sub>2</sub>Cl<sub>2</sub>. Purified to obtain 52.0 mg (89%) of a colorless oil.  $[\alpha]_D^{25} = 26.6$ ,  $c$  0.775 (CH<sub>2</sub>Cl<sub>2</sub>); HRMS ( $m/z$ ): [M+Na]<sup>+</sup> calcd. for C<sub>30</sub>H<sub>38</sub>O<sub>7</sub>Na 533.2510, found 533.2525; <sup>1</sup>H NMR (250 MHz, CDCl<sub>3</sub>) δ 8.12 (d,  $J = 7.0$  Hz, 2H), 8.05 (d,  $J = 7.1$  Hz, 2H), 7.57 (m, 2H), 7.46 (m, 4H), 5.17 (m, 2H), 4.95 (s, 1H), 4.12 (dq,  $J = 12.6, 6.6$  Hz, 1H), 3.84 (m, 1H), 2.43 (m, 3H), 2.14 (m, 4H), 1.54 (m, 10H), 1.29 (d,  $J = 6.2$  Hz, 3H), 1.19 (d,  $J = 6.0$  Hz, 3H); <sup>13</sup>C NMR (100 MHz, CDCl<sub>3</sub>): δ 209.0; 165.7; 165.6; 133.11; 133.07; 129.9; 129.7; 129.5; 128.3; 93.6; 72.5; 72.4; 71.1; 70.5; 66.8; 43.6; 36.9; 36.8; 29.7; 29.6; 29.3; 29.0; 25.5; 23.6; 19.2; 17.8.

Method A:

Representative procedure for methanolysis with K<sub>2</sub>CO<sub>3</sub> – synthesis of **asc-C8-OH**:

To a suspension of 10.8 mg (0.0223 mmol) saturated alcohol **9** in 1.5 mL MeOH was added 1.8 mg (0.013 mmol) K<sub>2</sub>CO<sub>3</sub> at once. The resulting solution was allowed to stir at reflux for 5 h and allowed to cool to 25°C. The reaction mixture was concentrated to 17.3 mg of colorless oil. HPLC purification afforded 2.7 mg (44%) of a colorless oil.  $[\alpha]_D^{25} = -22$ ,  $c$  0.14 (CH<sub>3</sub>OH); HRMS ( $m/z$ ): [M+Na]<sup>+</sup> calcd. for C<sub>14</sub>H<sub>28</sub>O<sub>5</sub>Na 299.1829, found 299.1838; <sup>1</sup>H NMR (400 MHz, CD<sub>3</sub>OD): δ 4.64 (s, 1H), 3.74 (m, 5H), 3.51 (ddd,  $J = 11.4, 9.3, 4.5$  Hz, 1H), 1.94 (dddd,  $J = 13.0, 4.4, 3.2, 1.0$  Hz, 1H), 1.76 (ddd,  $J = 13.1, 11.3, 3.1$  Hz, 1H), 1.44 (m, 8H), 1.21 (m, 3H), 1.14 (dd,  $J = 6.3, 1.9$  Hz, 3H), 1.12 (d,  $J = 6.0$  Hz, 3H); <sup>13</sup>C NMR (100 MHz, CDCl<sub>3</sub>): δ 96.1; 71.6; 70.0; 69.5; 68.34; 68.28; 39.5; 37.2; 35.4; 26.0; 25.9; 24.0; 19.2; 17.9.

Method B:

Representative procedure for hydrolysis with LiOH/MeOH - synthesis of **asc-C10-OH**:

To a suspension of 141.3 mg (0.2756 mmol) saturated alcohol **11** in 20 mL MeOH was added 20 mL sat. 1M LiOH at once. The resulting solution was allowed to stir at 23°C for 24 h.

10 mL 20% *i*PrOH in CH<sub>2</sub>Cl<sub>2</sub> was added to the reaction mixture, and the layers were separated. The aqueous layer was extracted with an additional 5x 10 mL 20% *i*PrOH in CH<sub>2</sub>Cl<sub>2</sub>. Solid NaCl was then added until saturation was obtained, and the aqueous layer was further extracted with 3 x 10 mL 20% *i*PrOH in CH<sub>2</sub>Cl<sub>2</sub>. The combined organic layers were dried over Na<sub>2</sub>SO<sub>4</sub> and filtered. Evaporation of solvent afforded 117.2 mg of an oil. Silica gel column chromatography (46.72 g silica gel, gradient run from 5% *i*PrOH in CH<sub>2</sub>Cl<sub>2</sub> to 20% *i*PrOH in CH<sub>2</sub>Cl<sub>2</sub>) afforded 78.9 mg (94%) of a colorless oil.  $[\alpha]_D^{25} = -35.3$ ,  $c$  1.43 (CH<sub>3</sub>OH); HRMS ( $m/z$ ): [M+Na]<sup>+</sup> calcd. for C<sub>16</sub>H<sub>32</sub>O<sub>5</sub>Na 327.2142, found 327.2133; <sup>1</sup>H NMR (400 MHz, CD<sub>3</sub>OD):  $\delta$  4.64 (s, 1H), 3.69 (m, 4H), 3.52 (ddd,  $J = 11.3, 9.3, 4.6$  Hz, 1H), 1.95 (dt,  $J = 13.1, 3.8$  Hz, 1H), 1.76 (m, 1H), 1.44 (m, 12H), 1.21 (d,  $J = 6.2$  Hz, 3H), 1.13 (dd,  $J = 9.9, 6.1$  Hz, 6H); <sup>13</sup>C NMR (100 MHz, CD<sub>3</sub>OD):  $\delta$  97.7; 72.6; 71.3; 70.1; 68.7; 68.4; 40.3; 38.5; 36.1; 30.9; 30.8; 27.0; 26.9; 23.6; 19.5; 18.2.

#### Synthesis of **asc-C9-OH**:

Started with 344.5 mg (0.6909 mmol) alcohol **10** and 49.0 mL sat. 1 M LiOH in 49.0 mL MeOH. Purified to obtain 178.5 mg (89%) of a colorless oil.  $[\alpha]_D^{25} = -49.1$ ,  $c$  2.53 (CH<sub>3</sub>OH); HRMS ( $m/z$ ): [M+Na]<sup>+</sup> calcd. for C<sub>15</sub>H<sub>30</sub>O<sub>5</sub>Na 313.1985, found 313.1979; <sup>1</sup>H NMR (400 MHz, CD<sub>3</sub>OD):  $\delta$  4.63 (s, 1H), 3.69 (m, 4H), 3.51 (ddd,  $J = 11.4, 9.4, 4.6$  Hz, 1H), 1.94 (dt,  $J = 13.1, 3.9$  Hz, 1H), 1.76 (ddd,  $J = 13.2, 11.3, 3.0$  Hz, 1H), 1.42 (m, 10H), 1.21 (d,  $J = 6.1$  Hz, 3H), 1.12 (dd,  $J = 10.3, 6.1$  Hz, 6H); <sup>13</sup>C NMR (100 MHz, CD<sub>3</sub>OD):  $\delta$  97.7; 72.7; 71.3; 70.1; 68.7; 68.5; 40.3; 38.5; 36.1; 30.9; 27.03; 27.0; 23.6; 19.5; 18.3.

#### Synthesis of **asc-C8-MK**:

Started with 49.7 mg (0.103 mmol) ketone **12** and 7.1 mL sat. 1 M LiOH in 7.1 mL MeOH. Purified to obtain 21.7 mg (77%) of a colorless oil.  $[\alpha]_D^{25} = -71.0$ ,  $c$  1.15 (CH<sub>3</sub>OH); HRMS ( $m/z$ ): [M+Na]<sup>+</sup> calcd. for C<sub>14</sub>H<sub>26</sub>O<sub>5</sub>Na 297.1672, found 297.1670; <sup>1</sup>H NMR (400 MHz,



CD<sub>3</sub>OD):  $\delta$  4.67 (s, 1H), 3.67 (m, 4H), 2.53 (t,  $J = 7.3$  Hz, 2H), 2.16 (s, 3H), 1.98 (dddd,  $J = 13.0, 4.4, 3.2, 1.1$  Hz, 1H), 1.79 (ddd,  $J = 13.0, 11.2, 3.1$  Hz, 1H), 1.53 (m, 6H), 1.24 (d,  $J = 6.1$  Hz, 3H), 1.15 (d,  $J = 6.0$  Hz, 3H); <sup>13</sup>C NMR (100 MHz, CDCl<sub>3</sub>):  $\delta$  209.8; 96.0; 71.1; 70.0; 69.4; 68.2; 43.8; 37.1; 35.4; 30.2; 25.4; 23.9; 19.1; 17.9.

#### Synthesis of **asc-C9-MK**:

Started with 234.1 mg (0.4714 mmol) ketone **13** and 33.3 mL sat. 1 M LiOH in 33.3 mL MeOH. Purified to obtain 103.4 mg (76%) of a colorless oil.  $[\alpha]_D^{25} = -40.0$ ,  $c$  3.11 (CH<sub>3</sub>OH); HRMS ( $m/z$ ):  $[M+Na]^+$  calcd. for C<sub>15</sub>H<sub>28</sub>O<sub>5</sub>Na 311.1829, found 311.1830; <sup>1</sup>H NMR (250 MHz, CD<sub>3</sub>OD):  $\delta$  4.63 (s, 1H), 3.62 (m, 4H), 2.48 (t,  $J = 7.3$  Hz, 2H), 2.12 (s, 3H), 1.94 (dddd,  $J = 13.1, 4.4, 3.3, 1.0$  Hz, 1H), 1.75 (ddd,  $J = 12.9, 11.1, 3.0$  Hz, 1H), 1.44 (m, 8H), 1.20 (d,  $J = 6.0$  Hz, 3H), 1.11 (d,  $J = 6.1$  Hz, 3H); <sup>13</sup>C NMR (100 MHz, CD<sub>3</sub>OD):  $\delta$  212.1; 97.5; 72.4; 71.2; 69.9; 68.3; 44.3; 38.2; 36.0; 30.2; 29.8; 26.7; 24.8; 19.3; 18.1.

#### Synthesis of **asc-C10-MK**:

Started with 36.9 mg (0.0723 mmol) ketone **14** and 5.3 mL sat. 1 M LiOH in 5.3 mL MeOH. Purified to obtain 18.3 mg (84%) of a colorless oil.  $[\alpha]_D^{25} = -42$ ,  $c$  0.28 (CH<sub>3</sub>OH); HRMS ( $m/z$ ):  $[M+Na]^+$  calcd. for C<sub>16</sub>H<sub>30</sub>O<sub>5</sub>Na 325.1985, found 325.1987; <sup>1</sup>H NMR (250 MHz, CD<sub>3</sub>OD):  $\delta$  4.63 (s, 1H), 3.62 (m, 4H), 2.47 (t,  $J = 7.3$  Hz, 2H), 2.12 (s, 3H), 1.94 (dt,  $J = 13.1, 4.0$  Hz, 1H), 1.75 (ddd,  $J = 13.0, 10.8, 2.9$  Hz, 1H), 1.46 (m, 10H), 1.20 (d,  $J = 6.0$  Hz, 3H), 1.11 (d,  $J = 6.1$  Hz, 3H); <sup>13</sup>C NMR (100 MHz, CD<sub>3</sub>OD):  $\delta$  212.2; 97.6; 72.5; 71.2; 70.0; 68.3; 44.3; 38.3; 36.0; 30.5; 30.2; 29.8; 26.7; 24.9; 19.3; 18.1.

## 1.5 References

1. Brenner, S., Nature's Gift to Science (Nobel lecture). *ChemBiochem* **2003**, *4* (8), 683-7.

2. Wood, W. B., Introduction to *C. elegans* Biology. In *The Nematode Caenorhabditis elegans*, Cold Springs Harbor Laboratory Press: Cold Springs Harbor, NY, 1988; pp 1-16.
3. Altun, Z. F., Introduction to *C. elegans* Anatomy. In *Wormatlas*, 2005.
4. Cheung, B. H.; Cohen, M.; Rogers, C.; Albayram, O.; de Bono, M., Experience-Dependent Modulation of *C. elegans* Behavior by Ambient Oxygen. *Curr. Biol.* **2005**, *15* (10), 905-17.
5. Hulme, S. E.; Whitesides, G. M., Chemistry and the Worm: *Caenorhabditis elegans* as a Platform for Integrating Chemical and Biological Research. *Angew. Chem. Int. Ed.* **2011**, *50* (21), 4774-807.
6. Barriere, A.; Felix, M. A., High Local Genetic Diversity and Low Outcrossing Rate in *Caenorhabditis elegans* Natural Populations. *Curr. Biol.* **2005**, *15* (13), 1176-84.
7. Murakami, S., *Caenorhabditis elegans* As a Model System to Study Aging of Learning and Memory. *Mol. Neurobiol.* **2007**, *35* (1), 85-94.
8. Kaletta, T.; Hengartner, M. O., Finding Function in Novel Targets: *C. elegans* as a Model Organism. *Nat. Rev. Drug Discov.* **2006**, *5* (5), 387-98.
9. Hu, P. J., Dauer. In *WormBook : the Online Review of C. elegans Biology*, 2007; pp 1-19.
10. Cassada, R. C. R., R. L., The Dauerlarva, a Post-Embryonic Developmental Variant of the Nematode *Caenorhabditis elegans*. *Dev. Biol.* **1975**, *46* (2), 326-342.
11. (a) Vowels, J. J. T., J. H., Genetic Analysis of Chemosensory Control of Dauer Formation in *Caenorhabditis elegans*. *Genetics* **1992**, *130*, 105-123; (b) Thomas, J. H. B., D. A.; Vowels, J. J., Evidence for Parallel Processing of Sensory Information Controlling Dauer Formation in *Caenorhabditis elegans*. *Genetics* **1993**, *134*, 1105-1117; (c) Riddle, D. L.; Swanson, M. M.; Albert, P. S., Interacting Genes in Nematode Dauer Larva Formation. *Nature* **1981**, *290*, 668-671; (d) Jia, K.; Albert, P.; Riddle, D., DAF-9, a Cytochrome P450 Regulating *C. elegans* Larval Development and Adult Longevity. *Dev. Biol.* **2002**, *129*, 221-231; (e) Gottlieb, S.; Ruvkun, G., Daf-2, daf-16 and daf-23: Genetically Interacting Genes Controlling Dauer Formation in *Caenorhabditis elegans*. *Genetics* **1994**, *137*, 107-120.
12. Butcher, R. A.; Fujita, M.; Schroeder, F. C.; Clardy, J., Small-Molecule Pheromones that Control Dauer Development in *Caenorhabditis elegans*. *Nat. Chem. Biol.* **2007**, *3* (7), 420-2.
13. Golden, J.; Riddle, D., A Pheromone Influences Larval Development in the Nematode *Caenorhabditis elegans*. *Science* **1982**, *218*, 578-580.

14. Butcher, R.; Ragains, J.; Kim, E.; Clardy, J., A Potent Dauer Pheromone Component in *Caenorhabditis elegans* that Acts synergistically with Other Components. *Proc. Natl. Acad. Sci. U.S.A.* **2008**, *105*, 14288-14292.
15. Butcher, R.; Ragains, J.; Clardy, J., An Indole-Containing Dauer Pheromone Component with Unusual Dauer Inhibitory Activity at Higher Concentrations. *Org. Lett.* **2009**, *11*, 3100-3103.
16. Pungaliya, C.; Srinivasan, J.; Fox, B.; Malik, R.; Ludewig, A.; Sternberg, P.; Schroeder, F., A Shortcut to Identifying Small Molecule Signals that Regulate Behavior and Development in *Caenorhabditis elegans*. *Proc. Natl. Acad. Sci. U.S.A.* **2009**, *106*, 7708-7713.
17. Golden, J.; Riddle, D., *Caenorhabditis elegans* Dauer Larva: Developmental Effects of Pheromone, Food and Temperature. *Dev. Biol.* **1984**, *102*, 368-378.
18. Ward, S.; Thomson, N.; White, J.; Brenner, S., Electron Microscopical Reconstruction of the Anterior Sensory Anatomy of the Nematode *Caenorhabditis elegans*. *J. Comp. Neurol.* **1975**, *160*, 313-337.
19. Zwaal, R.; Mendel, J.; Sternberg, P.; Plasterk, R., Two Neuronal G Proteins are Involved in Chemosensation of the *Caenorhabditis elegans* Dauer-Inducing Pheromone. *Genetics* **1997**, *145*, 715-727.
20. (a) Ren, P.; Lim, c.; Johnsen, R.; Albert, P.; Pilgrim, D.; Riddle, D., Control of *C. elegans* Larval Development by Neuronal Expression of a TGF-Beta Homolog. *Science* **1996**, *274*, 1389-1391; (b) Larsen, P.; Albert, P.; Riddle, D., Genes that Regulate Both Development and Longevity in *Caenorhabditis elegans*. *Genetics* **1995**, *139*, 1567-1583.
21. Dorman, J.; Albinder, B.; Shroyer, T.; Kenyon, C., The Age-1 and Daf-2 Genes Function in a Common Pathway to Control the Lifespan of *Caenorhabditis elegans*. *Genetics* **1995**, *141*, 1399-1406.
22. Bartke, A., Single-Gene Mutations and Healthy Ageing in Mammals. *Philos. Trans. R. Soc. B.* **2011**, *366*, 28-34.
23. Arnaldez, F.; Helman, L., Targeting the Insulin Growth Factor Receptor 1. *Hematol. Oncol. Clin. North Am.* **2012**, *26*, 527-542.
24. McCarty, M., Vegan Proteins May Reduce Risk of Cancer, Obesity, and Cardiovascular Disease by Promoting Increased Glucagon Activity. *Med. Hypotheses* **1999**, *53*, 459-485.
25. Padua, D.; Massague, J., Roles of TGF-Beta in Metastasis. *Cell Res.* **2009**, *19*, 89-102.
26. Swardfager, W.; Lanctot, K.; Rothenburg, L.; Wong, A.; Cappell, J.; Herrmann, N., A Meta-Analysis of Cytokines in Alzheimer's Disease. *Biol. Psychiatry* **2010**, *68*, 930-941.

27. von Reuss, S. H.; Bose, N.; Srinivasan, J.; Yim, J. J.; Judkins, J. C.; Sternberg, P. W.; Schroeder, F. C., Comparative Metabolomics Reveals Biogenesis of Ascarosides, a Modular Library of Small-Molecule Signals in *C. elegans*. *J. Am. Chem. Soc.* **2012**, *134* (3), 1817-24.
28. Agbaga, M.; Brush, R.; Mandal, N.; Henry, K.; Elliott, M.; Anderson, R., Role of Stargardt-3 Macular Dystrophy Protein (ELOVL4) in the Biosynthesis of Very Long Chain Fatty Acids. *Proc. Natl. Acad. Sci. U.S.A.* **2008**, *105*, 12843-12848.
29. Reddy, J.; Hashimoto, T., Peroxisomal  $\beta$ -Oxidation and Peroxisome Proliferator-Activated Receptor  $\alpha$ : An Adaptive Metabolic System. *Annu. Rev. Nutr.* **2001**, *21*, 193-230.
30. Srinivasan, J.; von Reuss, S.; Bose, N.; Zaslaver, A.; Mahanti, P.; Ho, M.; O'Doherty, O.; Edison, S.; Sternberg, P.; Schroeder, F., A Modular Library of Small Molecule Signals Regulates Social Behaviors in *Caenorhabditis elegans*. *PLoS Biol.* **2012**, *10*, e1001237.
31. Hollister, K. A.; Conner, E. S.; Zhang, X.; Spell, M.; Bernard, G. M.; Patel, P.; de Carvalho, A. C.; Butcher, R. A.; Ragains, J. R., Ascaroside Activity in *Caenorhabditis elegans* is Highly Dependent on Chemical Structure. *Bioorg. Med. Chem.* **2013**, *21* (18), 5754-69.
32. Jeong, P.; Jung, M.; Yim, Y.; Kim, H.; Park, M.; Hong, E.; Lee, W.; Kim, Y.; Kim, K.; Paik, Y., Chemical Structure and Biological Activity of the *Caenorhabditis elegans* Dauer-Inducing Pheromone. *Nature* **2005**, *433*, 541.
33. Butcher, R.; Ragains, J.; Li, W.; Ruvkun, G.; Clardy, J.; Mak, H., Biosynthesis of the *Caenorhabditis elegans* Dauer Pheromone. *Proc. Natl. Acad. Sci. U.S.A.* **2009**, *106*, 1875-1879.
34. Louie, J.; Bielawski, C.; Grubbs, R., Tandem Catalysis: The Sequential Mediation of Olefin Metathesis, Hydrogenation, and Hydrogen Transfer with Single-Component Ru Complexes. *J. Am. Chem. Soc.* **2001**, *123*, 11312-11313.
35. Felix, M.; Duveau, F., Population Dynamics and Habitat Sharing of Natural Populations of *Caenorhabditis elegans* and *C. briggsae*. *BMC Biol.* **2012**, *10*, 59.
36. Pangborn, A.; Giardello, M.; Grubbs, R.; Rosen, R.; Timmers, F., Safe and Convenient Procedure for Solvent Purification. *Organometallics* **1996**, *15*, 1518-1520.

## CHAPTER 2: SYNTHESIS AND BIOLOGICAL EVALUATION OF THE INFECTIVE JUVENILE HORMONE OF *HETERORHABDITIS BACTERIOPHORA*

### 2.1 Introduction

#### 2.1.1 Life Cycle

*Heterorhabditis bacteriophora*, an entomopathogenic nematode (roundworm insect parasitoid), has a life cycle homologous to that of *C. elegans* (Figure 2.1).<sup>1</sup> The parasite exists in the soil as an infective juvenile (IJ), a dauer-like, nonfeeding and developmentally arrested stage of the nematode. This infective juvenile seeks out an appropriate insect host and eventually causes its death using its symbiotic relationship with *Photorhabdus luminescens*. This symbiotic

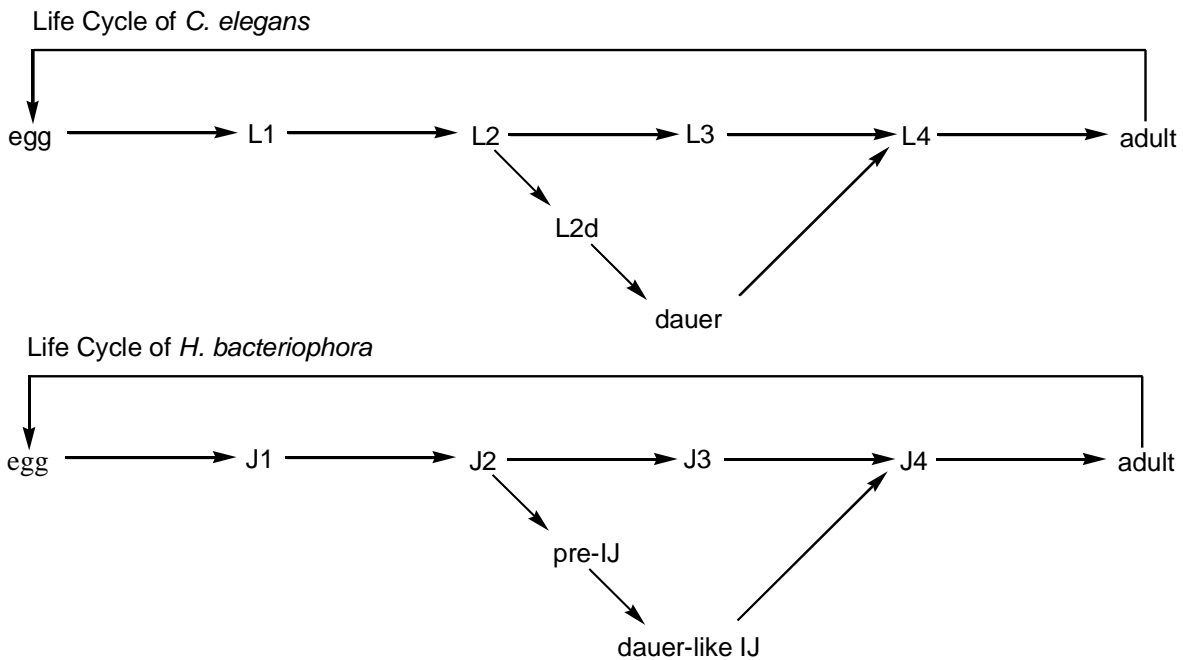


Figure 2.1 Comparison of life cycles of *C. elegans* and *H. bacteriophora*

partner is a bacteria that resides in the gut of *H. bacteriophora*, and it allows the nematode to develop, proliferate and kill its insect host, which acts as an essential source for nutrients.<sup>2</sup> After finding an insect host to inhabit, the IJ uses a relatively large buccal tooth to cut into the insect cuticle and facilitate entry into the host's gut.<sup>3</sup> Approximately 30 minutes after the IJ selects and

inhabits an insect hemocoel, the primary body cavity containing the circulatory fluid, it regurgitates the symbiotic bacteria, which multiply and grow inside the gut of the insect, killing it within 24 hours.<sup>4</sup> In a study where *P. luminescens* bacteria were injected straight into the insect's hemocoel, they exhibited a LC<sub>50</sub> value of <10 cells.<sup>5</sup>

*H. bacteriophora*, after it regurgitates the *P. luminescens* bacteria, then recovers from the IJ stage and enters the J4 stage, progressing towards adulthood.<sup>6</sup> These adults then continue through 1-2 generation cycles in the insect carcass, laying eggs that develop through J1-J4, bypassing IJ formation. After these few cycles, when food availability from nutrients in the insect host becomes low<sup>7</sup> and population density is high, eggs begin to accumulate within the nematode.<sup>8</sup> The eggs then hatch while still inside the body cavity of *H. bacteriophora*, producing pre-IJ's which feed off of the tissues of its host mother, resulting in maternal death and IJ production and release. This process is called *endotokia matricida*.

The study of the biological processes of *H. bacteriophora* is an important step in biological pesticide research. *H. bacteriophora* or chemicals associated with its propagation and parasitic properties could be used as a natural insecticide effective at eradicating a wide range of insects without introducing other synthetic agents which could be harmful to the environment. ARBICO Organics, a company focused on providing organic options for lawn and garden care, is marketing the product NemaSeek™. This product is simply *H. bacteriophora* nematodes dispersed in a solution which is advertised as a pesticide for common garden pests that won't affect other animals. NemaSeek™ is mixed with water and sprayed over any infected area for the control of unwanted insects.

### 2.1.2 Symbiosis and *Photorhabdus luminescens*

*H. bacteriophora* has become of interest, in part, because of its interesting symbiotic relationship with *P. luminescens*, a gram negative bacteria belonging to the family Enterobacteriaceae.<sup>9</sup> The bacterium is dependent upon the nematode for dispersal and food supply (from the host insect). Naturally-occurring, free-living *P. luminescens* have not been found in either water or soil samples, suggesting its dependence on a host.<sup>9</sup> The nematode, in turn, relies on *P. luminescens* for potential nutrients,<sup>9</sup> protection from the insect host's immune system<sup>10</sup> and deterrence of other microorganisms. *H. bacteriophora* reproduces more readily when *P. luminescens* is prevalent, demonstrating that the bacterium may act as a source of nutrients or partial food supply for the nematode.<sup>9</sup> Once *P. luminescens* is regurgitated from *H. bacteriophora*, it enters the stationary phase, secreting various lipases, phospholipases, proteases and antibiotics into the insect host's hemocoel. The antibiotics serve a two-part function: protecting the developing nematode from the insect's defense mechanisms and keeping the insect cadaver from contamination by competing microorganisms.<sup>10</sup>

### 2.1.3 Regulation of Processes in *H. bacteriophora* Using Chemical Cues

As previously discussed, an array of small molecule chemical cues regulates various processes in *C. elegans* such as dauer formation and recovery. Like *C. elegans*, *H. bacteriophora* use chemosensation to navigate the world around them. Several processes in the nematode are regulated by small molecules. For example, *H. bacteriophora* find potential prey through chemosensation of carbon dioxide, long-chain alcohols produced by insects<sup>11</sup> and (*E*)-beta-caryophyllene, a molecule secreted by plant roots after herbivore damage.<sup>12</sup> This chemosensation allows *H. bacteriophora* to locate areas with high herbivore (potentially insect) activity. Once *H. bacteriophora* has entered the insect host, regurgitation of the symbiont

bacteria is induced by chemical cues in the insect's hemolymph,<sup>4</sup> and IJ recovery to L4 is regulated by small molecules produced by the bacteria.<sup>13</sup>

The importance of chemosensation in regulating various aspects of *H. bacteriophora*'s existence, as well as the similarity between the IJ stage of this nematode and the dauer phase of *C. elegans*, has led Butcher and workers on a search for an IJ hormone, a small molecule that would inhibit IJ recovery after *endotokia matricida*.<sup>1</sup> Using bioassay-guided fractionation with an IJ recovery assay, the IJ hormone was isolated (Figure 2.2). First, the infective juveniles were cultivated in high densities by growing adults on a split Petri lipid-agar/saline plate. After *endotokia matricida*, the infective juveniles would migrate from the lipid-agar side to the saline section of the plate, where they were collected. The lipid-agar side of the plate was then extracted with methanol.

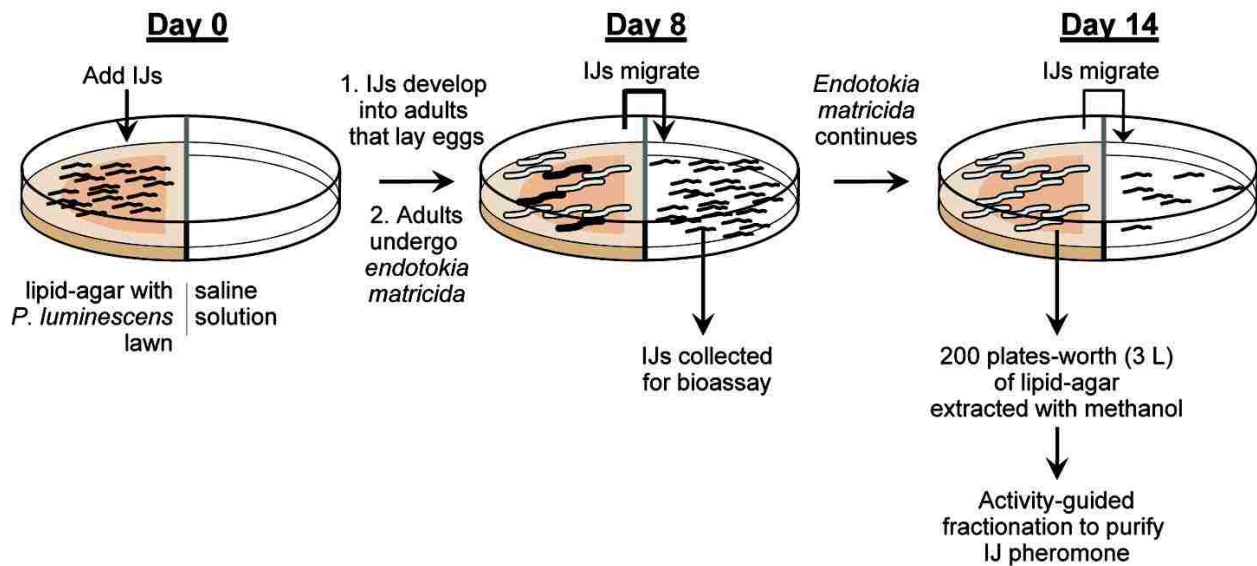


Figure 2.2 Isolation of crude IJ hormones

This crude pheromone was then purified using  $C_{18}$  chromatography, and the fractions were collected and analyzed for any biological activity. Fractions exhibiting activity towards inhibiting IJ recovery to adulthood were further purified using reverse-phase HPLC. The active



fractions from this round of purification contained a single compound, which was characterized by NMR ( $^1\text{H}$ ,  $^{13}\text{C}$ , dfq-COSY, HSQC, HMBC, and ROESY) and mass spectrometry. The structure of ascaroside C11 ethanolamide (**asc-C11EA 25**) was then tentatively assigned (Figure 2.3).

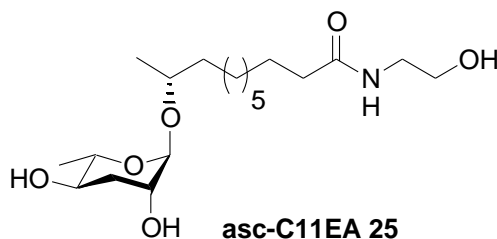
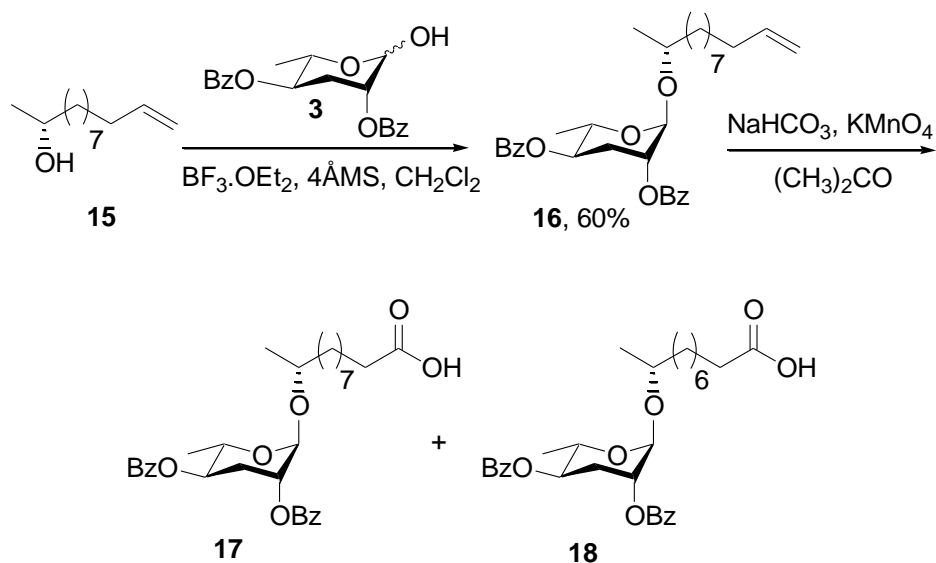


Figure 2.3 Structure of **asc-C11EA 25**

## 2.2 Results and Discussion

### 2.2.1 Synthesis of Infective Juvenile Hormone

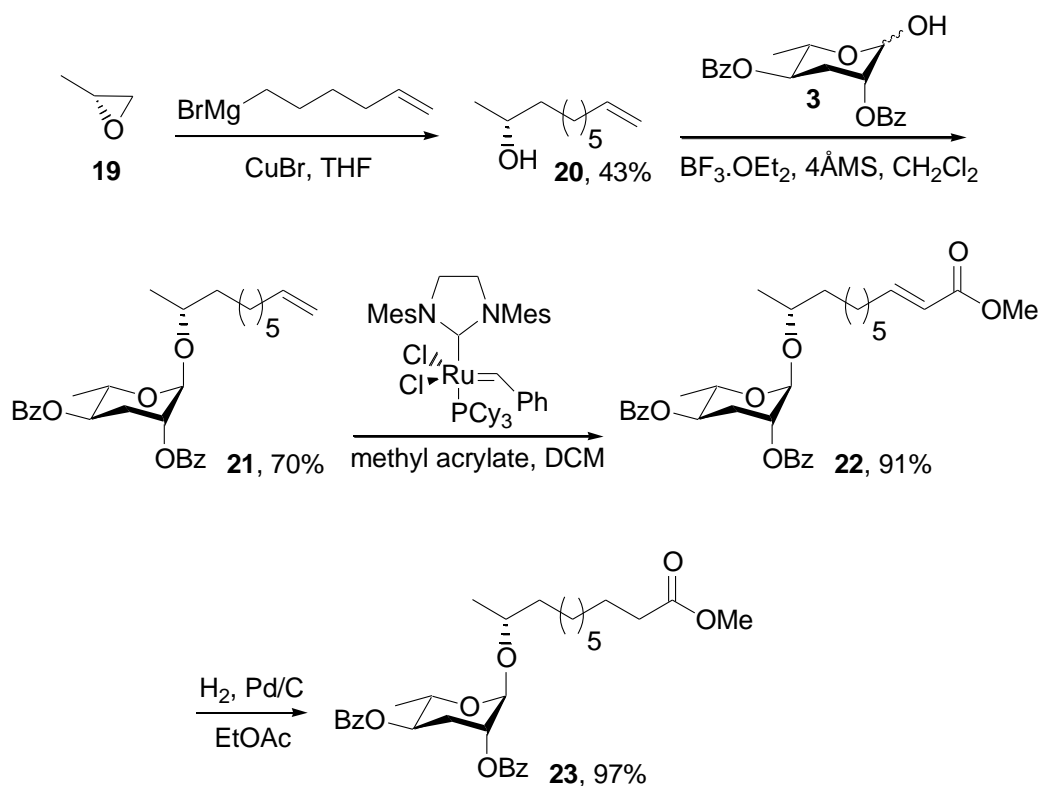
In order to verify the structure of the suggested hormone and to determine its exact stereochemistry, the putative hormone **25** was to be synthesized first. After the compound was created, its NMR spectra were then to be compared with the isolated hormone to confirm structure and stereochemistry. Initially, a synthetic scheme was envisioned where the intermediate sugar **22**, with a side chain containing 12 carbons and a terminal carboxylic acid, would be functionalized with ethanolamine to give the desired amide **25**. To accomplish this synthesis, glycosylation of the previously synthesized (*R*)-(+)-11-dodecen-2-ol (**15**) with dibenzoyl ascarlyose **3** provided sugar **16** in 60% yield (Scheme 2.1). As with the glycosylations accomplished in Chapter 1, only oxygenation at the  $\alpha$ -position was observed due to neighboring group participation from the benzoate protecting group. These protecting groups block the bottom face of the intermediate from attack by the alkenol **15**. Oxidation of the terminal alkene in compound **16** to the corresponding carboxylic acid was then attempted using  $\text{KMnO}_4$  oxidation.



Scheme 2.1 Attempt at the synthesis of oxidized product **17**

However, this method was unsuccessful. After oxidation, compound characterization ( $^1\text{H}$  NMR and  $^{13}\text{C}$  NMR) indicated conversion to a carboxylic acid. But a closer look at the mass spectrometry data illustrated that extensive loss of a side chain methylene group led to an inseparable contaminant, illustrated by sugars **17** and **18** in Scheme 2.1. Another route towards the synthesis of **asc-C11EA 25** was then necessary (Scheme 2.2). In this synthetic outline, the intermediate 12 carbon chain ester **22** would be made via cross metathesis of alkene **21** and methyl acrylate.

The resulting ester, after hydrogenation of the alkene, could then undergo aminolysis to give the desired putative IJ hormone, **asc-C11EA 25**. The first step in this new process was the synthesis of starting alcohol **20** via an organocuprate addition to the less sterically hindered carbon of (*R*)-(+)-propylene (Scheme 2.2). This was accomplished with the modest yield of 43%. Glycosylation of alcohol **20** with dibenzoyl ascarylose **3** gave the major  $\beta$  anomer **21** in 70% yield.

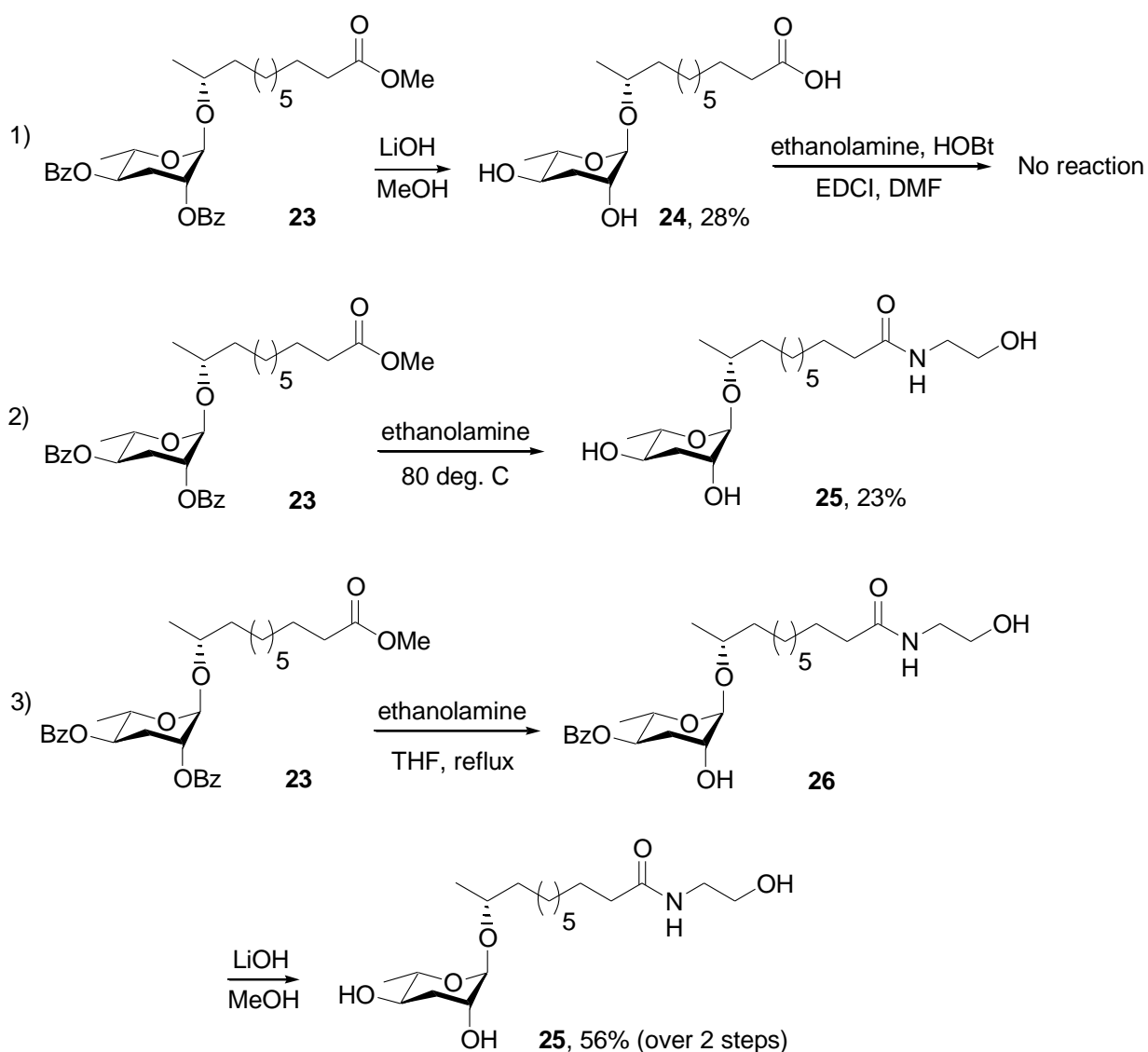


Scheme 2.2 Synthesis of the saturated methyl ester **23**

Alkene **21** underwent olefin cross metathesis with methyl acrylate, using Grubbs 2<sup>nd</sup> generation ruthenium catalyst, to produce ascaroside **22** in an excellent yield of 91%. Unlike the products of cross metathesis in Chapter 1 where a mixture of stereoisomers were produced, the  $\alpha,\beta$ -unsaturated methyl ester **22** was synthesized solely in the *E* configuration. This selectivity is a result of the difference in stability between the *cis* and *trans* conformers. The *cis* isomer is considerably less stable due to the strain between the carbonyl on the ester and the side chain attached to the alkene. After purification of the  $\alpha, \beta$ -unsaturated methyl ester, the double bond was then hydrogenated using H<sub>2</sub> and Pd/C at atmospheric pressure to afford the saturated ester **23** in 97% yield.

The last step in the synthesis of **asc-C11EA 25** was the transformation of the terminal ester to the ethanolamide moiety. In the first attempt, hydrolysis of the benzoate groups to give

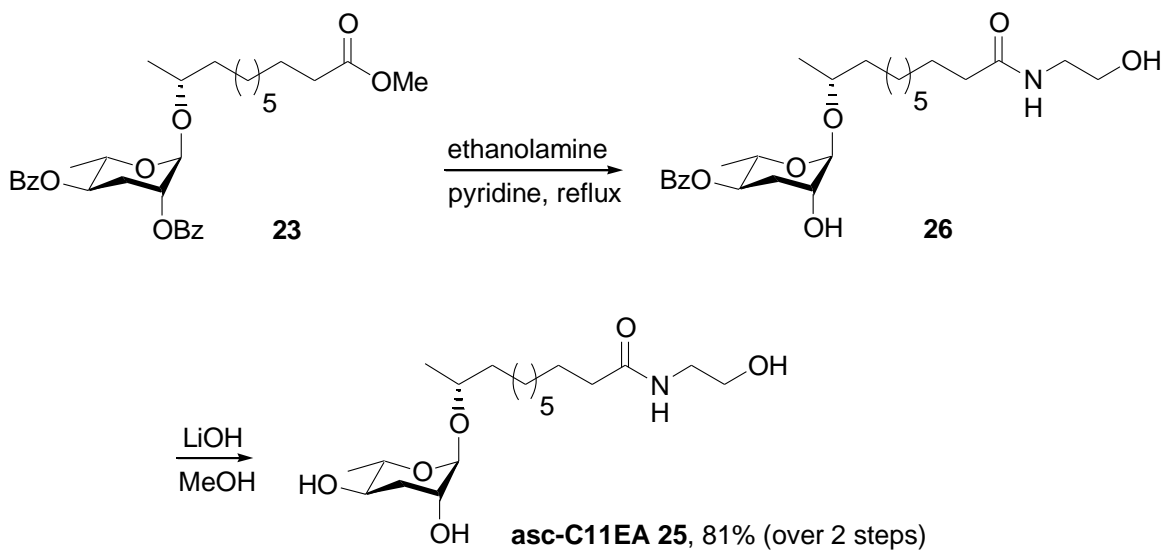
alcohols and the terminal methyl ester to the carboxylic acid was accomplished in 28% using LiOH in MeOH (Scheme 2.3, Entry 1). Coupling of the carboxylic acid with ethanolamine using HOBt and EDCI led to no desired product. No conversion of starting material was observed. Several attempts at aminolysis of the ester **23** were then performed. Stirring of ester **23** in ethanolamine at 80° C gave the desired product, **asc-C11EA 25**, in low yield (23%) (Scheme 2.3, Entry 2). Next, refluxing ethanolamine and the ester **23** in THF for two weeks only gave the monodebenzoylated ethanolamide **26**.



Scheme 2.3 Attempts at aminolysis

Hydrolysis with LiOH in MeOH was used to give the final product in 56% yield over 2 steps. Monodebenzoylation only occurred in the axial position possibly due to the gauche interaction between the equatorial benzoate group and the methyl group on the ring, which rendered it inaccessible to attack by ethanolamine.

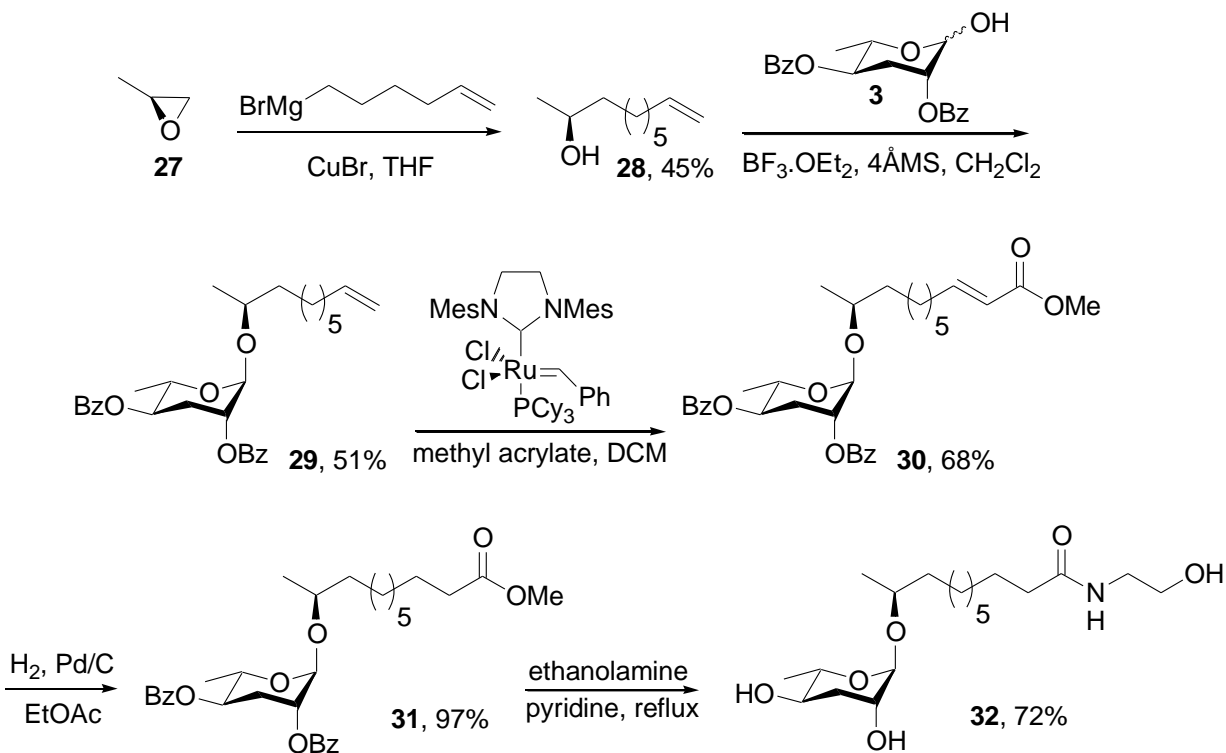
Although 56% was a decent yield, the reaction was further optimized with the intention of increasing reaction efficiency. Therefore, the solvent was changed from THF in favor of pyridine (Scheme 2.4). Pyridine was seen as a more suitable solvent, because it would create a polar environment and reflux at a higher temperature than THF, which would increase the overall reactivity. Aminolysis of **23** using ethanolamine in refluxing pyridine gave the monodebenzoylated ethanolamide **26**. This intermediate was then carried directly to the next step. Hydrolysis of the remaining protecting benzoyl group gave desired product **asc-C11EA 25** in 81% yield over 2 steps.



Scheme 2.4 Successful synthesis of amide **asc-C11EA 25**

Although NMR spectra of both the isolated IJ hormone and **asc-C11EA 25** were a match, when the optical rotation of **asc-C11EA 25** was compared to that of the naturally occurring isolated IJ hormone, it was found that the two were not even close to one another. Therefore, the

epimer **32** at the  $\omega$ -1 center was synthesized via the same route as that of the synthesis of **asc-C11EA 25** (Scheme 2.5). The first step was the synthesis of (*S*)-(-)-11-dodecen-2-ol **28** from (*S*)-(-)-propylene oxide **27**. Once again, this synthesis was accomplished via an organocuprate ring opening of the epoxide, providing compound **28** in 45% yield. Next in the synthesis was the glycosylation of the alkenol **28** with dibenzoyl ascrylose **3** to give the sugar **29** in 51% yield. This sugar then underwent cross metathesis with methyl acrylate, producing the  $\alpha,\beta$ -unsaturated methyl ester **30** in the *E* configuration in 68%. Hydrogenation of the alkene was then successfully performed in an excellent yield of 97%. Aminolysis of **31** to form the epimer **32** at the  $\omega$ -1 center was straightforward in comparison to the synthesis of **asc-C11EA 25**. Reflux of **31** and ethanolamine in pyridine was sufficient in removing both benzoate groups and producing epimer **32** in 72% yield. No hydrolysis was needed.



Scheme 2.5 Synthesis of amide **32**

In comparison of the NMRs of the two synthesized epimers and that of the isolated ascaroside hormone, it was clear that the ascaroside containing the *R* stereocenter (**asc-C11EA**) was the correct structure for the naturally occurring IJ hormone of *H. bacteriophora*. It is likely that the optical rotations of the synthetic **asc-C11EA 25** and isolated hormones initially did not match because of impurities present in the isolated hormone.

### 2.2.2 Biological Evaluation of IJ hormone and asc-C11

After synthesis of IJ hormone, biological evaluation was performed by the Butcher lab at the University of Florida. This compound was submitted to an IJ recovery assay (Figure 2.4). In this assay, the hormone was mixed with an agar medium containing a *P. luminescens* culture. After incubation for 24 hours at 28°C, eighty 7 or 8 day old infective juveniles were added to the sample. This mixture was then allowed to incubate for an additional 18 hours at 28°C, and all resulting infective juveniles and recovered adult worms were counted.

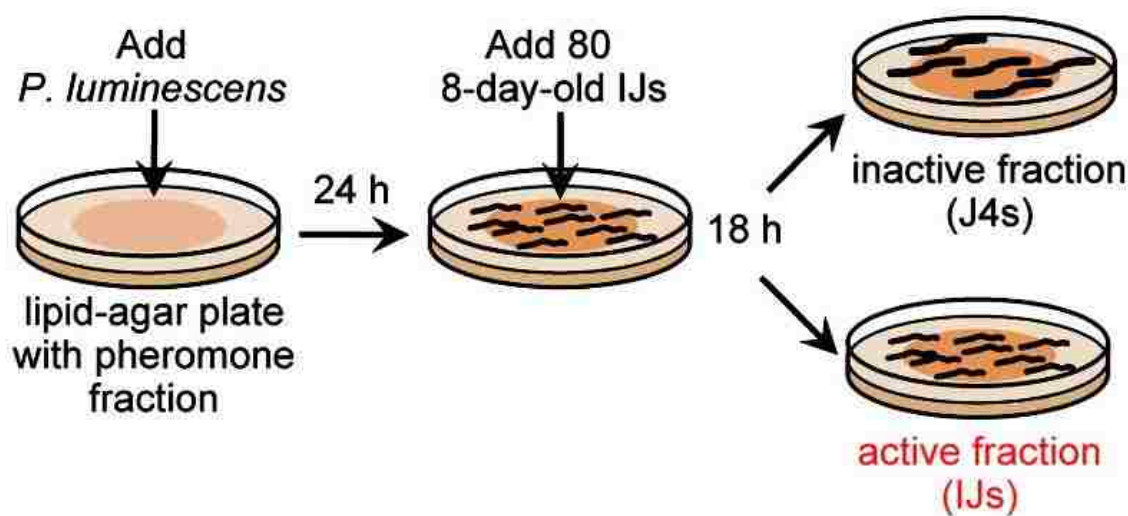
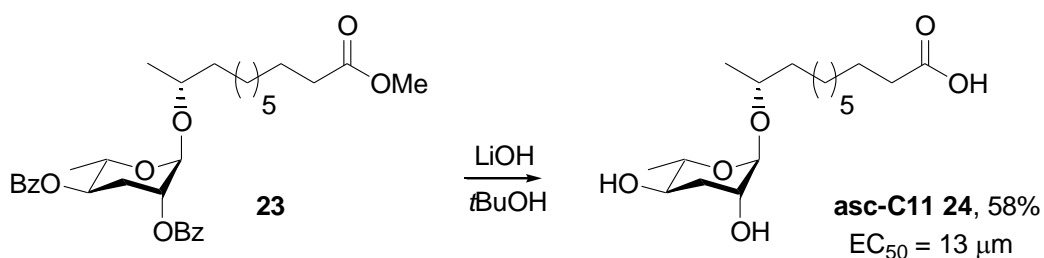


Figure 2.4 IJ recovery assay

This compound exhibited an  $EC_{50}$  value of 25 nM in an IJ recovery assay, where an  $EC_{50}$  value is defined as the concentration at which the sample reached half of its maximal activity for

inhibiting IJ recovery to adulthood. In order to confirm that this activity was mostly due to the hormone and not to other molecules present in the crude pheromone, the IJ recovery activities of both the hormone and the crude pheromone were compared. In an IJ recovery assay at a concentration of 1  $\mu\text{M}$ , the synthetic hormone **asc-C11 EA** and the crude pheromone exhibited the comparable percent IJ formations of ~30% and ~40%. This indicates that the synthesized **asc-C11 EA** is the active species of the crude pheromone.

In order to determine the ethanolamide moiety's significance in IJ recovery inhibition, **asc-C11 24** was also synthesized (Scheme 2.6). **Asc-C11 24** only differs structurally from the IJ hormone by the absence of the ethanolamide moiety. Instead, it contains a terminal carboxylic acid. **Asc-C11 24** was synthesized via the hydrolysis of **23** with LiOH in *t*BuOH. *t*BuOH was a better solvent than the previously utilized MeOH, due to better solvation of reagents. **Asc-C11 24** has an  $\text{EC}_{50}$  value of 13  $\mu\text{m}$  in an IJ recovery assay, which is 500-fold less than that of the ethanolamide-containing hormone. This decrease in potency demonstrates that the ethanolamide moiety plays an integral role in IJ hormone receptor binding.



Scheme 2.6 Synthesis of **asc-C11 24**

### 2.3 Conclusions

*H. bacteriophora* exists in the soil as an infective juvenile, which bears a remarkable resemblance to the dauer stage in *C. elegans*. Like *C. elegans*, the IJ stage is characterized by its non-aging nature and the cessation of feeding. This dauer-like stage of *H. bacteriophora* serves



as an excellent model for studying parasitism and symbiosis. A compound was isolated by the Butcher laboratory at the University of Florida which was determined to inhibit IJ recovery to adulthood. Chapter 2 describes the synthesis and characterization of this naturally-occurring IJ hormone **asc-C11EA 25**, its epimer at the  $\omega$ -1 position **32**, and **asc-c11 24**. The  $\omega$ -1 (*R*) epimer **asc-C11EA 25** was originally thought to be the compound most likely to be the hormone due to the structural similarity between this compound and ascarosides comprising the dauer pheromone of *C. elegans*. At first, the synthesis of carboxylic acid **17** was attempted via  $\text{KMnO}_4$  oxidation of the alkene **16**. However, this proved to be unsuccessful due to extensive loss of a methylene group on the carbon side chain, which produced an inseparable mixture of desired product and lower molecular weight impurity. As an alternate route towards the synthesis of **asc-C11EA 25**, alkene **21** underwent cross metathesis with methyl acrylate to give  $\alpha,\beta$ -unsaturated methyl ester **22**, which was then hydrogenated to yield saturated ascaroside **23**. Aminolysis of compound **23** led to the desired product **asc-C11EA 25**. Optical rotation of the synthesized **asc-C11EA 25** did not match with that of the isolated hormone, so the  $\omega$ -1 (*S*) epimer **32** was synthesized. This synthesis was accomplished using the same route as **asc-C11EA 25** (glycosylation, cross metathesis, hydrogenation and aminolysis). After comparison of the NMRs of the two epimers and the IJ hormone, it was determined that the correct structure of the hormone was **asc-C11EA 25**. In an IJ recovery assay, the synthesized hormone was shown to have an  $\text{EC}_{50}$  value of 25 mM. In order to determine the importance of the terminal ethanolamide moiety on **asc-C11EA 25**, **asc-C11 24** was synthesized via the hydrolysis of methyl ester **23**. The activity of this carboxylic acid was 500 times less than that of **asc-C11EA 25**, demonstrating that the ethanolamide moiety was crucial in inhibiting IJ recovery.

## 2.4 Experimental

### 2.4.1 Procedures and Characterization

Representative procedure for epoxide opening – synthesis of **20**:

To a suspension of 82.4 mg (3.39 mmol) of magnesium turnings in 0.44 mL dry THF was added 0.52 mL (3.4 mmol) 7-bromo-1-heptene in 2.9 mL dry THF dropwise over the course of 4 minutes. The resulting suspension was brought to reflux and stirred for 12 h until all magnesium had been consumed. The resulting cloudy, pale-yellow mixture was allowed to cool to 25°C. To a separate flask was added 34.2 mg (0.238 mmol) CuBr in 5 mL dry THF. This suspension was cooled to -78°C. To this chilled suspension was added the previously synthesized 7-heptenylmagnesium bromide dropwise over 3 minutes via syringe. This resulting suspension was allowed to stir for 10 minutes, upon which it turned dark gray with black solids. To this suspension was added 0.17 mL (2.4 mmol) (R)-(+)-propylene oxide at once, upon which it turned from dark gray to black. The suspension was allowed to warm to 25°C and was stirred for 3 h. To the black suspension was added 4 mL sat. NH<sub>4</sub>Cl at once. The aqueous layer was separated from the organic layer and then extracted with 3 x 10 mL THF. The resulting organic extracts were dried over MgSO<sub>4</sub> and filtered to obtain 509.3 mg of dark yellow oil. Silica gel column chromatography (54.9 g silica gel, 20% ethyl acetate in hexanes) afforded 225.2 mg (43%) of a colorless oil.  $[\alpha]_D^{25} = -19.8$ ,  $c$  1.87 (CH<sub>2</sub>Cl<sub>2</sub>); IR (cm<sup>-1</sup>): 3334; <sup>1</sup>H NMR (400 MHz, CDCl<sub>3</sub>):  $\delta$  5.79 (ddt, 1H, J=17.1 Hz, J=10.2 Hz, J=6.7 Hz); 4.97 (d, 1H, J=17.2 Hz); 4.91 (d, 1H, J=10.2 Hz); 3.76 (m, 1H); 2.02 (q, 2H, J=6.9 Hz); 1.36 (m, 10H); 1.16 (d, 3H, J=6.2 Hz); <sup>13</sup>C NMR (100 MHz, CDCl<sub>3</sub>):  $\delta$  139.1; 114.2; 68.2; 39.3; 33.8; 29.5; 29.1; 28.8; 25.7; 23.5.

Representative procedure for glycosylation – synthesis of **21**:

A suspension of 500.3 mg (1.404 mmol) dibenzoyl ascarylose **3**, 350.4 mg (2.242 mmol) alcohol **20** and 166.0 mg 4Å molecular sieves in 16 mL CH<sub>2</sub>Cl<sub>2</sub> was cooled to 0°C. To this

suspension was added 0.77 mL (6.1 mmol)  $\text{BF}_3 \cdot \text{OEt}_2$  at once. The resulting suspension was stirred at  $0^\circ\text{C}$  for 2.5 h. 20 mL saturated  $\text{NaHCO}_3$  solution was then added. Upon cessation of effervescence, the aqueous layer was separated from the organic layer and then extracted with 3 x 10 mL 20% *i*PrOH in  $\text{CH}_2\text{Cl}_2$ . The resulting organic extracts were dried over  $\text{MgSO}_4$  and filtered to obtain 847.3 mg of oil. Silica gel column chromatography (53 g silica gel, gradient run from 50% hexanes in  $\text{CH}_2\text{Cl}_2$  to 100%  $\text{CH}_2\text{Cl}_2$ ) afforded 487.6 mg (70%) of a colorless syrup.  $[\alpha]_{\text{D}}^{25} = -14.0$ ,  $c$  2.33 ( $\text{CH}_2\text{Cl}_2$ ); IR ( $\text{cm}^{-1}$ ): 1722; HRMS ( $m/z$ ):  $[\text{M}+\text{Na}]^+$  calcd. for  $\text{C}_{30}\text{H}_{38}\text{O}_6\text{Na}$  517.2561, found 517.2564;  $^1\text{H}$  NMR (400 MHz,  $\text{CDCl}_3$ ):  $\delta$  8.12 (d, 2H,  $J=7.2$  Hz); 8.05 (d, 2H,  $J=7.2$  Hz); 7.58 (t, 2H,  $J=6.8$  Hz); 7.46 (m, 4H); 5.82 (ddt, 1H,  $J=17.1$ ,  $J=10.2$  Hz,  $J=6.7$  Hz); 5.19 (td, 1H,  $J=10.5$  Hz,  $J=4.1$  Hz); 5.15 (m, 1H); 5.00 (d, 1H,  $J=17.2$  Hz); 4.96 (s, 1H); 4.94 (d, 1H,  $J=11.1$  Hz); 4.13 (dq, 1H,  $J=9.7$  Hz,  $J=6.2$  Hz); 3.85 (m, 1H); 2.42 (dt, 1H,  $J=13.3$  Hz,  $J=3.4$  Hz); 2.22 (td, 1H,  $J=11.0$  Hz,  $J=12.4$  Hz,  $J=2.9$  Hz); 2.07 (q, 2H,  $J=6.8$  Hz); 1.65 (m, 1H); 1.45 (m, 9H); 1.29 (d, 3H,  $J=6.2$  Hz), 1.19 (d, 3H,  $J=6.0$  Hz);  $^{13}\text{C}$  NMR (100 MHz,  $\text{CDCl}_3$ ):  $\delta$  165.8; 165.6; 139.1; 133.2; 133.1; 130.0; 129.8; 129.6; 128.4; 114.2; 93.8; 72.6; 71.2; 70.7; 66.9; 37.1; 33.8; 29.7; 29.4; 29.1; 28.9; 25.7; 19.2; 17.9.

Representative procedure for cross metathesis – synthesis of **22**:

To a solution of 480.2 mg (0.9367 mmol) alkene **21** and 0.42 mL (4.7 mmol) methyl acrylate in 29.8 mL  $\text{CH}_2\text{Cl}_2$  at reflux was added 79.5 mg (0.0937 mmol) Grubbs 2<sup>nd</sup> generation ruthenium catalyst at once. The resulting solution was allowed to stir at reflux for 6 h. The reaction mixture was concentrated to 404.0 mg of brown oil. Silica gel column chromatography (41 g silica gel, gradient run from 2% diethyl ether in hexanes to 10% diethyl ether in hexanes) afforded 485.1 mg (91%) of a yellow oil.  $[\alpha]_{\text{D}}^{25} = -1.3$ ,  $c$  2.75 ( $\text{CH}_2\text{Cl}_2$ ); IR ( $\text{cm}^{-1}$ ): 1721; HRMS ( $m/z$ ):  $[\text{M}+\text{Na}]^+$  calcd. for  $\text{C}_{32}\text{H}_{40}\text{O}_8\text{Na}$  575.2615, found 575.2606;  $^1\text{H}$  NMR (400 MHz,  $\text{CDCl}_3$ ):  $\delta$  8.11 (d, 2H,  $J=7.1$  Hz); 8.04 (d, 2H,  $J=7.2$  Hz); 7.58 (t, 2H,  $J=7.2$  Hz); 7.46 (m, 4H); 6.98 (dt,

1H, J=15.6 Hz, J=6.9 Hz); 5.82 (d, 1H, J=15.6 Hz); 5.18 (td, 1H, J=10.5 Hz, J=4.0 Hz); 5.15 (m, 1H); 4.95 (s, 1H); 4.11 (dq, 1H, J=9.7 Hz, J=6.1 Hz); 3.84 (m, 1H); 3.70 (s, 3H); 2.42 (dt, 1H, J=13.3 Hz, J=3.7 Hz); 2.22 (m, 3H); 1.67 (m, 1H); 1.43 (m, 9H); 1.28 (d, 3H, J=6.2 Hz); 1.19 (d, 3H, J=6.0 Hz); <sup>13</sup>C NMR (100 MHz, CDCl<sub>3</sub>): δ 167.1; 165.7; 165.6; 149.6; 133.2; 133.1; 130.0; 129.8; 129.5; 128.4; 120.9; 93.8; 72.6; 71.2; 70.6; 66.9; 51.3; 37.0; 32.1; 29.7; 29.3; 29.1; 28.0; 25.6; 19.1; 17.8.

Representative procedure for hydrogenation – synthesis of **23**:

A suspension of 422.8 mg (0.7650 mmol) unsaturated ester **22** and 50.4 mg 10 % palladium on activated carbon in 46.0 mL EtOAc was vacuum purged and back filled with H<sub>2</sub> from a balloon. The resulting suspension was allowed to stir at 23°C for 22 h. The reaction mixture was filtered through Celite<sup>®</sup> and concentrated to obtain 411.5 mg (97%) of colorless oil that required no further purification.  $[\alpha]_D^{25} = -2.1, c 4.04$  (CH<sub>2</sub>Cl<sub>2</sub>); IR (cm<sup>-1</sup>): 1722; HRMS (*m/z*): [M+Na]<sup>+</sup> calcd. for C<sub>32</sub>H<sub>42</sub>O<sub>8</sub>Na 577.2772, found 577.2779; <sup>1</sup>H NMR (400 MHz, CDCl<sub>3</sub>): δ 8.11 (d, 2H, J=7.4 Hz); 8.04 (d, 2H, J=7.4 Hz); 7.57 (t, 2H, J=6.8 Hz); 7.45 (m, 4H); 5.18 (td, 1H, J=10.4 Hz, J=4.2 Hz); 5.15 (m, 1H); 4.95 (s, 1H); 4.12 (dq, 1H, J=9.7 Hz, J=6.1 Hz); 3.84 (m, 1H); 3.64 (s, 3H); 2.42 (dt, 1H, J=13.3 Hz, J=4.1 Hz); 2.29 (t, 2H, J=7.5 Hz); 2.21 (td, 1H, J=12.4 Hz, J=2.8 Hz); 1.70 (m, 3H); 1.42 (m, 11H); 1.28 (d, 3H, J=6.2 Hz); 1.18 (d, 3H, J=6.0 Hz); <sup>13</sup>C NMR (100 MHz, CDCl<sub>3</sub>): δ 174.1; 165.6; 165.5; 133.1; 133.0; 129.9; 129.7; 129.5; 128.3; 93.7; 72.5; 71.1; 70.6; 66.8; 51.3; 37.0; 33.9; 29.6; 29.4; 29.3; 29.1; 29.0; 25.6; 24.8; 19.1; 17.8.

Synthesis of **asc C11 EA 25**:

To a solution of 57.8 mg (0.104 mmol) saturated ester **23** in 4.3 mL pyridine at reflux was added 0.1 mL (2 mmol) ethanolamine at once. The resulting solution was allowed to stir at reflux for 48 h, in which time formation of the amide bond and monodebenzoylation occurred (as

judged with  $^1\text{H}$  NMR). The reaction mixture was concentrated to a yellow syrup. This syrup was dissolved in 7.3 mL *t*BuOH. 7.3 mL 1M LiOH was then added at once. This solution was allowed to stir for 24 h at 23°C. 1N HCl was then added dropwise until the reaction mixture reached a pH=5. 5.0 mL 20% *i*PrOH in  $\text{CH}_2\text{Cl}_2$  was then added to the acidified reaction mixture and the layers were separated. The aqueous layer was extracted with an additional 6 x 5 mL 20% *i*PrOH in  $\text{CH}_2\text{Cl}_2$ . The aqueous layer was then saturated with solid NaCl and further extracted with 3 x 5 mL 20% *i*PrOH in  $\text{CH}_2\text{Cl}_2$ . The combined organic layers were dried over  $\text{Na}_2\text{SO}_4$ , filtered and concentrated to a pale yellow oil. HPLC purification afforded 31.5 mg (81%, 2 steps) of a colorless oil.  $[\alpha]_{\text{D}}^{25} = -49.4$ ,  $c$  1.56 ( $\text{CH}_3\text{OH}$ ); IR ( $\text{cm}^{-1}$ ): 3314; 1651; HRMS ( $m/z$ ):  $[\text{M}+\text{Na}]^+$  calcd. for  $\text{C}_{19}\text{H}_{37}\text{NO}_6\text{Na}$  398.2513, found 398.2496;  $^1\text{H}$  NMR (700 MHz,  $\text{CD}_3\text{OD}$ ):  $\delta$  4.64 (s, 1H); 3.76 (m, 1H); 3.71 (m, 1H); 3.62 (dq, 1H,  $J=9.1$  Hz,  $J=6.3$  Hz); 3.58 (t, 2H,  $J=5.6$  Hz); 3.51 (td, 1H,  $J=10.9$  Hz,  $J=3.9$  Hz); 3.28 (t, 2H,  $J=5.6$  Hz); 2.20 (t, 2H,  $J=7.7$  Hz); 1.95 (dt, 1H,  $J=13.0$  Hz,  $J=3.3$  Hz); 1.76 (td, 1H,  $J=12.3$  Hz,  $J=2.8$  Hz); 1.60 (m, 2H); 1.54 (m, 1H); 1.39 (m, 11H); 1.21 (d, 3H,  $J=6.3$  Hz); 1.12 (d, 3H,  $J=5.6$  Hz);  $^{13}\text{C}$  NMR (100 MHz,  $\text{CD}_3\text{OD}$ ):  $\delta$  176.8; 97.7; 72.6; 71.3; 70.1; 68.4; 61.8; 43.0; 38.5; 37.2; 36.1; 30.8; 30.7; 30.6; 30.4; 27.1; 27.0; 19.5; 18.3.

Synthesis of **28** (Same procedure as **20**):

HRMS ( $m/z$ ):  $[\text{M}+\text{H}]^+$  calcd. for  $\text{C}_{10}\text{H}_{21}\text{O}$  157.1587, found 157.1591;  $^1\text{H}$  NMR (250 MHz,  $\text{CDCl}_3$ ):  $\delta$  5.81 (m, 1H); 4.95 (m, 2H); 3.78 (m, 1H); 2.05 (q, 2H,  $J=6.3$  Hz); 1.40 (m, 11H); 1.19 (d, 3H,  $J=7.5$  Hz).

Synthesis of **29** (Same procedure as **21**):

HRMS ( $m/z$ ):  $[\text{M}+\text{Na}]^+$  calcd. for  $\text{C}_{30}\text{H}_{38}\text{O}_6\text{Na}$  517.2561, found 517.2569;  $^1\text{H}$  NMR (400 MHz,  $\text{CDCl}_3$ ):  $\delta$  8.12 (m, 2H); 8.05 (m, 2H); 7.59 (m, 2H); 7.47 (m, 4H); 5.82 (m, 1H); 5.18 (m, 2H); 5.02 (dq, 1H,  $J=16.0$  Hz,  $J=4.0$  Hz); 4.93 (m, 2H); 4.17 (m, 1H); 3.80 (sextet, 1H,  $J=8.0$  Hz);

2.41 (dt, 1H, J=16.0 Hz, J=3.6 Hz); 2.22 (m, 1H); 2.05 (m, 2H); 1.59 (m, 1H); 1.40 (m, 9H); 1.29 (d, 6H, J=6.0 Hz); <sup>13</sup>C NMR (62.5 MHz, CDCl<sub>3</sub>): δ 165.74; 165.66; 139.2; 133.2; 133.1; 130.0; 129.8; 129.6; 128.4; 114.1; 96.1; 75.4; 71.0; 70.7; 66.8; 36.4; 33.8; 29.7; 29.5; 29.0; 28.9; 25.3; 21.3; 17.8.

Synthesis of **30** (Same procedure as **22**):

HRMS (*m/z*): [M+Na]<sup>+</sup> calcd. for C<sub>32</sub>H<sub>40</sub>O<sub>8</sub>Na 575.2615, found 575.2623; <sup>1</sup>H NMR (400 MHz, CDCl<sub>3</sub>): δ 8.12 (m, 2H); 8.05 (m, 2H); 7.58 (m, 2H); 7.46 (m, 4H); 6.97 (dt, 1H, J=16.0 Hz, J=8.0 Hz); 5.82 (dt, 1H, J=15.6 Hz, J=2.0 Hz); 5.19 (m, 2H); 4.92 (s, 1H); 4.17 (m, 1H); 3.79 (m, 1H); 3.71 (s, 3H); 2.41 (dt, 1H, J=12.0 Hz, J=3.9 Hz); 2.20 (m, 3H); 1.59 (m, 1H); 1.39 (m, 9H); 1.28 (d, 6H, J=6.0 Hz).

Synthesis of **31** (Same procedure as **23**):

HRMS (*m/z*): [M+Na]<sup>+</sup> calcd. for C<sub>32</sub>H<sub>42</sub>O<sub>8</sub>Na 577.2772, found 577.2789; <sup>1</sup>H NMR (400 MHz, CDCl<sub>3</sub>): δ 8.12 (d, 2H, J=8.0 Hz); 8.05 (d, 2H, J=8.0 Hz); 7.58 (m, 2H); 7.47 (m, 4H); 5.19 (m, 2H); 4.92 (s, 1H); 4.17 (m, 1H); 3.80 (m, 1H); 3.66 (s, 3H); 2.42 (dt, 1H, J=12.0 Hz, J=4.0 Hz); 2.30 (t, 2H, J=7.8 Hz); 2.22 (m, 1H); 1.62 (m, 3H); 1.40 (m, 11H); 1.30 (d, 3H, J=6.5 Hz); 1.29 (d, 3H, J=6.2 Hz); <sup>13</sup>C NMR (100 MHz, CDCl<sub>3</sub>): δ 174.3; 165.8; 165.7; 133.21; 133.15; 130.1; 129.94; 129.87; 129.6; 128.4; 96.1; 75.5; 71.0; 70.8; 66.9; 51.4; 36.5; 34.1; 29.7; 29.6; 29.4; 29.2; 29.1; 25.3; 24.9; 21.3; 17.8.

Synthesis of **32**:

HRMS (*m/z*): [M+Na]<sup>+</sup> calcd. for C<sub>19</sub>H<sub>37</sub>NO<sub>6</sub>Na 398.2513, found 398.2522; <sup>1</sup>H NMR (400 MHz, CD<sub>3</sub>OD): δ 4.58 (s, 1H); 3.73-3.61 (m, 3H); 3.57 (t, 2H, J=5.8 Hz); 3.50 (m, 1H); 3.27 (t, 2H, J=5.8 Hz); 2.18 (t, 2H, J=7.7 Hz); 1.93 (dt, 1H, J=13.2 Hz, J=3.6 Hz); 1.76 (td, 1H, J=11.4 Hz, J=3.0 Hz); 1.59 (m, 2H); 1.50 (m, 1H); 1.37 (m, 11H); 1.20 (d, 3H, J=6.2 Hz); 1.19

(d, 3H, J=6.2 Hz);  $^{13}\text{C}$  NMR (100 MHz,  $\text{CD}_3\text{OD}$ ):  $\delta$  176.7; 100.2; 75.6; 71.0; 69.7; 68.4; 61.7; 42.9; 37.5; 37.1; 35.9; 30.7; 30.5; 30.35; 30.26; 27.0; 26.4; 21.7; 18.0.

#### Synthesis of **asc C11 (free acid) 24**:

To a suspension of 55.8 mg (0.101 mmol) saturated ester **23** in 7.9 mL *t*BuOH was added 7.9 mL sat. 1M LiOH at once. The resulting solution was allowed to stir at 23°C for 19 h. 1N HCl was then added dropwise until the reaction mixture reached a pH=3. 5.0 mL 20% *i*PrOH in  $\text{CH}_2\text{Cl}_2$  was added to the acidified reaction mixture, and the layers were separated. The aqueous layer was extracted with an additional 8 x 5 mL 20% *i*PrOH in  $\text{CH}_2\text{Cl}_2$ . Solid NaCl was then added until saturation was obtained, and the aqueous layer was further extracted with 3 x 5 mL 20% *i*PrOH in  $\text{CH}_2\text{Cl}_2$ . The combined organic layers were dried over  $\text{Na}_2\text{SO}_4$  and filtered. Evaporation of solvent afforded 128.3 mg of an oil. HPLC purification afforded 19.4 mg (58%) of a colorless oil.  $[\alpha]_{\text{D}}^{25} = -54.5$ ,  $c$  0.99 ( $\text{CH}_3\text{OH}$ ); IR ( $\text{cm}^{-1}$ ): 3390; 1737; HRMS ( $m/z$ ):  $[\text{M}+\text{Na}]^+$  calcd. for  $\text{C}_{17}\text{H}_{32}\text{O}_6\text{Na}$  355.2091, found 355.2074;  $^1\text{H}$  NMR (400 MHz,  $\text{CD}_3\text{OD}$ ):  $\delta$  4.68 (s, 1H); 3.77 (m, 2H); 3.68 (m, 1H); 3.58 (td, 1H, J=10.3 Hz, J=4.4 Hz); 2.29 (t, 2H, J=7.6 Hz); 2.06 (dt, 1H, J=13.0 Hz, J=3.8 Hz); 1.83 (td, 1H, J=12.3 Hz, J=2.9 Hz); 1.58 (m, 3H); 1.34 (m, 14H); 1.20 (d, 3H, J=6.1 Hz); 1.11 (d, 3H, J=6.1 Hz);  $^{13}\text{C}$  NMR (400 MHz,  $\text{CDCl}_3$ ):  $\delta$  174.5; 96.0; 71.6; 69.8; 69.3; 68.1; 37.1; 35.1; 34.1; 29.4; 29.3; 29.1; 29.0; 25.6; 24.9; 18.9; 17.6.

## 2.5 References

1. Noguez, J. H.; Conner, E. S.; Zhou, Y.; Ciche, T. A.; Ragains, J. R.; Butcher, R. A., A Novel Ascaroside Controls the Parasitic Life Cycle of the Entomopathogenic Nematode *Heterorhabditis bacteriophora*. *ACS Chem. Biol.* **2012**, 7 (6), 961-6.
2. Han, R.; Ehlers, R.-U., Pathogenicity, Development, and Reproduction of *Heterorhabditis bacteriophora* and *Steinernema carpocapsae* under Axenic in Vivo Conditions. *J. Invertebr. Pathol.* **2000**, 75 (1), 55-58.
3. Bedding, R. A.; Molyneux, A. S., Penetration of Insect Cuticle By Infective Juveniles of *Heterorhabditis* Spp. (*Heterorhabditidae*: Nematoda). *Nematologica* **1982**, 28 (3), 354-359.

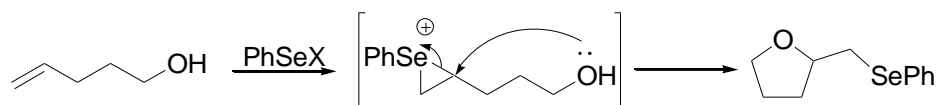
4. Ciche, T. A.; Ensign, J. C., For the Insect Pathogen *Photorhabdus luminescens*, Which End of a Nematode is Out? *Appl. Environ. Microbiol.* **2003**, *69*, 1890-1897.
5. Milstead, J. E., Heterorhabditis bacteriophora as a Vector for Introducing its Associated Bacterium into the Hemocoel of *Galleria mellonella* Larvae. *J. Invertebr. Pathol.* **1979**, *33* (3), 324-327.
6. Ciche, T., The biology and Genome of Heterorhabditis bacteriophora. *WormBook : the online review of C. elegans biology* **2007**, 1-9.
7. Johnigk, S.-A.; Ehlers, R.-U., Endotokia Matricida in Hermaphrodites of Heterorhabditis spp. and the Effect of the Food Supply. *Nematology* **1999**, *1* (7-8), 717-726.
8. Ciche, T. A.; Kim, K.-s.; Kaufmann-Daszczuk, B.; Nguyen, K. C. Q.; Hall, D. H., Cell Invasion and Matricide During *Photorhabdus luminescens* Transmission by Heterorhabditis bacteriophora Nematodes. *Appl. Environ. Microbiol.* **2008**, *74*, 2275-2287.
9. Forst, S. D., B.; Boemare, N.; Stackebrandt, E., Xenorhabdus and photorhabdus spp.: bugs that kill bugs. *Annu. Rev. Microbiol.* **1997**, *51*, 47-72.
10. Bode, H. B., Entomopathogenic Bacteria as a Source of Secondary Metabolites. *Curr. Opin. Chem. Biol.* **2009**, *13*, 224-230.
11. O'Halloran, D. M. B., A.M, Olfaction and Odour Discrimination in the Insect Parasitic Nematode *Heterorhabditis bacteriophora*. *Nematology* **2002**, *4*, 206.
12. Rasmann, S. K., T. G.; Degenhardt, J.; Hiltbold, I.; Toepfer, S.; Kulmann, U.; Gershenzon, J.; Turlings, T.C.J., Recruitment of Entomopathogenic Nematodes by Insect-Damaged Maize Roots. *Nature* **2005**, *434*, 732-737.
13. Aumann, J.; Ehlers, R.-U., Physico-Chemical Properties and Mode of Action of a Signal from the Symbiotic Bacterium *Photorhabdus luminescens* Inducing Dauer Juvenile Recovery in the Entomopathogenic Nematode Heterorhabditis bacteriophora. *Nematology* **2001**, *3* (8), 849-853.



## CHAPTER 3: DEVELOPMENT OF NOVEL VISIBLE LIGHT-PROMOTED METHOD FOR SELENO-AND TELLUROFUNCTIONALIZATION AND SYNTHESIS OF $\gamma$ -LYCORANE

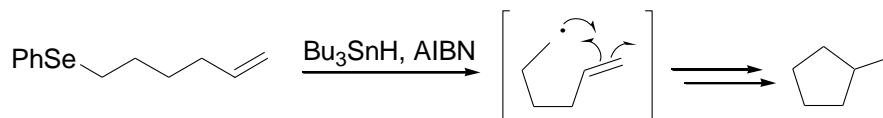
### 3.1 Introduction

The first organoselenium compound, diethyl selenide, was synthesized in 1836.<sup>1</sup> Since then, organoselenium chemistry has become an integral part of organic synthesis. In the 1950's, the addition of PhSeY (formed from PhSeX (X=Cl or Br) and AgY (Y=OAc)) to alkenes was introduced.<sup>2</sup> Selenocyclizations using PhSeX were the logical next step.<sup>3</sup> The mechanism for these transformations is well known.<sup>4</sup> Initially, a seleniranium ion intermediate is formed and then attacked by a nucleophile, resulting in a stereospecific anti-addition (Scheme 3.1).



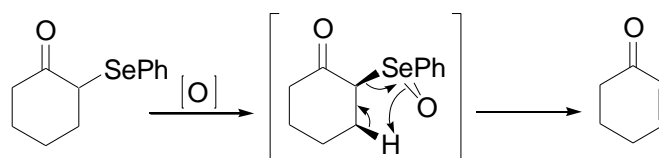
Scheme 3.1 Mechanism for selenocyclization

Selenofunctionalization has played an integral role in the synthesis of many natural and non-natural products.<sup>5</sup> Organoselenides act as important intermediates which can be transformed into the desired products via several methods. One method for manipulation of the selenofunctionalization product is C-Se bond homolysis.<sup>6</sup> This reaction usually takes place as a result of abstraction of the selenide by a tin or sulfur radical. As seen in Scheme 3.2, the abstraction of selenide generates a carbon-centered radical, which can react further intermolecularly or intramolecularly. For instance, this radical can cyclize onto an alkene.



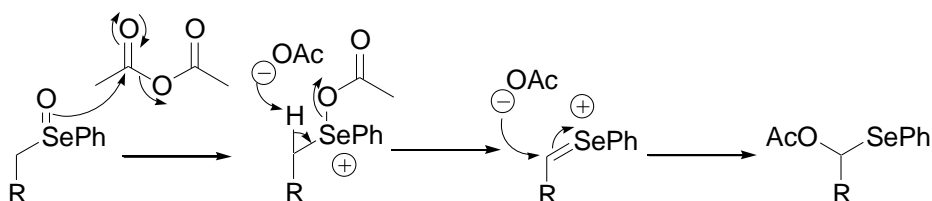
Scheme 3.2 C-Se bond homolysis

In addition to C-Se homolysis, a selenide intermediate can also undergo selenoxide elimination to form an alkene.<sup>7</sup> The first step in this elimination is the formation of the selenoxide moiety via oxidation of the selenide (Scheme 3.3). Oxidation can be accomplished using a variety of oxidations, the most common being hydrogen peroxide. Once the selenide is oxidized, the intermediate then experiences an intermolecular syn elimination of the selenoxide moiety to give the alkene.



Scheme 3.3 Selenoxide elimination

Another pathway for functionalizing a selenide intermediate is the Pummerer rearrangement.<sup>8</sup> In this step, a formed selenoxide interacts with an anhydride, usually acetic anhydride, to yield an  $\alpha$ -acyloxy selenoester (Scheme 3.4). This product can then undergo elimination, followed by the attack of an acetate anion to give the ester.<sup>9</sup>



Scheme 3.4 Pummerer rearrangement

Besides being important intermediates in organic synthesis, selenides have recently been determined to have potent anti-cancer properties (Figure 3.1).<sup>10</sup> The most studied and successful anti-cancer agent is Ebselen<sup>®</sup>, selenide **33**. It is currently in cancer clinical trials, and its possible use as a therapeutic agent for stroke and bipolar disorder is also being investigated. The role that selenium plays in this compound can be demonstrated by the complete inactivity of the sulfur

analog. Compound **34** also displays high activity, with growth inhibition in the nanomolar range, against several cancer cell lines including MCF-7, MCF-10A and HT-29.

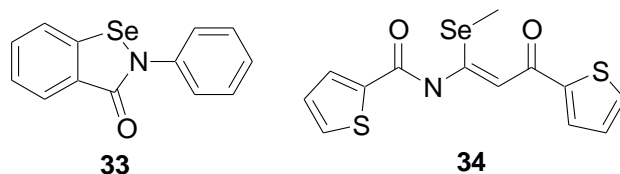
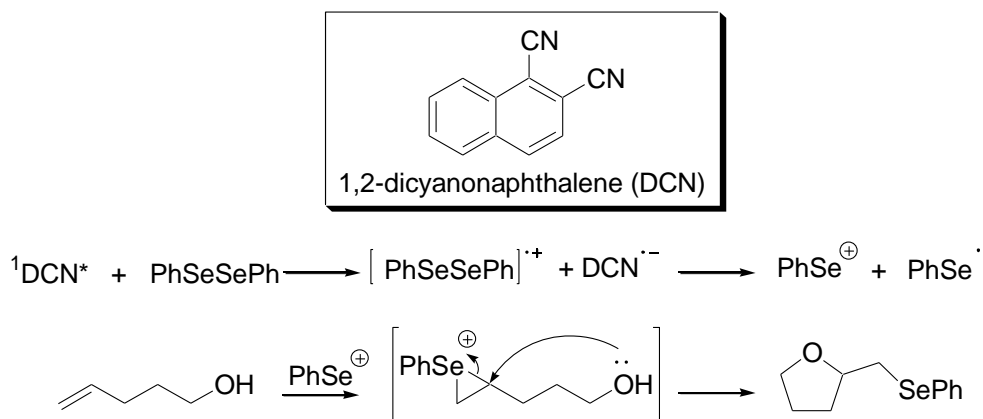


Figure 3.1 Selenium-containing anti-cancer agents

The reagent for selenofunctionalization most often used is phenylselenenyl bromide. It is commercially available; however, due its short shelf life, water sensitivity and relatively high price, it is generally synthesized via the reaction between diphenyl diselenide and molecular bromine.<sup>11</sup> Phenylselenenyl bromide also has a high toxicity. In an attempt to replace this water-sensitive, toxic, reactive species, Pandey and coworkers have developed a light-promoted selenocyclization method using diphenyl diselenide and 1,2-dicyanonaphthalene (DCN).<sup>12</sup>



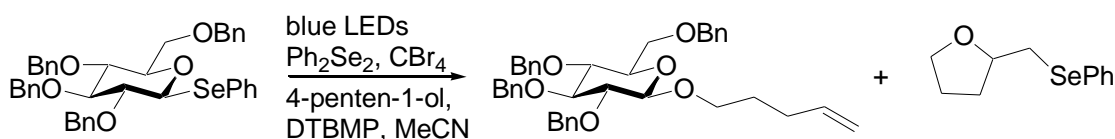
Scheme 3.5 Pandey's light-promoted selenocyclization

In this method,  ${}^1\text{DCN}^*$ , promoted to its excited state by UV light, accepts an electron from diphenyl diselenide (Scheme 3.5). The resulting diphenyl diselenide radical cation cleaves to form phenyl selenide radical, which may combine with other radicals to reform  $\text{Ph}_2\text{Se}_2$ , and phenyl selenide cation. This phenyl selenide cation is the species that reacts with the alkene to

form the seleniranium ion, which then undergoes cyclization. The generated DCN radical anion is oxidized by O<sub>2</sub> to reform more catalyst. Although Pandey and coworkers were successful in cyclizing a wide variety of substrates, their method suffered from several drawbacks. One was that the use of UV light was essential to the transformation. UV light sources are expensive and require complicated setups and cooling systems. Also, the yields obtained for the cyclized products were mediocre, ranging from 40% to 74%.

### 3.2 Results and Discussion

Initially, this seleno- and tellurofunctionalization project began as an investigation of a problem occurring in the  $\alpha$ -selective glycosylation of alcohols with selenoglycosides, promoted by visible light.<sup>13</sup> After the successful glycosylation of various alcohols including cyclohexanol, (-)-menthol and 1-octanol, the reaction was attempted using 4-penten-1-ol as the glucosyl acceptor (Scheme 3.6). The expected substitution of 4-penten-1-ol to the selenoglycoside occurred only in low yields, mostly producing the cyclized ether. This phenomenon led to the conclusion that there were possible competing reactions between the alkene, diphenyl diselenide and tetrabromomethane which were interfering with the glycosylation process.



Scheme 3.6 Attempted glycosylation using 4-peten-1-ol

In an effort to demonstrate that phenylselenenyl bromide was the reactive species which promoted the selenocyclizations, the blue LED irradiation of diphenyl diselenide and tetrabromomethane in both dichloromethane and acetonitrile was monitored over time using <sup>77</sup>Se NMR. The resulting NMR spectra were compared to that of phenylselenenyl bromide, which had been obtained from the reaction of Br<sub>2</sub> and diphenyl diselenide (Figure 3.2).<sup>11</sup> After 1.5 h, only

diphenyl diselenide at  $\delta$  464 ppm and no phenylselenenyl bromide was observed by  $^{77}\text{Se}$  NMR. After an additional 3 h, however, the phenylselenenyl peak at  $\delta$  867 ppm was beginning to show. Thus, phenylselenenyl bromide was generated *in situ* in the course of the selenocyclization reactions and was likely the reactive species.

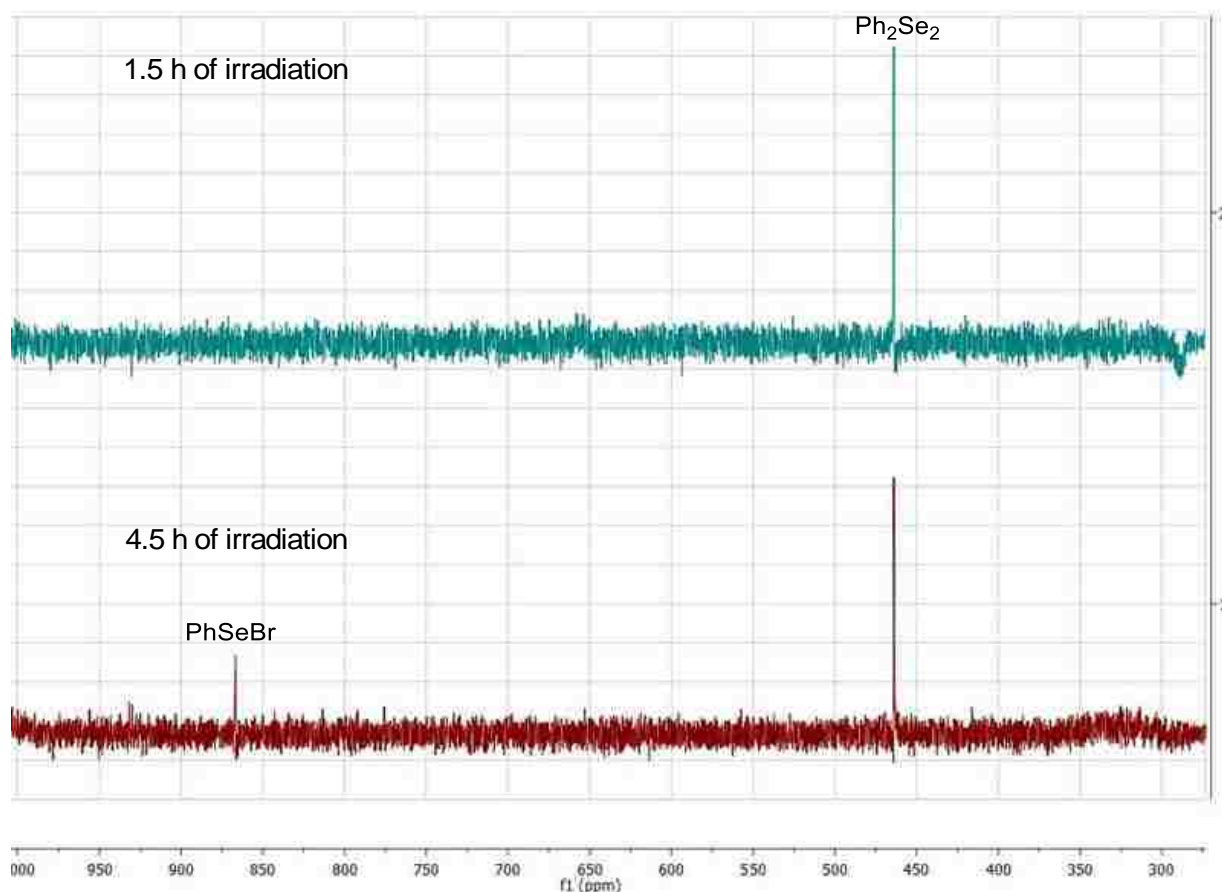
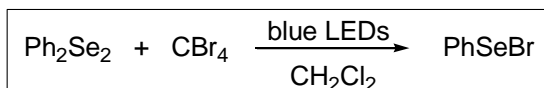
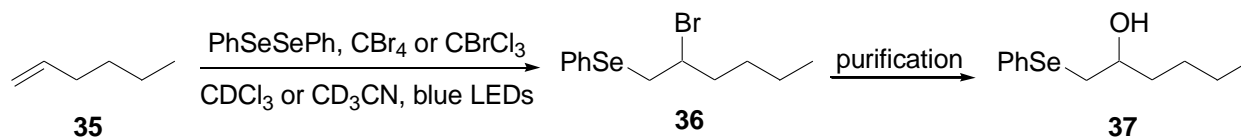


Figure 3.2  $^{77}\text{Se}$  NMR Studies

To investigate any possible side reactions between the alkene moiety on 4-penten-1-ol and the other reagents present in the reaction in Scheme 3.6, an NMR experiment was performed. In this experiment, an NMR tube was charged with diphenyl diselenide, tetrabromomethane (or bromotrichloromethane) and 1-hexene (**35**) in either acetonitrile- $\text{D}_3$  or

chloroform-D and placed in a small beaker surrounded by blue LEDs ( $\lambda_{\text{max}} = 455 \text{ nm}$ ). Over the course of the reaction, the addition of PhSeBr across the alkene was observed (Scheme 3.7). The relatively clean conversion of 1-hexene to the phenyl selenide/bromide adduct **36** was confirmed by  $^1\text{H}$  NMR and 2D NMR. Purification of the reaction mixture by column chromatography using silica gel, however, proved to be unproductive. Multiple attempts at purification were performed. Upon reflection on this issue, it was determined that the phenyl selenide/ bromide adduct was being hydrolyzed on the column to produce the phenyl selenide/ hydroxylated compound **37**.<sup>14</sup> To remedy this situation, silica gel was dried and dry solvents were used to elute the compound. After this was determined to be ineffective, dry neutral alumina was used as the solid phase media, without success. Even after taking these measures, the phenyl selenide/bromine adduct was still hydrolyzed to the alcohol.



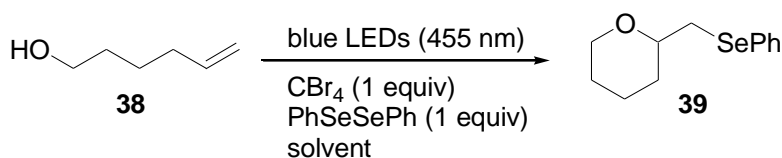
Scheme 3.7 Attempted addition of PhSeBr across an alkene

Since the bromide **36** appeared to be susceptible to nucleophilic attack, an intramolecular selenocyclization was then attempted using 5-hexen-1-ol (**38**). Initial experiments using 1 equivalent each of diphenyl diselenide and tetrabromomethane with a concentration of 5-hexen-1-ol of 200 mM in various solvents resulted in low and variable yields of the cyclized product **39** as well as relatively long reaction times, often over 24 h. After observing that the diphenyl diselenide was precipitating during the course of the reaction, a higher dilution of 50 mM was attempted with exciting results. The yields at this dilution were a great improvement over those at the higher concentration, and the reaction times were much shorter. At this time, it was also observed that the reaction proceeded efficiently under air, with no effect on yield or reaction

time. In an effort to optimize the conditions for this selenocyclization reaction, a battery of experiments using various solvents was performed (Table 3.1).

The use of tetrahydrofuran and diethyl ether (Entries 1 and 2) as solvent gave the cyclized ether product **39** in 70% and 84% yield, respectively, in 24.5 h. Although the yields were high, the reaction time was relatively long. The irradiation time and yield improved when dichloromethane was used as solvent, with complete conversion in 11 h with a yield of 93% (Entry 3).

Table 3.1 Solvent screen for selenocyclization of 5-penten-1-ol



Entry	Solvent	Irradiation Time (h)	Yield (%)
1	THF	24.5	70
2	Et <sub>2</sub> O	24.5	84
3	CH <sub>2</sub> Cl <sub>2</sub>	11	93
4	CH <sub>3</sub> CN	6	91
5	<i>i</i> PrOH	3.5	85
6	EtOH	5.5	90
7	MeOH	4	98
8*	MeOH	7	82
9 <sup>‡</sup>	CH <sub>2</sub> Cl <sub>2</sub>	120	0
10 <sup>†</sup>	CH <sub>2</sub> Cl <sub>2</sub>	120	0

<sup>a</sup>All reactions were performed on a 0.6 mmol scale at a concentration of 50 mM. \*Used CBrCl<sub>3</sub> instead of CBr<sub>4</sub>. <sup>‡</sup>Performed in the absence of light. <sup>†</sup>Performed in the absence of CBr<sub>4</sub>.

The use of acetonitrile as solvent decreased the reaction time even further to 6 h, with a similar yield of 91% (Entry 4). Isopropanol and ethanol as solvent produced reaction times of just 3.5 h and 5.5 h, respectively, with yields reaching 85% and 90% (Entries 5 and 6). The best combination of reaction time and yield was the result of using methanol as solvent. With methanol as solvent, the irradiation time needed to completely consume the starting material was

shortened to 4 h, and the yield was increased to 98% (Entry 7). Interestingly, no formation of the alkoxyseleination product resulting from the attack of solvent molecules on the seleniranium intermediate was observed. To determine the importance of the tetrabromomethane in the course of the reaction, the less expensive bromotrichloromethane was used (Entry 8). Although the reaction succeeded in generating the cyclization product, the yield was significantly lower (82%) and the reaction time was almost doubled (7 h). Next, various controls were run. When the reaction was run under the favored conditions without irradiation for 5 days, no product was observed. This result demonstrates that the selenocyclization is promoted by light. For the next control, tetrabromomethane was eliminated as a reagent, and starting material was not converted. As such, tetrabromomethane plays an integral role in the reaction.

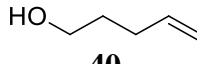
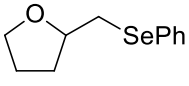
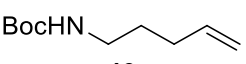
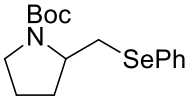
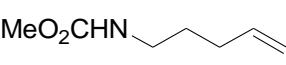
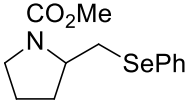
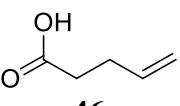
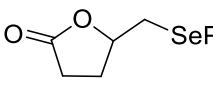
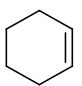
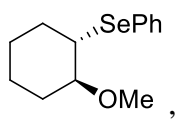
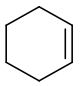
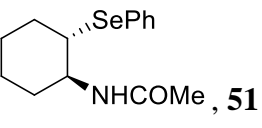
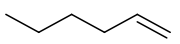
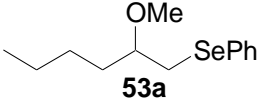
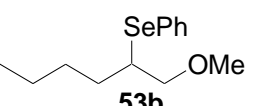
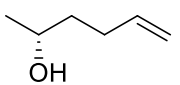
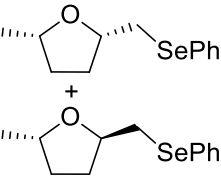
In order to expand our substrate scope, varying nucleophiles, chain lengths, stereochemistries and complexities were chosen to demonstrate the utility of the developed method (Table 3.2). To experiment with chain length, 4-penten-1-ol was irradiated with blue LEDs using the optimized conditions of 1 equivalent each of diphenyl diselenide and tetrabromomethane at a concentration of 50 mM. The resulting cyclized product was formed in 94% yield in 3.5 h (Entry 1). In order to demonstrate that the developed selenofunctionalization method was successful for a range of nucleophiles, unprotected pentenamine was submitted to the reaction conditions. Unfortunately, no cyclized product was formed. However, the reaction was successful when the amine was protected to form either the Boc-protect amine or the methyl carbamate. The Boc-protected amine was cyclized first under the standard conditions with methanol as solvent. No pyrrolidine product was observed. After changing the solvent to dichloromethane, the reaction proceeded as expected, and the Boc-protected amine was converted to the desired product in a modest yield of 62% over the course of 3.5 h (Entry 2).



The decrease in yield could have been due to the degradation of the Boc group of both the starting material and product by in situ-generated HBr. Using the methyl carbamate as the starting material instead of the Boc-protected analog as a way to circumvent degradation by HBr successfully increased the yield to 78% (Entry 3) with a longer irradiation time of 7 h. The last nucleophile that was explored was a carboxylic acid. When 4-pentenoic acid was irradiated with diphenyl diselenide and tetrabromomethane in methanol, substantial quantities of methoxyselenation products were observed. To avoid this issue, dichloromethane was used as the solvent and gave the desired product in 95% yield over 4 h (Entry 4). All of the substrates in this study thus far had involved the intramolecular attack of a pendant nucleophile. To demonstrate that the developed method was applicable to intermolecular systems, experiments were envisioned where the starting alkene would be converted to the methoxyselenation product. Cyclohexene was, therefore, reacted under the optimized conditions to give the expected methoxyselenation product in 97% yield after 17 h of irradiation (Entry 5). The methoxy group and phenyl selenide were on opposite faces due to the anti addition of methanol to the seleniranium ion. The Ritter reaction of cyclohexene was then attempted to demonstrate the intermolecular addition of acetonitrile and the following formation of the amide. Unfortunately, the desired product was formed in only a low yield of 43% over a long irradiation time of 12 days (Entry 6). The irradiation of 1-hexene under standard conditions also yielded the methoxyselenation products (Entry 7). The product consisted of a 3.3:1 ratio of regioisomers **53a** and **53b**, favoring the Markovnikov addition product with a combined yield of 97% over 7 h. Lastly, a secondary alcohol as nucleophile was utilized to give the product as a 1:1 mixture of diastereomers in 99% yield in the relatively short reaction time of 4 h (Entry 8). It should be noted that the purification via column chromatography of all selenocyclization products was

facile, due to the clean conversion of the starting material and the polarity difference between the product and the impurities (*e.g.* diphenyl diselenide).

Table 3.2 Substrate scope for selenofunctionalization

Entry	Substrate	Product	Yield (%)
1	 <b>40</b>	 , <b>41</b>	94
2 <sup>b</sup>	 <b>42</b>	 , <b>43</b>	62
3	 <b>44</b>	 , <b>45</b>	78
4 <sup>b</sup>	 <b>46</b>	 , <b>47</b>	95
5	 <b>48</b>	 , <b>49</b>	97
6 <sup>c</sup>	 <b>50</b>	 , <b>51</b>	43
7	 <b>52</b>	 <b>53a</b> +  <b>53b</b> (3.3:1)	97
8	 <b>54</b>	 , <b>55</b> (1:1)	99

<sup>a</sup>All reactions were performed on a 0.6 mmol scale at a concentration of 50 mM. <sup>b</sup>Reaction performed in CH<sub>2</sub>Cl<sub>2</sub> <sup>c</sup>Reaction performed in CH<sub>3</sub>CN/H<sub>2</sub>O

In order to demonstrate that the developed method was applicable to more complex structures, the total synthesis of ( $\pm$ )- $\gamma$ -lycorane, an Amaryllidaceae alkaloid, was undertaken. This natural product contains an interesting pentacyclic ring system (Figure 3.3). Although ( $\pm$ )- $\gamma$ -lycorane itself does not exhibit any biological properties, it is often synthesized as a route to more active lycorine alkaloids.<sup>15</sup>

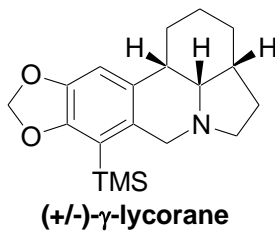
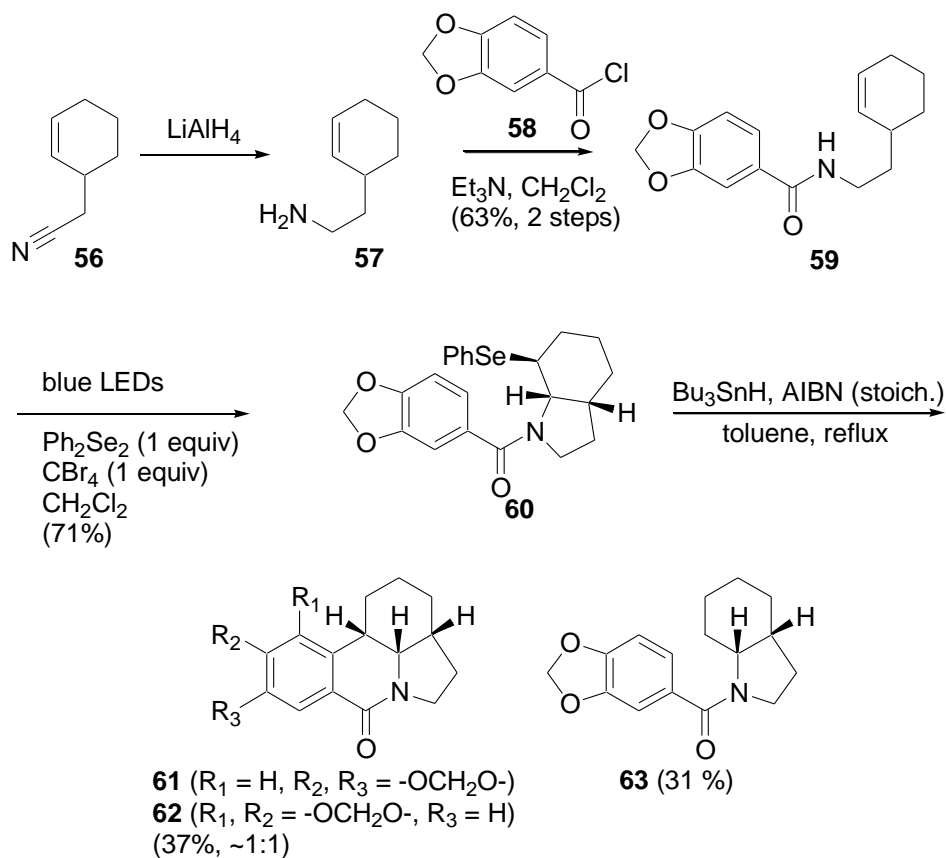


Figure 3.3 ( $\pm$ )- $\gamma$ -lycorane

The first step in the synthesis involves the reduction of the known nitrile **56** to amine **57**.<sup>20</sup> The amine **57** was then coupled with commercially available piperonyl chloride **58** using triethylamine in dichloromethane to form amide **59** in 63% yield over 2 steps. The standard conditions for the developed visible light-promoted selenocyclization method were then applied to amide **59**. The solvent that gave the best yield for this reaction was determined to be dichloromethane, which produced the desired perhydroindole **60** in 71% yield. The stereochemistry for this cyclized product was confirmed by 2D NMR (COSY and ROESY). The COSY NMR experiment did not show any correlation between the two bridging hydrogen atoms, while the ROESY NMR illustrated a strong correlation between the previously mentioned hydrogen atoms. Both of these results confirm the anti addition of the amide onto the formed seleniranium intermediate to give the cis-fused ring system **60** illustrated in Scheme 3.8. In the next step in the synthesis of ( $\pm$ )- $\gamma$ -lycorane, tributyltin hydride and AIBN were reacted with phenyl selenide to produce the carbon-centered radical intermediate which would cyclize onto the aromatic ring. Unfortunately, the amide **63**, a result of the carbon-centered radical

abstracting a hydrogen from tributyltin hydride, formed in 31% yield. Also, the cyclization of the radical intermediate onto the aromatic ring was not site-selective, giving the two regioisomers **61** and **62** as an inseparable 1:1 mixture with a combined yield of 37%.

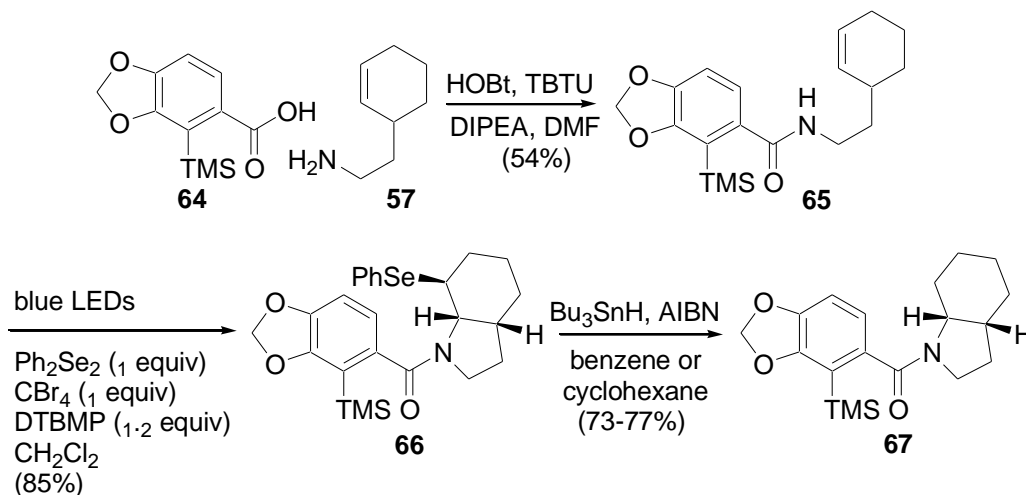


Scheme 3.8 First attempt at the synthesis of ( $\pm$ )- $\gamma$ -lycorane

To remedy this selectivity issue, a TMS protecting group was added to the aromatic ring to form the blocked substrate **64** (Scheme 3.9). This protection was achieved via a directed ortho metalation.<sup>16</sup> The TMS-protected carboxylic acid **64** was coupled with amine **57** using HOBT, TBTU and DIPEA in dichloromethane to form the TMS-protected amide **65** in 54% yield. When attempts were made to cyclize the amine onto the cyclohexene ring using the developed selenocyclization method in dichloromethane, the desired phenyl selenide **66** was not produced.

Although cyclization was observed, it was determined that the HBr generated in situ was leading to the protidesilylation and removal of the TMS-protecting group.

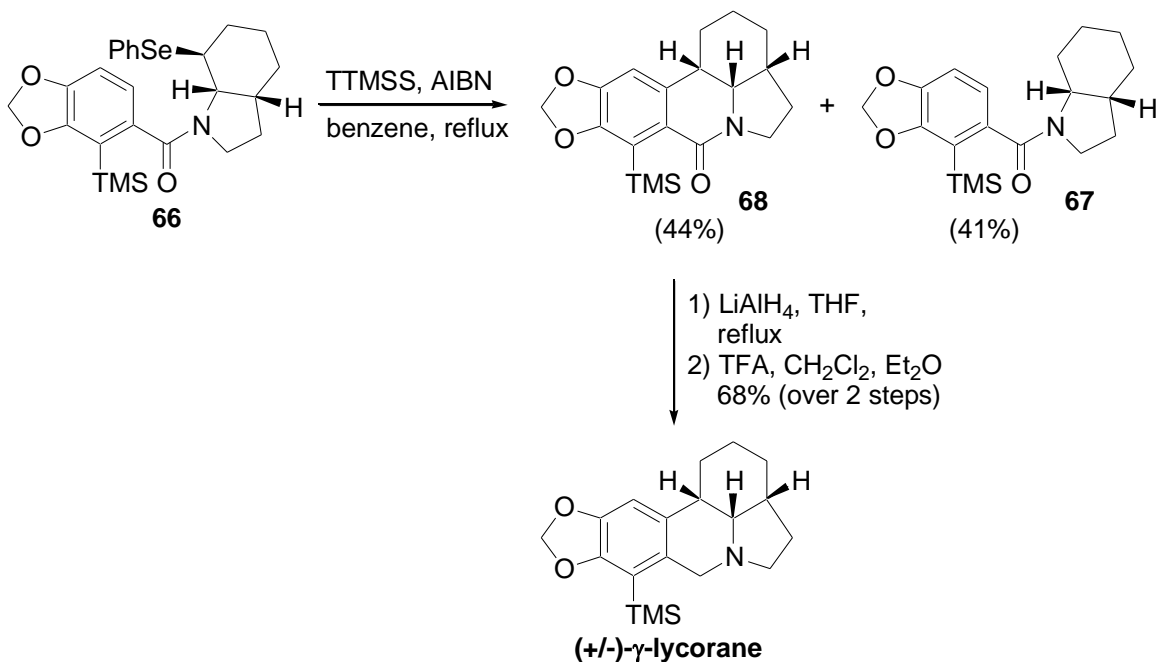
To neutralize any acid formed during the course of the reaction, 1.2 equivalents of 2,6-di-tert-butyl-4-methylpyridine (DTBMP) was added. After addition of base, the reaction proceeded smoothly to give the cyclized product **66** in 85% yield. The tin-promoted cyclization of **66** mainly produced small amounts of cyclized product **68** (Scheme 3.10), but mainly forming the hydrogen abstraction product **67** in yields ranging from 73% to 77%, depending upon the solvent used. Various changes were made to the reaction conditions to increase the yield of the cyclized product and decrease the amount of hydrogen abstraction. For example, both benzene and cyclohexane were utilized as solvents, but both led to the major hydrogen abstraction product. Slow addition of AIBN via syringe pump and varying the concentration of the phenyl selenide **66** were also attempted, with no increase in desired cyclized product **68**.



Scheme 3.9 Addition of TMS-protecting group

The undesired amide **67** was assumed to be the product of the abstraction of hydrogen from tributyltin hydride by the carbon-centered radical intermediate. Surmising that tributyltin hydride was too reactive as a hydrogen donor, TTMSS, a much less reactive species, was used as

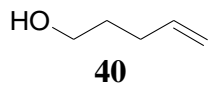
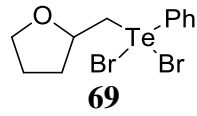
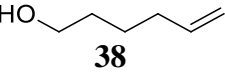
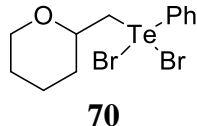
an alternative.<sup>17</sup> When this reagent was used in combination with AIBN, a separable mixture of the desired cyclized product (**68**) and the hydrogen abstraction product (**67**) was formed. To improve the yield of the cyclized product **68**, several solvent systems were pursued. The solvents chosen for the screen were toluene, cyclohexane and benzene which gave the corresponding yields of 15%, 22% and 44% of the cyclized product **68**. Once again, slow addition of the AIBN via syringe pump and varying the concentration were also attempted to decrease the amount of hydrogen abstraction product formed. Neither of these methods was successful in increasing the yield of cyclization. In the final two steps in the synthesis of ( $\pm$ )- $\gamma$ -lycorane, the amide was transformed into the amine via the reduction of the ketone by lithium aluminum hydride and then submitted to acidic conditions (TFA) to remove the TMS group to produce ( $\pm$ )- $\gamma$ -lycorane in 68% yield. Overall, the Amaryllidaceae alkaloid was synthesized in 3.4% yield over 7 steps.



Scheme 3.10 TTMSS as radical initiator

After the synthesis of ( $\pm$ )- $\gamma$ -lycorane, the developed visible light-promoted selenofunctionalization method was applied towards other systems. Tellurocyclizations were attempted via the irradiation of alkenols with diphenyl ditelluride and tetrabromomethane. At first, methanol was used as solvent for both the cyclization of 4-penten-1-ol and 5-penten-1-ol, as it was the solvent of choice for selenofunctionalizations. However, this gave no desired cyclic ether product. Dichloromethane was then used as an alternative solvent with success. Although the yields were decreased and the reaction times were increased from those of selenofunctionalization, tellurocyclization products were formed. With 4-penten-1-ol as the substrate, the desired product was formed in 75% yield over 47 h (Entry 1). The structure of compound **69** was confirmed by X-ray crystallography to be the dibromotelluride. When 5-hexen-1-ol was submitted to the same conditions with dichloromethane as solvent, the cyclic ether was again formed in 53% yield over the course of 44 h of irradiation (Entry 2). The dibromotelluride **69** was reduced to the telluride with sodium borohydride in ethanol to give the desired product in 99% yield.

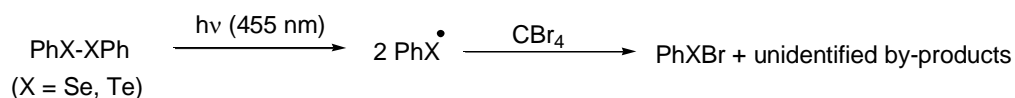
Table 3.3 Visible light-promoted tellurofunctionalization

Entry	Substrate	Reaction Time (h)	Product	Yield (%)
1	 <b>40</b>	47	 <b>69</b>	75
2	 <b>38</b>	44	 <b>70</b>	53

<sup>a</sup>Reactions were performed on a 0.6 mmol scale at a concentration of 50 mM.

As demonstrated by  $^{77}\text{Se}$  NMR, phenylselenenyl bromide is generated *in situ* during the course of the selenocyclization reactions. We proposed that the formation of this reactive species was due to the visible light-promoted homolysis of the Se-Se bond to generate two phenyl selenide radicals. These phenyl selenide radicals then would abstract a bromine atom from tetrabromomethane to form phenylselenenyl bromide. In order to determine the mechanism by which phenylselenenyl bromide was generated, Gaussian 2009 calculations were performed by Ranelka Fernando (Stanley group, LSU Department of Chemistry) who demonstrated that the phenyl selenide radical abstraction of bromine from tetrabromomethane was favorable by -9.3 kcal/mol (Scheme 3.11). The fate of the by-product tribromomethyl radical was studied as well. Some research suggests that the tribromomethyl radical can react to form tetrabromoethylene. In order to test this theory within the realms of our reaction conditions, diphenyl diselenide was irradiated with tetrabromomethane in both methanol and dichloromethane. GC-MS analysis of the resulting reaction mixture did not show any evidence of tetrabromoethylene in solution. The fate of the putative tribromomethyl radical is unknown.

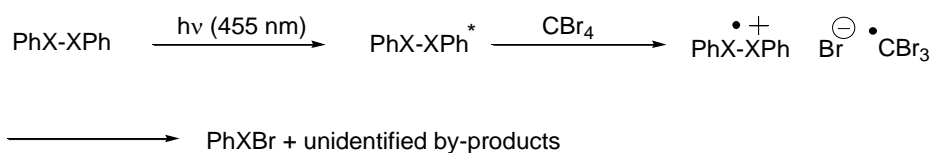
Mechanism 1: Homolysis



6-311G\*\* calculations:



Mechanism 2: Photoinitiated Electron Transfer



Scheme 3.11 Mechanistic considerations



A year after this work on seleno- and tellurofunctionalization was published, Xu and coworkers demonstrated a potential mechanistic pathway resulting from the visible light irradiation of diselenides.<sup>18</sup> In this study, it was concluded that scrambling occurred when a diaryl diselenide and dialkyl diselenide were irradiated, providing evidence towards the visible light-promoted Se-Se bond homolysis theory.

### 3.3 Conclusions

In this project, a method was developed for the visible light-promoted seleno- and tellurofunctionalization of alkenes. The method utilized mild, stable reagents with inexpensive experimental setups. Optimization of the developed method was accomplished by screening solvents, bromine sources, concentrations and light sources using 4-penten-1-ol as the starting material. The best reaction conditions were the irradiation of the starting material with diphenyl diselenide and tetrabromomethane as bromine source in methanol at a concentration of 50 mM. The reaction proceeds under aerobic conditions, without any negative effects on yield. To prove that selenofunctionalization was possible with a wide variety of substrates, starting materials with different nucleophiles and chain lengths were irradiated under the optimized conditions to give the desired functionalized products in good to excellent yields ranging from 43% to 99%. The developed method was then applied to the total synthesis of Amaryllidaceae alkaloid, ( $\pm$ )- $\gamma$ -lycorane, which was made in 3.4% yield in 7 steps from the commercially available starting material. The key visible light-promoted selenocyclization reaction proceeded in excellent yield (85%), and the stereochemistry was confirmed using 2D NMR (ROESY and COSY). Next, tellurocyclization was explored. Using 4-penten-1-ol and 6-hexen-1-ol as substrates, the desired cyclized products **40** and **38** were isolated in mediocre yields. Attempts at generating the carbon-centered radical via C-Te bond cleavage were unsuccessful.

The reactive species present in the selenofunctionalization reactions was PhSeBr. In order to determine the mechanism by which PhSeBr was generated, computational studies were performed. Computational data using Gaussian 2009 calculations demonstrated that the Se-Se bond homolysis followed by selenide radical abstraction of bromine was favorable by -9.3 kcal/mole. Xu and coworkers demonstrated the feasibility of diselenide radicals through homolysis.

### **3.4 Experimental**

#### **3.4.1 General Methods**

Flash column chromatography was performed using BDH 60Å silica gel. <sup>1</sup>H NMR and <sup>13</sup>C NMR spectroscopy were performed on a Bruker AV-400, DPX 400 or DPX 250 spectrometer. Mass spectra were obtained using an Agilent 6210 electrospray time-of-flight mass spectrometer. Unless otherwise noted, all materials were obtained from commercial suppliers and used without further purification. Analytical TLC was conducted on aluminum-backed sheets (Merck, silica gel 60, F254). Compounds were visualized by UV absorption (254 nm) and staining with anisaldehyde or KMnO<sub>4</sub>. Deuterated solvents were obtained from Cambridge Isotope Labs. All solvents except MeOH, <sup>i</sup>PrOH and EtOH were purified according to the method of Grubbs.<sup>19</sup> MeOH, <sup>i</sup>PrOH and EtOH were obtained from Sigma-Aldrich®. Diffraction data were obtained on a Bruker Kappa Apex-II DUO diffractometer using a graphite monochromated Mo K $\alpha$  radiation.

#### **3.4.2 Experimental Setup**

The experimental setup and reaction conditions for the seleno- and tellurofunctionalization transformations were simple. Blue LEDs were purchased from Creative Lighting Solutions at a low cost and wrapped around the exterior of an evaporating dish. The

reaction flasks were placed directly up against the light and stirred vigorously. Since air did not have any effect on yield, a septum was placed on the reaction vial under air just to eliminate the possibility of stray particles from falling into the reaction. The solution temperature stayed within the range 25-29 °C, demonstrating that adventitious heating by the LEDs was not responsible for any reactivity of the reaction. There was no workup for the seleno- and tellurofunctionalizations. Once the reaction was complete by TLC, the solvent was removed *in vacuo*.



Figure 3.4: Experimental setup

### 3.4.3 Procedures and Characterization

Representative procedure for selenocyclization – synthesis of **39**:

To a round bottom flask containing 199.0 mg (0.6000 mmol) of tetrabromomethane and 187.3 mg (0.6000 mmol) diphenyl diselenide in 12.0 mL CH<sub>3</sub>OH was added 72 μL (0.60 mmol) **38** at once. The reaction was placed approximately 5 mm from the irradiation source (blue LEDs – see Figure 3.4) and allowed to stir under irradiation for 4 h when complete conversion of starting alcohol was observed by TLC. The crude reaction mixture was then concentrated *in*

*vacuo*. Silica gel chromatography (silica gel, gradient run from 100% hexanes to 10% ethyl acetate in hexanes) afforded 149.5 mg (98%) of a pale yellow oil. <sup>1</sup>H NMR (400 MHz, CDCl<sub>3</sub>): δ 7.50 (m, 2H), 7.22 (m, 3H), 4.00 (m, 1H), 3.44 (m, 2H), 3.06 (dd, J = 12.2, 6.9 Hz, 1H), 2.92 (dd, J = 12.1, 5.6 Hz, 1H), 1.78 (m, 2H), 1.51 (m, 3H), 1.31 (m, 1H); <sup>13</sup>C NMR (100 MHz, CDCl<sub>3</sub>): δ 132.5, 130.9, 129.1, 126.8, 77.2, 68.8, 33.8, 31.9, 25.9, 23.5; HRMS m/z calcd for C<sub>12</sub>H<sub>17</sub>OSe (M+H)<sup>+</sup> 257.0433, found 257.0445.

#### Synthesis of **41**:

Started with 199.0 mg (0.6000 mmol) tetrabromomethane, 187.3 mg (0.6000 mmol) diphenyl diselenide and 62 μL (0.60 mmol) **40** in 12.0 mL CH<sub>3</sub>OH. Irradiated for 3.5 h. Solvent was then removed *in vacuo*. Silica gel chromatography (silica gel, gradient run from 100% hexanes to 10% ethyl acetate in hexanes) afforded 135.7 mg (94%) of a colorless oil. <sup>1</sup>H NMR (400 MHz, CDCl<sub>3</sub>): δ 7.52 (m, 2H), 7.24 (m, 3H), 4.09 (quintet, J = 6.7 Hz, 1H), 3.91 (m, 1H), 3.76 (m, 1H), 3.12 (dd, J = 12.1, 5.8 Hz, 1H), 2.99 (dd, J = 12.2, 6.8 Hz, 1H), 2.06 (m, 1H), 1.91 (m, 2H), 1.62 (m, 1H); <sup>13</sup>C NMR (100 MHz, CDCl<sub>3</sub>): δ 132.5, 130.3, 129.0, 126.8, 78.3, 68.3, 33.0, 31.5, 25.9; HRMS m/z calcd for C<sub>11</sub>H<sub>15</sub>OSe (M+H)<sup>+</sup> 243.0276, found 243.0283.

#### Synthesis of **43**:

Started with 199.0 mg (0.6000 mmol) tetrabromomethane, 187.3 mg (0.6000 mmol) diphenyl diselenide and 111.0 mg (0.6000 mmol) **42** in 12.0 mL CH<sub>2</sub>Cl<sub>2</sub>. Irradiated for 3.5 h. Solvent was then removed *in vacuo*. Silica gel chromatography (silica gel, gradient run from 100% hexanes to 10% ethyl acetate in hexanes) afforded 127.2 mg (62%) of a colorless oil. <sup>1</sup>H NMR (400 MHz, CD<sub>3</sub>CN, 343K): δ 7.59 (m, 2H), 7.30 (m, 3H), 4.01 (m, 1H), 3.36 (m, 3H), 2.98 (dd, J = 12.0, 9.4 Hz, 1H), 2.07 (m, 1H), 1.91 (m, 2H), 1.79 (m, 1H), 1.43 (s, 9H); <sup>13</sup>C NMR

(125 MHz, (CD<sub>3</sub>)<sub>2</sub>SO):  $\delta$  153.2, 131.4, 129.7, 128.8, 126.3, 78.3, 56.5, 46.3, 30.9, 30.0, 27.9, 22.4; HRMS m/z calcd for C<sub>16</sub>H<sub>24</sub>NO<sub>2</sub>Se (M+H)<sup>+</sup> 342.0967, found 342.0985.

#### Synthesis of **45**:

Started with 199.0 mg (0.6000 mmol) tetrabromomethane, 187.3 mg (0.6000 mmol) diphenyl diselenide and 85.9 mg (0.600 mmol) **44** in 12.0 mL CH<sub>2</sub>Cl<sub>2</sub>. Irradiated for 7 h. Solvent was then removed *in vacuo*. Silica gel chromatography (silica gel, gradient run from 100% hexanes to 30% ethyl acetate in hexanes) afforded 138.7 mg (78%) of a colorless oil. <sup>1</sup>H NMR (400 MHz, CDCl<sub>3</sub>, 329K):  $\delta$  7.56 (m, 2H), 7.25 (m, 3H), 4.08 (m, 1H), 3.66 (s, 3H), 3.42 (m, 3H), 2.90 (m, 1H), 2.03 (m, 1H), 1.91 (m, 2H), 1.80 (m, 1H); <sup>13</sup>C NMR (100 MHz, CDCl<sub>3</sub>, 329K):  $\delta$  155.6, 132.4, 130.5, 129.2, 126.9, 57.9, 52.30, 52.26, 47.2, 30.9, 23.6; HRMS m/z calcd for C<sub>13</sub>H<sub>18</sub>NO<sub>2</sub>Se (M+H)<sup>+</sup> 300.0498, found 300.0497.

#### Synthesis of **47**:

Started with 199.0 mg (0.6000 mmol) tetrabromomethane, 187.0 mg (0.6000 mmol) diphenyl diselenide and 61  $\mu$ L (0.60 mmol) **46** in 12.0 mL CH<sub>2</sub>Cl<sub>2</sub>. Irradiated for 4 h. Solvent was then removed *in vacuo*. Silica gel chromatography (silica gel, gradient run from 100% hexanes to 50% ethyl acetate in hexanes) afforded 146.5 mg (95%) of a colorless oil. <sup>1</sup>H NMR (400 MHz, CDCl<sub>3</sub>):  $\delta$  7.54 (m, 2H), 7.28 (m, 3H), 4.65 (m, 1H), 3.28 (dd, J = 12.8, 4.8 Hz, 1H), 3.01 (dd, J = 12.8, 7.9 Hz, 1H), 2.49 (m, 3H), 1.95 (m, 1H); <sup>13</sup>C NMR (100 MHz, CDCl<sub>3</sub>):  $\delta$  176.7, 133.4, 129.5, 129.0, 127.8, 79.5, 32.0, 28.9, 27.8; HRMS m/z calcd for C<sub>11</sub>H<sub>13</sub>O<sub>2</sub>Se (M+H)<sup>+</sup> 257.0075, found 257.0071.

#### Synthesis of **49**:

Started with 199.0 mg (0.6000 mmol) tetrabromomethane, 187.3 mg (0.6000 mmol) diphenyl diselenide and 61  $\mu$ L (0.60 mmol) **48** in 12.0 mL CH<sub>3</sub>OH. Irradiated for 17 h. Solvent

was then removed *in vacuo*. Silica gel chromatography (silica gel, gradient run from 100% hexanes to 10% ethyl acetate in hexanes) afforded 157.3 mg (97%) of a colorless oil.  $^1\text{H}$  NMR (400 MHz,  $\text{CDCl}_3$ ):  $\delta$  7.58 (m, 2H), 7.24 (m, 3H), 3.36 (s, 3H), 3.26 (m, 1H), 3.16 (m, 1H), 2.13 (m, 1H), 1.99 (m, 1H), 1.71 (m, 1H), 1.58 (m, 1H), 1.49 (m, 1H), 1.27 (m, 3H);  $^{13}\text{C}$  NMR (100 MHz,  $\text{CDCl}_3$ ):  $\delta$  135.3, 129.0, 128.8, 127.4, 82.2, 26.4, 47.4, 32.1, 30.3, 25.8, 23.5; HRMS  $m/z$  calcd for  $\text{C}_{12}\text{H}_{15}\text{Se}$  ( $\text{M} - \text{OMe}$ ) $^+$  239.0333, found 239.0338.

#### Synthesis of **51**:

Started with 199.0 mg (0.6000 mmol) tetrabromomethane, 187.3 mg (0.6000 mmol) diphenyl diselenide, 13  $\mu\text{L}$  (0.72 mmol)  $\text{H}_2\text{O}$  and 61  $\mu\text{L}$  (0.60 mmol) **50** in 12.0 mL  $\text{CH}_3\text{CN}$ . Irradiated for 12 days. Solvent was then removed *in vacuo*. Silica gel chromatography (silica gel, gradient run from 20% EtOAc in hexanes to 100% EtOAc) afforded 76.6 mg (43%) of a colorless oil.  $^1\text{H}$  NMR (400 MHz,  $\text{CDCl}_3$ ):  $\delta$  7.57 (m, 2H), 7.28 (m, 3H), 5.71 (d,  $J = 7.3$  Hz), 3.82 (m, 1H), 3.03 (td,  $J = 11.2, 3.7$  Hz, 1H), 2.14 (m, 2H), 1.91 (s, 3H), 1.67 (m, 2H), 1.52 (dq,  $J = 12.2, 3.0$  Hz, 1H), 1.27 (m, 3H);  $^{13}\text{C}$  NMR (62.5 MHz,  $\text{CDCl}_3$ ):  $\delta$  169.2, 135.3, 128.9, 128.2, 127.7, 53.1, 47.8, 40.0, 33.7, 26.6, 24.5, 23.3; HRMS  $m/z$  calcd for  $\text{C}_{14}\text{H}_{20}\text{NOSe}$  ( $\text{M} + \text{H}$ ) $^+$  292.0764, found 292.0746.

#### Synthesis of **53a** and **53b**:

Started with 199.0 mg (0.6000 mmol) tetrabromomethane, 187.3 mg (0.6000 mmol) diphenyl diselenide and 74  $\mu\text{L}$  (0.60 mmol) **52** in 12.0 mL  $\text{CH}_3\text{OH}$ . Irradiated for 7 h. Solvent was then removed *in vacuo*. Silica gel chromatography (silica gel, gradient run from 100% hexanes to 10% ethyl acetate in hexanes) afforded 157.6 mg (97%) of a colorless oil. (\* indicates signals for minor isomer)  $^1\text{H}$  NMR (400 MHz,  $\text{CDCl}_3$ ) (mixture of regioisomers):  $\delta$  7.55\* (m, 2H), 7.51 (dd,  $J = 1.7, 7.3$  Hz, 2H), 7.22 (m, 3H), 3.51\* (m, 2H), 3.35 (m, 1H), 3.32 (s,

3H), 3.31\* (s, 3H), 3.29\* (m, 1H); 3.09 (dd, J = 12.2, 5.5 Hz, 1H), 2.99 (dd, J = 12.2, 6.1 Hz, 1H), 1.82\* (m, 1H), 1.57 (m, 2H), 1.35 (m, 4H), 0.88 (m, 3H); <sup>13</sup>C NMR (100 MHz, CDCl<sub>3</sub>) (mixture of regioisomers): δ 134.8\*, 132.6, 130.8, 129.05, 128.95\*, 127.5\*, 126.8, 80.5, 75.9\*, 58.70\*, 56.95, 44.9\*, 33.6, 31.99, 31.96\*, 29.9\*, 27.4, 22.77, 22.59\*, 14.1, 14.0\*; HRMS m/z calcd for C<sub>12</sub>H<sub>17</sub>Se (M - OMe)<sup>+</sup> 241.0490, found 241.0493.

#### Synthesis of **55**:

Started with 199.0 mg (0.6000 mmol) tetrabromomethane, 187.3 mg (0.6000 mmol) diphenyl diselenide and 73 μL (0.60 mmol) **54** in 12.0 mL CH<sub>3</sub>OH. Irradiated for 4 h. Solvent was then removed *in vacuo*. Silica gel chromatography (silica gel, gradient run from 100% hexanes to 10% ethyl acetate in hexanes) afforded 152.8 mg (99%) of a colorless oil. <sup>1</sup>H NMR (400 MHz, CDCl<sub>3</sub>) (1:1 mixture of diastereomers): δ 7.51 (m, 4H), 7.22 (m, 6H), 4.19 (m, 2H), 4.02 (m, 2H), 3.14 (dd, J = 12.1, 5.3 Hz, 2H), 2.96 (m, 2H), 2.05 (m, 4H), 1.67 (m, 2H), 1.47 (m, 2H), 1.23 (d, J = 6.0 Hz, 3H), 1.19 (d, 6.1 Hz, 3H); <sup>13</sup>C NMR (100 MHz, CDCl<sub>3</sub>) (1:1 mixture of diastereomers): δ 132.5, 132.4, 130.5, 130.3, 129.0, 126.80, 126.76, 78.5, 77.9, 76.1, 75.4, 34.0, 33.5, 33.4, 33.0, 32.4, 31.5, 21.4, 21.3; HRMS m/z calcd for C<sub>12</sub>H<sub>17</sub>OSe (M+H)<sup>+</sup> 257.0439, found 257.0445.

#### Synthesis of **56**<sup>20</sup>

#### Synthesis of **59**:

To a round bottom flask containing 367.2 mg (3.030 mmol) **56** in 5 mL Et<sub>2</sub>O at 0°C was added 4.6 mL (4.6 mmol) LiAlH<sub>4</sub> (1.0 M in Et<sub>2</sub>O) dropwise. Reaction was allowed to stir under N<sub>2</sub> at room temperature for 5 h when complete conversion of starting nitrile was observed on TLC. Reaction was once again cooled to 0°C. To the reaction mixture was added dropwise, in succession, 7 mL Et<sub>2</sub>O, 0.18 mL deionized water, 0.18 mL 10 N NaOH, then 0.53 mL deionized

water. The reaction was then allowed to stir at room temperature for 1.5 h to ensure complete quenching of excess  $\text{LiAlH}_4$ . The resulting aluminum salts were filtered off and the filter cake was washed with  $\text{Et}_2\text{O}$ . The filtrate was dried over  $\text{Na}_2\text{SO}_4$ , filtered and carefully concentrated *in vacuo* to avoid loss of volatile amine product **57**. The resulting amine **57** was added to a round bottom flask containing 0.83 mL (6.0 mmol)  $\text{Et}_3\text{N}$  in 10 mL  $\text{CH}_2\text{Cl}_2$  at room temperature. To this mixture was added 1.006 g (5.450 mmol) **58** in 15 mL  $\text{CH}_2\text{Cl}_2$  at once. The reaction was allowed to stir under  $\text{N}_2$  at room temperature for 2 h when amine **57** was completely consumed as judged by TLC. To the reaction mixture was added 15 mL  $\text{H}_2\text{O}$  and brought to a  $\text{pH} > 11$  with the dropwise addition of 1M  $\text{K}_2\text{CO}_3$ . The aqueous layer was separated from the organic layer and then extracted with 4x15mL  $\text{CH}_2\text{Cl}_2$ . The resulting organic extracts were dried over  $\text{Na}_2\text{SO}_4$ , filtered and concentrated *in vacuo*. Silica gel chromatography (silica gel, gradient run from 70%  $\text{CH}_2\text{Cl}_2$  in hexanes to 15%  $^i\text{PrOH}$  in  $\text{CH}_2\text{Cl}_2$ ) afforded 515.9 mg (62% over 2 steps) of a colorless oil.  $^1\text{H}$  NMR (400 MHz,  $\text{CDCl}_3$ ):  $\delta$  7.28 (m, 2H), 6.80 (d,  $J = 7.8$  Hz, 1H), 6.17 (m, 1H), 6.01 (s, 2H), 5.71 (m, 1H), 5.58 (m, 1H), 3.49 (dt,  $J = 7.36, 5.72$  Hz, 2H), 2.18 (m, 1H), 1.98 (m, 2H), 1.82 (m, 1H), 1.73 (m, 1H), 1.58 (m, 3H), 1.28 (m, 1H);  $^{13}\text{C}$  NMR (100 MHz,  $\text{CDCl}_3$ ):  $\delta$  166.9, 150.3, 148.1, 131.2, 129.2, 127.9, 121.5, 108.1, 107.8, 101.8, 38.1, 36.2, 33.2, 29.0, 25.4, 21.5; HRMS  $m/z$  calcd for  $\text{C}_{16}\text{H}_{20}\text{NO}_3$  ( $\text{M}+\text{H}$ ) $^+$  274.1438, found 274.1440.

#### Synthesis of **60**:

Started with 36.5 mg (0.110 mmol) tetrabromomethane, 34.3 mg (0.110 mmol) diphenyl diselenide and 30.1 mg (0.110 mmol) **59** in 2.2 mL  $\text{CH}_2\text{Cl}_2$ . Irradiated for 2 days. Solvent was then removed *in vacuo*. Silica gel chromatography (silica gel, gradient run from 100% hexanes to 40% ethyl acetate in hexanes) afforded 33.4 mg (71%) of a pale yellow oil.  $^1\text{H}$  NMR (400 MHz,  $\text{CDCl}_3$ ):  $\delta$  7.69 (m, 2H), 7.26 (m, 3H), 7.03 (d,  $J = 7.0$  Hz, 1H), 6.99 (s, 1H), 6.79 (d,  $J =$



8.0 Hz, 1H), 5.99 (d, J = 1.4 Hz, 2H), 4.52 (m, 1 H), 3.70 (m, 2H), 3.37 (m, 1H), 2.43 (m, 1H), 1.98 (m, 1H), 1.84 (m, 2H), 1.56 (m, 5H);  $^{13}\text{C}$  NMR (100 MHz,  $\text{CDCl}_3$ ):  $\delta$  170.7, 149.1, 147.4, 134.5, 131.0, 129.5, 128.8, 127.1, 122.3, 108.5, 107.8, 101.2, 61.4, 48.0, 43.2, 37.1, 30.7, 28.1, 26.1, 21.3; HRMS m/z calcd for  $\text{C}_{22}\text{H}_{24}\text{NO}_3\text{Se}$  ( $\text{M}+\text{H}$ ) $^+$  430.0916, found 430.0902.

#### Synthesis of **61** and **62**:

To a round bottom flask containing 13.2 mg (0.0306 mmol) selenide **60** in 1.57 mL anhydrous toluene was added 16.7  $\mu\text{L}$  (0.0621 mmol)  $\text{Bu}_3\text{SnH}$  and 0.26 mg (0.0016 mmol – 0.13 mL taken from previously freeze-pump-thawed stock solution of 3.9 mg AIBN in 2 mL anhydrous toluene) AIBN. The reaction mixture was freeze-pump-thawed three times and allowed to stir at reflux under  $\text{N}_2$ . After 6, 24 and 32 h, 0.26 mg (0.0016 mmol – 0.13 mL taken from previously mentioned degassed stock solution) AIBN was added. The reaction was stopped after 48 h and concentrated *in vacuo* when complete consumption of starting selenide was observed on TLC. Solvent was then removed *in vacuo*. Silica gel chromatography (silica gel, gradient run from 100% hexanes to 40% EtOAc in hexanes) afforded 3.1 mg (37%) of a 1:1 mixture of regioisomers **61** and **62**.  $^1\text{H}$  NMR data matched with spectrum kindly provided by S. Z. Zard.<sup>21</sup> HRMS m/z calcd for  $\text{C}_{16}\text{H}_{18}\text{NO}_3$  ( $\text{M}+\text{H}$ ) $^+$  272.1281, found 272.1279.

#### Synthesis of **64**<sup>22</sup>

#### Synthesis of **65**:

To a solution containing 50.1 mg (0.210 mmol) carboxylic acid **64** in 2.0 mL 20% DIPEA/ 80% DMF was added 32.2 mg (0.210 mmol) HOBt and 67.4 mg (0.210 mmol) TBTU at once. The reaction was allowed to stir at room temperature for 30 mins. To the reaction mixture was then added 26.3 mg (0.210 mmol) amine **57** in 1 mL 18% DIPEA/82% DMF dropwise. The reaction was allowed to stir under  $\text{N}_2$  at room temperature for 5 h when complete conversion of

starting materials were observed by  $^1\text{H}$  NMR of a reaction aliquot. To the reaction mixture was added 5 mL  $\text{H}_2\text{O}$  and 10 mL  $\text{Et}_2\text{O}$ . The aqueous layer was separated from the organic layer and then extracted with 4x10 mL  $\text{Et}_2\text{O}$ . The resulting organic extracts were dried over  $\text{Na}_2\text{SO}_4$ , filtered and concentrated *in vacuo*. Silica gel chromatography (silica gel, gradient run from 20%  $\text{CH}_2\text{Cl}_2$  in hexanes to 100%  $\text{CH}_2\text{Cl}_2$  and 10%  $\text{EtOAc}$  in  $\text{CH}_2\text{Cl}_2$  to 100%  $\text{EtOAc}$ ) afforded 39.4 mg (54%) of a white solid.  $^1\text{H}$  NMR (400 MHz,  $\text{CDCl}_3$ ):  $\delta$  6.91 (d,  $J = 7.8$  Hz, 1H), 6.73 (d,  $J = 7.8$  Hz, 1H), 5.93 (s, 2H), 5.80 (m, 1H), 5.71 (m, 1H), 5.57 (m, 1H), 3.45 (dt,  $J = 7.3, 5.7$  Hz, 2H), 2.19 (m, 1H), 1.99 (m, 2H), 1.83 (m, 1H), 1.62 (m, 4H), 1.28 (m, 1H) 0.33 (s, 9H);  $^{13}\text{C}$  NMR (100 MHz,  $\text{CDCl}_3$ ):  $\delta$  170.7, 153.3, 147.5, 136.9, 130.9, 127.8, 120.8, 118.7, 108.0, 100.3, 37.9, 35.9, 32.9, 28.8, 25.2, 21.3, 0.52; HRMS  $m/z$  calcd for  $\text{C}_{19}\text{H}_{28}\text{NO}_3\text{Si}$  ( $\text{M}+\text{H}$ ) $^+$  346.1833, found 346.1832.

#### Synthesis of **66**:

Started with 46.4 mg (0.140 mmol) tetrabromomethane, 43.7 mg (0.1400 mmol) diphenyl diselenide, 34.9 mg (0.170 mmol) DTBMP and 48.7 mg (0.141 mmol) **65** in 4.0 mL  $\text{CH}_2\text{Cl}_2$ . Irradiated for 3 days. Silica gel chromatography (silica gel, gradient run from 100% hexanes to 20% ethyl acetate in hexanes) afforded 59.8 mg (85%) of a yellow oil.  $^1\text{H}$  NMR (400 MHz,  $\text{CDCl}_3$ ):  $\delta$  7.65 (m, 2H), 7.25 (m, 3H), 6.73 (m, 2H), 5.923 (d,  $J = 12.2$  Hz, 1H), 5.920 (d,  $J = 12.3$  Hz, 1H), 4.43 (dd,  $J = 8.4, 6.1$  Hz, 1H), 3.74 (td,  $J = 9.2, 3.5$  Hz, 1H), 3.55 (m, 1H), 3.28 (m, 1H), 2.46 (m, 1H), 1.97 (m, 1H), 1.85 (m, 2H), 1.60 (m, 5H), 0.30 (s, 9H);  $^{13}\text{C}$  NMR (100 MHz,  $\text{CDCl}_3$ ):  $\delta$  172.4, 153.0, 146.6, 136.7, 134.0, 130.0, 128.9, 126.9, 121.1, 117.6, 108.3, 100.2, 60.1, 48.4, 43.2, 37.2, 31.1, 27.7, 26.0, 21.6, 0.16; HRMS  $m/z$  calcd for  $\text{C}_{25}\text{H}_{32}\text{NO}_3\text{SeSi}$  ( $\text{M}+\text{H}$ ) $^+$  502.1318, found 502.1313.

#### Synthesis of **67** and **68**:

To a round bottom flask containing 9.9 mg (0.020 mmol) selenide **66** in 5.5 mL benzene was added 7.4  $\mu$ L (0.024 mmol) TTMS and 1.6 mg (0.0097 mmol) AIBN. The reaction mixture was freeze-pump-thawed three times and allowed to stir at reflux under N<sub>2</sub>. After 5 h, another 1.6 mg (0.0097 mmol) AIBN was added, and reaction mixture was once again freeze-pump-thawed three times and brought to reflux. The reaction was allowed to stir at reflux for an additional 15 h and concentrated *in vacuo* when complete consumption of starting selenide was observed on TLC. Silica gel chromatography (silica gel, gradient run from 100% hexanes to 10% EtOAc in hexanes) afforded 2.8 mg (41%) of **67** and 3.0 mg (44%) of **68**.

Characterization for **67**: <sup>1</sup>H NMR (400 MHz, CDCl<sub>3</sub>) (mixture of rotamers):  $\delta$  6.76 (m, 2H), 6.71 (m, 2H), 5.94 (d, J = 2.0 Hz, 2H), 5.92 (d, J = 3.7 Hz, 2H), 4.18 (m, 1H), 3.63 (m, 2H), 3.49 (m, 1H), 3.40 (dt, J = 10.2, 2.5 Hz, 1H), 3.19 (m, 1H), 2.35 (m, 1H), 2.26 (m, 1H), 2.18 (m, 1H), 2.00 (m, 2H), 1.84 (m, 1H), 1.48 (m, 14H), 0.97 (m, 1H); 0.87 (m, 1H), 0.30 (s, 9H), 0.29 (s, 9H); <sup>13</sup>C NMR (125 MHz, CDCl<sub>3</sub>) (mixture of rotamers):  $\delta$  170.6, 170.1, 153.0, 152.9, 146.13, 146.07, 137.0, 136.4, 120.5, 120.4, 117.01, 116.99, 108.6, 108.4, 100.3, 100.2, 58.7, 56.1, 48.2, 44.5, 37.6, 36.6, 28.4, 27.5, 26.8, 26.2, 26.1, 25.3, 24.0, 23.5, 21.2, 20.1, -0.06, -0.25; HRMS m/z calcd for C<sub>19</sub>H<sub>28</sub>NO<sub>3</sub>Si (M+H)<sup>+</sup> 346.1833, found 346.1825.

Characterization for **68**: <sup>1</sup>H NMR (400 MHz, CDCl<sub>3</sub>):  $\delta$  6.63 (s, 1H), 5.938 (d, J = 10.5 Hz, 1H), 5.935 (d, J = 10.5 Hz, 1H), 3.88 (t, J = 4.7 Hz, 1H), 3.70 (m, 2H), 2.78 (dt, J = 12.1, 4.9 Hz, 1H), 2.32 (sextet, J = 5.6 Hz, 1H), 1.99 (m, 1H), 1.72 (m, 4H), 1.28 (m, 2H), 1.13 (m, 1H), 0.38 (s, 9H); <sup>13</sup>C NMR (125 MHz, CDCl<sub>3</sub>):  $\delta$  163.8, 152.8, 148.6, 138.9, 127.7, 120.5, 107.8, 100.2, 57.2, 43.1, 40.2, 38.1, 29.8, 29.4, 26.5, 23.8, 2.7; HRMS m/z calcd for C<sub>19</sub>H<sub>26</sub>NO<sub>3</sub>Si (M+H)<sup>+</sup> 344.1676, found 344.1679.

Synthesis of ( $\pm$ )- $\gamma$ -lycorane:

To a round bottom flask containing 21.7 mg (0.571 mmol)  $\text{LiAlH}_4$  and 1 mL previously distilled THF under  $\text{N}_2$  at  $0^\circ\text{C}$  was added dropwise a solution of 9.8 mg (0.029 mmol) **68** in 3.5 mL previously distilled THF. The reaction mixture was allowed to stir at reflux for 19 h until complete consumption of starting material was observed on TLC. Reaction was once again cooled to  $0^\circ\text{C}$ . To the reaction mixture was added dropwise, in succession, 3 mL THF, 0.05 mL deionized water, 0.05 mL 10N NaOH, then 0.1 mL deionized water. The reaction was then allowed to stir at room temperature for 2 h to ensure complete quenching of excess  $\text{LiAlH}_4$ . The resulting aluminum salts were filtered off and the resulting filter cake was washed with THF. The filtrate was dried over  $\text{Na}_2\text{SO}_4$ , filtered and carefully concentrated *in vacuo* to give 11.1 mg of a 1:1 mixture of the desired product and the TMS-protected product. To this mixture was added 1 mL DCM, 0.1 mL  $\text{Et}_2\text{O}$  and 1 mL TFA. The reaction mixture was allowed to stir at room temperature under  $\text{N}_2$  for 6 h at which point the mixture was concentrated *in vacuo*. To the concentrated reaction mixture was added enough  $^i\text{PrOH}$  to dissolve the crude material. 10M NaOH was then added until the reaction reached a pH =12. To this basic mixture was added 5 mL 20%  $^i\text{PrOH}$ / 80% DCM. The aqueous layer was separated from the organic layer and then extracted with 4x5 mL 20%  $^i\text{PrOH}$ / 80% DCM. The resulting organic extracts were dried over  $\text{Na}_2\text{SO}_4$ , filtered and concentrated *in vacuo*. Unfortunately, the crude  $^1\text{H}$  NMR demonstrated that the amine had been reprotonated by small amounts of HCl present in the  $\text{CDCl}_3$ . Therefore, the concentrated reaction mixture needed to be re-basified and was added enough  $^i\text{PrOH}$  to dissolve the crude material. 10M NaOH was then added until the reaction reached a pH =13. To this basic mixture was added 5 mL 20%  $^i\text{PrOH}$ / 80% DCM. The aqueous layer was separated from the organic layer and then extracted with 4x5 mL 20%  $^i\text{PrOH}$ / 80% DCM. The resulting organic extracts were dried over  $\text{Na}_2\text{SO}_4$ , filtered and concentrated *in vacuo*. Silica gel chromatography

in a pipet column (silica gel, gradient run from 100% hexanes to 100% EtOAc) afforded 5.0 mg (68% over 2 steps) of (+/-)- **$\gamma$ -lycorane** as a white powder.  $^1\text{H}$  NMR (400 MHz,  $\text{CDCl}_3$ ):  $\delta$  6.61 (s, 1H), 6.49 (s, 1H), 5.89 (m, 2H), 4.02 (d,  $J = 14.4$  Hz, 1H), 3.38 (m, 1H), 3.22 (d,  $J = 14.2$  Hz, 1H), 2.74 (dt,  $J = 12.1, 4.6$  Hz, 1H), 2.38 (m, 1H), 2.18 (m, 2H), 2.02 (m, 1H), 1.71 (m, 3H), 1.47 (m, 2H) 1.30 (m, 2H);  $^{13}\text{C}$  NMR (500 MHz,  $\text{CDCl}_3$ ):  $\delta$  146.1, 145.7, 133.2, 127.3, 108.3, 106.3, 100.7, 62.9, 57.1, 53.7, 39.5, 37.4, 31.7, 30.4, 29.3, 25.2; HRMS  $m/z$  calcd for  $\text{C}_{16}\text{H}_{20}\text{NO}_2$  ( $\text{M}+\text{H}$ ) $^+$  258.1489, found 258.1489.

#### Synthesis of **69**:

Started with 199.0 mg (0.6000 mmol) tetrabromomethane, 245.6 mg (0.6000 mmol) diphenyl ditelluride and 62  $\mu\text{L}$  (0.60 mmol) **40** in 12.0 mL  $\text{CH}_2\text{Cl}_2$ . Irradiated for 47 h. Solvent was then removed *in vacuo*. Silica gel chromatography (silica gel, gradient run from 100% hexanes to 10% ethyl acetate in hexanes) afforded 203.3 mg (75%) of a pale yellow solid.  $^1\text{H}$  NMR (400 MHz,  $\text{CDCl}_3$ ):  $\delta$  8.11 (m, 2H), 7.49 (m, 3H), 4.91 (m, 1H), 4.18 (m, 1H), 4.07 (m, 2H), 3.85 (m, 1H), 2.15 (m, 3H), 1.81 (m, 1H);  $^{13}\text{C}$  NMR (100 MHz,  $\text{CDCl}_3$ ):  $\delta$  134.6, 131.6, 130.2, 128.7, 73.5, 69.5, 59.3, 32.3, 26.4.

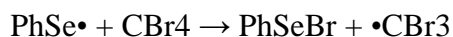
#### Synthesis of **70**:

Started with 199.0 mg (0.6000 mmol) tetrabromomethane, 245.6 mg (0.6000 mmol) diphenyl ditelluride and 72  $\mu\text{L}$  (0.60 mmol) **38** in 12.0 mL  $\text{CH}_2\text{Cl}_2$ . Irradiated for 44 h. Solvent was then removed *in vacuo*. Silica gel chromatography afforded (silica gel, gradient run from 100% hexanes to 60% ethyl acetate in hexanes) 147.8 mg (53%) of a pale orange solid.  $^1\text{H}$  NMR (400 MHz,  $\text{CDCl}_3$ ):  $\delta$  8.09 (m, 2H), 7.47 (m, 3H), 4.24 (m, 1H), 4.11 (m, 1H), 4.00 (m, 2H), 3.56 (dt,  $J = 11.5, 2.0$  Hz, 1H), 1.94 (m, 1H), 1.80 (m, 1H), 1.58 (m, 4H);  $^{13}\text{C}$  NMR (100 MHz,

CDCl<sub>3</sub>):  $\delta$  134.5, 131.3, 129.9, 128.9, 72.6, 69.6, 57.0, 32.1, 25.1, 22.9; HRMS m/z calcd for C<sub>12</sub>H<sub>16</sub>BrOTe (M-Br)<sup>+</sup> 384.9441, found 384.9415.

### 3.4.4 Computational Methods

DFT calculations were performed using Gaussian 09 C.01 64-bit version.<sup>23</sup> The hybrid B3LYP functional and 6-311G\*\* basis set were employed to optimize all structures and to obtain the thermochemical data. PhSe•, CBr<sub>4</sub>, PhSeBr and •CBr<sub>3</sub> were optimized in the absence of solvents (in a vacuum). The calculated thermodynamic values for the following process are shown in Figure S3:



These structures were optimized in the presence of three solvents (CH<sub>2</sub>Cl<sub>2</sub>, MeOH, CH<sub>3</sub>CN). All of the structures were optimized using the 6-311G\*\* basis set. The Polarizable Continuum Model (PCM) using the integral equation formalism variant (IEFPCM) was employed to perform calculations in the presence of solvents.

Table 3.4 Gaussian 2009 calculated enthalpies, entropies, and Gibbs free energies

	$\Delta H_{\text{rxn}}$ (kcal/mol)	$\Delta S_{\text{rxn}}$ (kcal/mol)	$\Delta G_{\text{rxn}}$ (kcal/mol) @ 298 K
No solvent model	-8.369	0.0029	-9.25
CH <sub>2</sub> Cl <sub>2</sub> model	-8.384	0.0029	-9.25
CH <sub>3</sub> OH model	-8.336	0.0028	-9.17
CH <sub>3</sub> C≡N model	-8.333	0.0028	-9.17

### 3.4.5 Crystal Structures

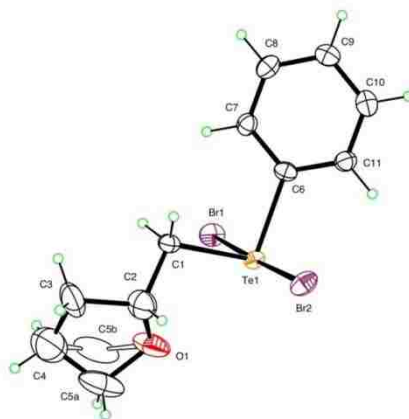


Figure 3.5 Crystal structure of telluride **69**

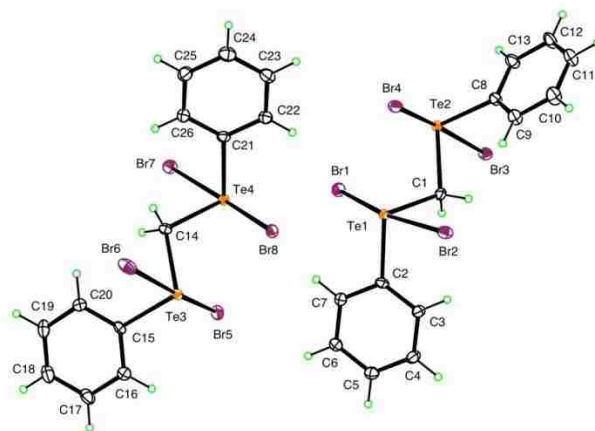


Figure 3.6 Crystal structure of **71**

### 3.5 References

1. Mukherjee, A. J.; Zade, S. S.; Singh, H. B.; Sunoj, R. B., Organoselenium Chemistry: Role of Intramolecular Interactions. *Chem. Rev.* **2010**, *110*, 4357-4416.
2. Writh, T., *Organoselenium Chemistry*. John Wiley & Sons: 2012.
3. (a) Tiecco, M.; Testaferri, L.; Tingoli, M.; Bartoli, D.; Balducci, R., Ring-closure reactions initiated by the peroxydisulfate ion oxidation of diphenyl diselenide. *J. Org. Chem.* **1990**, *55*, 429-34; (b) Clive, D. L. J.; Farina, V.; Singh, A.; Wong, C. K.; Kiel, W. A.; Menchen, S. M., Cyclofunctionalization of olefinic urethanes using benzeneselenenyl

- chloride in the presence of silica gel: a general route to nitrogen heterocycles. *J. Org. Chem.* **1980**, *45*, 2120-6.
- (a) Wirth, T.; Fragale, G.; Spichty, M., Mechanistic Course of the Asymmetric Methoxyselenenylation Reaction. *J. Am. Chem. Soc.* **1998**, *120*, 3376-3381; (b) Rvovic, M. D.; Divac, V. M.; Puchta, R.; Bugarcic, Z. M., Mechanistic investigation of the base-promoted cycloselenoetherification of pent-4-en-1-ol. *J. Mol. Model.* **2011**, *17*, 1251-1257.
  - (a) Nicolau, K. C., *Selenium in Natural Product Synthesis*. Philadelphia, 1984; (b) Ranganathan, S.; Muraleedharan, K. M.; Vaish, N. K.; Jayaraman, N., Halo- and selenolactonisation: the two major strategies for cyclofunctionalisation. *Tetrahedron* **2004**, *60* (25), 5273-5308.
  - Renaud, P., Radical reactions using selenium precursors. *Top. Curr. Chem.* **2000**, *208*, 81-112.
  - Nishibayashi, Y.; Uemura, S., Selenium compounds as ligands and catalysts. *Top. Curr. Chem.* **2000**, *208*, 201-233.
  - Akai, S.; Kita, Y., Recent advances in Pummerer reactions. *Top. Curr. Chem.* **2007**, *274*, 35-76.
  - Gilmour, R.; Prior, T.; Burton, J.; Holmes, A., An organocatalytic approach to the core of eunicellin. *Chem. Comm.* **2007**, *38*, 3954-3956.
  - Seng, H.; Tiekink, E., Anti-cancer potential of selenium- and tellurium-containing species: opportunities abound. *Appl. Organometal. Chem.* **2012**, *26*, 655-662.
  - Page, P. C. B.; Harkin, S. A.; Marchington, A. P.; Van, N. M. B., Addition of aminoketene dithioacetals to  $\alpha,\beta$ -unsaturated ketones. Synthesis and reactions of cyclohex-2-en-1,4-dione monodithioacetals. *Tetrahedron* **1989**, *45*, 3819-38.
  - Pandey, G.; Sekhar, B. B. V. S., In situ generation and utilization of electrophilic selenium species (PhSe<sup>+</sup>) by photooxidative (single electron transfer) cleavage of diphenyl diselenide (PhSeSePh). *J. Org. Chem.* **1992**, *57*, 4019-23.
  - Spell, M.; Wang, X.; Wahba, A.; Conner, E. S.; Ragains, J., An  $\alpha$ -selective, visible light photocatalytic glycosylation of alcohols with selenoglycosides. *Carbohydrate Res.* **2013**, *369*, 42-47.
  - Beckwith, A. L. J.; Page, D. M., Formation of Some Oxygen-Containing Heterocycles by Radical Cyclization: The Stereochemical Influence of Anomeric Effects. *J. Org. Chem.* **1998**, *63*, 5144-5153.



15. Osornio, Y. M.; Miranda, L. D., Formal synthesis of ( $\pm$ )- $\gamma$ -lycorane. *Rev. Soc. Quim. Mex.* **2004**, *48*, 288-292.
16. Josien, H.; Ko, S.; Bom, D.; Curran, D., A general synthetic approach to the (20S)-camptothecin family of antitumor agents by a regiocontrolled cascade radical cyclization of aryl isonitriles. *Chem. - Eur. J.* **1998**, *4*, 67-83.
17. Crich, D.; Yao, Q., Generation of Acyl Radicals from Thioesters by Intramolecular Homolytic Substitution at Sulfur. *J. Org. Chem.* **1996**, *61*, 3566-3570.
18. Ji, S.; Cao, W.; Yu, Y.; Xu, H., Dynamic diselenide bonds: exchange reaction induced by visible light without catalysis. *Angewandte Chemie* **2014**, *53*, 6781-5.
19. Pangborn, A. B. G., M. A.; Grubbs, R. H.; Rosen, R. K.; Timmers, F. J., Safe and Convenient Procedure for Solvent Purification. *Organometallics* **1996**, *15*, 1518.
20. Lovick, H. M. M., F.E., Metal-Free Highly Regioselective Aminotrifluoroacetoxylation of Alkenes. *J. Am. Chem. Soc.* **2010**, *132* (1249).
21. Haong-Cong, X. Q.-S., B.; Zard, S.Z., An Expedient Synthesis of (+/-)- $\gamma$ -Lycorane. *Tetrahedron Lett.* **1999**, *40*, 2125.
22. Josien, H. K., S.; Bom, D.; Curran, D.P., A general synthetic approach to the (20S)-camptothecin family of antitumor agents by a regiocontrolled cascade radical cyclization of aryl isonitriles. *Chem. Eur. J.* **1998**, *4*, 67.
23. Frisch, M.; Trucks, G.; Schlegel, H.; Scuseria, G.; Robb, M.; Cheeseman, J.; Scalmani, G.; Barone, V.; Mennucci, B.; Petersson, G.; Nakatsuji, H.; Caricato, M.; Li, X.; Hratchian, H.; Izmaylov, A.; Bloino, J.; Zheng, G.; Sonnenberg, J.; Hada, M.; Ehara, M.; Toyota, K.; Fukuda, R.; Hasegawa, J.; Ishida, M.; Nakajima, T.; Honda, Y.; Kitao, O.; Nakai, H.; Vreven, T.; Montgomery, J., J.; Peralta, J.; Ogliaro, F.; Bearpark, M.; Heyd, J. J.; Brothers, E.; Kudin, K.; Staroverov, V.; Kobayashi, R.; Normand, J.; Raghavachari, K.; Rendell, A.; Burant, J.; Iyengar, S.; Tomasi, J.; Cossi, M.; Rega, N.; Millam, J.; Klene, M.; Knox, J.; Cross, J.; Bakken, V.; Adamo, C.; Jaramillo, J.; Gomperts, R.; Stratmann, R.; Yazyev, O.; Austin, A.; Cammi, R.; Pomelli, C.; Ochterski, J.; Martin, R.; Morokuma, K.; Zakrzewski, V.; Voth, G.; Salvador, P.; Dannenberg, J.; Dapprich, S.; Daniels, A.; Farkas, Ö.; Foresman, J.; Ortiz, J. V.; Cioslowski, J.; Fox, D. J., Gaussian 09, Revision C.01. Gaussian, I., Ed. Wallingford, CT, 2009.

## **CHAPTER 4: DEVELOPMENT OF VISIBLE LIGHT PHOTOCATALYTIC METHOD FOR ORGANIC THIN FILM FORMATION ON GOLD USING ARYL IODIDES**

### **4.1 Introduction**

#### **4.1.1 History and Significance of Organic Thin Films**

Organic thin films play an important role in everyday life. Knowledge and utilization of organic thin films has existed for over millennia. Circa 1800 BC in Babylonia and Assyria, a form of divination involved pouring hydrocarbon-based oils on water and interpreting a person's future based on the way the oil would spread over the water surface and against the container.<sup>1</sup> In the early 1<sup>st</sup> century CE, Roman philosopher Pliny the Elder observed that divers would often pour oil onto a body of water in order to make the water clearer and easier to see to the bottom, where the desired objects, like clams or oysters, would be.<sup>2</sup> Benjamin Franklin ran an experiment which consisted of pouring a teaspoon of oil onto a pond. The oil spread out over the entire pond and made the water so that it appeared "as smooth as a looking-glass." To explain this phenomenon, Lord Rayleigh theorized that oil would spread until it was one molecule thick, thus forming a monolayer.<sup>3</sup>

Over forty years later, a major breakthrough in thin film technology was accomplished by Irving Langmuir and Katharine Blodgett when they realized that organic multilayers could be synthesized by repeatedly submerging glass plates into a solution of calcium stearate in polar solvents.<sup>4</sup> They found that the carboxylate head groups of the stearate moiety would attach to glass surface forming the thin layer. Repeated dipping of the glass substrate into the calcium stearate solution could produce multilayers up to 200 multilayers thick. These films had applications as antireflection coatings.

Today, organic thin films are used in a wide variety of applications like biosensors, coatings for medical devices, anti-corrosion resists, and organic thin film transistors.<sup>5</sup> Organic

thin films provide a barrier between solid matter and a liquid or gaseous phase. Thin films also provide an opportunity to functionalize a solid surface, where thickness and functionality can be controlled to synthesize designer interfaces.

#### **4.1.2 Methods for Thin Film Formation**

The most popular method for thin film formation is via the grafting of thiol precursors to metals like gold and platinum. Thin film formation prior to the 1980's consisted of attaching a molecule with a polar functional group to a surface, as described in the previous section. Although these films provided an important step in materials research, they were often weakly bound to the surface and were structurally uninteresting. Any functional group that would be of any use was bound to the surface and unable to undergo further reaction. The only part of the layer that was available was usually an unreactive hydrocarbon chain.

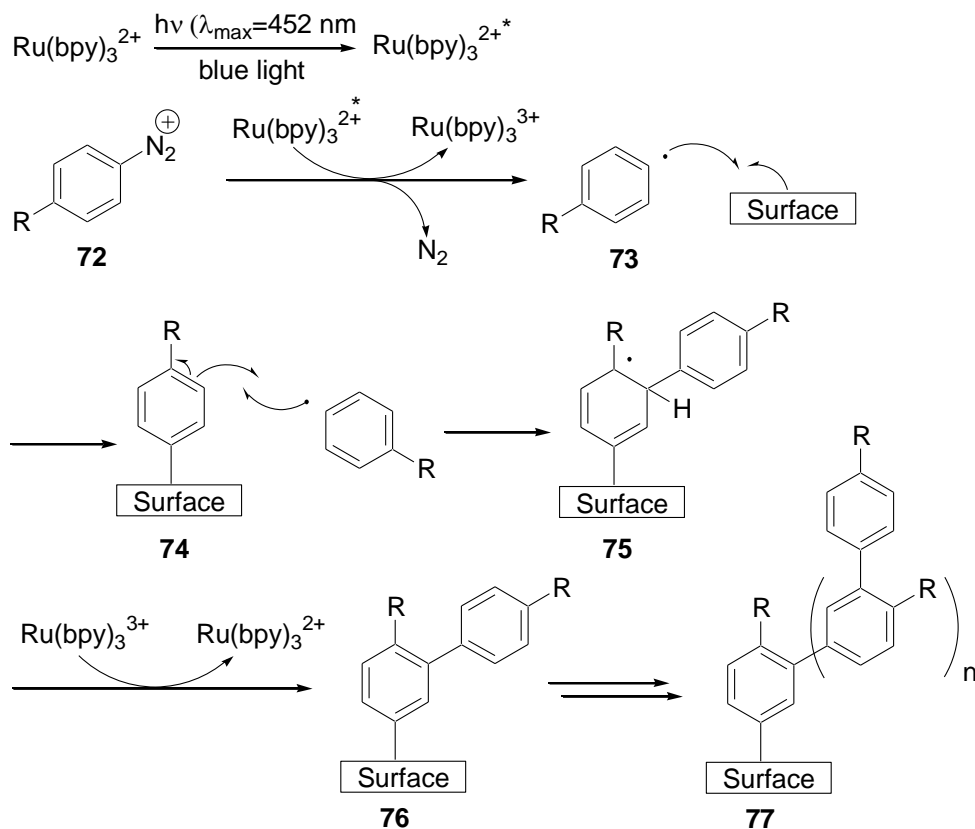
In search of a method to functionalize surfaces with coatings containing interesting terminal groups, organic chemists Ralph Nuzzo and David Allara performed research on the formation of thin films from thiol precursors. They found that monolayers of thiol-containing compounds were spontaneously formed when gold was submerged in a thiol solution.<sup>6</sup> Sulfur has a strong affinity for metal surfaces, and thiols outcompete carboxylates or other functional groups from grafting onto metals.<sup>5f</sup> Therefore, molecules to be attached to a gold surface can have pendant functional groups that will be on the outer surface of the layer and available for further reaction. Relatively homogenous mixed thiol monolayers can also be easily made through the immersion of a gold plate in a solution of two or more thiols.<sup>7</sup> Since Nuzzo and Allara's discovery, thiol self-assembled monolayers have become integral parts of nanotechnology research. However, these thiol self-assembled monolayers suffer from several

drawbacks. They are relatively unstable toward oxidation and thermal desorption. For example, dodecanethiol monolayers undergo desorption at 100°C and are unstable to oxidation.<sup>5e, 8</sup>

As a way to produce more stable thin films, other methods for synthesizing organic thin films were explored. The most notable method was developed initially in the 1990's. This method entailed the grafting of aryl radicals, generated *in situ* via the UV irradiation or cathodic reduction of diazonium salts, onto carbon materials to form multilayers.<sup>5a</sup> These synthesized layers overcame problems presented by thiol-derived thin films. For instance, the films were considerably more stable, with no thermal desorption occurring up to a temperature of 427°C on glassy carbon.<sup>5c</sup> These multilayers were also relatively stable to oxidation, being able to withstand storage in air for several months. The same multilayers were not removed or degraded by sonication and boiling solvents. The stability of the formed multilayers stems from the strength of the covalent bonding of carbon, on the arene ring, and the metal or carbon surface. The presence of the covalent bond between the organic substrate and a gold surface has been demonstrated by both X-ray photoelectron spectroscopy (XPS)<sup>9</sup> and high resolution electron energy loss spectroscopy (HREELS).<sup>10</sup> The covalent gold-carbon bond strength was determined to be ~30 kcal/mole by Scherlis and coworkers using computational methods.<sup>10</sup> This bond is, therefore, similar in strength to that in I<sub>2</sub>.

As previously mentioned, the original method for generation of aryl radicals from diazonium salts involved either the irradiation by UV light or the cathodic reduction of arendiazonium salts to generate aryl radicals that graft to surfaces. Both of these methods, however, require advanced and expensive experimental setups. In an effort to improve the ease of grafting of aryl radicals, generated from diazonium salts, a visible light-promoted method was developed.<sup>11</sup> In this photocatalytic method, blue LED irradiation coupled with the photocatalyst,

$\text{Ru}(\text{bpy})_3^{2+}$ , generated aryl radicals from diazonium salts. The initiation step in the process was the promotion of the catalyst to its excited state,  $[\text{Ru}(\text{bpy})_3^{2+}]^*$ , by the absorption of a photon from a visible light source (Scheme 4.1). After undergoing intersystem crossing to the triplet state, the excited state photocatalyst donates an electron to the diazonium salt **72**, which loses  $\text{N}_2$  to generate the aryl radical **73**. The aryl radical **73** can then attach to the Au surface to form a covalent gold-carbon bond **74**. Polymerization, and thus multilayer formation, occurs when another aryl radical intercepts the arene already grafted to the surface. Regeneration of the photocatalyst is then accomplished via oxidation of the dimer radical **75** to form the cation, which then quickly rearomatizes to the desired grafted product. The thickness of the multilayers can be modified by varying the irradiation time. The longer the irradiation time is, the thicker the polymer thin film **77** will be.<sup>11a</sup>



Scheme 4.1 Photografting of arene diazonium salts<sup>11b</sup>

Although the multilayers formed via visible light photografting of arenes are stable to oxidation and thermal desorption due to the strength of the gold-carbon covalent bond, the method has several limitations. For instance, diazonium salts are themselves relatively unstable. Because diazonium salts undergo decomposition within days, even under N<sub>2</sub> at -20°C, they cannot be stored for long periods of time. The diazonium moiety is also extremely polar and sensitive to acidic conditions. Traditional purification methods by chromatography, therefore, are difficult and present many problems. Another method for generation of aryl radicals for grafting onto surfaces would be beneficial.

#### 4.1.3 Photocatalytic Generation of Aryl Radicals from Aryl Iodides

Electrografting of aryl iodides is not possible. This is due to the overreduction of the aryl iodide to the aryl carbanion instead of the desired aryl radical at potentials low enough to convert aryl iodide to aryl radical.<sup>12</sup> However, recent research has been performed demonstrating the generation of aryl radicals from aryl iodides using visible light photocatalysis.<sup>13</sup> Stephenson and coworkers used the photocatalyst Ir(ppy)<sub>3</sub> (Figure 4.1) to accomplish the generation of aryl radicals. Aryl iodides have a reduction potential ranging from -1.6V to -2.2V vs. SCE. Ir(ppy)<sub>3</sub><sup>\*</sup> has a reduction potential of -1.73V (versus SCE), making it an ideal candidate for single-electron transfer (SET) to and reduction of aryl iodides.

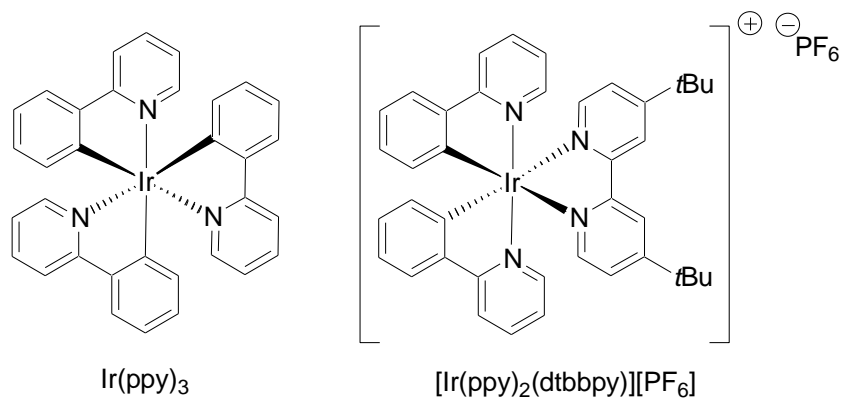
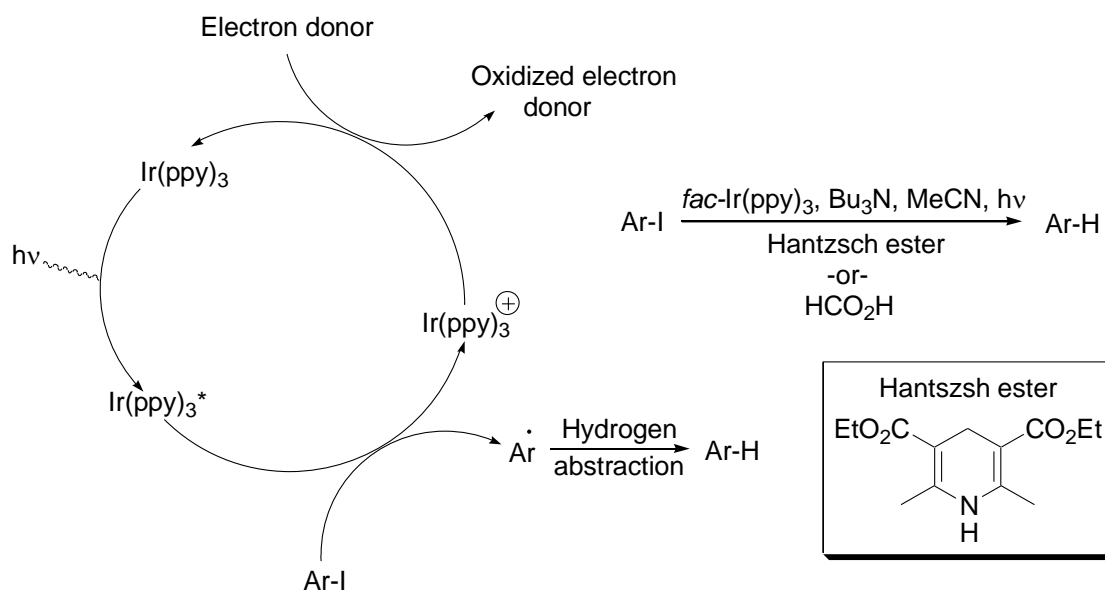


Figure 4.1 Iridium catalysts

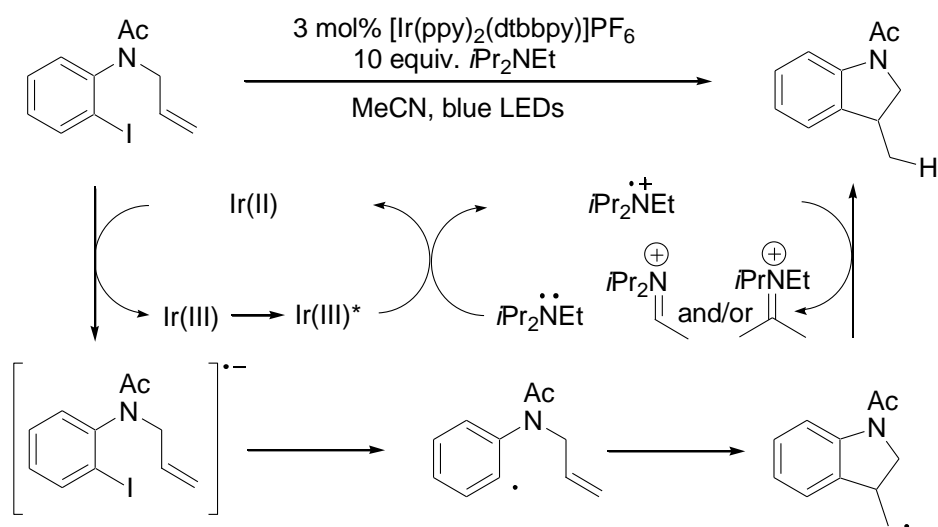
In Stephenson's work, several aryl iodides underwent transformation to the corresponding arene via the intermediacy of an aryl radical (Scheme 4.2). The photocatalyst  $\text{Ir(ppy)}_3$ , upon irradiation by visible light, was brought to its excited state  $\text{Ir(ppy)}_3^*$ . This excited state photocatalyst was then able to reduce the aryl iodide to the aryl radical, with the leaving of iodide. The aryl radical was then able to abstract a hydrogen atom from tributylamine radical cation, Hantzsch ester or formic acid. The photocatalyst was regenerated by the one electron oxidation of either tributylamine or the Hantzsch ester (Scheme 4.2). The substrate scope for this transformation was broad, with yields ranging from 92-98%. Evidence that the reaction was occurring via the oxidative quenching cycle was found in a control experiment when the reaction proceeded without the Hantzsch ester, formic acid or tributylamine, albeit at a lower percent yield.



Scheme 4.2 Proposed mechanism for aryl radical generation under the Stephenson conditions<sup>13a</sup>

Kim and Lee also developed a photocatalytic method for aryl radical formation from aryl radical precursors.<sup>13b</sup> In Lee's method, the photocatalyst used was  $[\text{Ir(ppy)}_2(\text{dtbbpy})][\text{PF}_6]$ , having a reduction potential of -1.51V (versus SCE) in the excited state (Figure 4.1). Both  $\text{Ir(ppy)}_3$  and  $[\text{Ir(ppy)}_2(\text{dtbbpy})][\text{PF}_6]$  have metal-to-ligand-charge-transfer (MLCT) bands at 400-

500 nm, making them susceptible to excitation by blue LEDs ( $\lambda_{\text{max}}=455\text{nm}$ ). In the mechanism for the conversion of aryl iodide to the hydrogen abstraction product under Lee's conditions, the iridium catalyst is first excited by visible light (Scheme 4.3). The excited state photocatalyst is then reduced by diisopropylethylamine (DIPEA) to the iridium (II) species. It is then able to undergo a single electron transfer (SET) to the aryl iodide, which loses iodide anion to give the aryl radical, regenerating the iridium catalyst in the process. This aryl radical can then cyclize onto any present pendant alkenes. In the termination step of the mechanism, the radical abstracts a hydrogen atom from the previously oxidized DIPEA to give the desired product. Yields under Lee's conditions were also excellent, ranging from 82-96%.



Scheme 4.3 Proposed mechanism for aryl radical generation under the Lee conditions<sup>13b</sup>

#### 4.1.4 Brief Overview of Atomic Force Microscopy

Our primary method for surface analysis in this section is atomic force microscopy (AFM). Since its introduction in the 1980's, AFM has been indispensable as tool for characterizing thin films on a variety of surfaces.<sup>14</sup> In general for a topographical image, the AFM gathers information from a sample by scanning the surface with a silicon or  $\text{Si}_3\text{N}_4$  cantilever (Figure 4.2). This information can be used to create an image. As the cantilever is



scanned over the surface of a sample, the tip is displaced upward or downward as a function of constant force between the tip and the sample. This movement is measured by a laser diode which reflects off the top of the cantilever to be collected by a detector consisting of two photodiodes. As the angular displacement of the laser changes, the amount of light that is collected by one of the diodes will be greater than the other. This produces an output signal which can be translated into depth analysis of the surface.

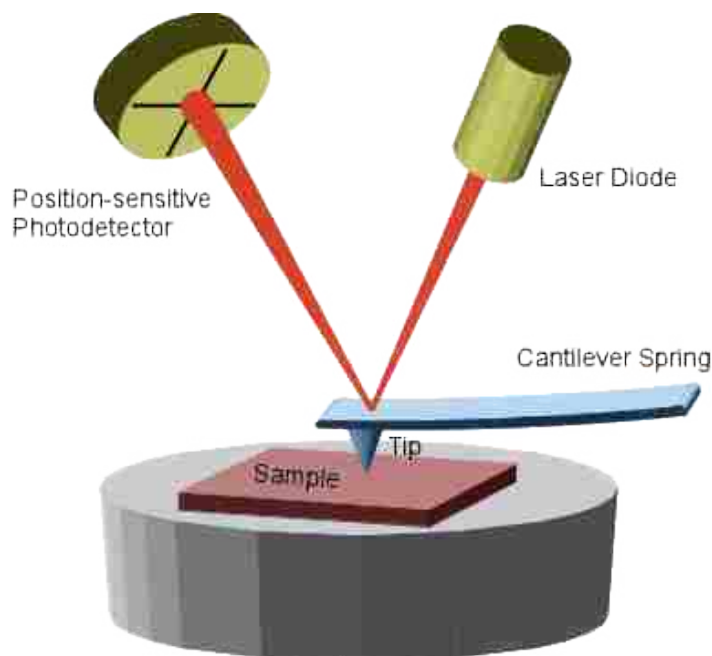


Figure 4.2 Basic experimental setup for AFM

In addition to providing an image of a surface, AFM coupled with particle lithography can be implemented to measure the depth of a thin film. Particle lithography often involves the addition of silica mesospheres to a clean surface before grafting of any organic thin film. Upon formation of the thin film, the mesospheres effectively mask the surface at the areas of contact while the thin film forms around them (Figure 4.3). After formation of the films, the mesospheres are removed via sonication in ethanol. Where the silica mesospheres were once located, nanopores are formed. The depth of the organic layer can then be measured by scanning

the AFM cantilever over the nanopores and measuring the distance between the substrate and the top of the thin films as a function of constant force.

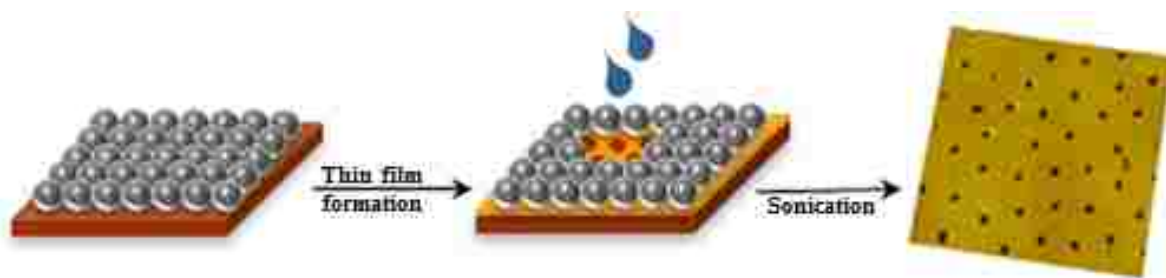


Figure 4.3 Immersion particle lithography<sup>11a</sup>

## 4.2 Results and Discussion

In order to provide a way to better synthesize thin layers of arenes on gold surfaces without suffering the limitations of electrografting or photografting of diazonium salts, aryl radicals generated from aryl iodides were grafted to atomically flat Au(111) surfaces via visible light photocatalysis. The resulting films were then characterized by AFM, water contact angle measurements and X-ray photoelectron spectroscopy (XPS).

4-Iodoanisole was chosen as the first molecule to be grafted, initially using Stephenson's conditions (Scheme 4.2). The hypothesis was that 4-anisyl radicals, formed from the photocatalytic reduction of 4-iodoanisole, would graft to the surface forming a covalent gold-carbon bond. To accomplish this goal, 4-iodoanisole was placed into an Erlenmeyer flask with Ir(ppy)<sub>3</sub>, Hantzsch ester, tributylamine and MeCN in the presence of a gold substrate accompanied by vigorous stirring and irradiated with blue LEDs for 18.5 hours. Formic acid was not used as a hydrogen donor due to the possible removal of the mesospheres under acidic conditions. Aliquots of the solution were analyzed by <sup>1</sup>H NMR over time, and 4-iodoanisole was completely converted to anisole after 18.5 hours. After irradiation, the template-stripped-gold (111) (TSG)<sup>15</sup> substrates with 500 nm mesospheres deposited via immersion particle lithography

were analyzed with AFM. The initial images illustrated the formation of thin films of ~2 nm in thickness (Figure 4.4). However, after multiple experiments at varying concentrations, uniform and consistent grafting of anisole onto the gold surface proved to be unreliable with grafting occurring only on patches of the gold if at all. The initial results were not reproducible.

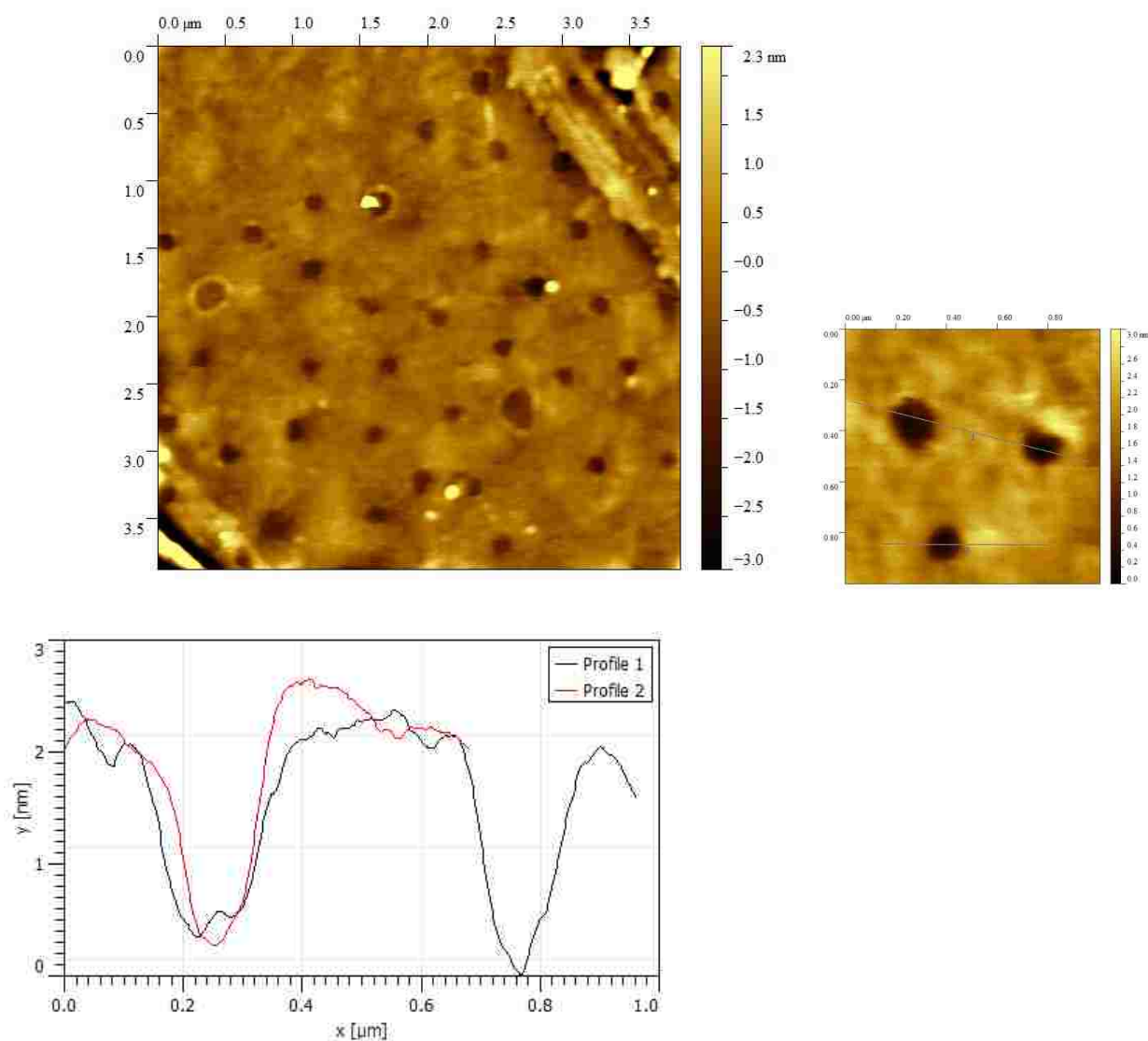
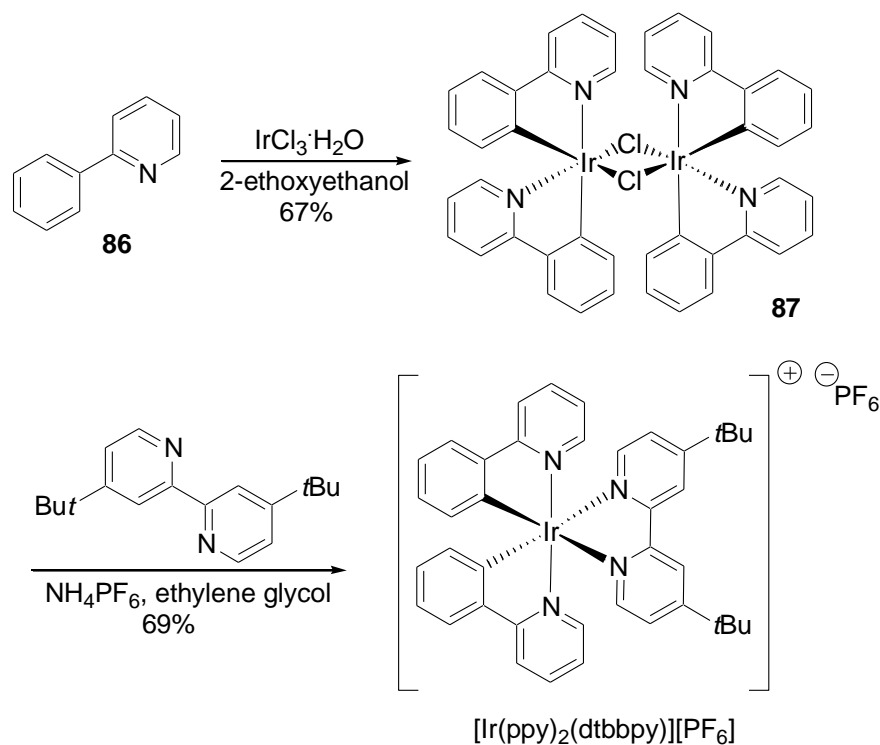


Figure 4.4 AFM images of 4-anisyl on gold using Stephenson's conditions

With the possibility that the formed aryl radical was simply abstracting a hydrogen atom from either the Hantzsch ester or the tributylamine before being able to reach the gold surface, another route towards the synthesis of an anisole thin film was deemed necessary. Lee's

conditions for the generation of aryl radicals from aryl iodides were then attempted (Scheme 4.3).

Before photografting under Lee's conditions could be accomplished,  $[\text{Ir}(\text{ppy})_2(\text{dtbbpy})][\text{PF}_6]$  was synthesized (Scheme 4.4). Phenylpyridine **86** was first reacted with iridium (III) chloride hydrate in 2-ethoxyethanol to give the bimetallic species **87** in 67% yield. The bimetallic intermediate **87** then underwent a ligand exchange with 4,4'-di-*tert*-butyl-2,2'-bipyridyl in ethylene glycol with ammonium hexafluorophosphate to produce the desired photocatalyst in 69% yield.



Scheme 4.4 Synthesis of  $[\text{Ir}(\text{dtbbpy})(\text{ppy})_2][\text{PF}_6]$

For thin film synthesis under Lee's conditions, 4-iodoanisole at an initial concentration of 0.01 M was placed in an Erlenmeyer flask with  $[\text{Ir}(\text{dtbbpy})(\text{ppy})_2][\text{PF}_6]$ , DIPEA and MeCN in the presence of TSG AFM gold plates<sup>15</sup> and irradiated for 18.5 hours. After removal of the silica

mesospheres by sonication in ethanol, AFM images illustrated that a uniform thin film was formed, but only at a thickness of  $\sim 1$  nm (Figure 4.5).

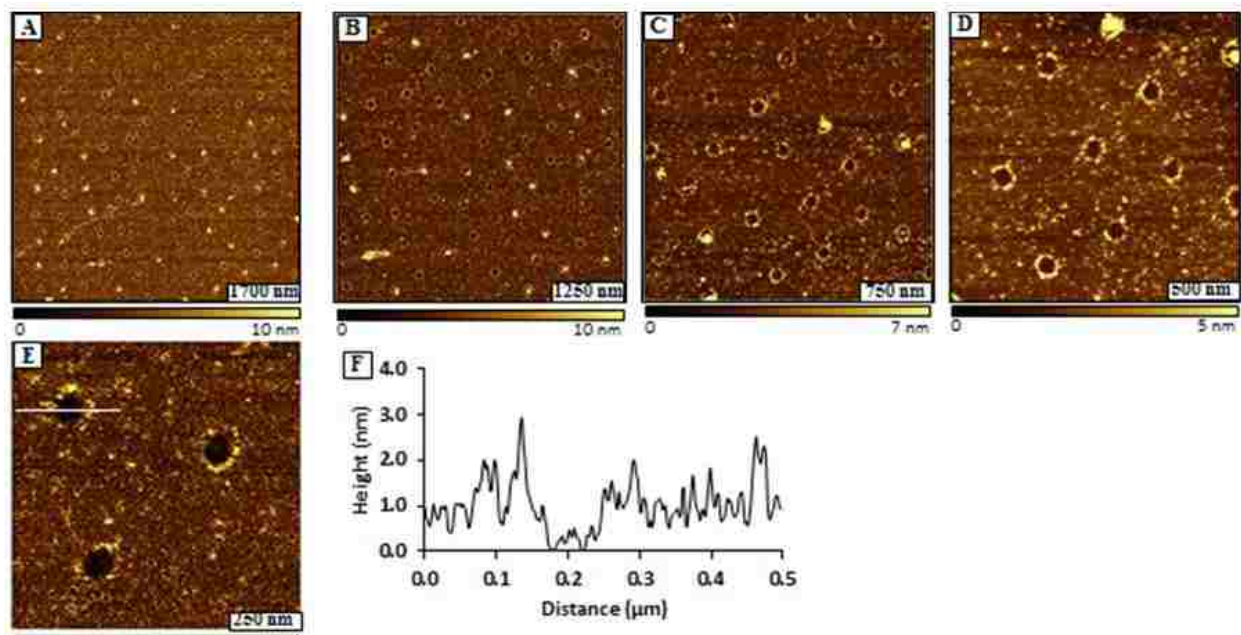


Figure 4.5 AFM image of 4-anisyl on gold using Lee's conditions with a 4-iodoanisole concentration of 0.01 M

Because thicker films are often useful for further analysis by infrared reflection-absorption spectroscopy (IRRAS) and XPS, the concentration of 4-iodoanisole was increased to 0.1M. Upon irradiation at this concentration and subsequent removal of the mesospheres, the depth of the formed nanopores was determined to be 2 nm by AFM (Figure 4.6). To further increase the anisole layer thickness, the 4-iodoanisole concentration was increased to 0.3 M and irradiated for 18.5 hours. The resulting film, however, was demonstrated by AFM to be not uniform in thickness across the entire surface, varying from 1-4 nm in depth. The most consistent and homogenous result, therefore, was obtained by using the 4-iodoanisole concentration of 0.1 M. To demonstrate that the thin film seen on AFM was not a result of grafting of DIPEA or MeCN, a control experiment was run where only  $[\text{Ir}(\text{dtbbpy})(\text{ppy})_2][\text{PF}_6]$ , DIPEA and MeCN was irradiated with the Au(111) substrate. No film was present on AFM.

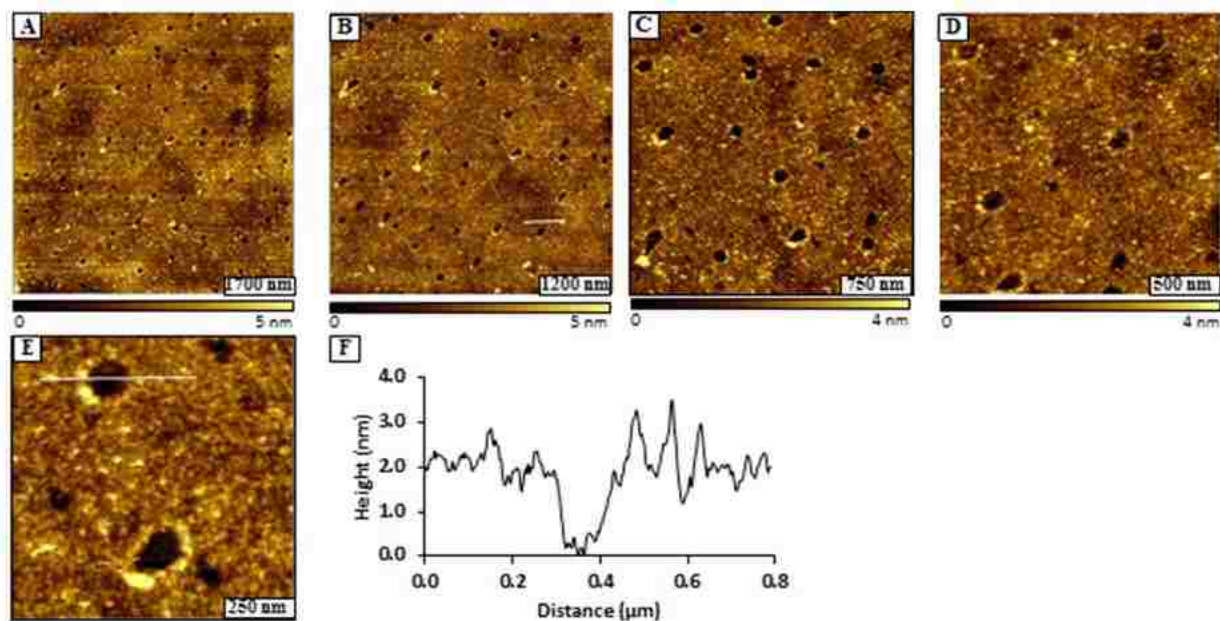


Figure 4.6 AFM image of 4-anisyl on gold using a 4-iodoanisole concentration of 0.1 M

In order to determine the elemental analysis of the surface, XPS was necessary. First, large Au(111) slides were bought and cleaned via UV irradiation over 6 hours. Water contact angles were determined to be  $62^\circ \pm 2^\circ$ . This corresponded to the literature value for contact angle measurement of  $57^\circ \pm 4^\circ$  of a bare gold surface.<sup>11b</sup> This slide was then irradiated under the favorable conditions (0.1 M 4-iodoanisole concentration). After irradiation, the water contact angle was measured to be  $75^\circ \pm 2^\circ$ . The increase in water contact angle illustrates that the gold surface is more hydrophobic(Figure 4.7).

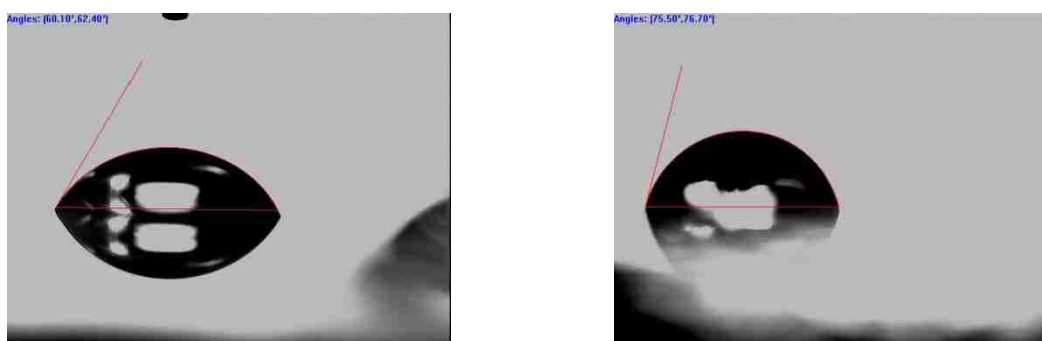


Figure 4.7 Water contact angles of gold plate before and after grafting of anisole

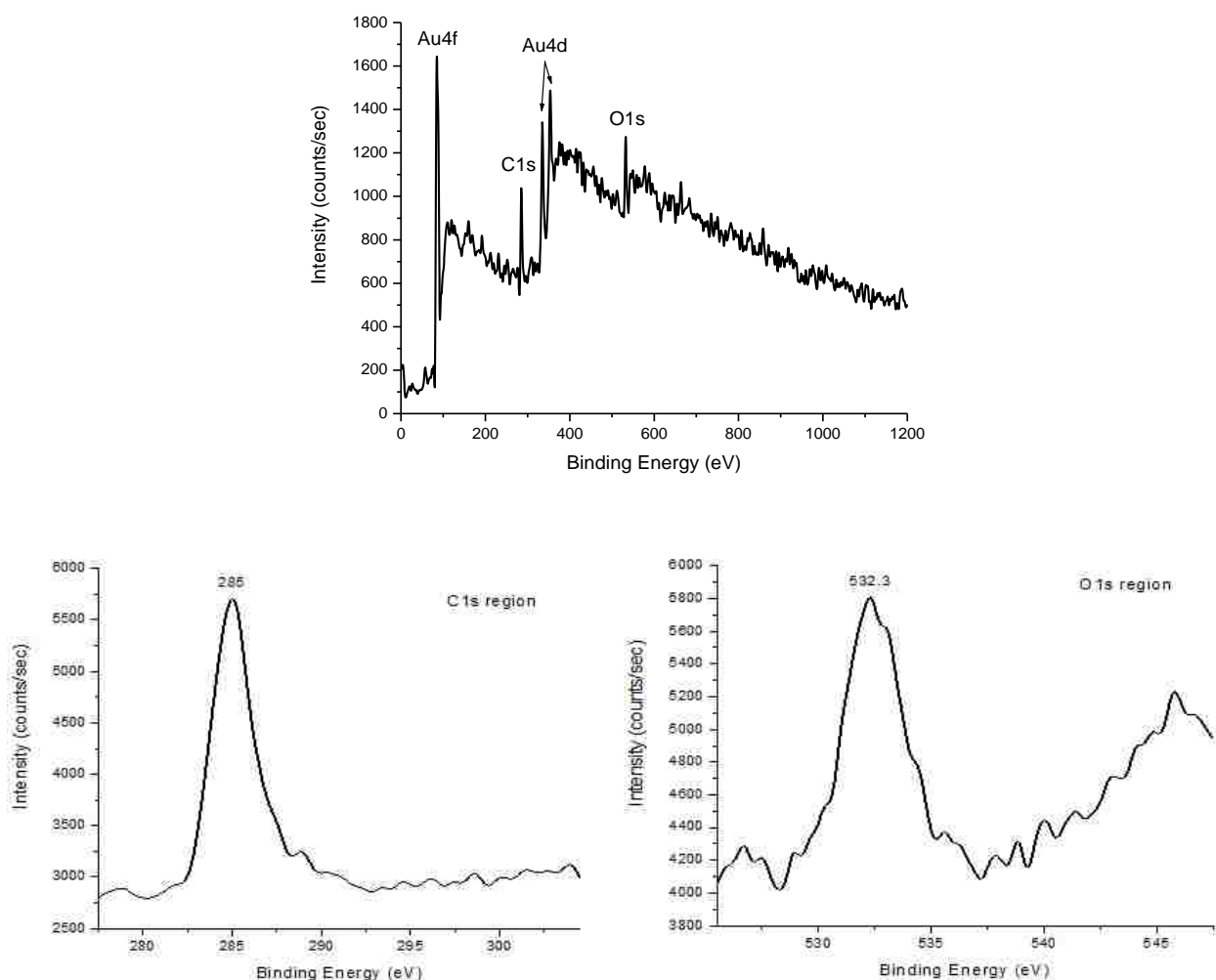


Figure 4.8 XPS spectrum of anisole thin film on gold plate

XPS data collected from the gold slide after irradiation confirmed the formation of anisole thin films on the surface (Figure 4.8). The elements detected were Au(4f<sub>7/2</sub>, 4d<sub>5/2</sub>, 4d<sub>3/2</sub>), C1s and O1s with no indication of the presence of nitrogen, demonstrating that DIPEA had not grafted. The notation after the element symbol corresponds to the orbital in which the electrons are excited. The observed binding energies for carbon and oxygen were 285.0 eV and 532.3 eV, respectively. The binding energy for oxygen is close to that of anisole O1s presented in the literature, suggesting the presence of an anisole thin film on the gold surface.<sup>16</sup>

### 4.3 Future Work

In order to increase the substrate scope for this developed method, many other aryl iodides will be used (Figure 4.9). The aryl iodides will first only vary in terminal functionality. For example, the methoxy group in 4-iodoanisole will be replaced by a nitrile, protected amine, methyl group or bromine. This will demonstrate that the developed method is applicable towards a large variety of functional groups. More complex structures will also be attempted to show that specially designed thin films are possible and can be synthesized with only one grafting procedure instead of two or more. Infrared Reflection-Absorption Spectroscopy (IRRAS) will also be used for all synthesized thin films to better characterize the multilayers present on the gold surface. This technique will provide IR data of the thin film.

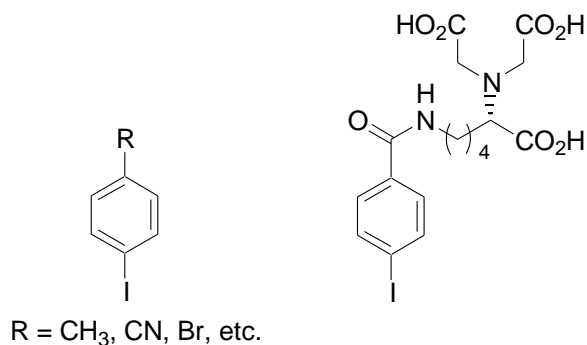
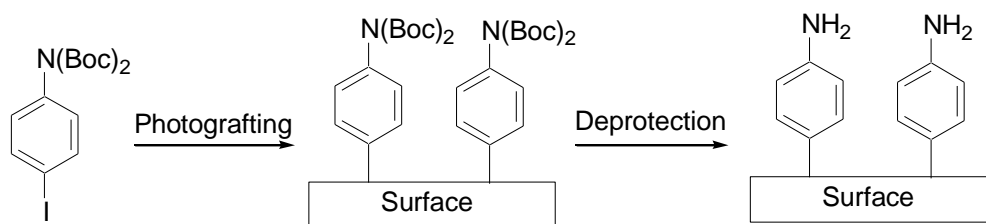


Figure 4.9 Proposed substrate scope

Monolayer formation via the use of removable protecting groups will also be explored. Currently, multilayers are formed due to the attack of additional aryl radicals onto the *meta* position of the already formed anisole monolayer (Scheme 4.1). The multilayers attack at the *meta* position, because the *para* position is already functionalized and the *ortho* position is too sterically hindered. To prevent this attack from occurring, substrates will be made containing removable protecting groups, like a doubly Boc-protected amine (Scheme 4.5). The protected amine would first be grafted under the developed conditions. The Boc groups would sterically



prevent any further polymerization during irradiation. Once grafting is complete, the protecting groups will be removed to reveal a monolayer.



Scheme 4.5 Monolayers resulting from removable blocking groups

## 4.4 Conclusions

Organic thin films play an integral role in nanoscience and surface science. In general, these films are generated from the immersion grafting of thiols onto metal surfaces. The synthesized thiol monolayers, however, are unstable to oxidation and are susceptible to thermal desorption, even at relatively low temperatures under inert atmosphere. One way of providing more stable thin films is the grafting of aryl radicals generated from diazonium salts. The resulting carbon-gold bond is extremely stable towards oxidation and high temperatures. The methods used to generate these aryl radicals from diazonium salts often require complex experimental setups, and the diazonium salts cannot withstand multistep synthesis. To overcome these issues, a visible light photocatalytic method of grafting aryl radicals, generated from aryl iodides, onto gold surfaces was developed. AFM confirmed the presence of an anisole thin film, ranging from 1-4 nm, and XPS spectra indicated that carbon and oxygen were on the surface. This method will be applied to many other aryl iodides in the future.

## 4.5 Experimental

### 4.5.1 General Methods

Gold slides were obtained from Evaporated Metal Films (Product # CA134). They consist of a glass slide coated with a 50 Å chromium binder layer followed by a 1,000 Å gold

layer. 4-Iodoanisole,  $[\text{Ir}(\text{dtbbpy})(\text{ppy})_2][\text{PF}_6]$ , and absolute ethanol were obtained from Sigma-Aldrich, and the corresponding catalog numbers were 17608, 688096, and 459844. Diisopropylethylamine was obtained from Acros Organics, and the catalog number was 367840010. These chemicals were used without purification. Acetonitrile was purified according to the method of Grubbs.<sup>17</sup>

#### **4.5.2 Synthesis of $[\text{Ir}(\text{dtbbpy})(\text{ppy})_2][\text{PF}_6]$**

Synthesis of  $[\text{Ir}(\text{dtbbpy})(\text{ppy})_2][\text{PF}_6]$  was accomplished according to the procedures of Polosan<sup>18</sup> and Lowry<sup>19</sup>.

#### **4.5.3 Procedure for Immersion Particle Lithography**

Two types of substrates were used for preparing samples. Ultraflat gold films were prepared on mica(0001) by evaporative deposition. Template-stripped, gold substrates were prepared by a previously reported procedure.<sup>15</sup> Glass discs were glued to freshly prepared gold films using an epoxy (EPO-TEK, Billerica, MA). Pieces of ultraflat gold/glass were stripped from mica to expose a clean, atomically flat Au(111) surface. Size-sorted silica mesospheres with an average diameter of 500 nm (Thermo Scientific) were cleaned by centrifugation and suspension in water (three cleaning cycles). A 40  $\mu\text{L}$  drop of the silica mesosphere suspension was placed onto the template-stripped gold substrates, dried in air for 2 h, and then oven-dried at 150 °C for at least 14 h. The final heating step was used to temporarily anneal the silica spheres to the substrate to prevent displacement during immersion in solutions. After completion of the chemical reactions, removal of the surface mask was accomplished by sonication in clean solvents.

#### **4.5.4 Cleaning of Large Au (111) Slides**

The gold plates, once obtained from Evaporated Metal Films, were placed in a triangular prism-shaped box made from cardboard (see below) with a UV penlight attachment. The plates

were then irradiated for 24 h in the presence of O<sub>2</sub> and transferred immediately to a reaction vessel for use in experiments. The water contact angle was 62° for freshly-irradiated Au (111) plates.



Figure 4.10 Apparatus for cleaning of gold slides

#### 4.5.5 Experimental Setup



Figure 4.11 Photografting experimental setup

#### 4.5.6 Photografting Procedure for AFM TSG Au Plates

The Au (111) plate was placed gold side up on one side of a 60 mL Erlenmeyer flask. A flea stir bar was placed in the Erlenmeyer flask on the opposite side so that the stir bar did not disturb the gold surface. For the samples run at a concentration of 0.01 M, the flask was then charged with 1.9 mg (0.0021 mmol)  $[\text{Ir}(\text{dtbbpy})(\text{ppy})_2][\text{PF}_6]$  and 16.4 mg (0.0700 mmol) 4-iodoanisole. A septum was then placed over the top of the flask and 0.12 mL (0.70 mmol) DIPEA and 6.9 mL MeCN was added at once via syringe. The reaction was then placed in an evaporating dish surrounded by blue LEDs (see Experimental Setup) and allowed to stir under  $\text{N}_2$  for 18.5 h (sparging not necessary). The gold plate was then carefully removed from the Erlenmeyer flask and rinsed first with 5 mL DI  $\text{H}_2\text{O}$  and then 5 mL absolute EtOH before setting on a paper towel to air dry. The samples were sonicated in EtOH for 1 min to remove the mesospheres and any remaining non-covalently bound residues. [Note: Photografting procedure for concentration of 0.1M was the same as above except the following amounts of reagents were used: 19.2 mg (0.0210 mmol)  $[\text{Ir}(\text{dtbbpy})(\text{ppy})_2][\text{PF}_6]$ , 163.8 mg (0.7000 mmol) 4-iodoanisole, 1.22 mL DIPEA and 5.78 mL MeCN.]

#### 4.5.7 Photografting Procedure for XPS Large Au Slides (0.1 M)

A 125 mL Erlenmeyer flask was charged with 57.6 mg (0.0630 mmol)  $[\text{Ir}(\text{dtbbpy})(\text{ppy})_2][\text{PF}_6]$  and 491.4 mg (2.100 mmol) 4-iodoanisole. The Au (111) plate was then placed gold side up on one side of the flask. A stir bar was placed in the Erlenmeyer flask on the opposite side of the flask so that the stir bar did not disturb the gold surface. A septum was then placed over the top of the flask and 3.66 mL DIPEA and 17.34 mL MeCN was added at once via syringe. The reaction was then placed in an evaporating dish surrounded by blue LEDs (see Experimental Setup) and allowed to stir under  $\text{N}_2$  for 18.5 hr (sparging not necessary). The gold

plate was then carefully removed from the Erlenmeyer flask and rinsed first with 5 mL DI H<sub>2</sub>O and then 5 mL absolute EtOH. The plate was then submerged in EtOH and sonicated for 5 minutes. After sonication, the plate was again rinsed first with 5 mL DI H<sub>2</sub>O and then 5 mL absolute EtOH before setting on a paper towel to air dry.

#### **4.5.8 Water Contact Angle Measurements on Large Au Slides**

Water contact angle measurements were obtained using a VCA Optima XE instrument. Two microliters of DI water were dropped onto the horizontal gold surface per measurement. At least six measurements were taken per sample in order to obtain a reliable value. The contact angle was calculated using the Sessile Drop method on AutoFAST Imaging software.

#### **4.5.9 X-ray Photoelectron Spectroscopy (XPS)**

Surface elemental analyses of the Au plates were performed using a Kratos Axis Ultra X-ray photoelectron spectroscopy system. The surface analysis chamber was equipped with aluminum K $\alpha$  X-ray gun and a 500 mm Rowland circle silicon single-crystal monochromator. The X-ray gun was operated using a 15 mA emission current at an accelerating voltage of 15 kV. Low-energy electrons were used for sample charge compensation. High-resolution spectra were acquired in the region of interest using the following experimental parameters: 20–40 eV energy window, pass energy of 20 eV, step size of 0.1 eV, and dwell time of 1000 ms. One sweep was used to acquire a survey spectrum of all binding regions (1200–0 eV) at a pass energy 160 eV, step size of 1 eV, and a dwell time of 100 ms. Samples were mounted by pressing them to indium foil for analysis. All spectra were calibrated using the adventitious Au4f peak at 84.0 eV. A Shirley-type background was subtracted from each spectrum to account for inelastically scattered electrons contributing to the broad background.

#### 4.5.10 Atomic Force Microscopy (AFM)

The samples were imaged using a model 5500 or model 5420 atomic force microscope with Pico View v.1.12 software (Agilent Technologies, Chandler, AZ). Non-conductive imaging probes from Bruker (MSCT, 0.01–0.6 N/m) were used to acquire contact-mode images. Images were processed and analyzed using Gwyddion (v. 2.22), an open-access processing software designed for AFM images, supported by the Czech Metrology Institute.<sup>20</sup>

#### 4.6 References

1. Oppenheim, A. L., *Ancient Mesopotamia: Portrait of a Dead Civilization*. U. Chicago Press: 1964.
2. Franklin, B., Of the Stilling of Waves by means of Oil. *Phil. Trans.* **1774**, *64*, 445.
3. Rayleigh, W.; Pockels, A., Prof. Van der Waals on the Continuity of the Liquid and Gaseous States. *Nature* **1891**, *43*, 437.
4. Blodgett, K., Films Built by Depositing Successive Monomolecular Layers on a Solid Surface. *J. Am. Chem. Soc.* **1935**, *57*, 1007-1022.
5. (a) Mahouche-Chergui, S.; Gam-Derouich, S.; Mangeney, C.; Chehimi, M., Aryl Diazonium Salts: A New Class of Coupling Agents for Bonding Polymers, Biomacromolecules and Nanoparticles to Surfaces. *Chem. Soc. Rev.* **2011**, *40*, 4143-4166; (b) Belanger, D.; Pinson, J., Electrografting: A Powerful Method for Surface Modification. *Chem. Soc. Rev.* **2011**, *40*, 3995-4048; (c) Pinson, J.; Podvorisca, F., Attachment of Organic Layers to Conductive or Semiconductive Surfaces by Reduction of Diazonium Salts. *Chem. Soc. Rev.* **2005**, *34*, 429-439; (d) Pensa, E.; Cortes, E.; Corthey, G.; Carro, P.; Vericat, C.; Fonticelli, M.; Benitez, G.; Rubert, A.; Salvarezza, R., The Chemistry of Sulfur-Gold Interface: In Search of a Unified Model. *Acc. Chem. Res.* **2012**, *45*, 1183-1192; (e) Vericat, C.; Vela, M.; Benitez, G.; Carro, P.; Salvarezza, R., Self-Assembled Monolayers of Thiols and Dithiols on Gold: New Challenges for a Well-Known System. *Chem. Soc. Rev.* **2010**, *39*, 1805-1834; (f) Love, J.; Estroff, L.; Kriebel, J.; Nuzzo, R.; Whitesides, G., Self-Assembled Monolayers of Thiolates on Metals as a Form of Nanotechnology. *Chem. Rev.* **2005**, *105*, 1103-1169; (g) Azzaroni, O.; Salvarezza, R., Chemisorbed Self-Assembled Monolayers. John Wiley & Sons, Ltd.: 2012; (h) Schreiber, F., Self-Assembled Monolayers: From 'Simple' Model Systems to Biofunctionalized Interfaces. *J. Phys.: Condens. Matter* **2004**, *16*, R881-R900.
6. Nuzzo, R.; Allara, D., Adsorption of Bifunctional Organic Disulfides on Gold Surfaces. *J. Am. Chem. Soc.* **1983**, *105*, 4481-4483.

7. Gooding, J.; Mearns, F.; Yang, W.; Liu, J., Self-Assembled Monolayers into the 21st Century: Recent Advances and Applications. *Electroanalysis* **2003**, *15*, 81-96.
8. Delamarche, E.; Bruno, M.; Biebuyck, H.; Gerber, C., Golden Interfaces: The Surface of Self-Assembled Monolayers. *Adv. Mater.* **1996**, *8*, 71-729.
9. Laforgue, A.; Addou, T.; Belanger, D., Characterization of the Deposition of Organic Molecules at the Surface of Gold by the Electrochemical Reduction of Aryldiazonium Cations. *Langmuir* **2005**, *21*, 6855-6865.
10. Laurentis, L.; Stoyanov, S.; Gusarov, S.; Kovalenko, A.; Du, R.; Lopinski, G.; McDermott, M. T., Diazonium-Derived Aryl Films on Gold Nanoparticles: Evidence for a Carbon-Gold Covalent Bond. *ACS Nano* **2011**, *5*, 4219-4227.
11. (a) Verberne-Sutton, S.; Quarels, R.; Garino, J.; Ragains, J., Application of Visible Light Photocatalysis with Particle Lithography. *J. Am. Chem. Soc.* **2014**, *136*, 14438-14444; (b) Bourgia, M.; Chehimi, M.; Combellas, C.; Decorse, P.; Kanoufi, F.; Deronzier, A.; Pinson, J., Sensitized Photografting of Diazonium Salts by Visible Light. *Chem. Mater.* **2013**, *25*, 90-97.
12. (a) Andrieux, C.; Pinson, J., The Standard Redox Potential of the Phenyl Radical/Anion Couple. *J. Am. Chem. Soc.* **2003**, *125*, 14801-14806; (b) Pause, L.; Robert, M.; Saveant, J., Can Single-Electron Transfer Break an Aromatic Carbon-Heteroatom Bond in One Step? A Novel Example of Transition between Stepwise and Concerted Mechanisms in the Reduction of Aromatic Iodides. *J. Am. Chem. Soc.* **1999**, *121*, 7158-7159.
13. (a) Nguyen, J.; D'Amato, E.; Narayanam, J.; Stephenson, C., Engaging Unactivated Alkyl, Alkenyl and Aryl Iodides in Visible-Light-Mediated Free Radical Reactions. *Nat. Chem.* **2012**, *4*, 854-859; (b) Kim, H.; Lee, C., Visible-Light-Induced Photocatalytic Reductive Transformations of Organohalides. *Angew. Chem. Int. Ed.* **2012**, *51*, 12303-12306.
14. Binnig, G.; Quate, C.; Gerber, C., Atomic Force Microscope. *Phys. Rev. Lett.* **1986**, *56*, 930-933.
15. Wagner, P.; Zaugg, F.; Kernen, P.; Hegner, M.; Semenza, G.,  $\omega$ -Functionalized Self-Assembled Monolayers Chemisorbed on Ultraflat Au(111) Surfaces for Biological Scanning Probe Microscopy in Aqueous Buffers. *J. Vac. Sci. Technol. B* **1996**, 1466-1471.
16. Folkesson, S.; Sundberg, P., A Reinvestigation of the Binding Energy versus Atomic Charge Relation for Oxygen from X-ray Photoelectron Spectroscopy. *Spectrosc. Lett.* **1987**, *20*, 193-200.
17. Pangborn, A.; Giardello, M.; Grubbs, R.; Rosen, R.; Timmers, F., Safe and Convenient Procedure for Solvent Purification. *Organometallics* **1996**, *15*, 1518-1520.

18. Polosan, S.; Radu, I., Mechanisms of the Charge Transfer in IrQ(ppy)<sub>2</sub>-5Cl Dual-Emitter Compound. *J. Nanosci. Nanotechnol.* **2013**, *13*, 5203-5208.
19. Lowry, M.; Hudson, W.; Pascal, R.; Bernhard, S., Accelerated Luminophore Discovery through Combinatorial Synthesis *J. Am. Chem. Soc.* **2004**, *126*, 14129-14135.
20. Necas, D.; Klapetek, P., *Central Eur. J. Phys.* **2012**, *10*, 181-188.



## APPENDIX A: COPYRIGHT RELEASES



RightsLink®

Home

Account Info

Help



**Title:** A Novel Ascaroside Controls the Parasitic Life Cycle of the Entomopathogenic Nematode Heterorhabditis bacteriophora

**Author:** Jaime H. Noguez, Elizabeth S. Conner, Yue Zhou, et al

**Publication:** ACS Chemical Biology

**Publisher:** American Chemical Society

**Date:** Jun 1, 2012

Copyright © 2012, American Chemical Society

Logged in as:  
Elizabeth Conner

LOGOUT

### PERMISSION/LICENSE IS GRANTED FOR YOUR ORDER AT NO CHARGE

This type of permission/license, instead of the standard Terms & Conditions, is sent to you because no fee is being charged for your order. Please note the following:

- Permission is granted for your request in both print and electronic formats, and translations.
- If figures and/or tables were requested, they may be adapted or used in part.
- Please print this page for your records and send a copy of it to your publisher/graduate school.
- Appropriate credit for the requested material should be given as follows: "Reprinted (adapted) with permission from (COMPLETE REFERENCE CITATION). Copyright (YEAR) American Chemical Society." Insert appropriate information in place of the capitalized words.
- One-time permission is granted only for the use specified in your request. No additional uses are granted (such as derivative works or other editions). For any other uses, please submit a new request.

BACK

CLOSE WINDOW

## ELSEVIER LICENSE TERMS AND CONDITIONS

Dec 01, 2014

---

This is a License Agreement between Elizabeth S Conner ("You") and Elsevier ("Elsevier") provided by Copyright Clearance Center ("CCC"). The license consists of your order details, the terms and conditions provided by Elsevier, and the payment terms and conditions.

**All payments must be made in full to CCC. For payment instructions, please see information listed at the bottom of this form.**

Supplier	Elsevier Limited The Boulevard, Langford Lane Kidlington, Oxford, OX5 1GB, UK
Registered Company Number	1982084
Customer name	Elizabeth S Conner
Customer address	3964 Gourrier Avenue BATON ROUGE, LA 70808
License number	3520431435664
License date	Dec 01, 2014
Licensed content publisher	Elsevier
Licensed content publication	Bioorganic & Medicinal Chemistry
Licensed content title	Ascaroside activity in <i>Caenorhabditis elegans</i> is highly dependent on chemical structure
Licensed content author	Kyle A. Hollister, Elizabeth S. Conner, Xinxing Zhang, Mark Spell, Gary M. Bernard, Pratik Patel, Ana Carolina G.V. de Carvalho, Rebecca A. Butcher, Justin R. Ragains
Licensed content date	15 September 2013
Licensed content volume number	21
Licensed content issue number	18
Number of pages	16
Start Page	5754
End Page	5769
Type of Use	reuse in a thesis/dissertation
Portion	full article
Format	both print and electronic
Are you the author of this Elsevier article?	Yes

Will you be translating?	No
Title of your thesis/dissertation	I. SYNTHESIS OF ASCAROSIDES FOR BIOLOGICAL EVALUATION AND II. DEVELOPMENT OF VISIBLE LIGHT-PROMOTED SELENOFUNCTIONALIZATION AND GRAFTING OF ARYL IODIDES
Expected completion date	Jan 2015
Estimated size (number of pages)	190
Elsevier VAT number	GB 494 6272 12
Permissions price	0.00 USD
VAT/Local Sales Tax	0.00 USD / 0.00 GBP
Total	0.00 USD
Terms and Conditions	

## ELSEVIER LICENSE TERMS AND CONDITIONS

Dec 01, 2014

---

This is a License Agreement between Elizabeth S Conner ("You") and Elsevier ("Elsevier") provided by Copyright Clearance Center ("CCC"). The license consists of your order details, the terms and conditions provided by Elsevier, and the payment terms and conditions.

**All payments must be made in full to CCC. For payment instructions, please see information listed at the bottom of this form.**

Supplier	Elsevier Limited The Boulevard,Langford Lane Kidlington,Oxford,OX5 1GB,UK
Registered Company Number	1982084
Customer name	Elizabeth S Conner
Customer address	3964 Gourrier Avenue BATON ROUGE, LA 70808
License number	3520440276548
License date	Dec 01, 2014
Licensed content publisher	Elsevier
Licensed content publication	Carbohydrate Research
Licensed content title	An $\alpha$ -selective, visible light photocatalytic glycosylation of alcohols with selenoglycosides
Licensed content author	Mark Spell,Xiaoping Wang,Amir E. Wahba,Elizabeth Conner,Justin Ragains
Licensed content date	22 March 2013
Licensed content volume number	369
Licensed content issue number	n/a
Number of pages	6
Start Page	42
End Page	47
Type of Use	reuse in a thesis/dissertation
Intended publisher of new work	other
Portion	full article
Format	both print and electronic
Are you the author of this Elsevier article?	Yes
Will you be translating?	No
Title of your thesis/dissertation	I. SYNTHESIS OF ASCAROSIDES FOR BIOLOGICAL EVALUATION

AND II. DEVELOPMENT OF VISIBLE LIGHT-PROMOTED  
SELENOFUNCTIONALIZATION AND GRAFTING OF ARYL IODIDES

Expected completion date	Jan 2015
Estimated size (number of pages)	190
Elsevier VAT number	GB 494 6272 12
Permissions price	0.00 USD
VAT/Local Sales Tax	0.00 USD / 0.00 GBP
Total	0.00 USD
Terms and Conditions	



**Title:** Visible-Light-Promoted Selenofunctionalization of Alkenes

**Author:** Elizabeth S. Conner, Katherine E. Crocker, Ranelka G. Fernando, et al

**Publication:** Organic Letters

**Publisher:** American Chemical Society

**Date:** Nov 1, 2013

Copyright © 2013, American Chemical Society

Logged in as:  
Elizabeth Conner

LOGOUT

## PERMISSION/LICENSE IS GRANTED FOR YOUR ORDER AT NO CHARGE

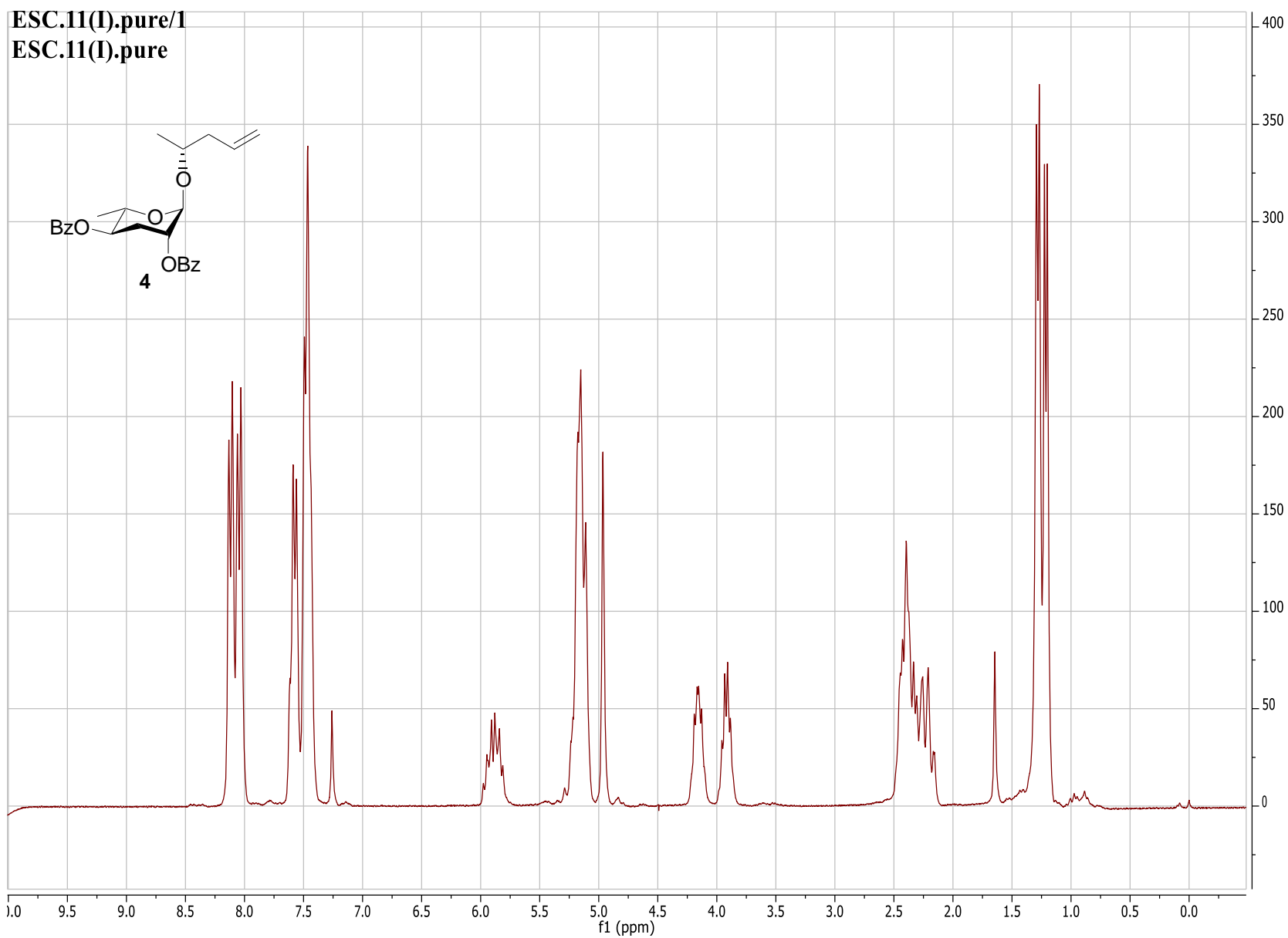
This type of permission/license, instead of the standard Terms & Conditions, is sent to you because no fee is being charged for your order. Please note the following:

- Permission is granted for your request in both print and electronic formats, and translations.
- If figures and/or tables were requested, they may be adapted or used in part.
- Please print this page for your records and send a copy of it to your publisher/graduate school.
- Appropriate credit for the requested material should be given as follows: "Reprinted (adapted) with permission from (COMPLETE REFERENCE CITATION). Copyright (YEAR) American Chemical Society." Insert appropriate information in place of the capitalized words.
- One-time permission is granted only for the use specified in your request. No additional uses are granted (such as derivative works or other editions). For any other uses, please submit a new request.

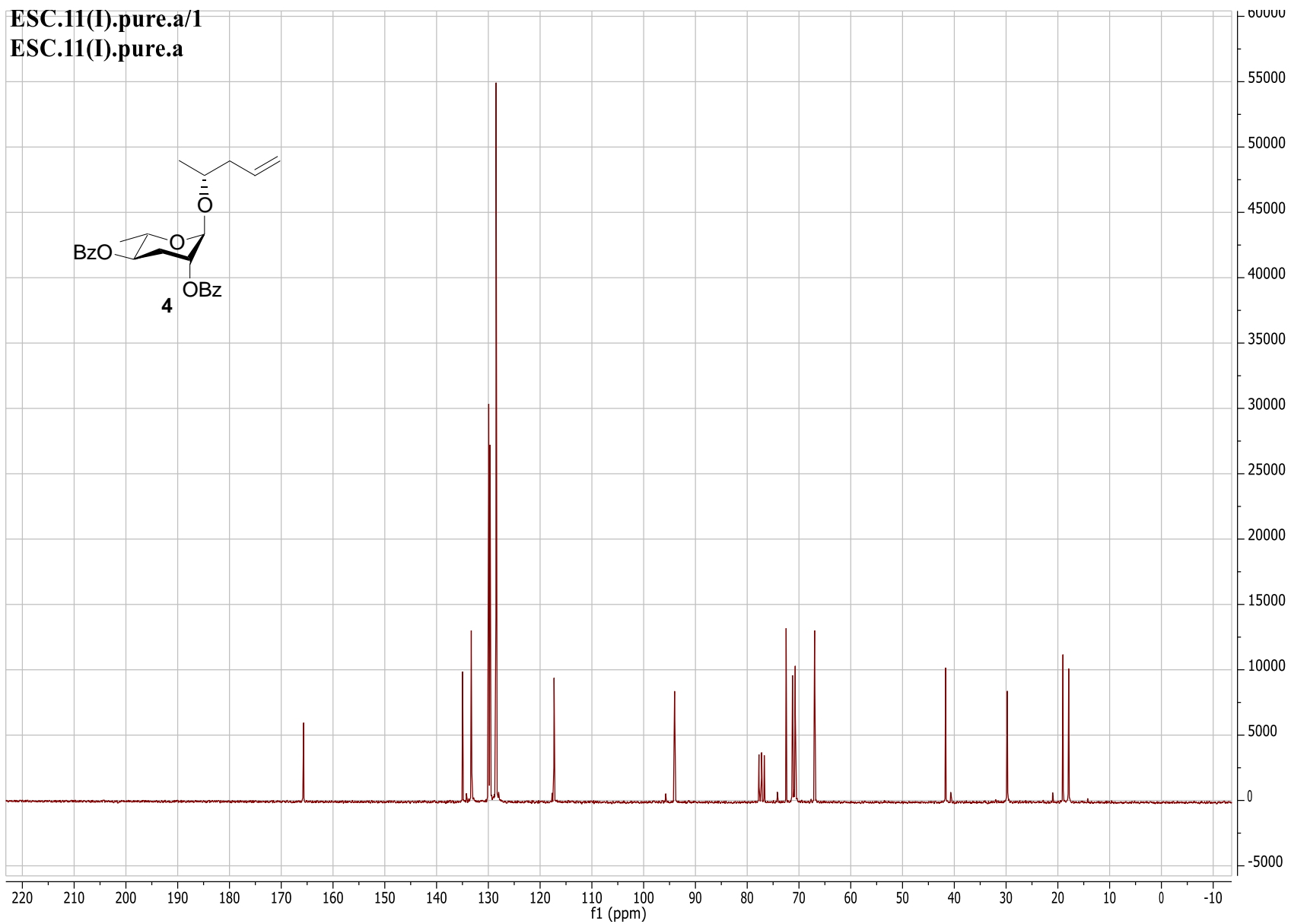
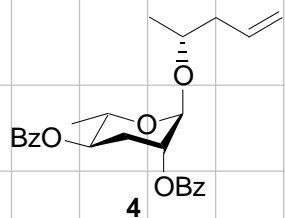
BACK

CLOSE WINDOW

APPENDIX B: NMR SPECTRA OF COUMPOUNDS FOUND IN CHAPTER 1

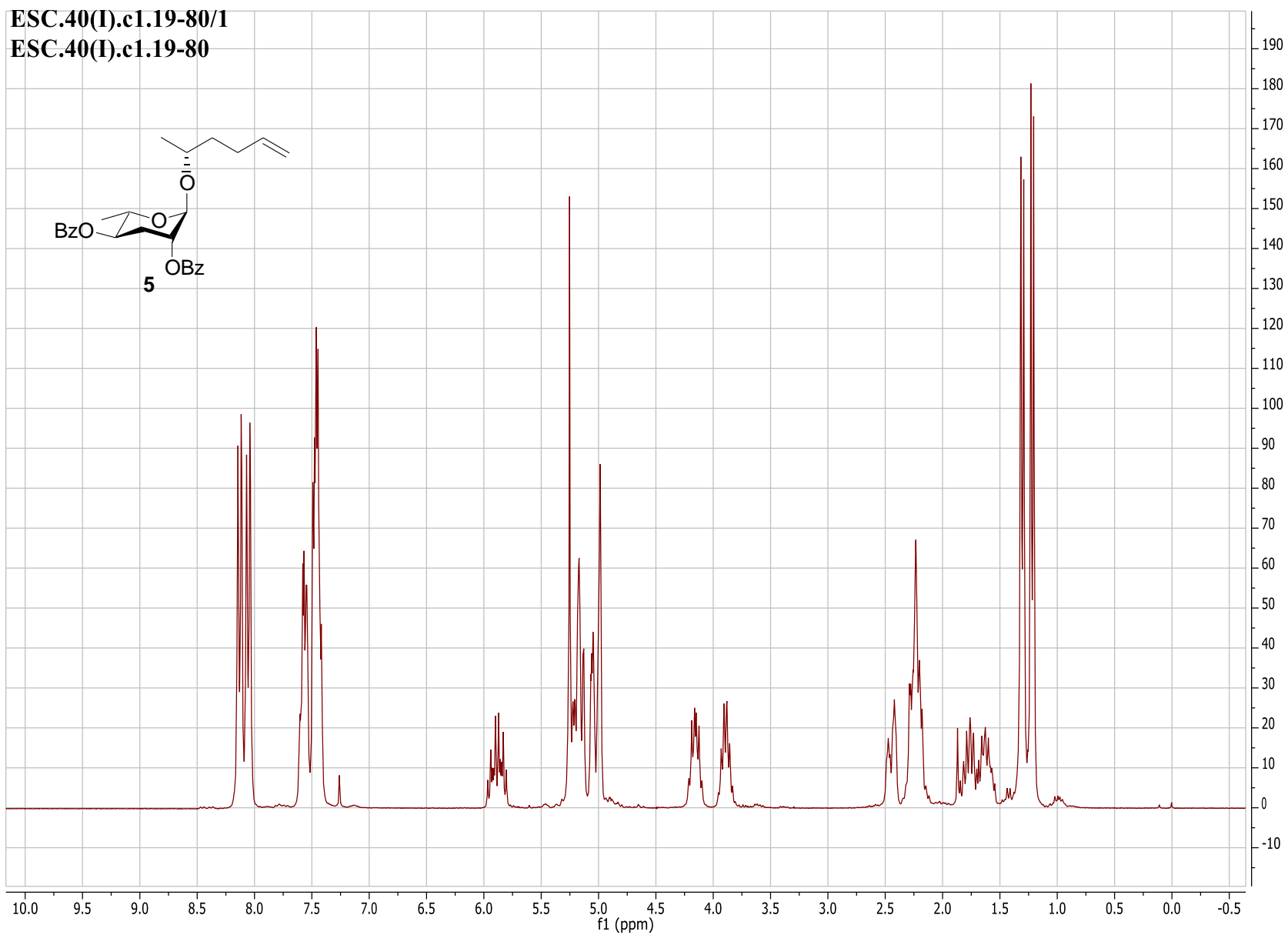


ESC.11(I).pure.a/1  
ESC.11(I).pure.a

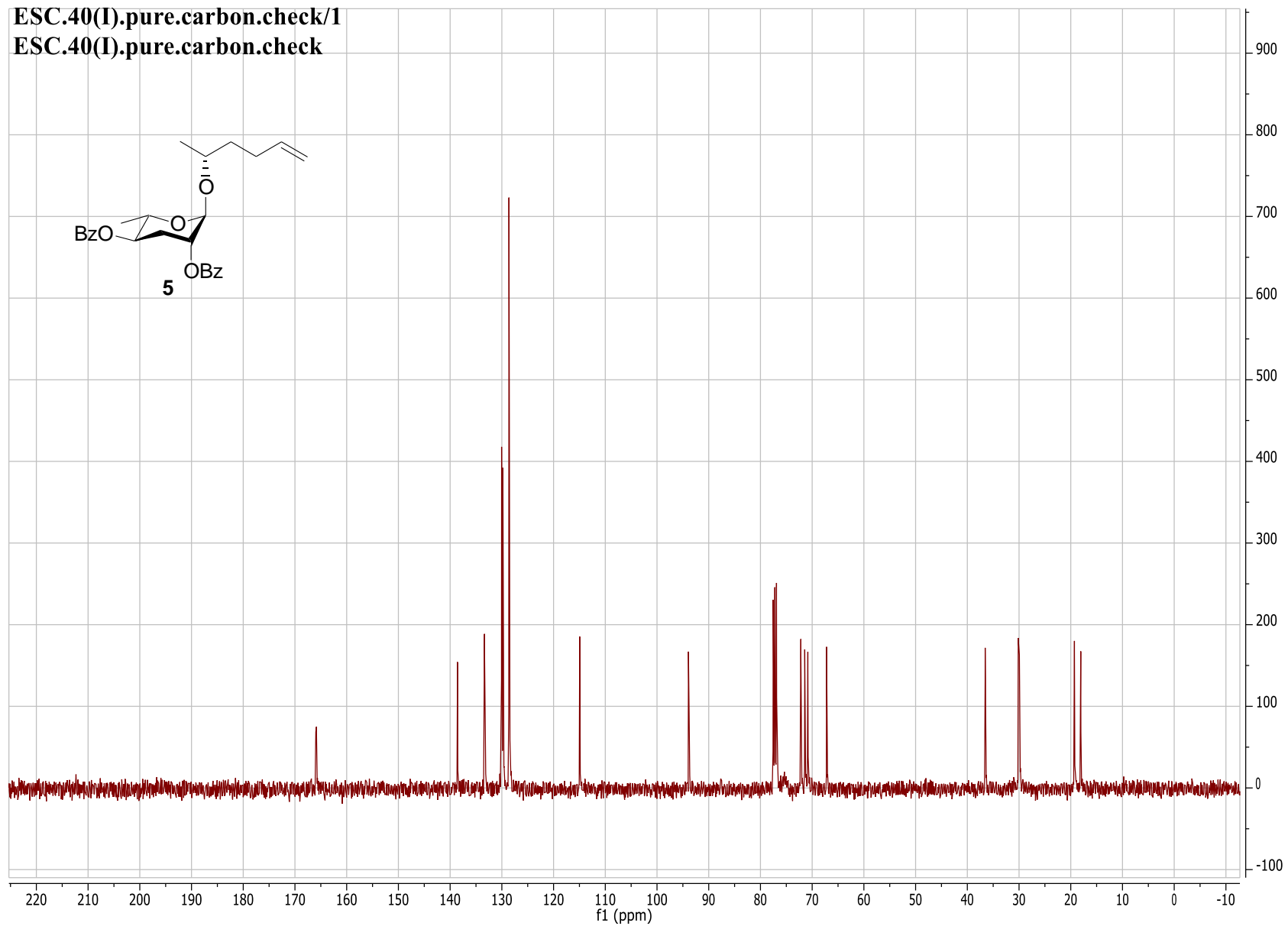
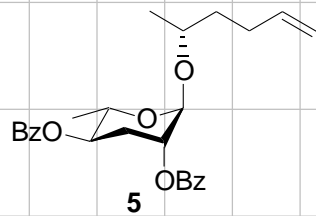




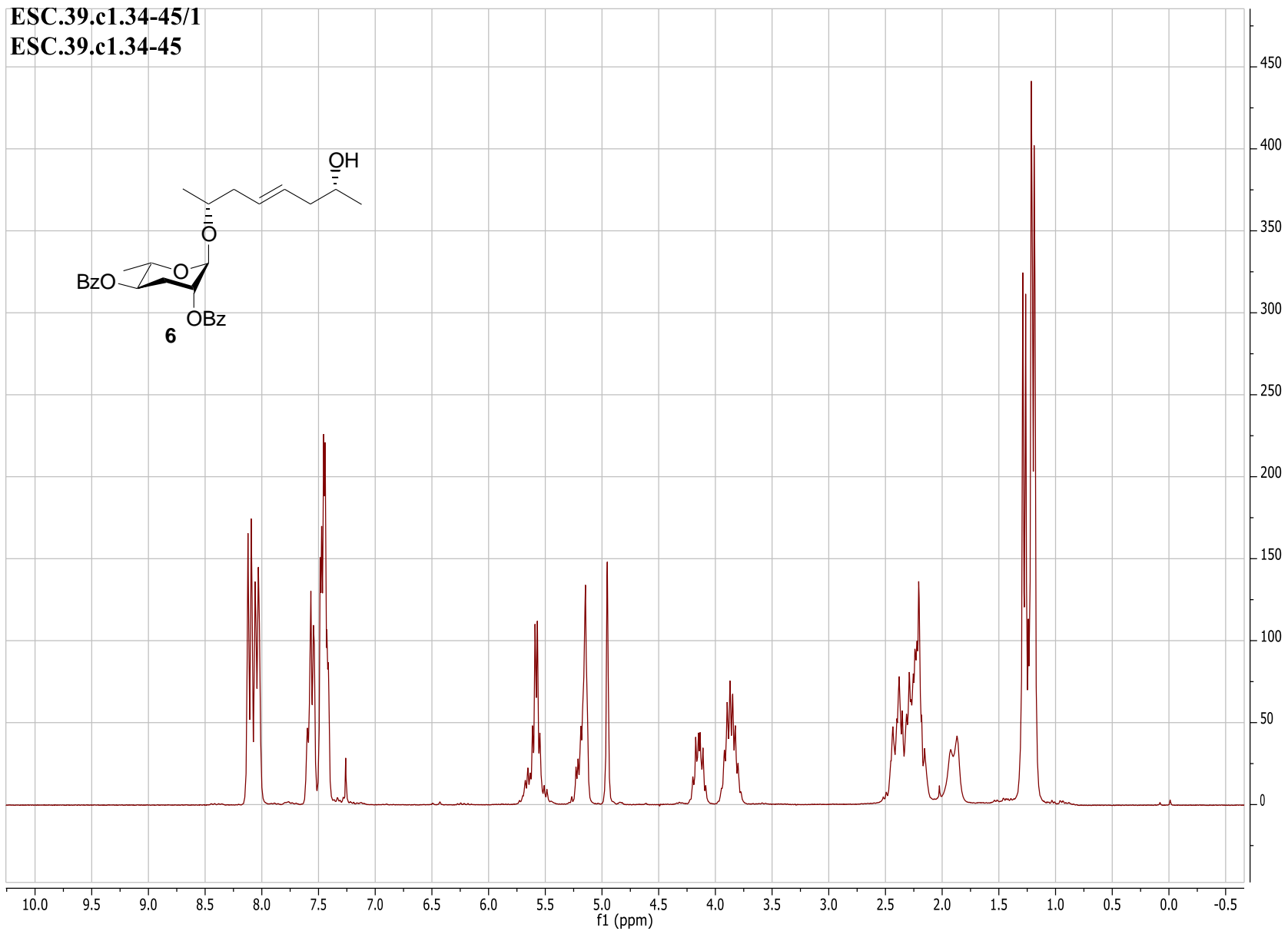
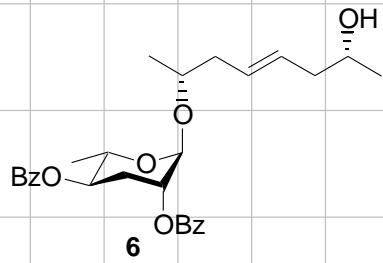
ESC.40(I).c1.19-80/1  
ESC.40(I).c1.19-80



ESC.40(I).pure.carbon.check/1  
ESC.40(I).pure.carbon.check

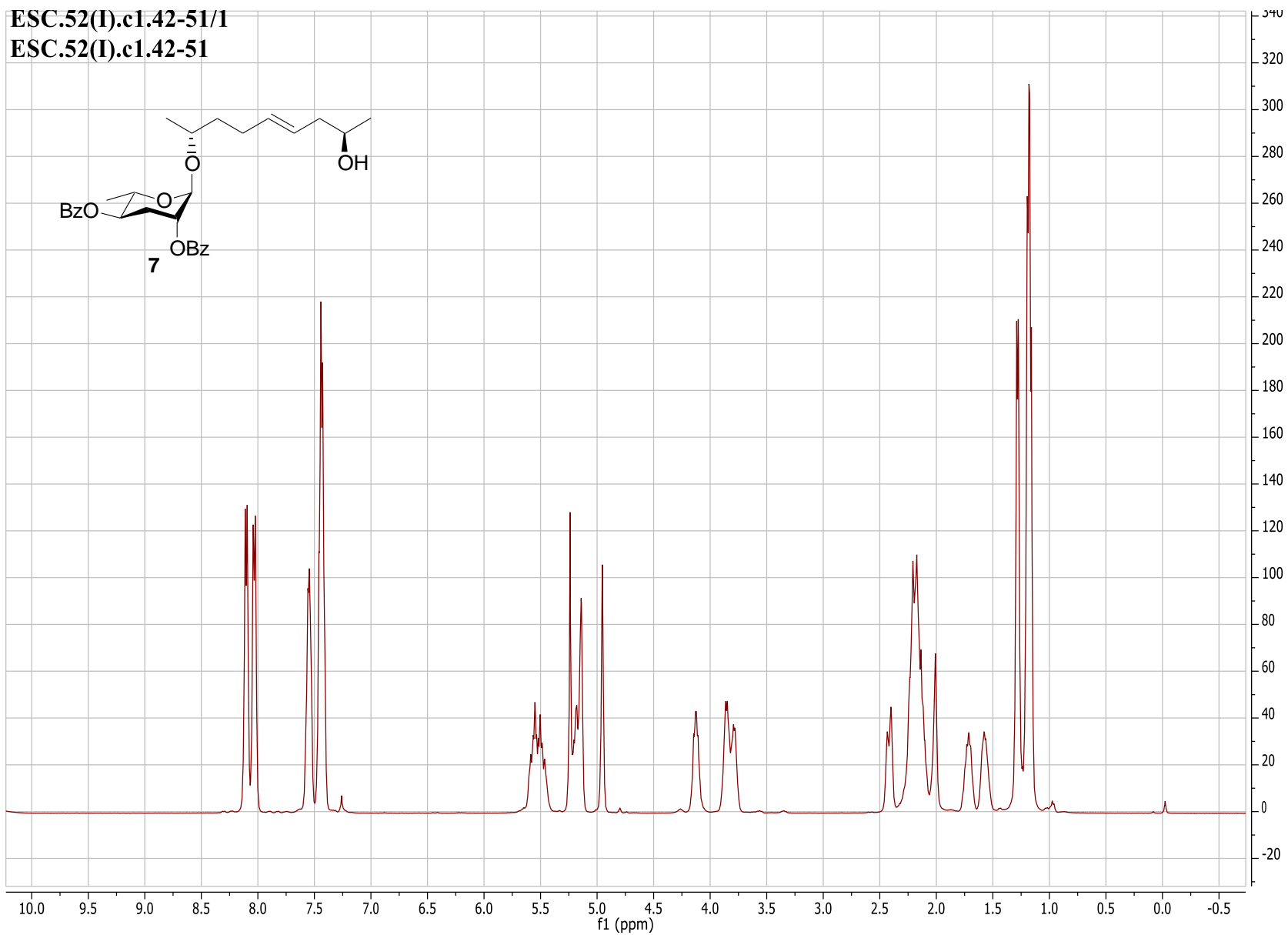
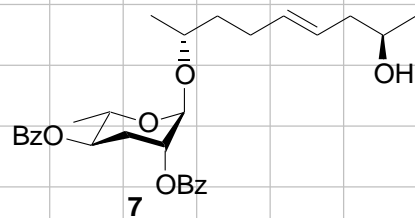


ESC.39.c1.34-45/1  
ESC.39.c1.34-45

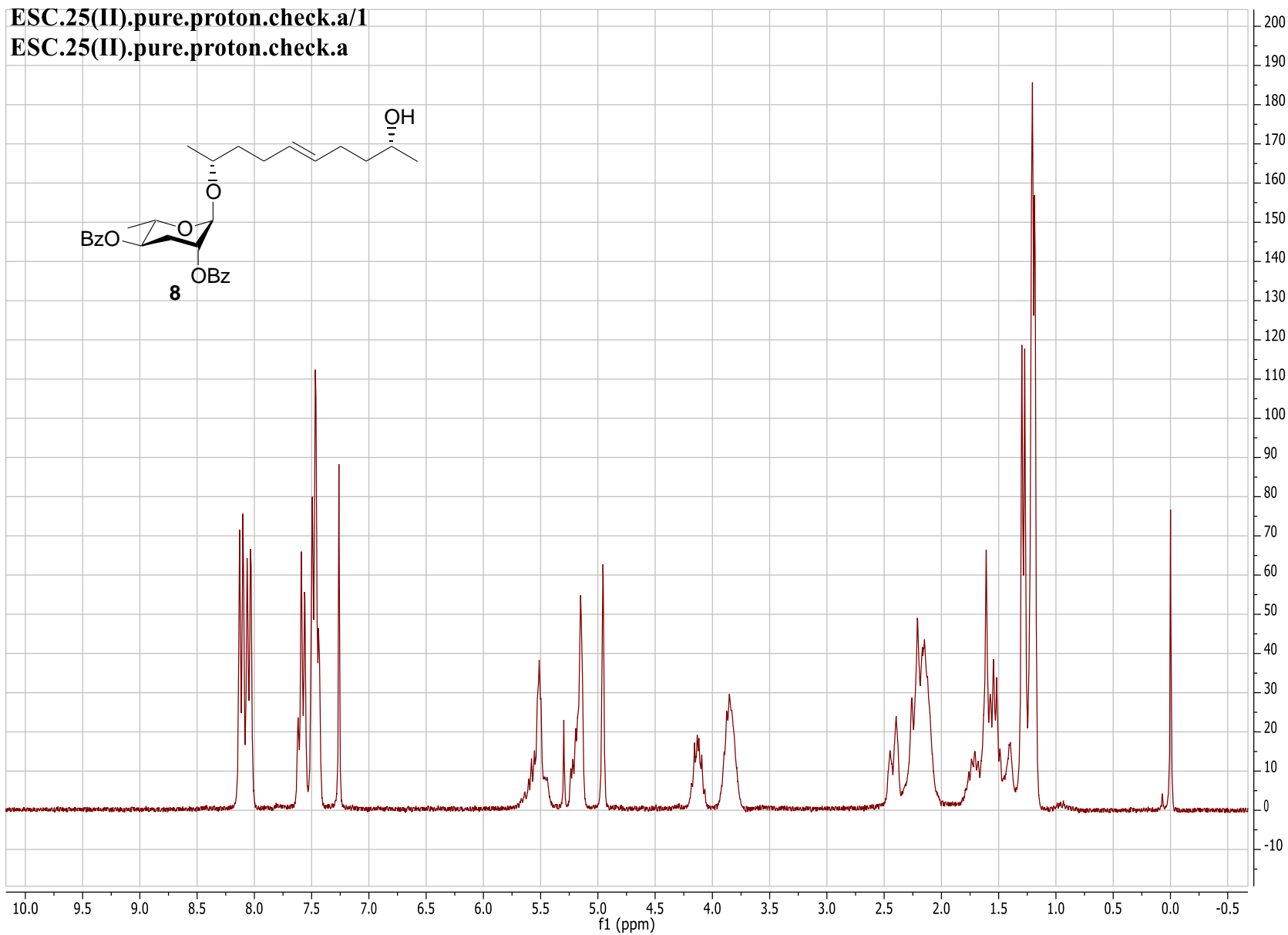


ESC.52(I).c1.42-51/1

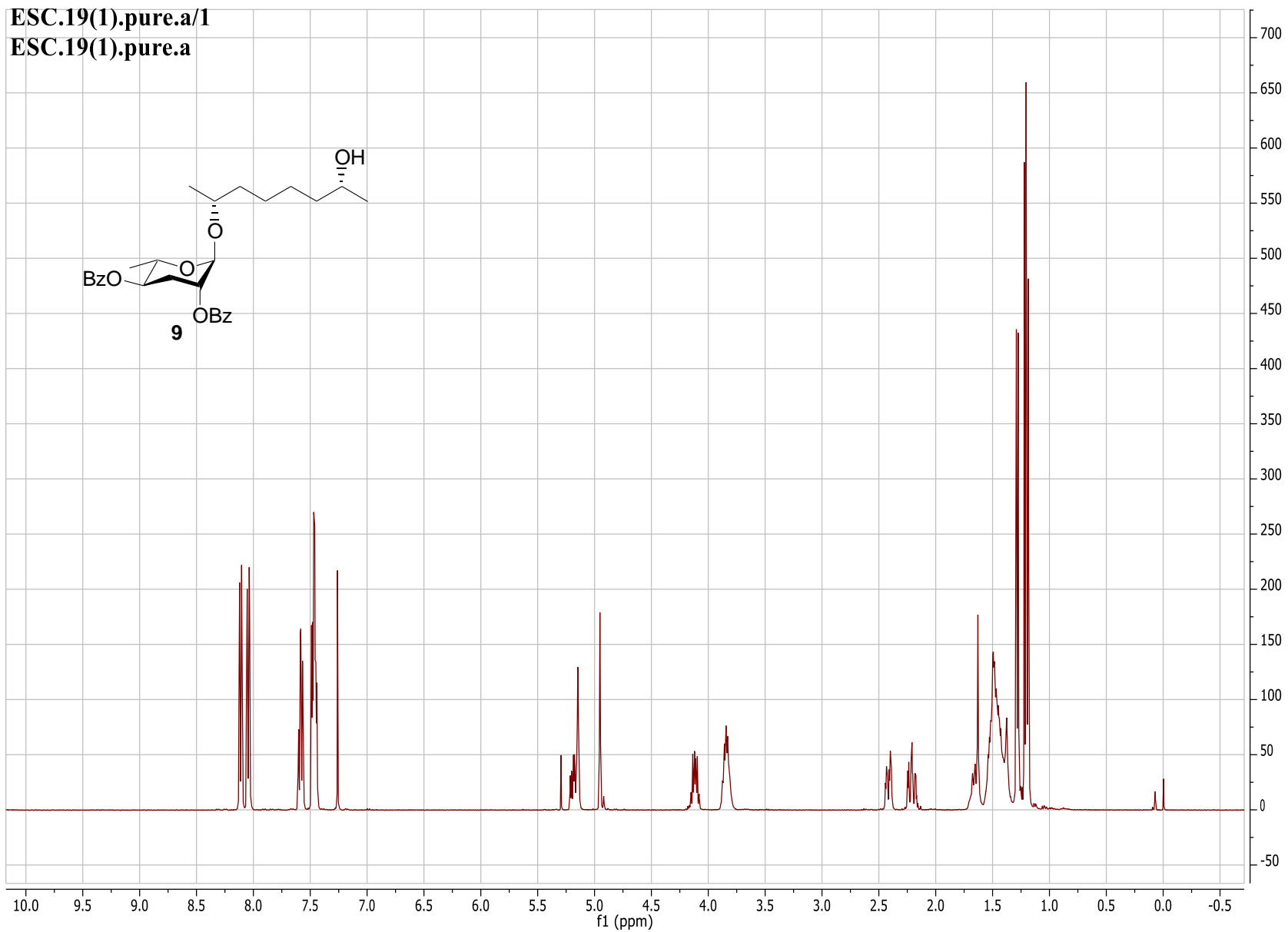
ESC.52(I).c1.42-51



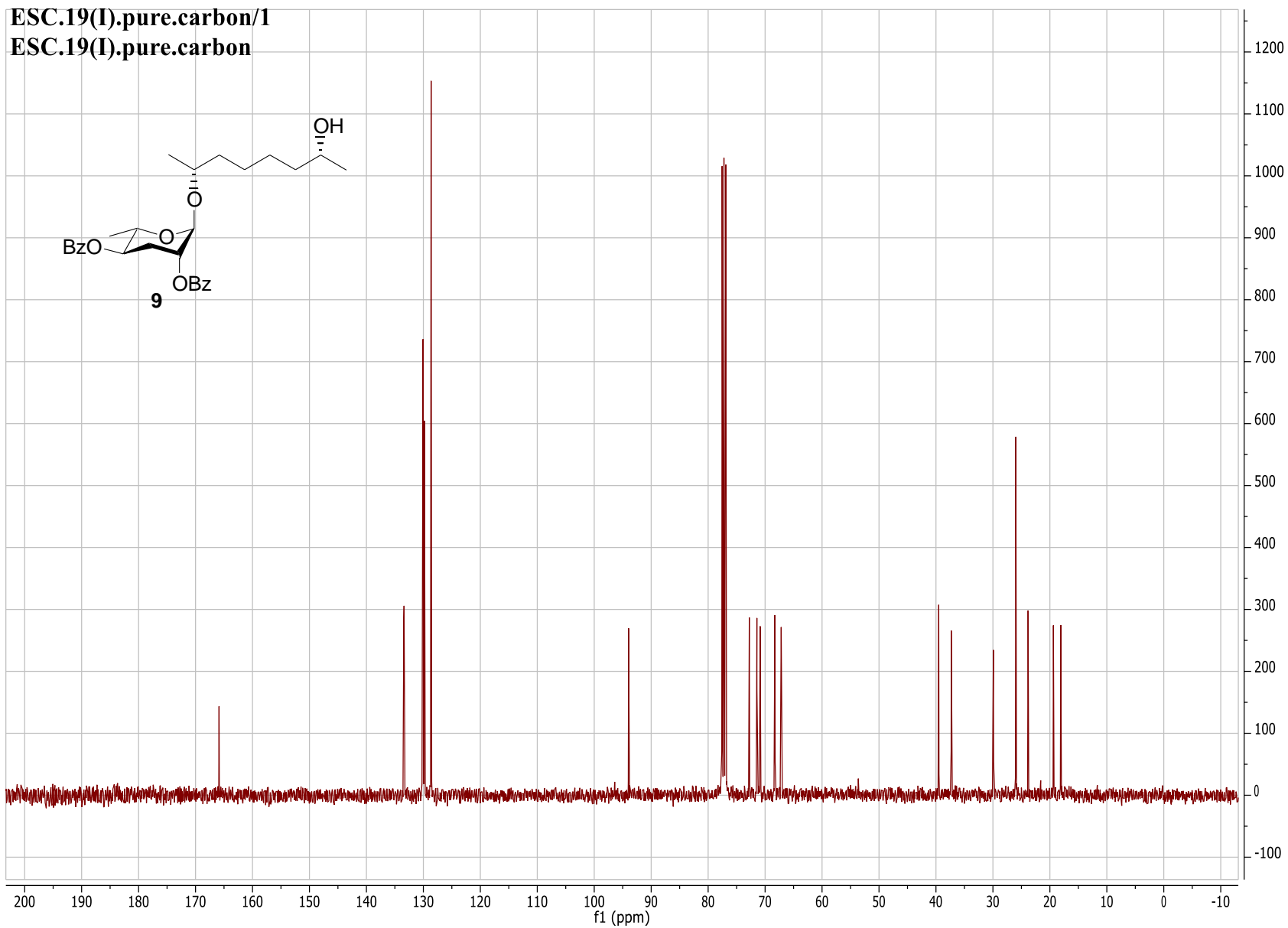
ESC.25(II).pure.proton.check.a/1  
ESC.25(II).pure.proton.check.a



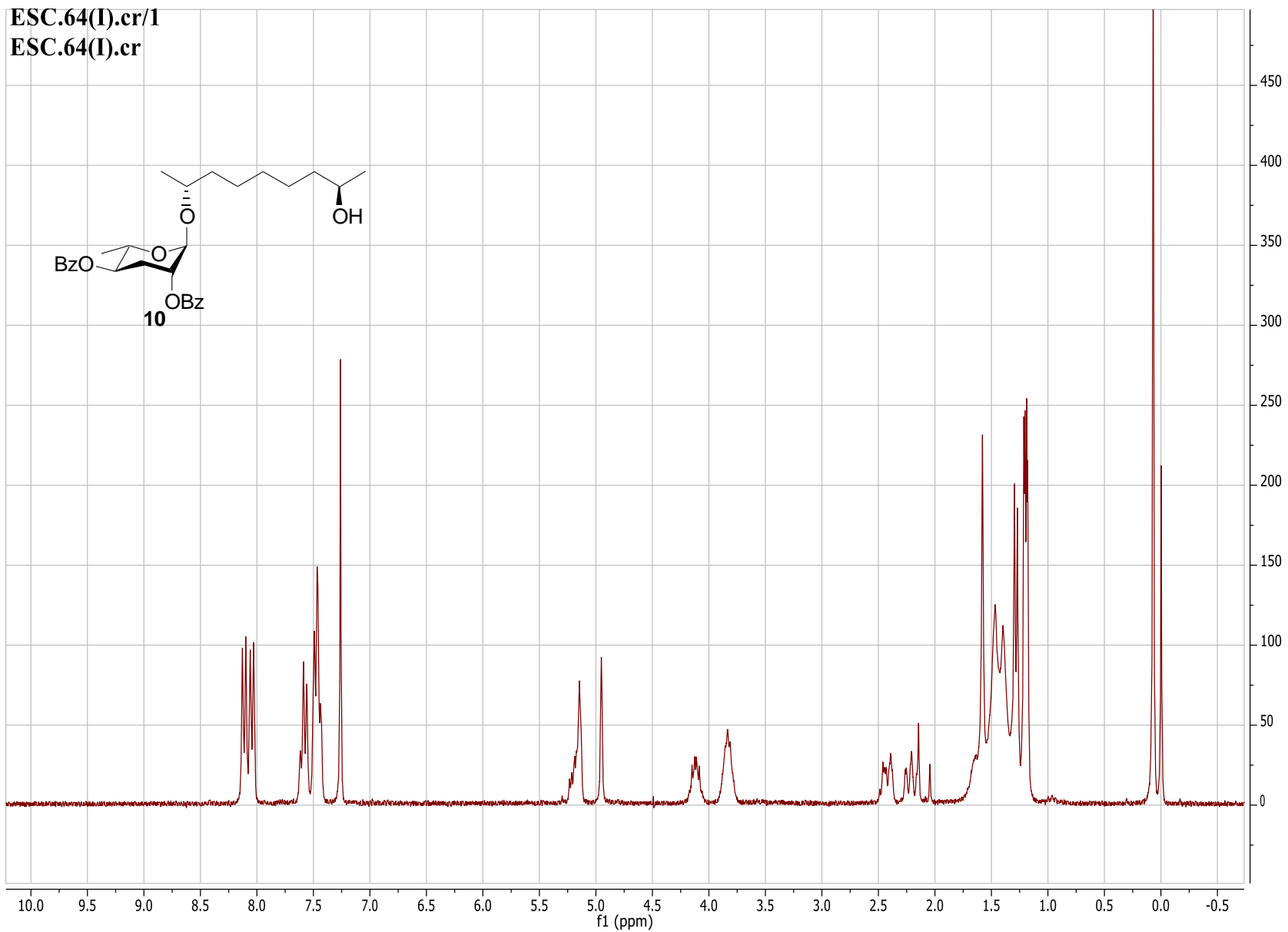
ESC.19(1).pure.a/1  
ESC.19(1).pure.a



ESC.19(I).pure.carbon/1  
ESC.19(I).pure.carbon

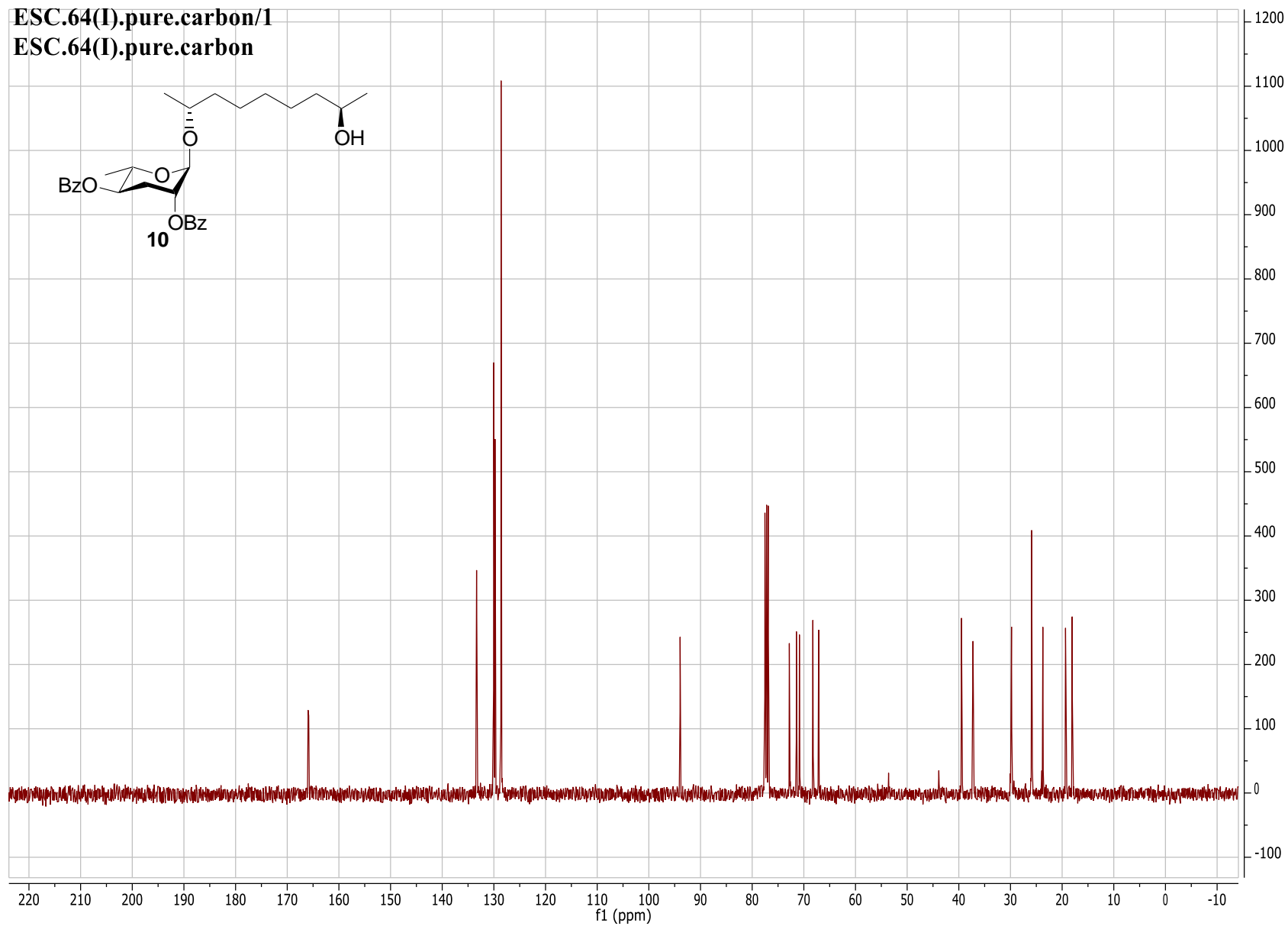
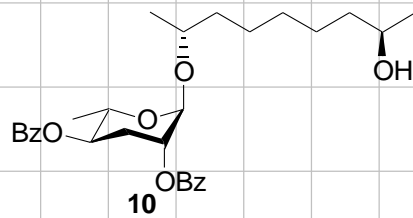


ESC.64(I).cr/1  
ESC.64(I).cr

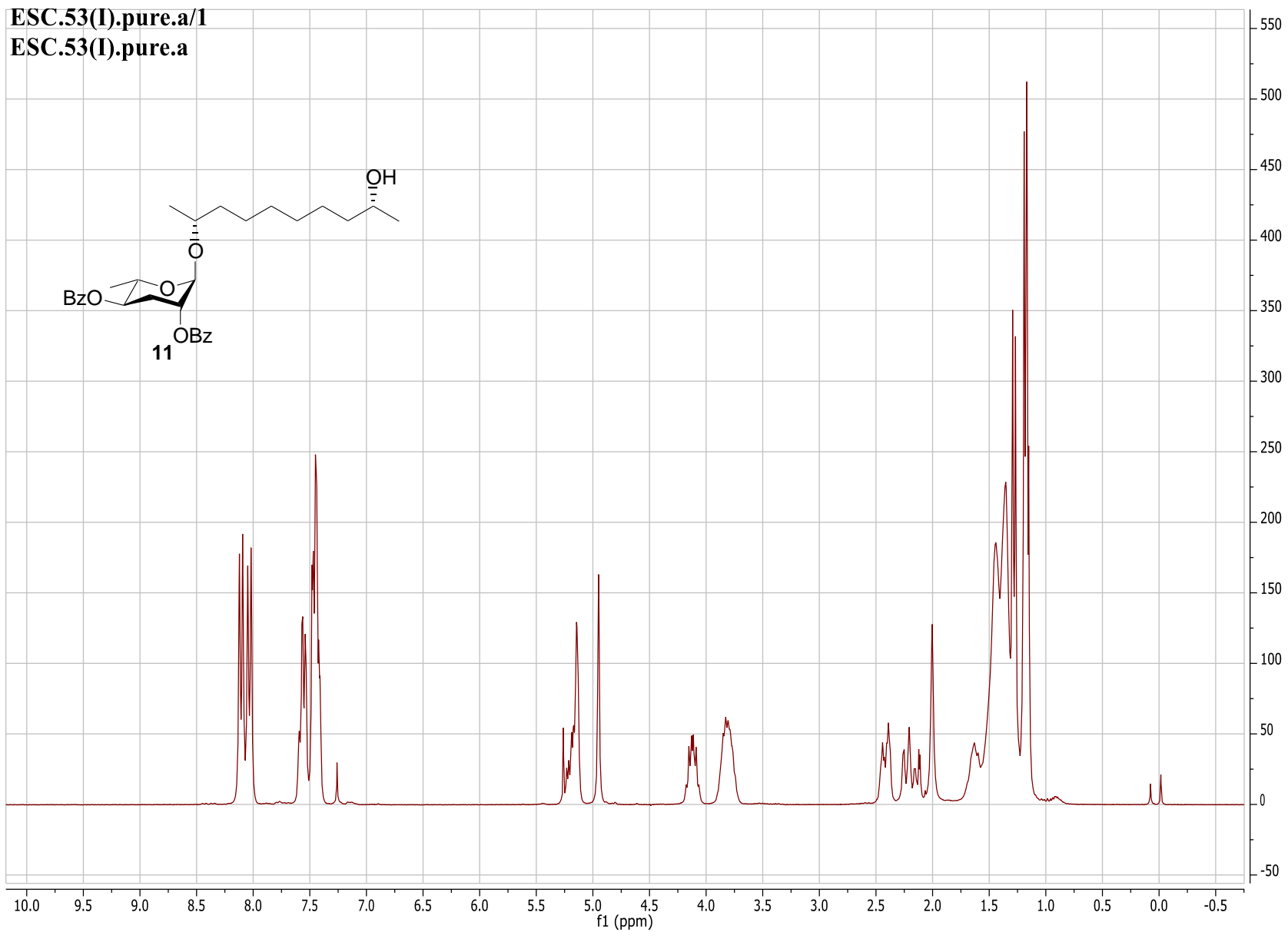
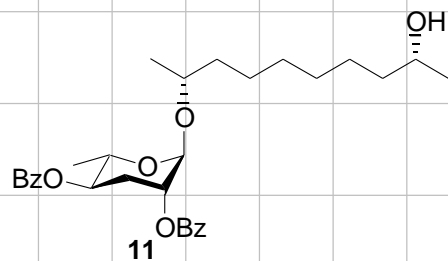




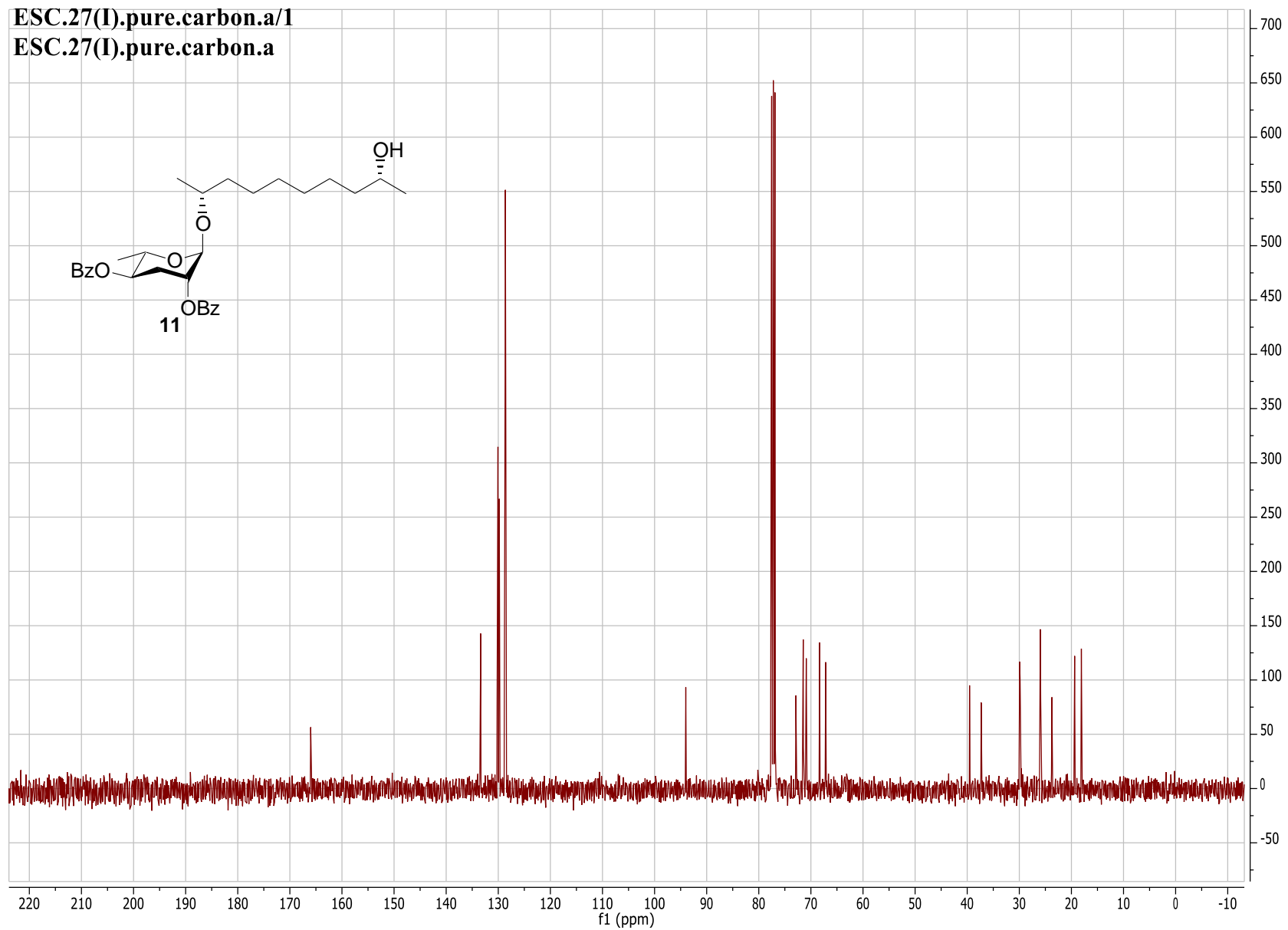
ESC.64(I).pure.carbon/1  
ESC.64(I).pure.carbon



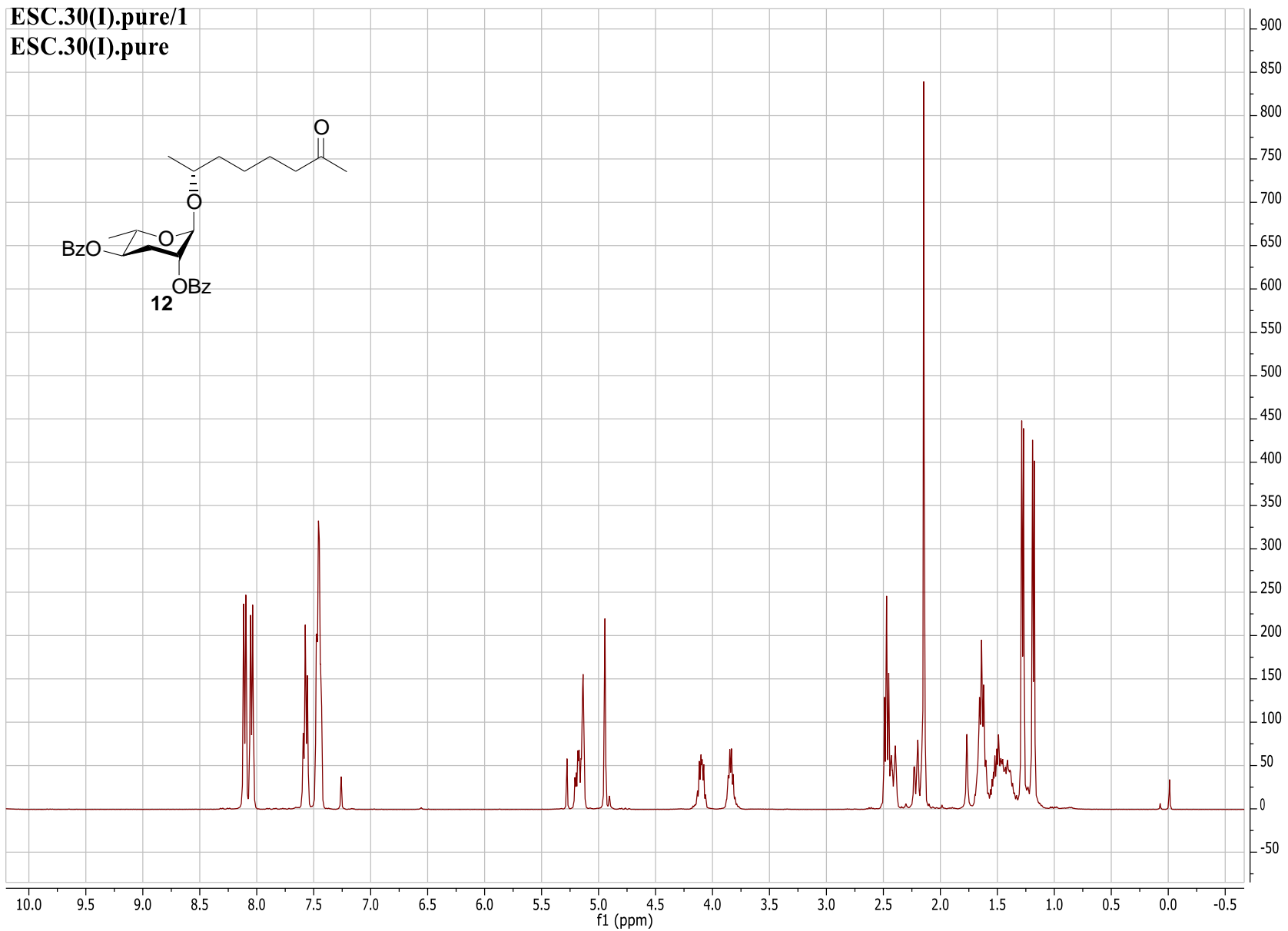
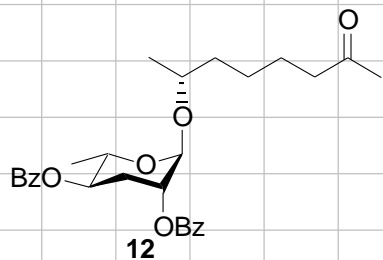
ESC.53(I).pure.a/1  
ESC.53(I).pure.a



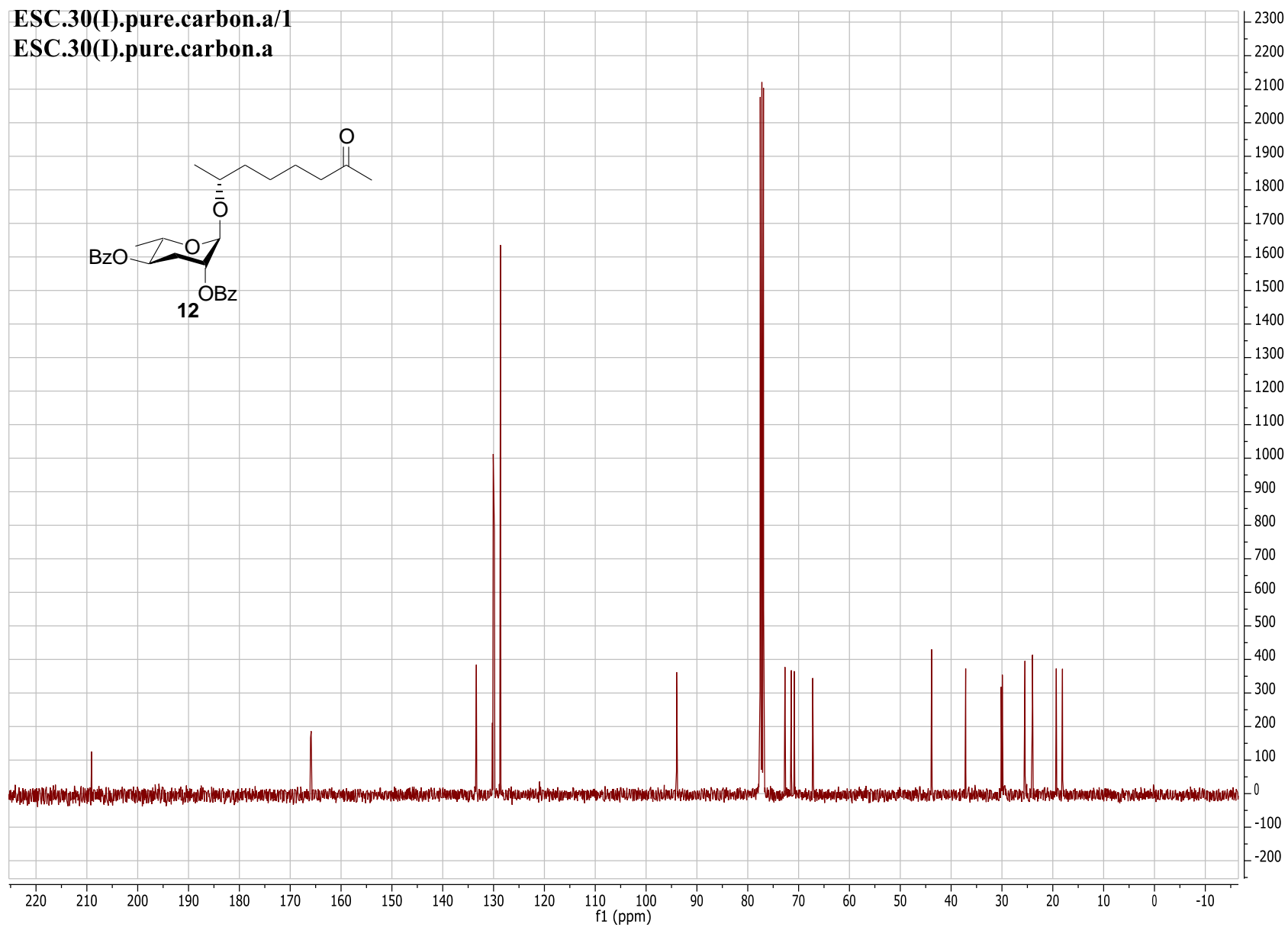
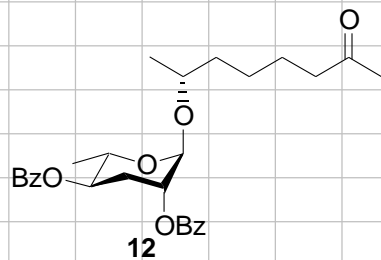
ESC.27(I).pure.carbon.a/1  
ESC.27(I).pure.carbon.a



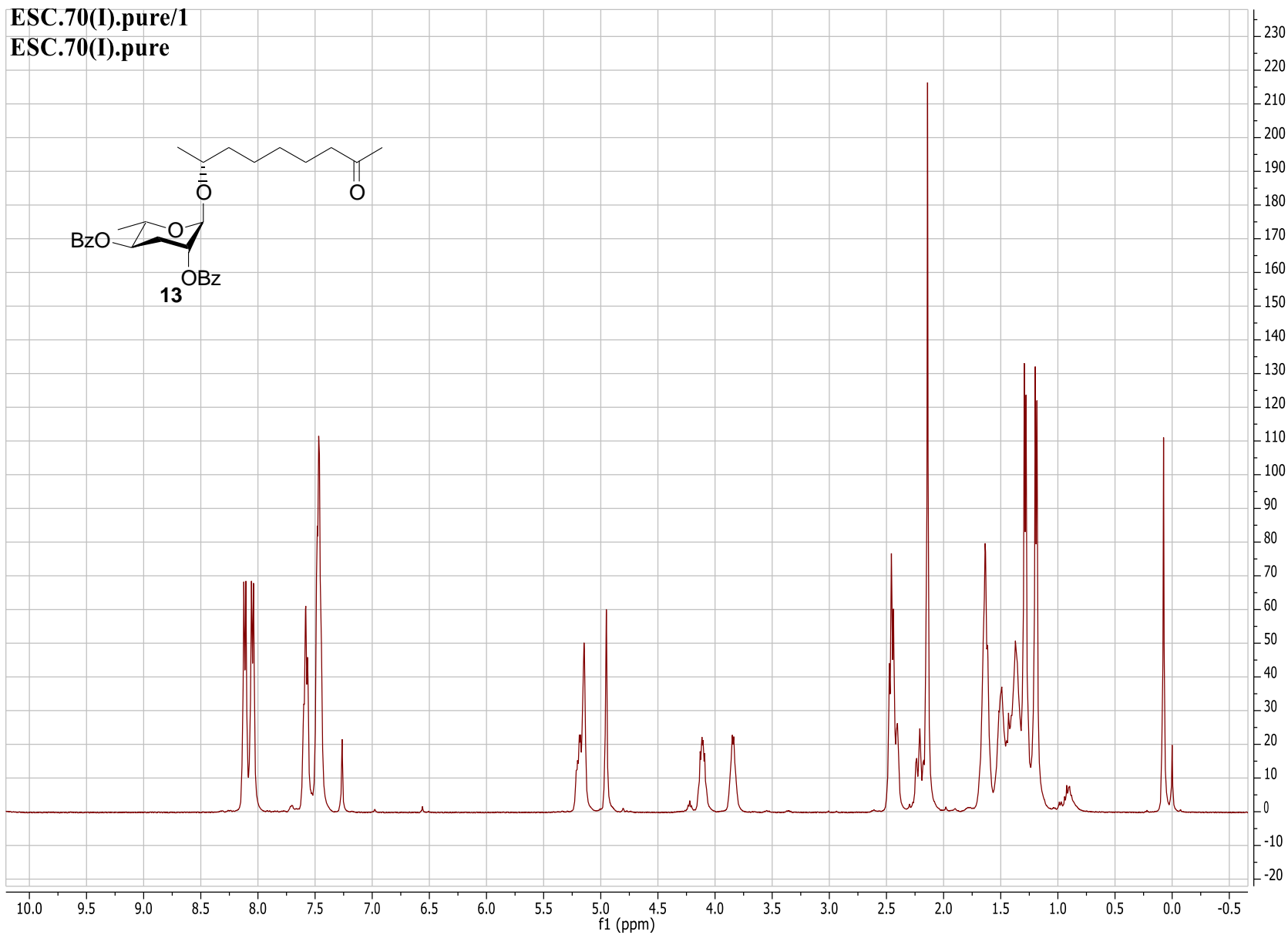
ESC.30(I).pure/1  
ESC.30(I).pure



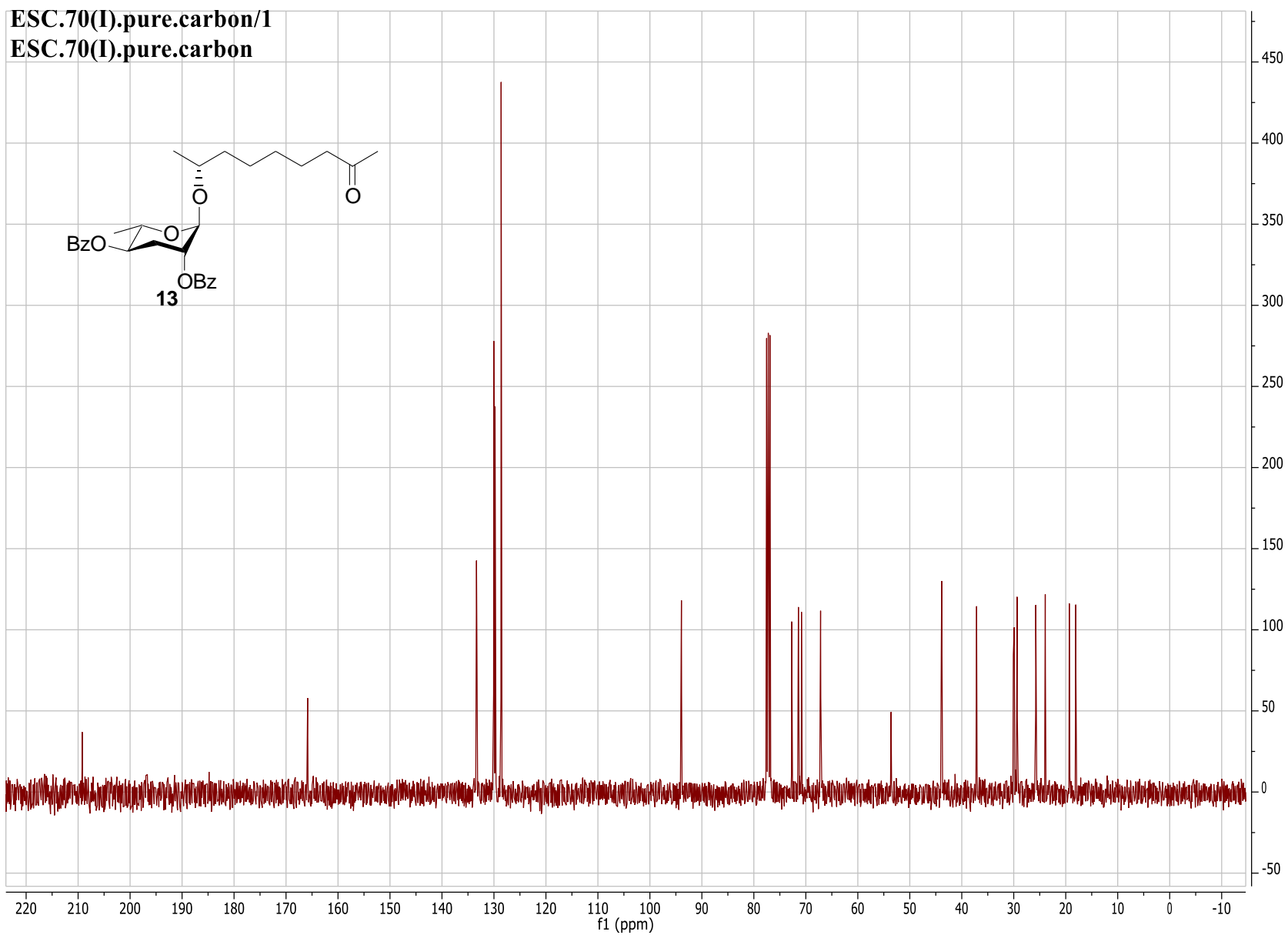
ESC.30(I).pure.carbon.a/1  
ESC.30(I).pure.carbon.a



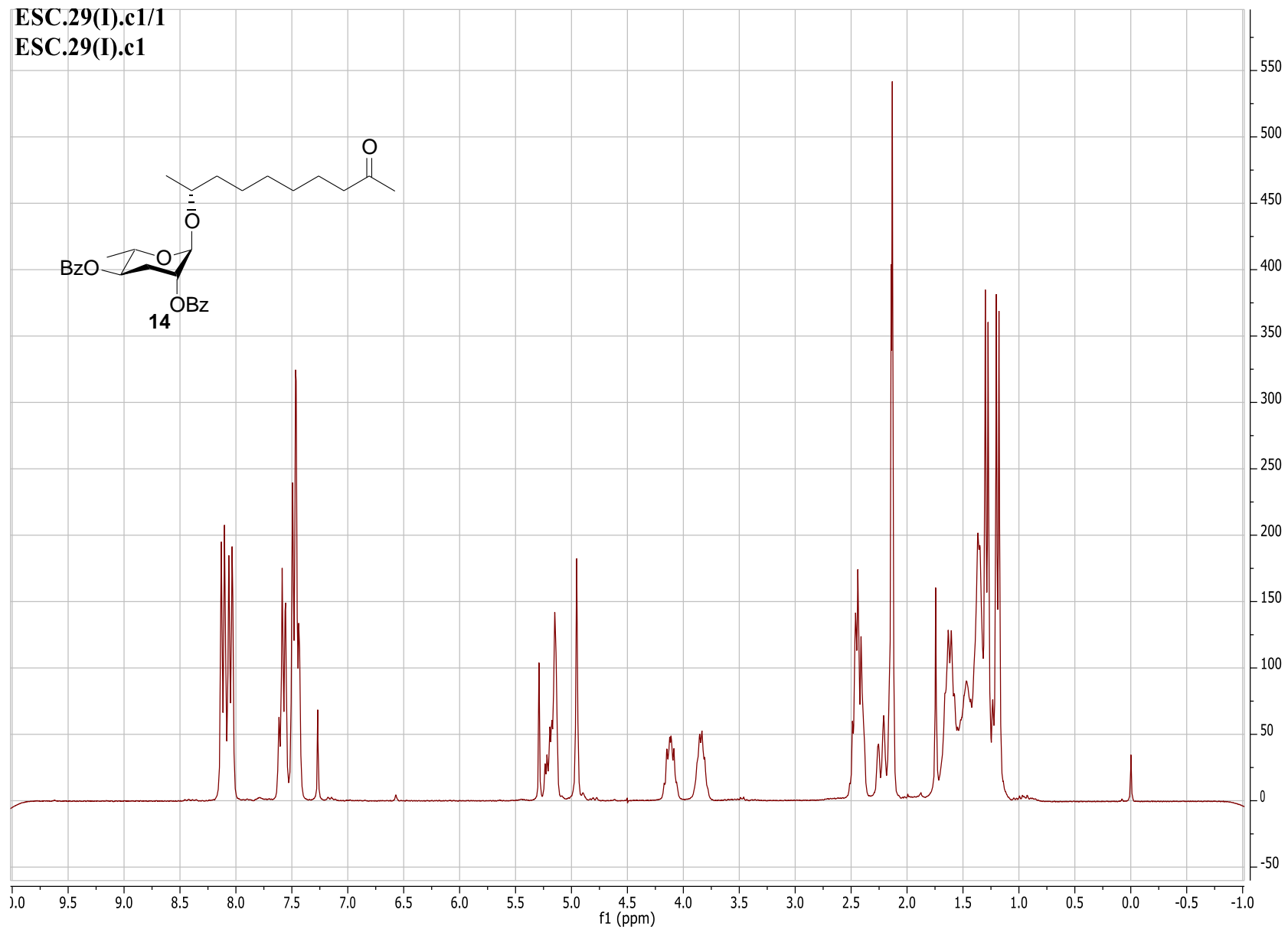
ESC.70(I).pure/1  
ESC.70(I).pure



ESC.70(I).pure.carbon/1  
ESC.70(I).pure.carbon

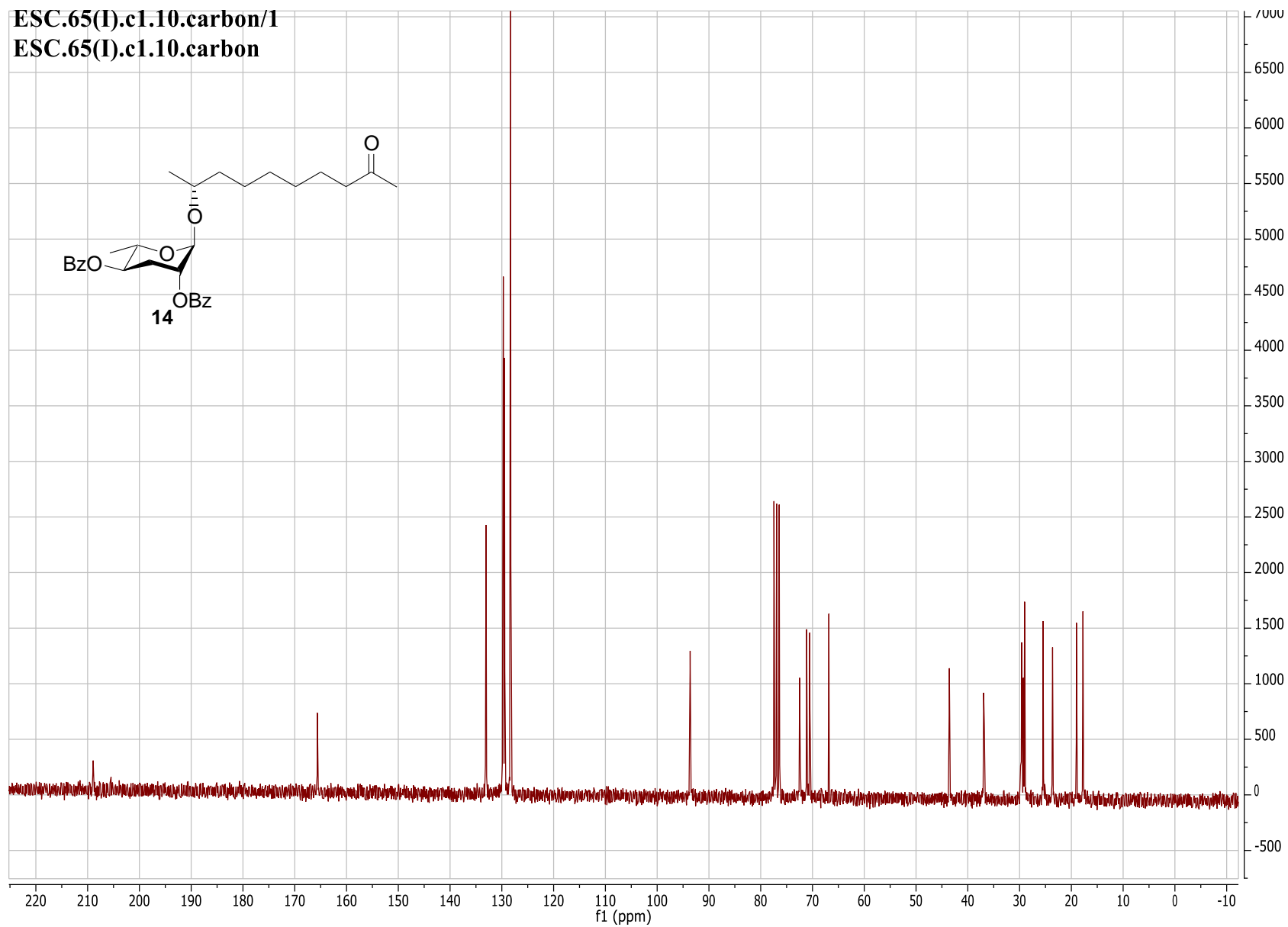


ESC.29(I).c1/1  
ESC.29(I).c1

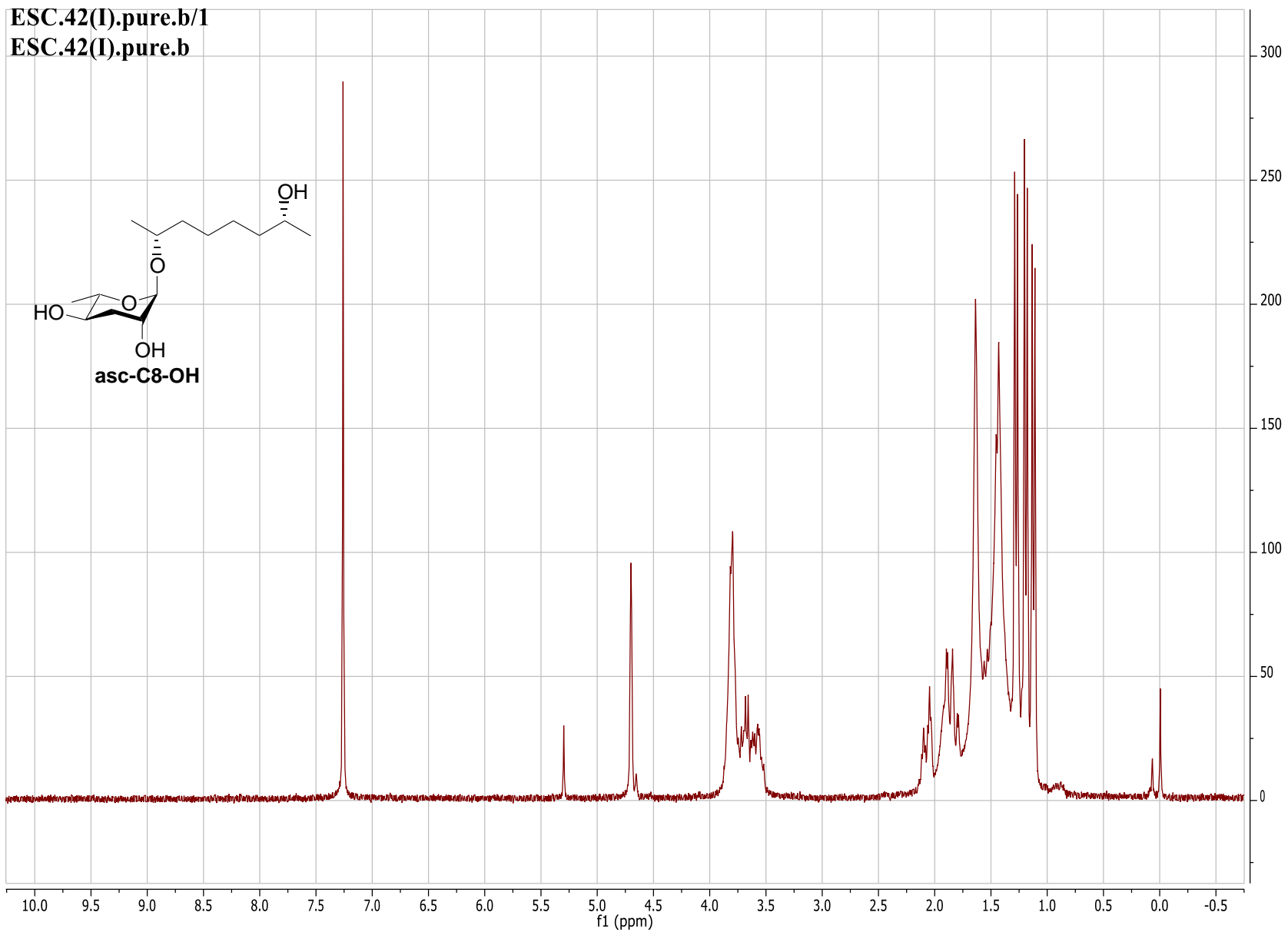




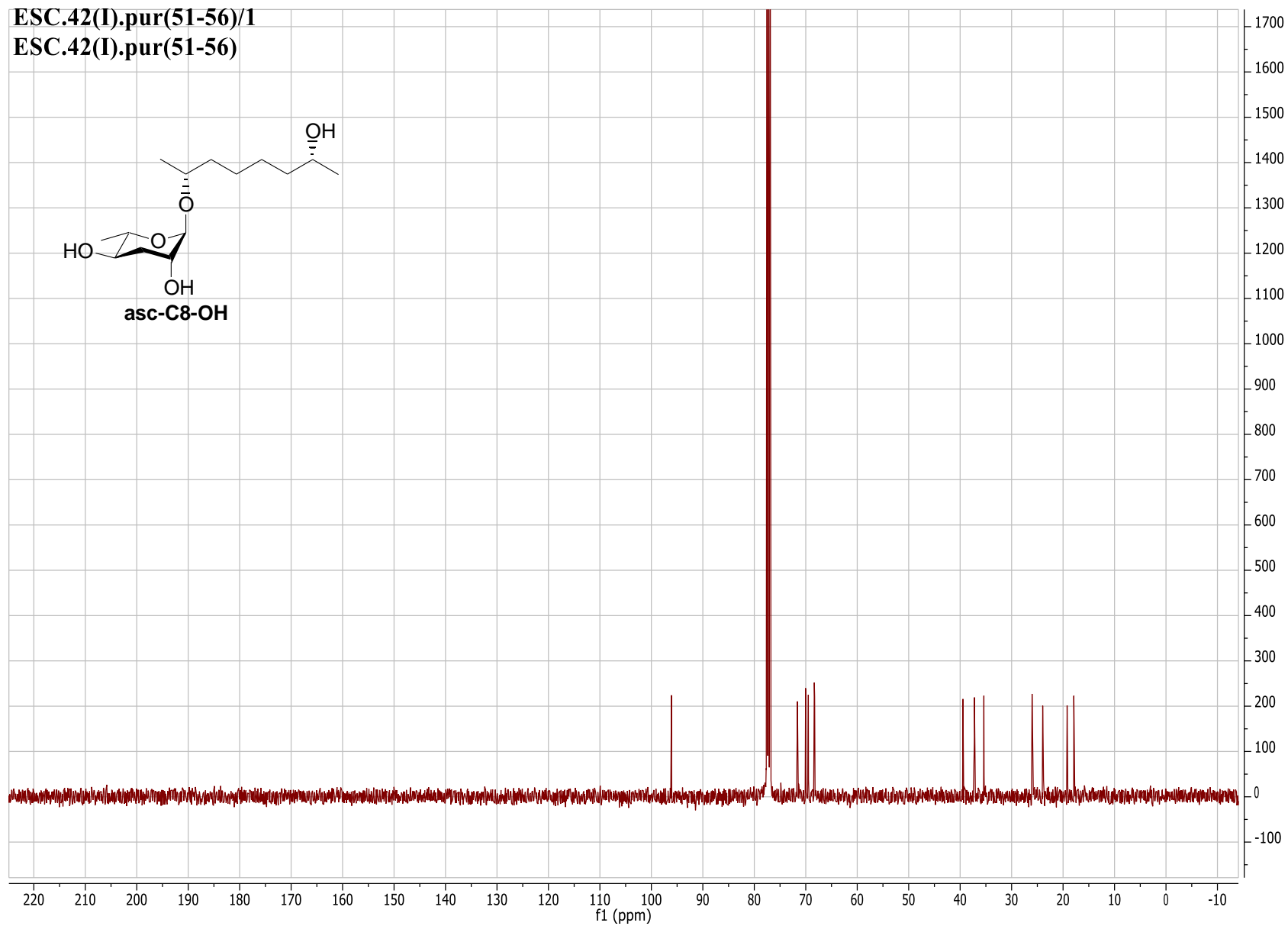
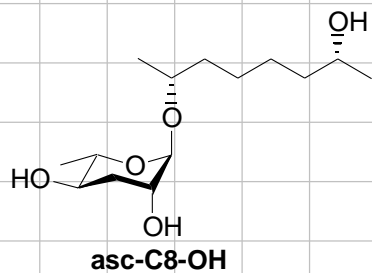
ESC.65(I).c1.10.carbon/1  
ESC.65(I).c1.10.carbon



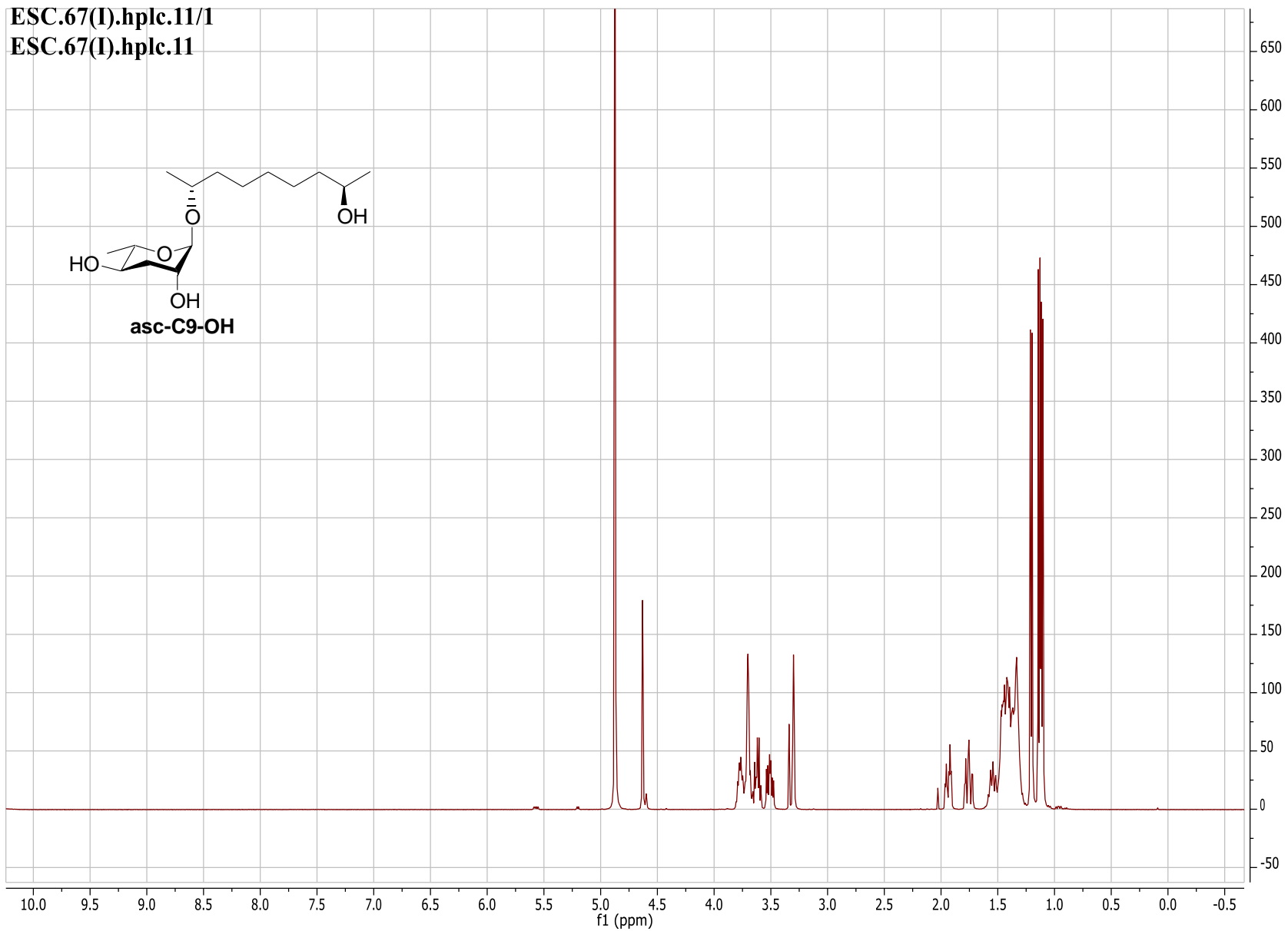
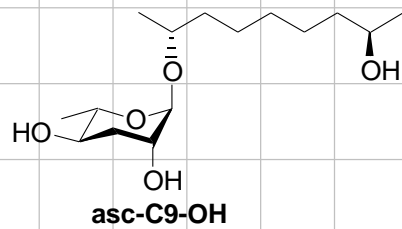
ESC.42(I).pure.b/1  
ESC.42(I).pure.b



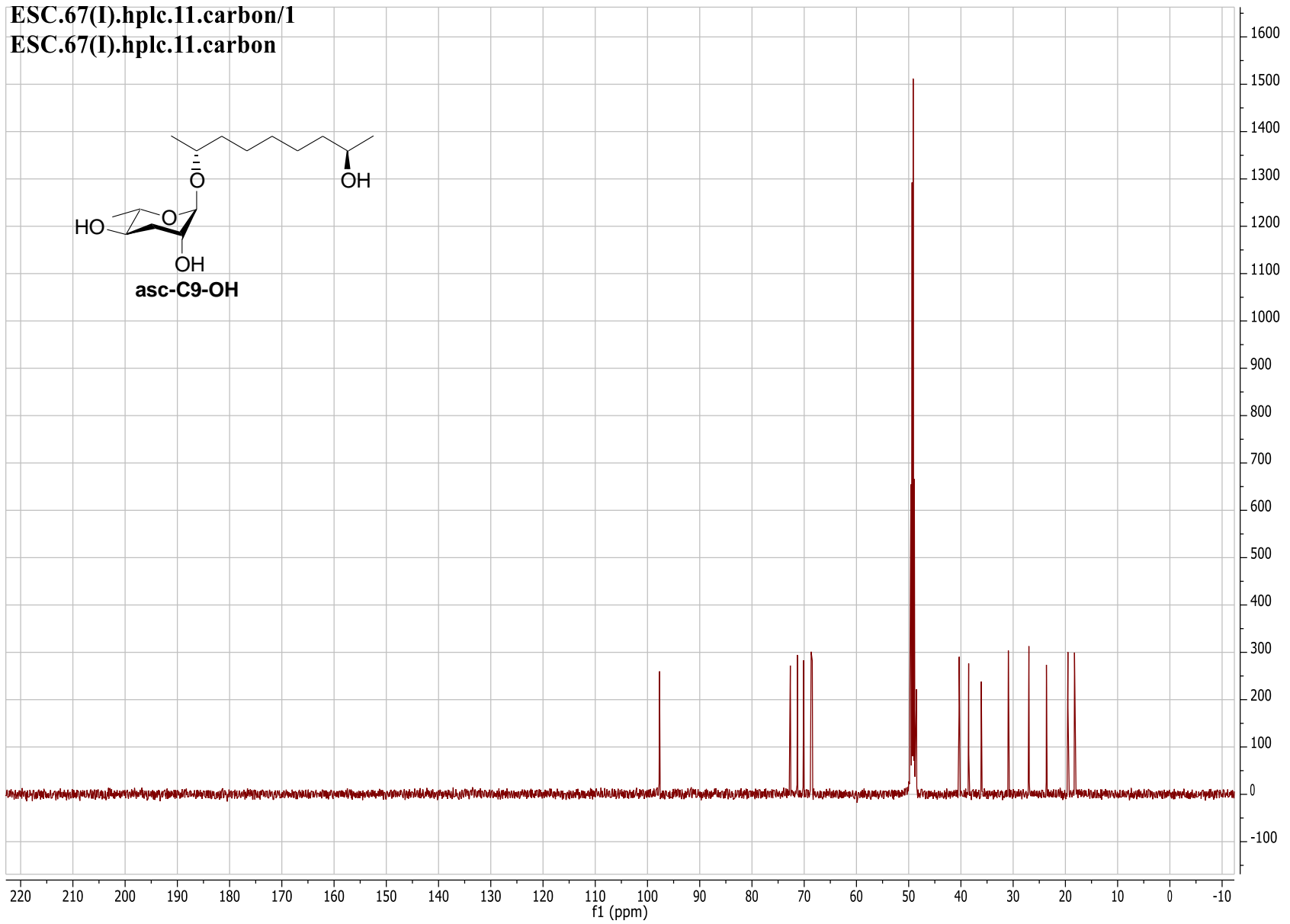
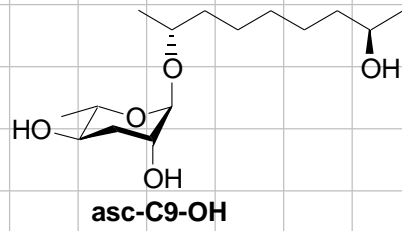
ESC.42(I).pur(51-56)/1  
ESC.42(I).pur(51-56)



ESC.67(I).hplc.11/1  
ESC.67(I).hplc.11

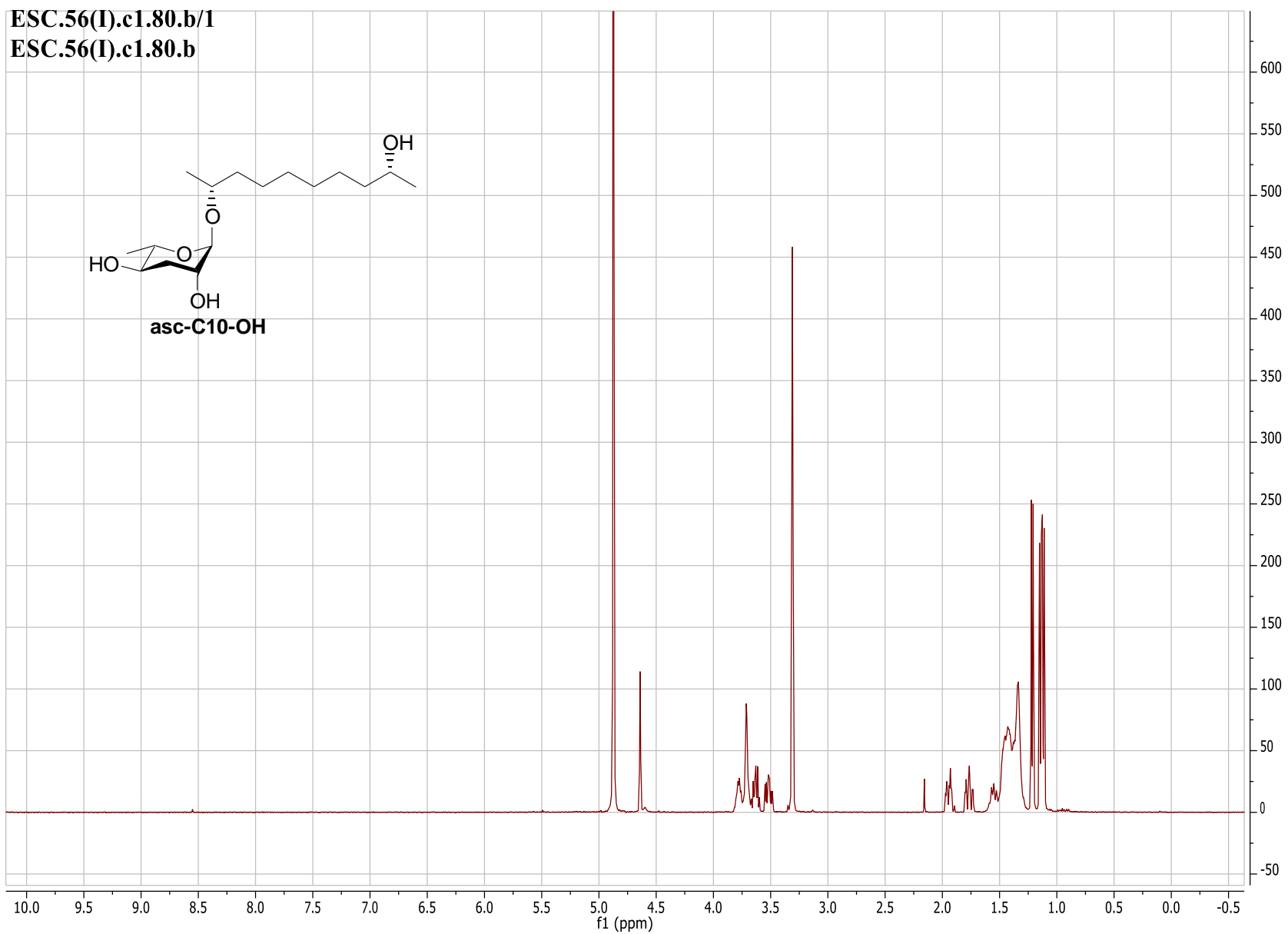
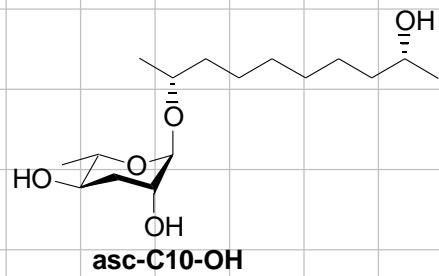


ESC.67(I).hplc.11.carbon/1  
ESC.67(I).hplc.11.carbon

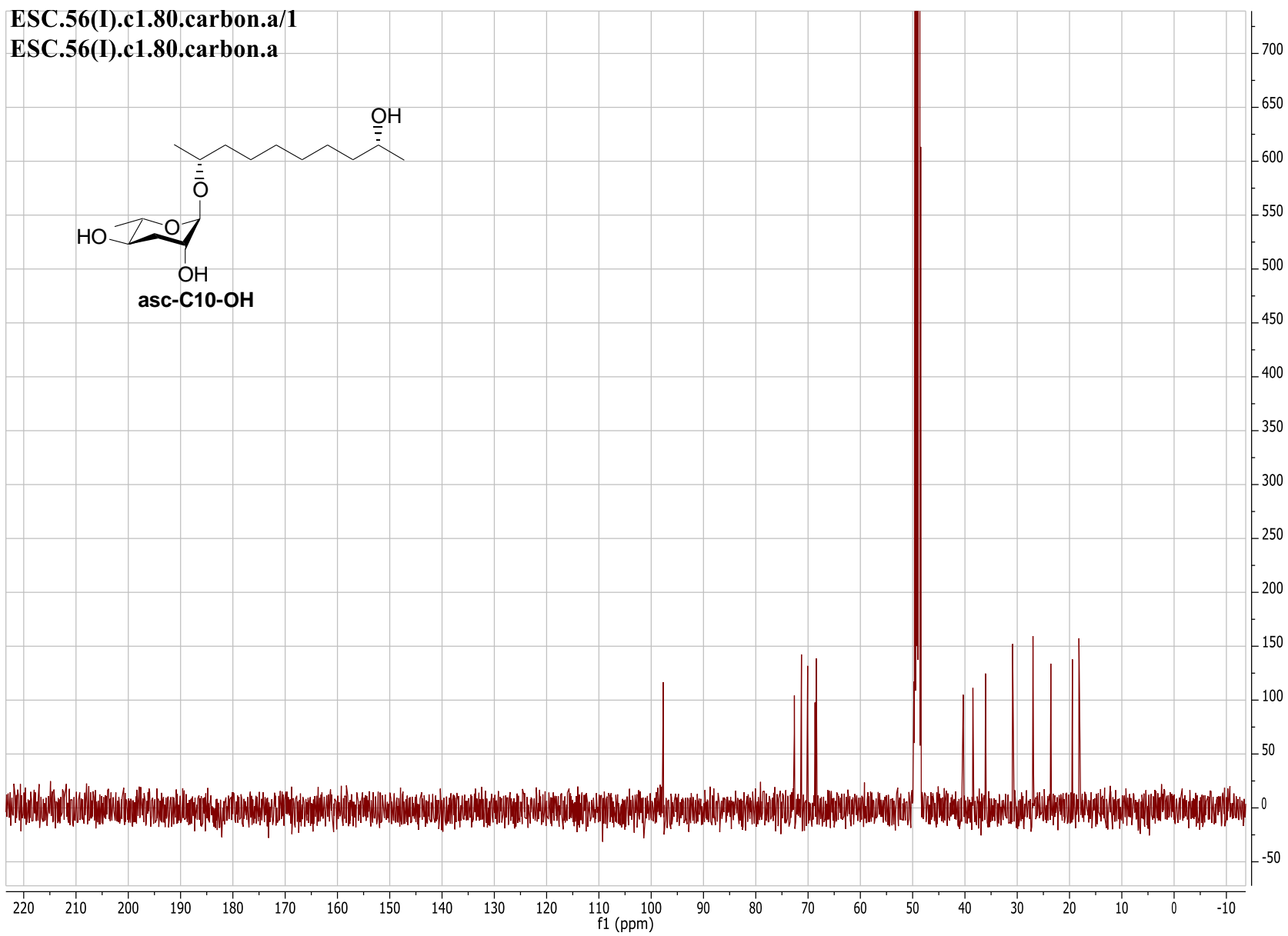
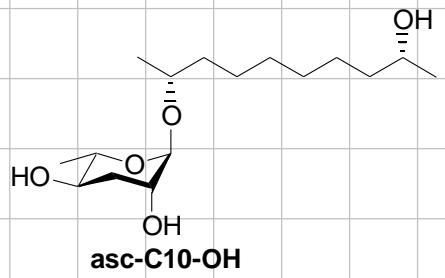


ESC.56(I).c1.80.b/1

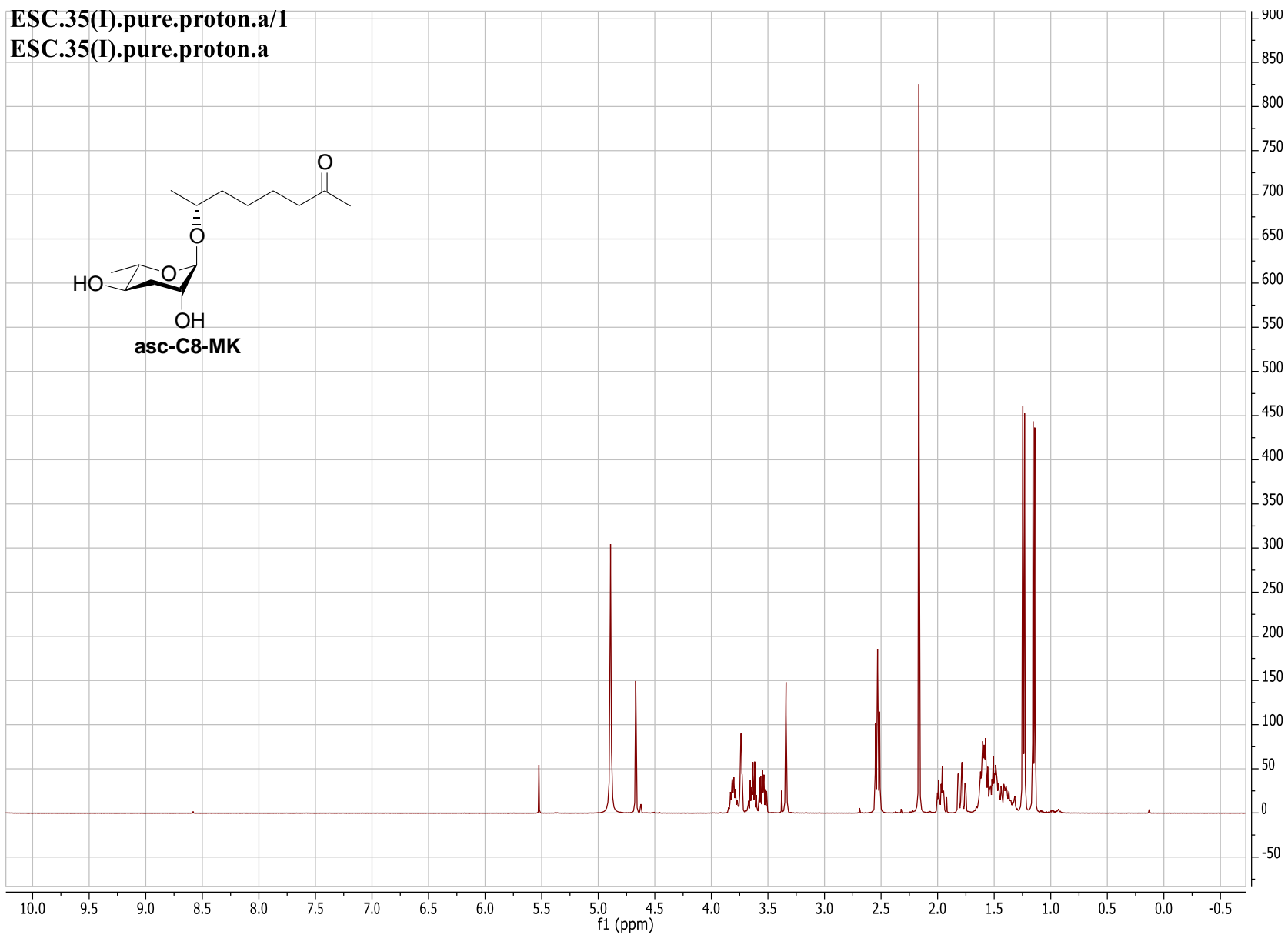
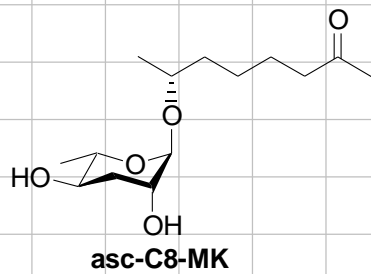
ESC.56(I).c1.80.b



ESC.56(I).c1.80.carbon.a/1  
ESC.56(I).c1.80.carbon.a

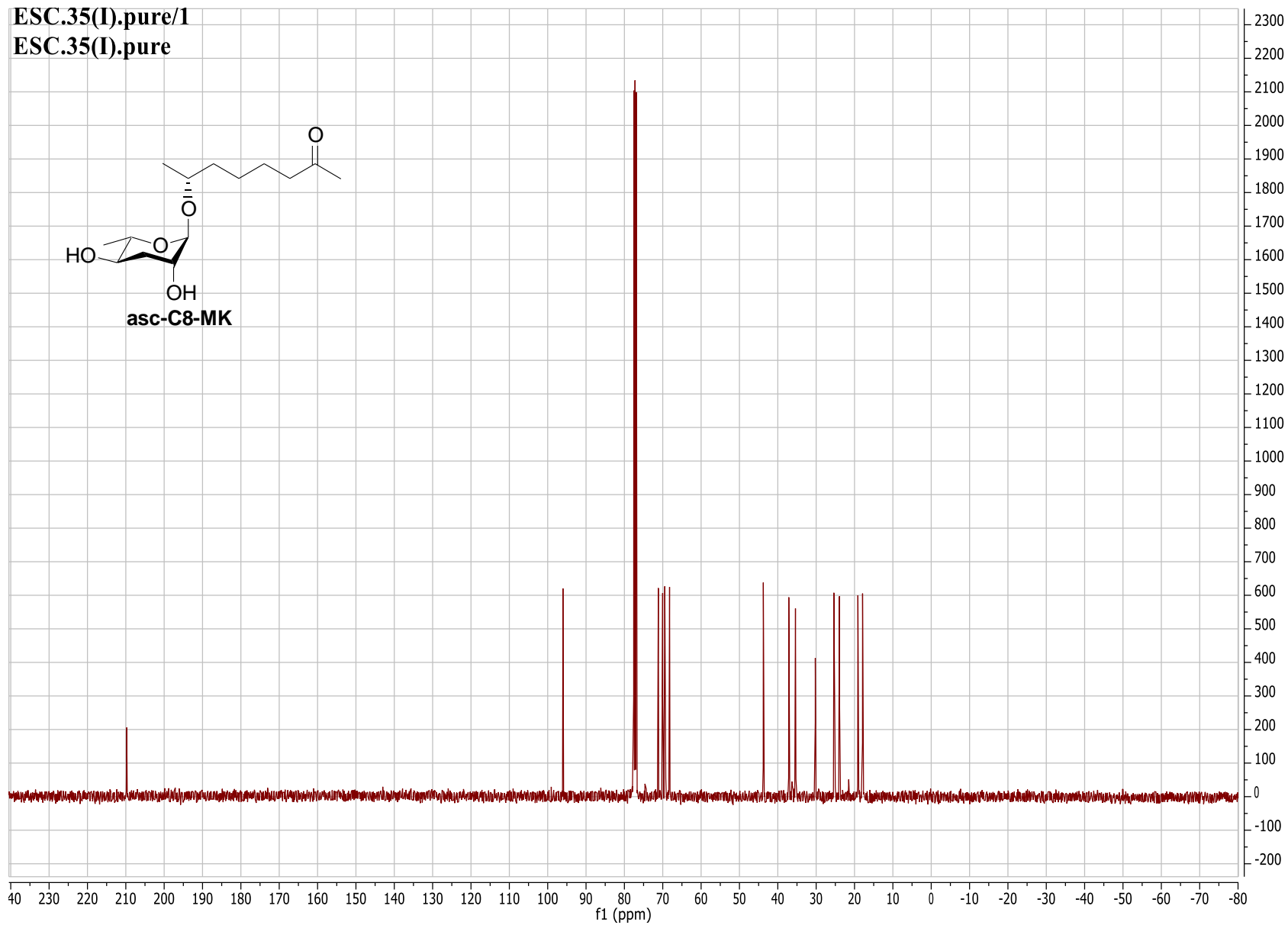
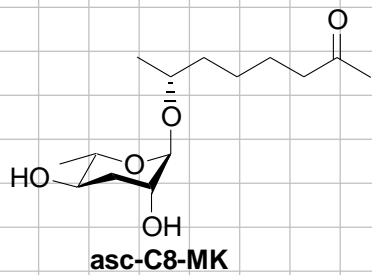


ESC.35(I).pure.proton.a/1  
ESC.35(I).pure.proton.a



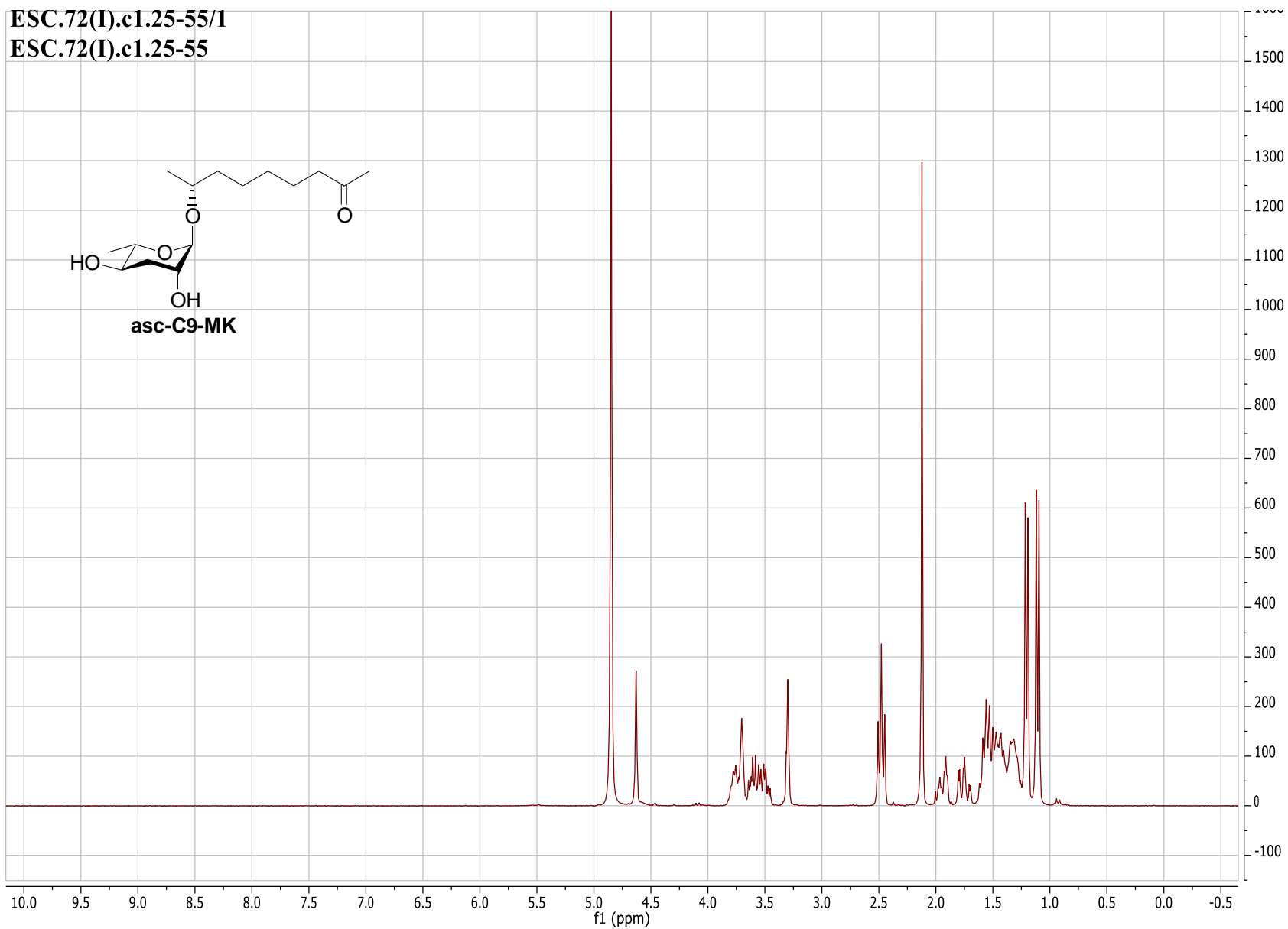
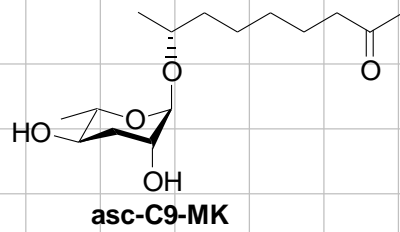


ESC.35(I).pure/1  
ESC.35(I).pure

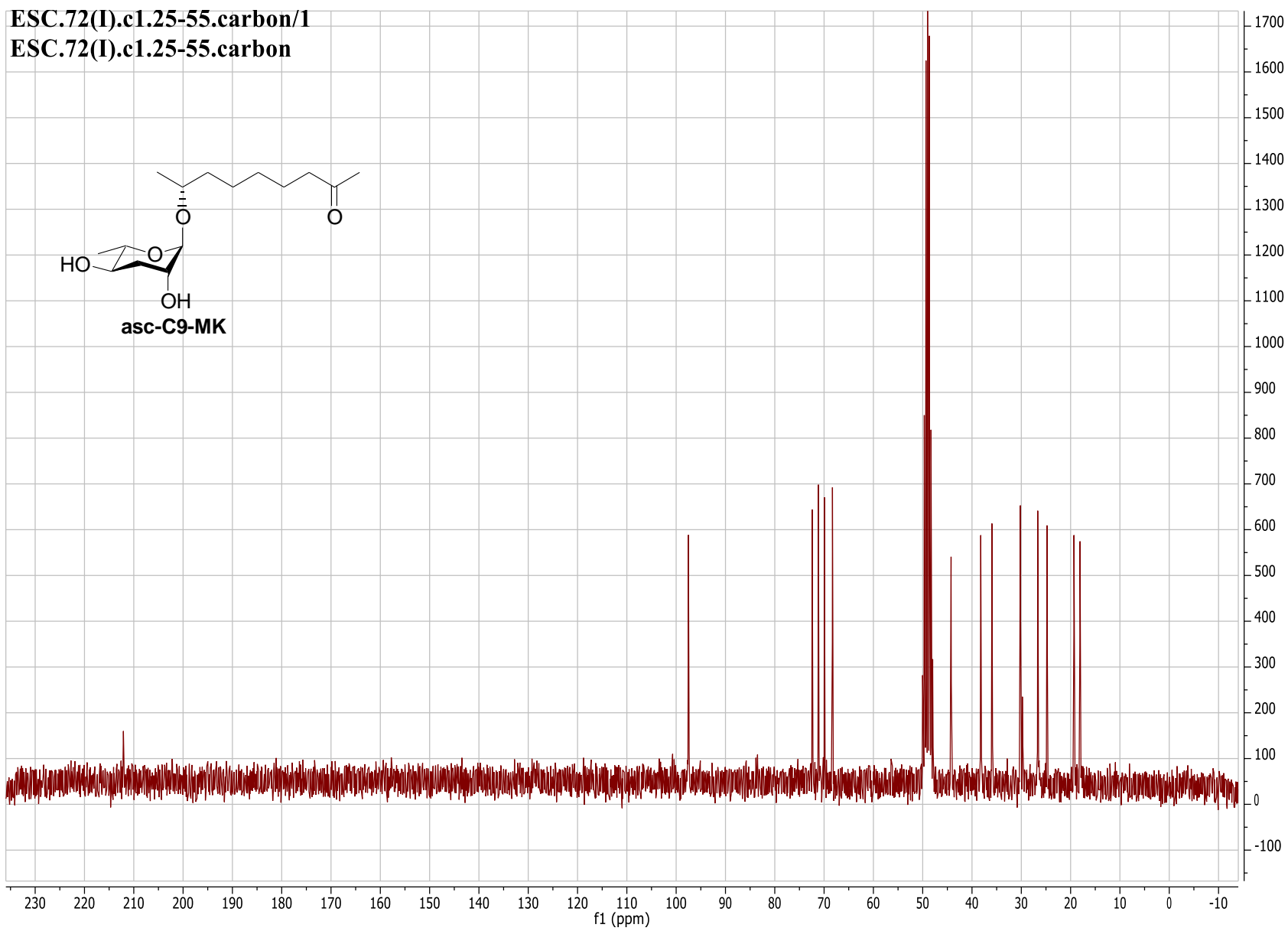
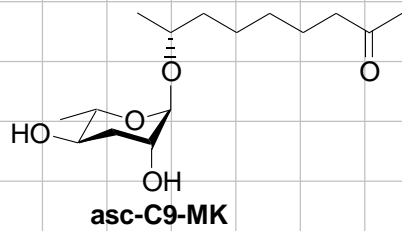


ESC.72(I).c1.25-55/1

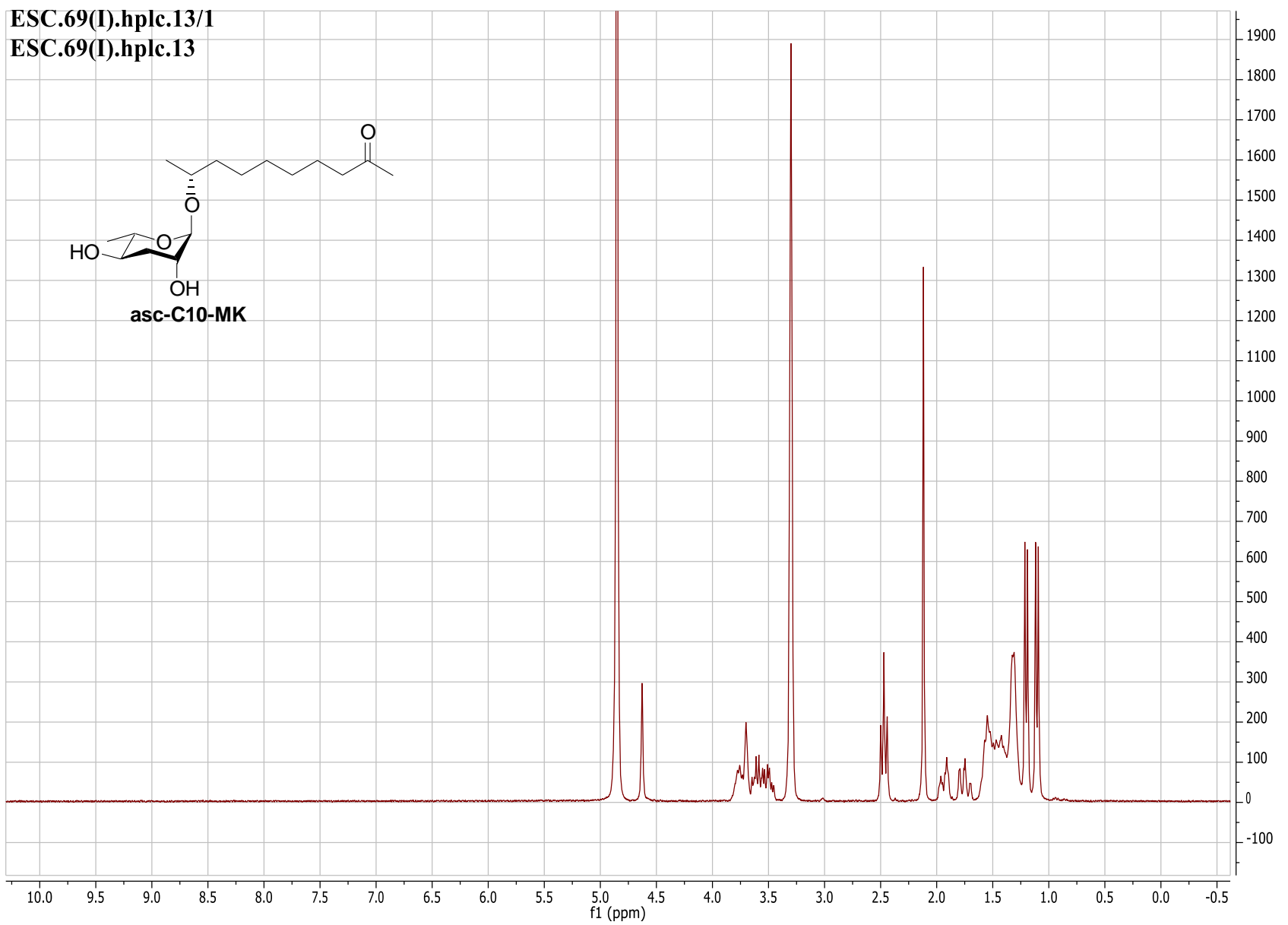
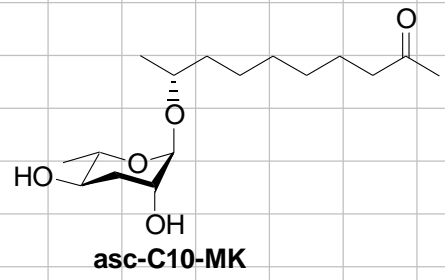
ESC.72(I).c1.25-55



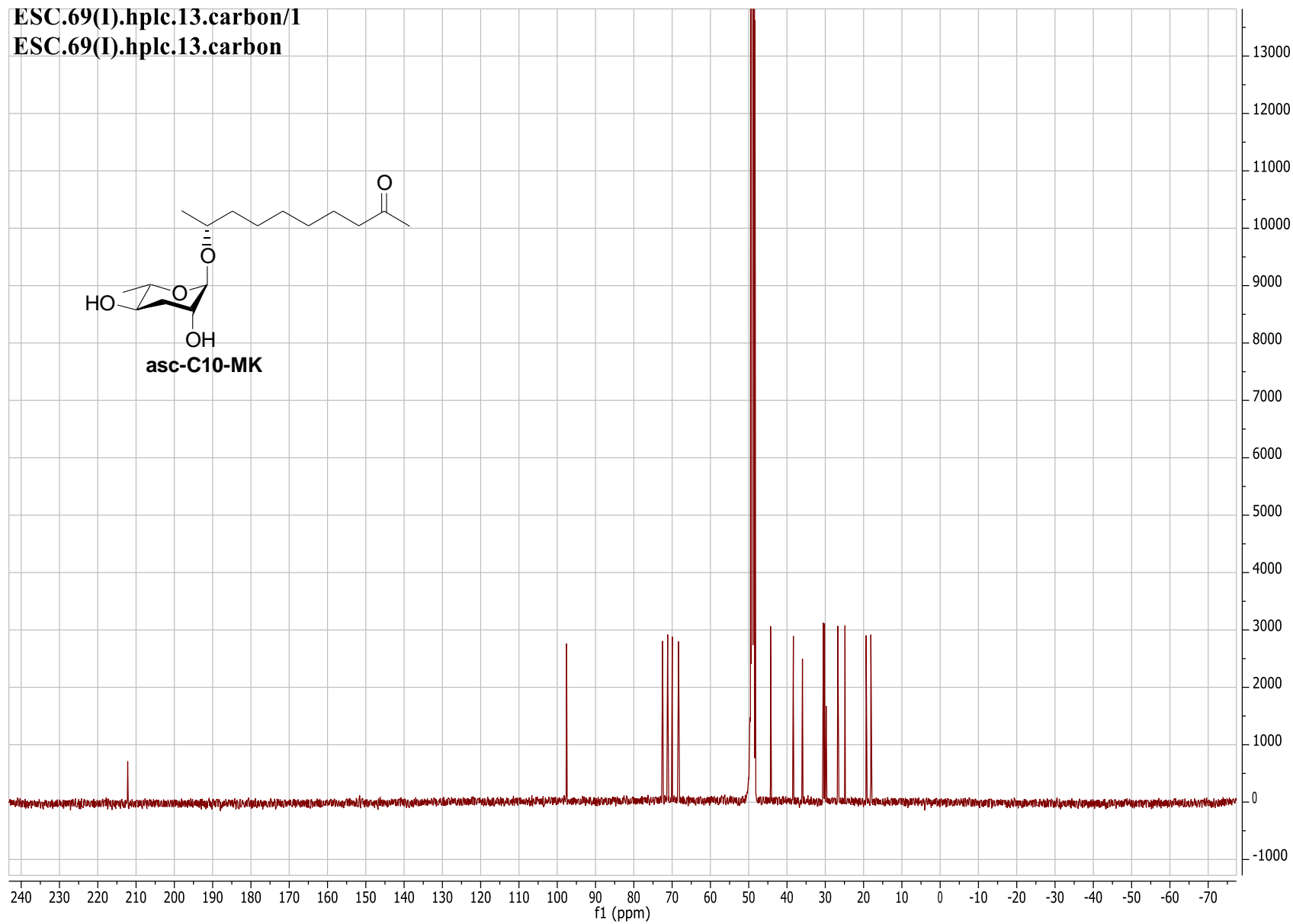
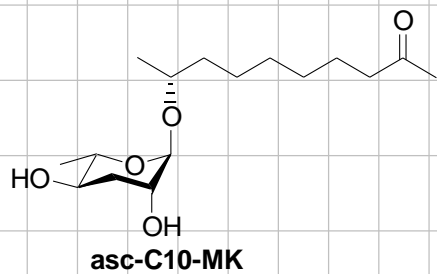
ESC.72(I).c1.25-55.carbon/1  
ESC.72(I).c1.25-55.carbon



ESC.69(I).hplc.13/1  
ESC.69(I).hplc.13



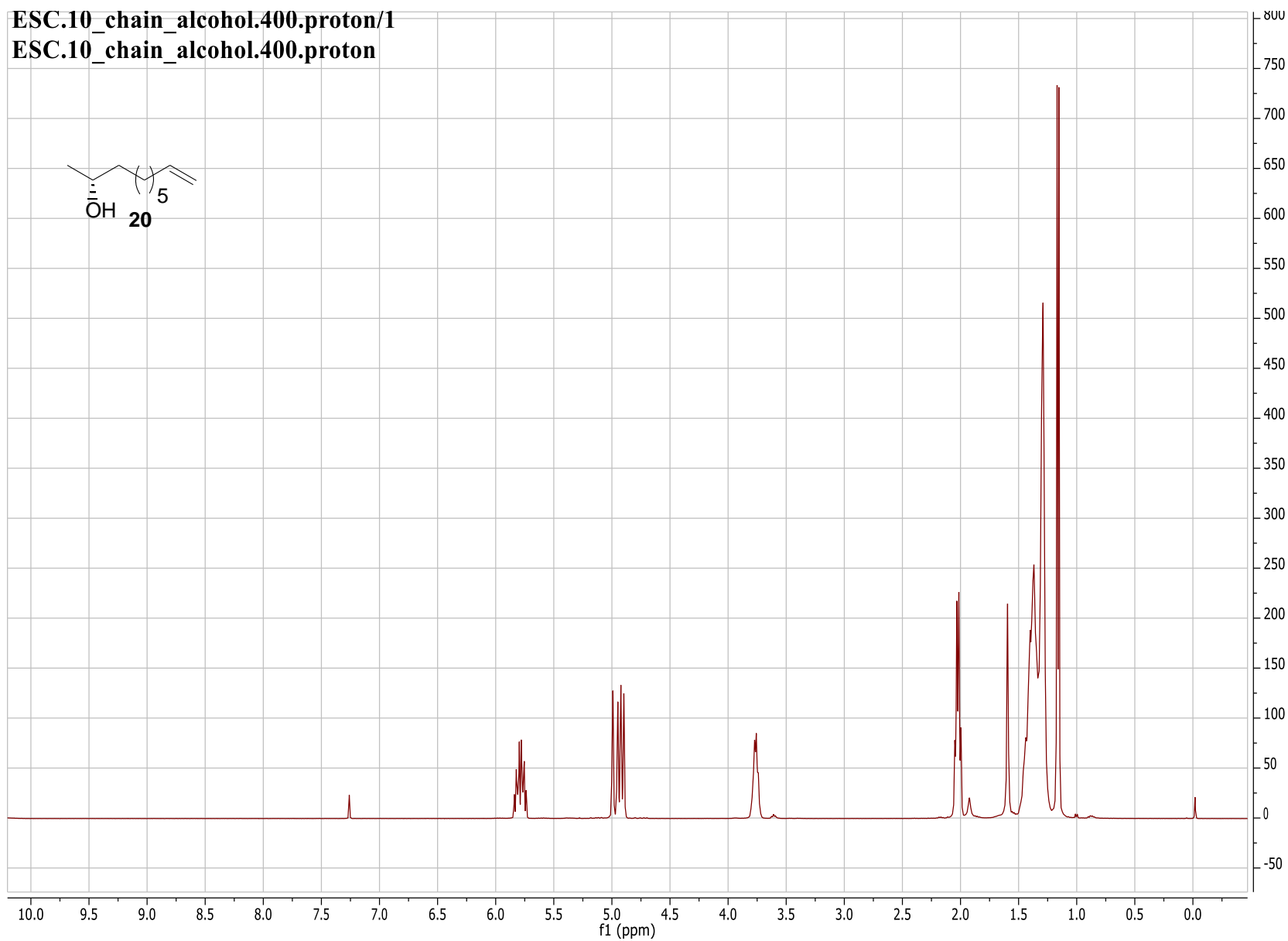
ESC.69(I).hplc.13.carbon/1  
ESC.69(I).hplc.13.carbon



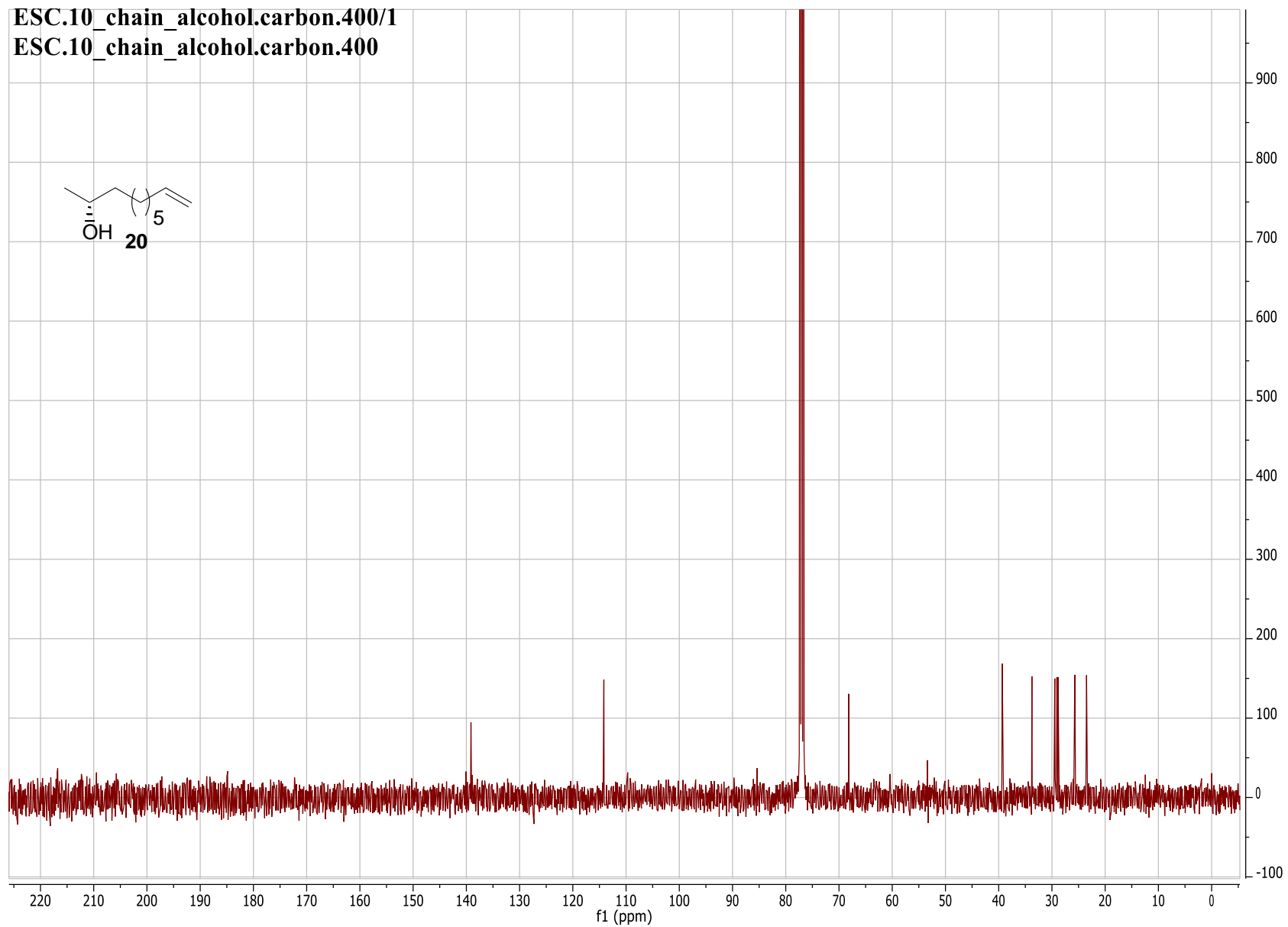
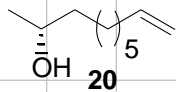
### APPENDIX C: NMR SPECTRA OF COMPOUNDS FOUND IN CHAPTER 2

ESC.10\_chain\_alcohol.400.proton/1

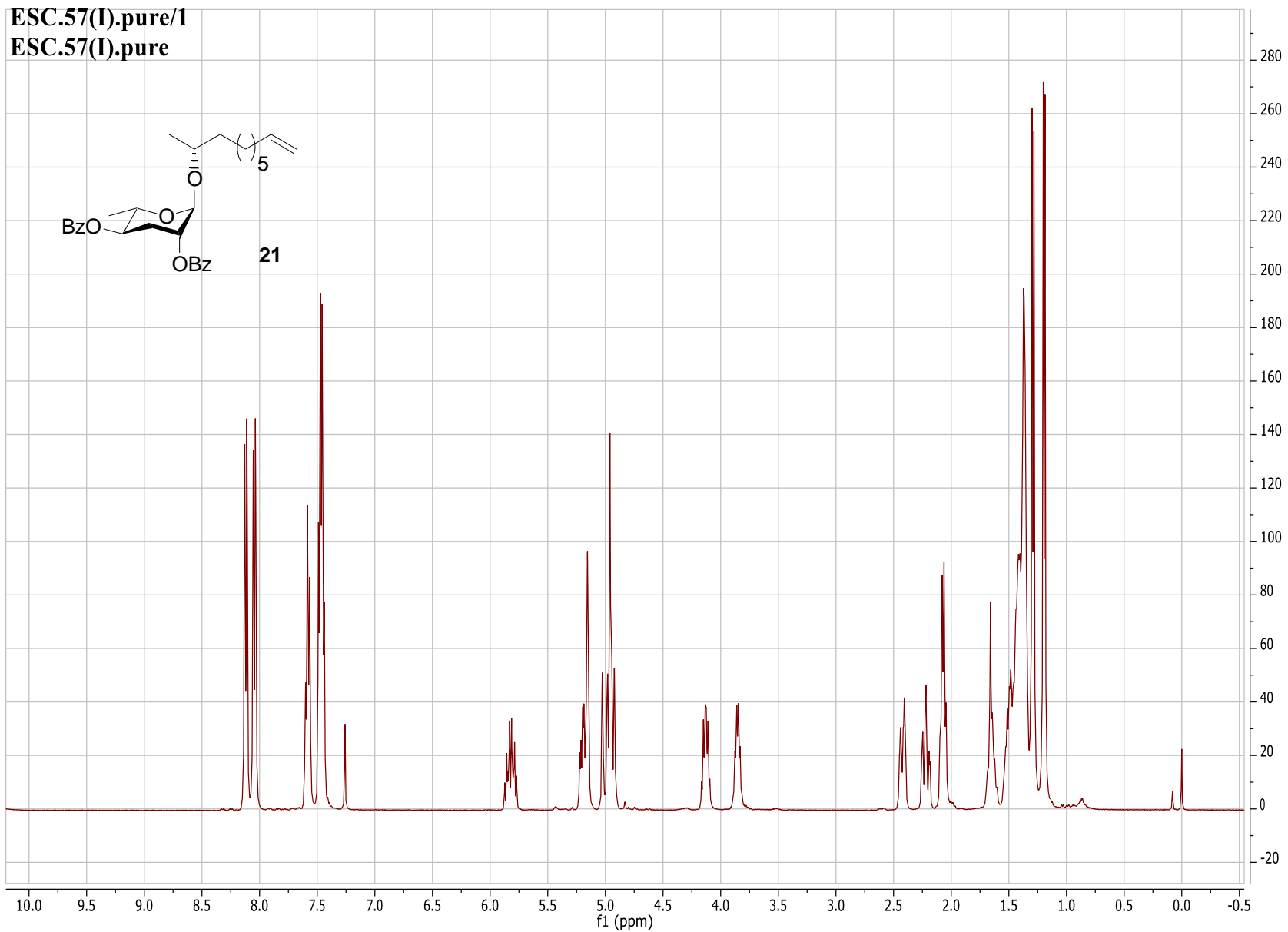
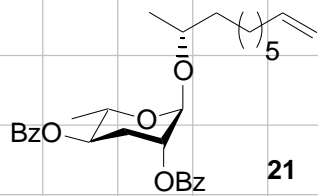
ESC.10\_chain\_alcohol.400.proton



ESC.10\_chain\_alcohol.carbon.400/1  
ESC.10\_chain\_alcohol.carbon.400

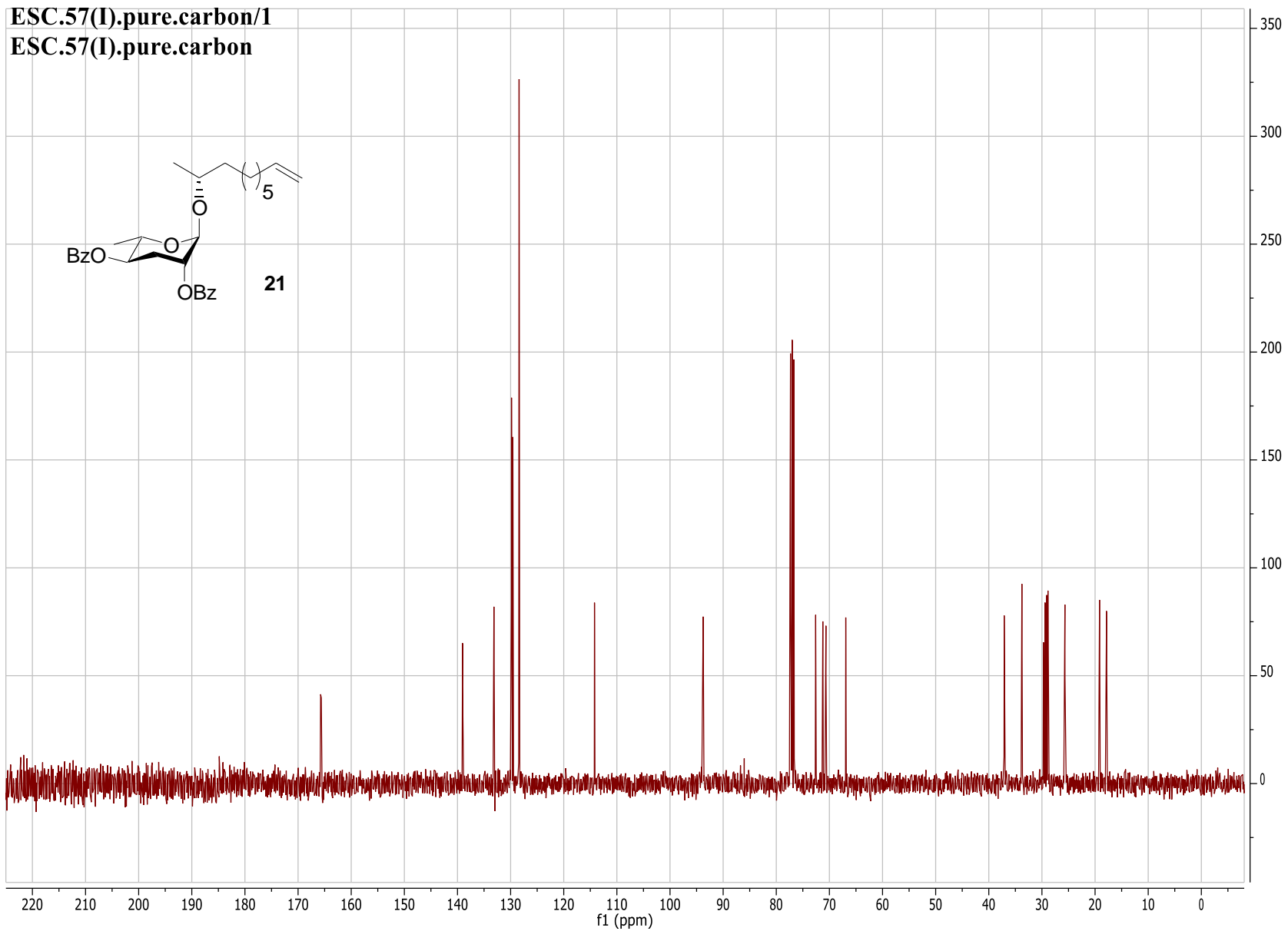
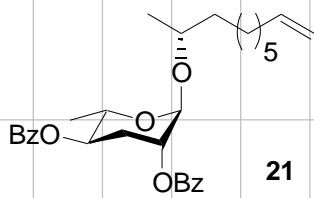


ESC.57(I).pure/1  
ESC.57(I).pure

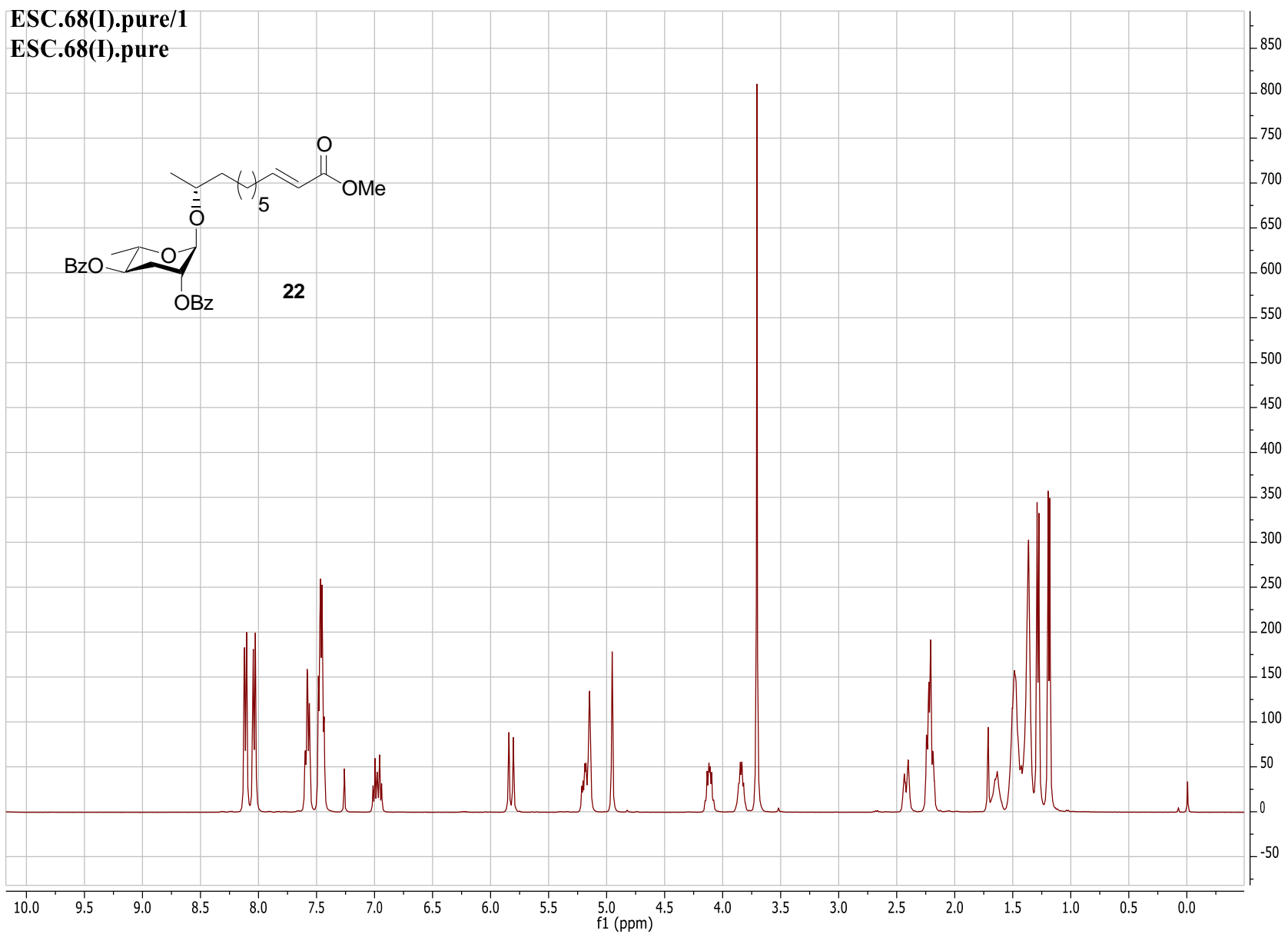




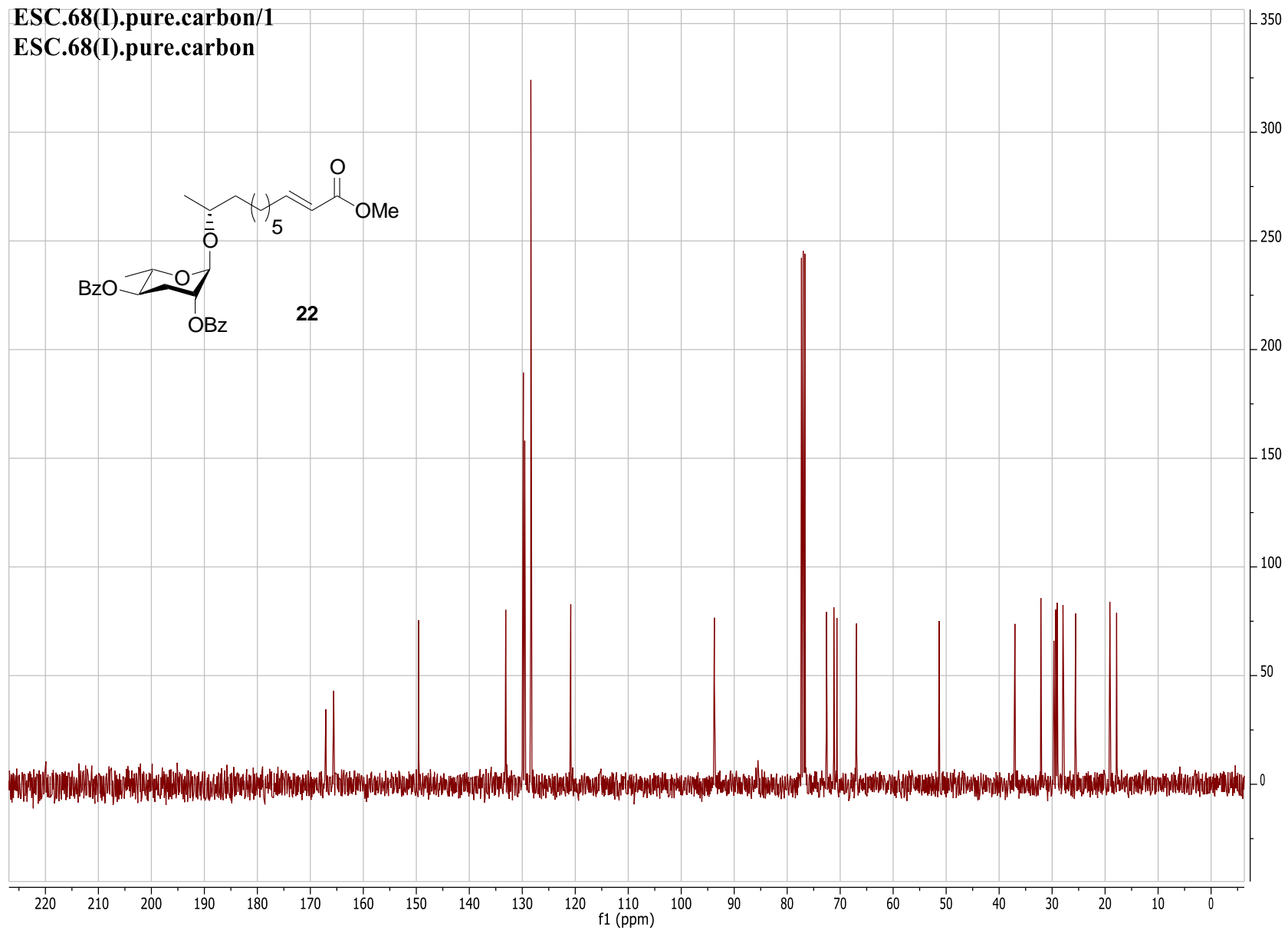
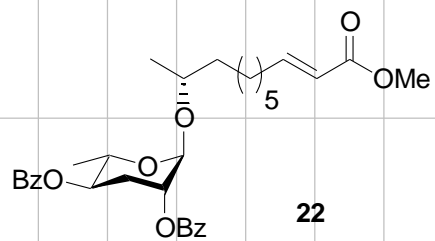
ESC.57(I).pure.carbon/1  
ESC.57(I).pure.carbon



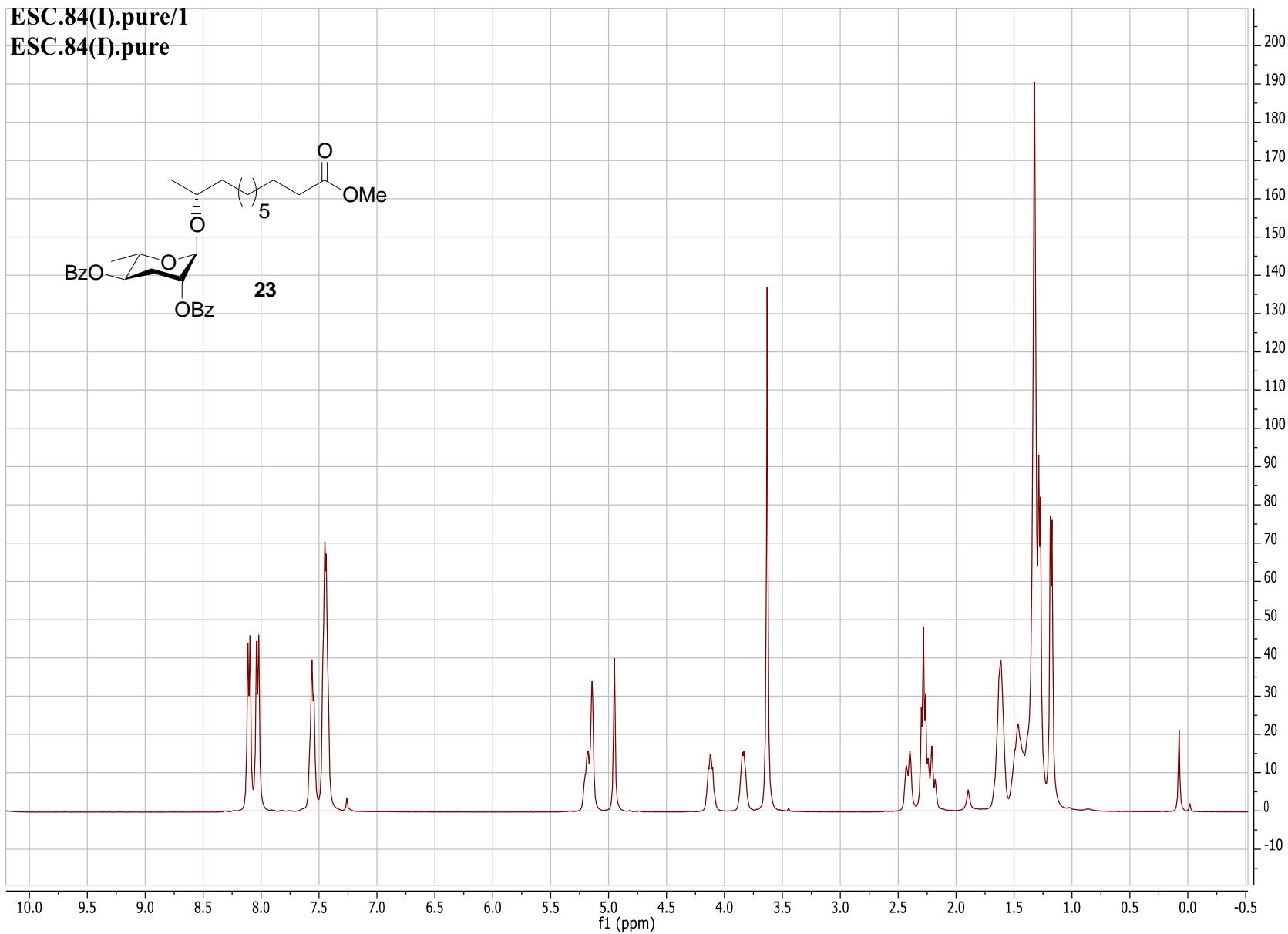
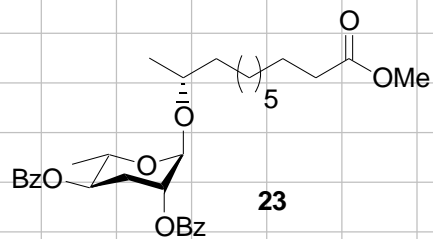
ESC.68(I).pure/1  
ESC.68(I).pure



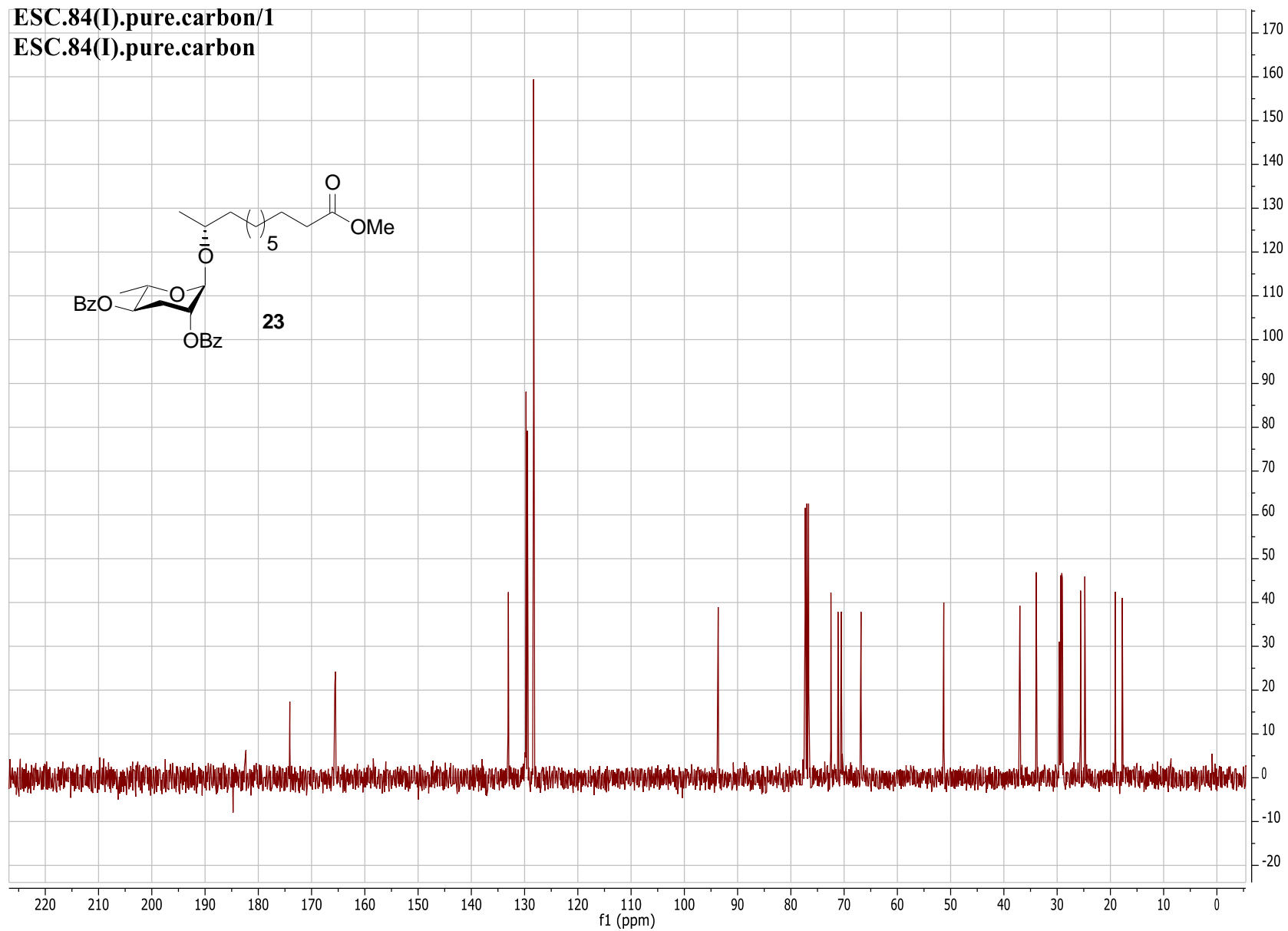
ESC.68(I).pure.carbon/1  
ESC.68(I).pure.carbon



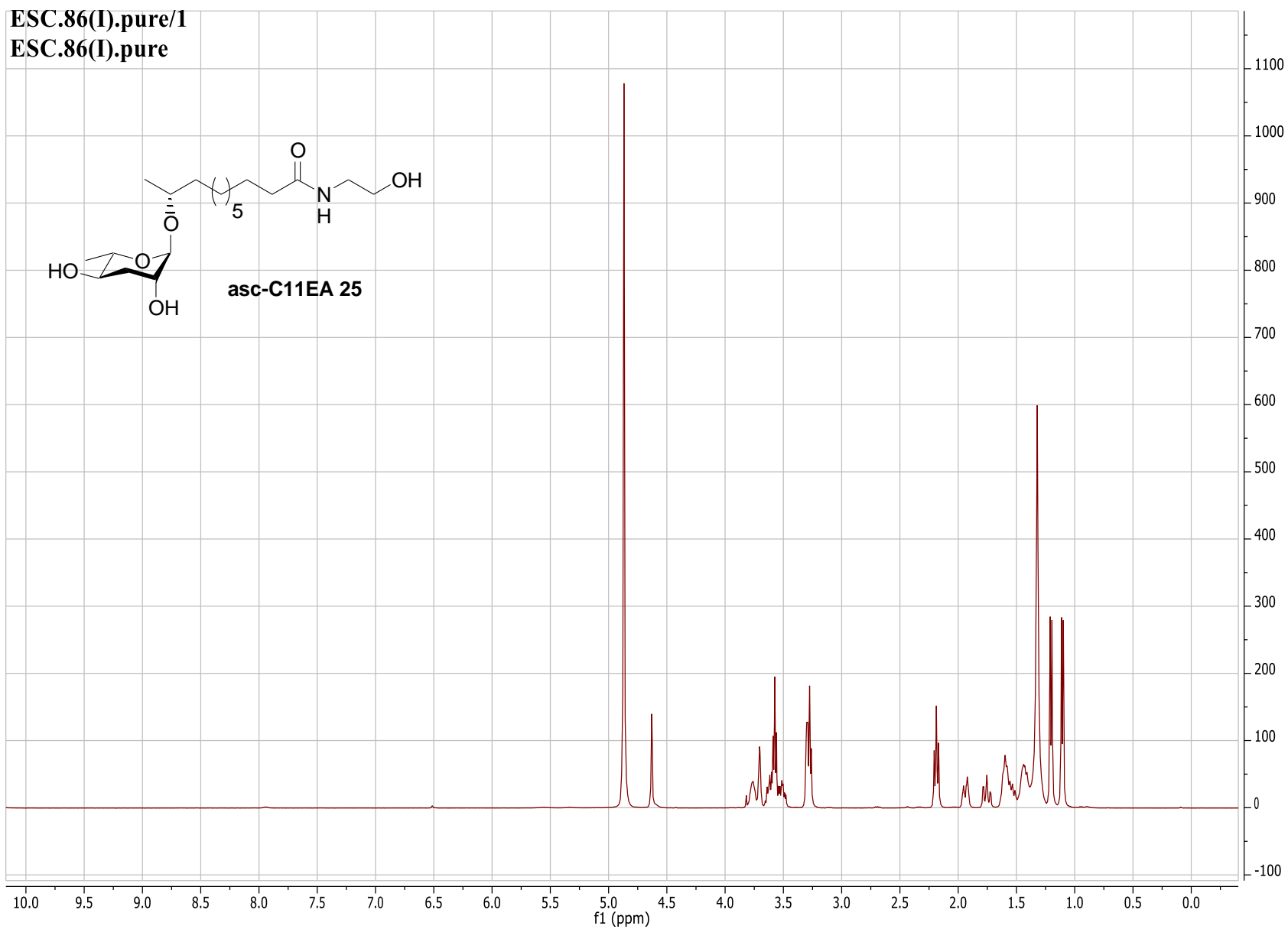
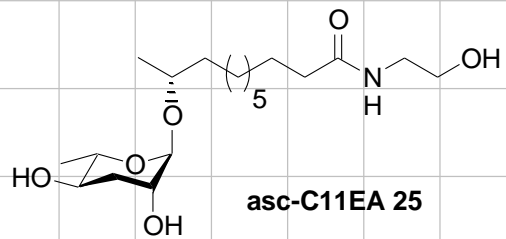
ESC.84(I).pure/1  
ESC.84(I).pure



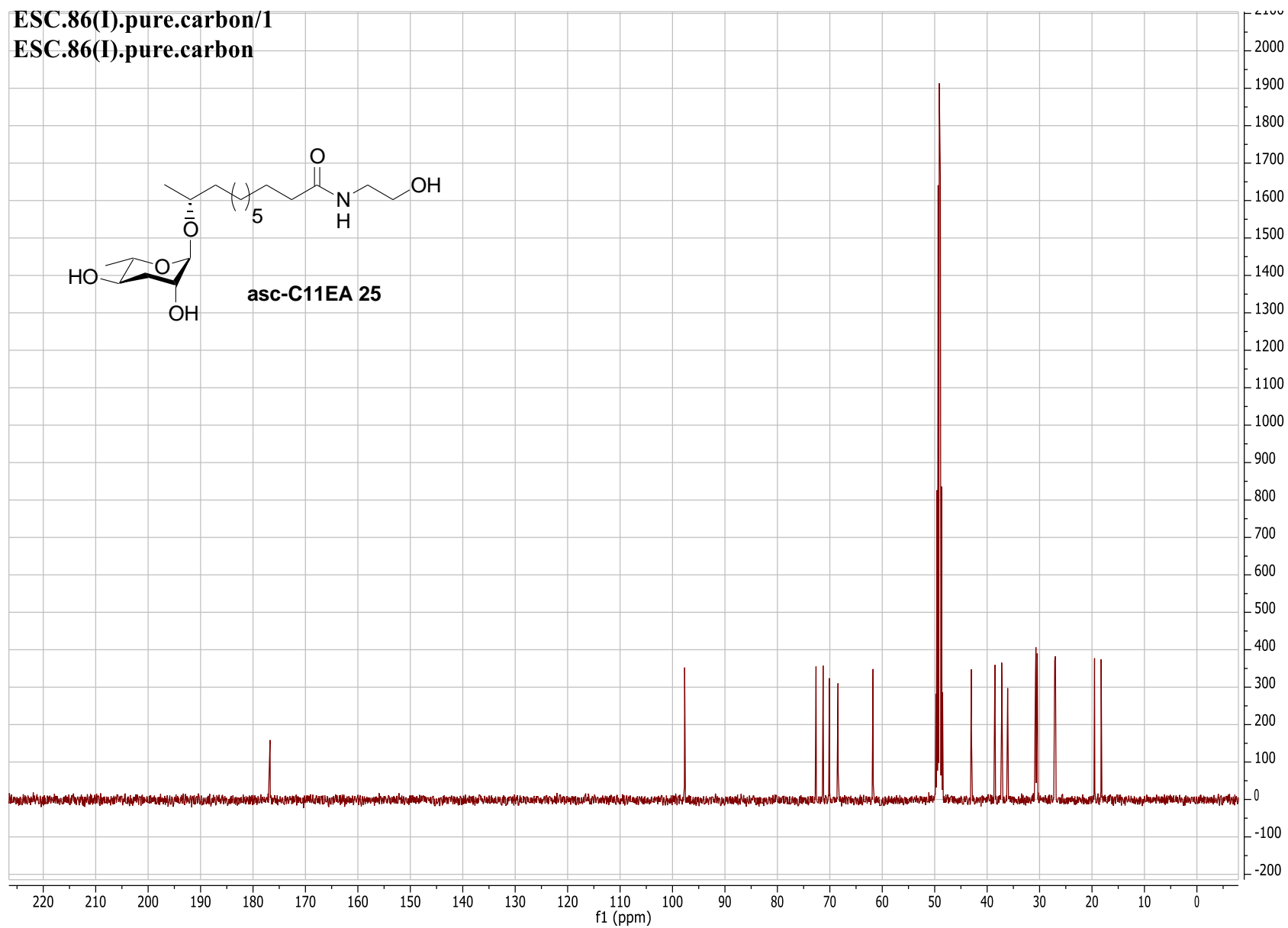
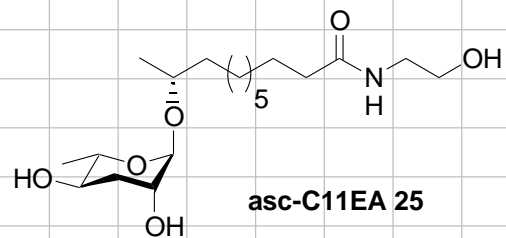
ESC.84(I).pure.carbon/1  
ESC.84(I).pure.carbon



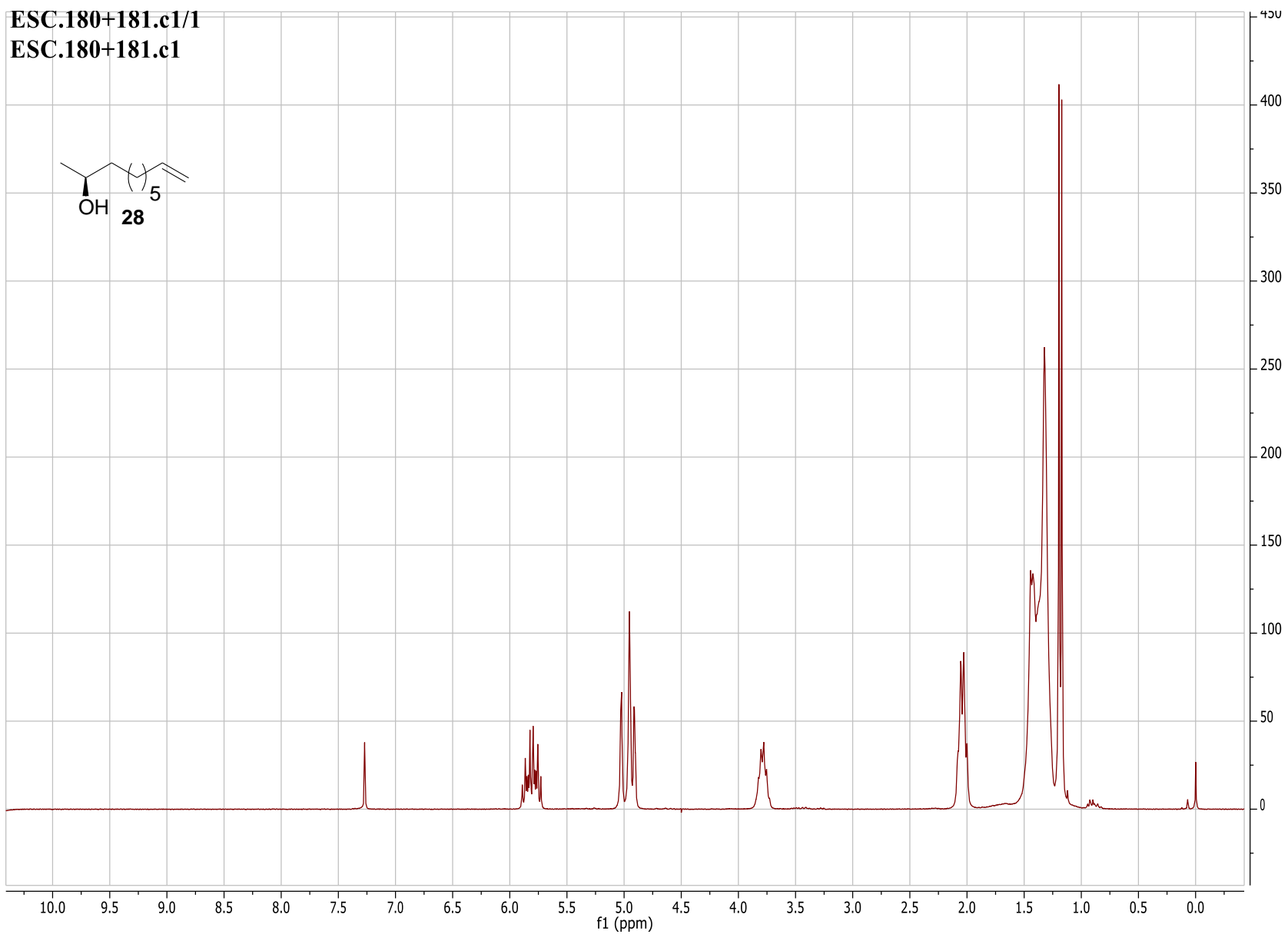
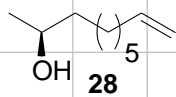
ESC.86(I).pure/1  
ESC.86(I).pure



ESC.86(I).pure.carbon/1  
ESC.86(I).pure.carbon

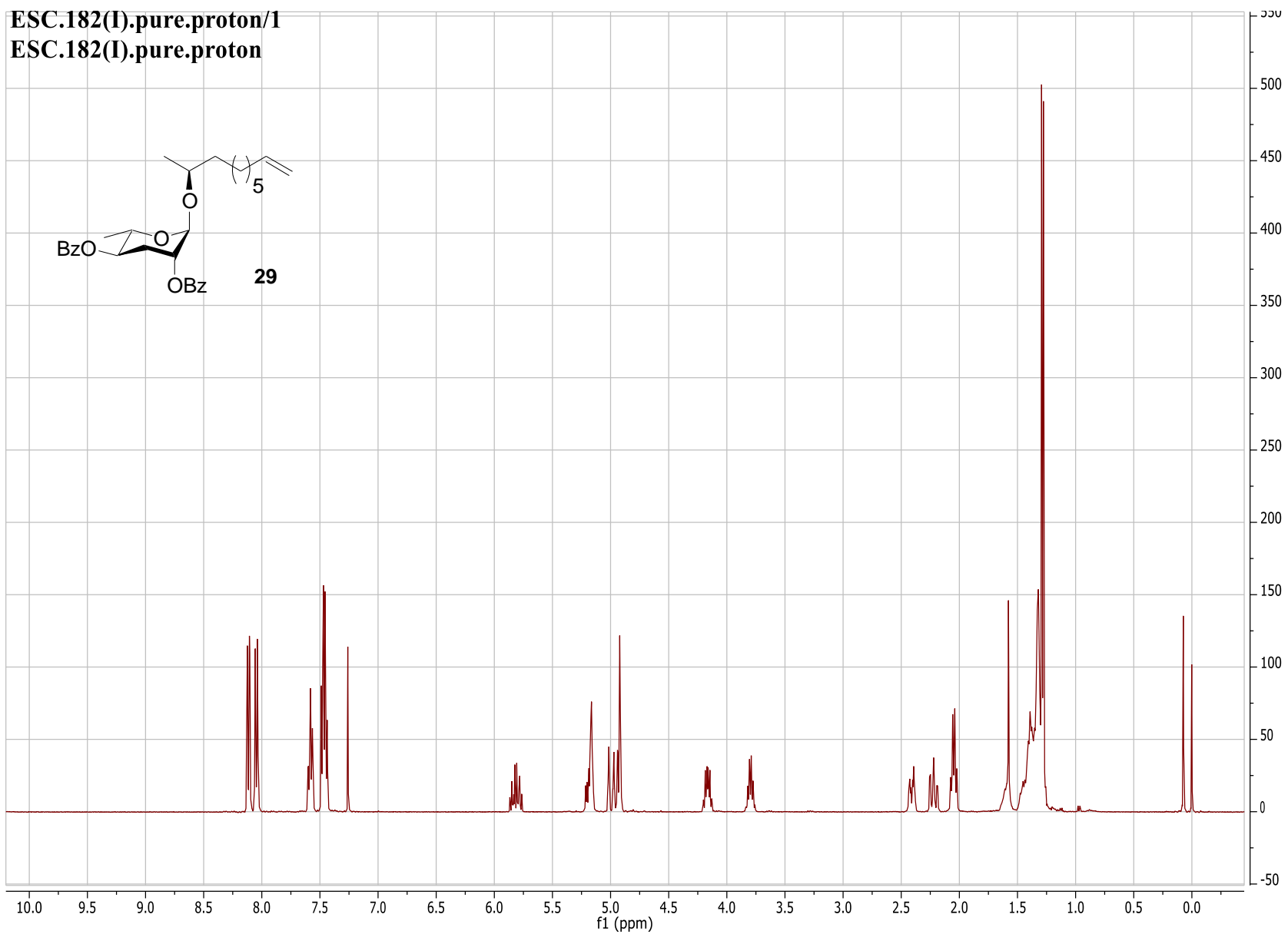
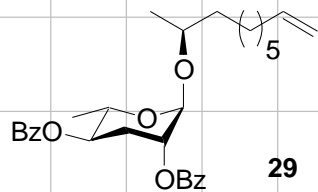


ESC.180+181.c1/1  
ESC.180+181.c1



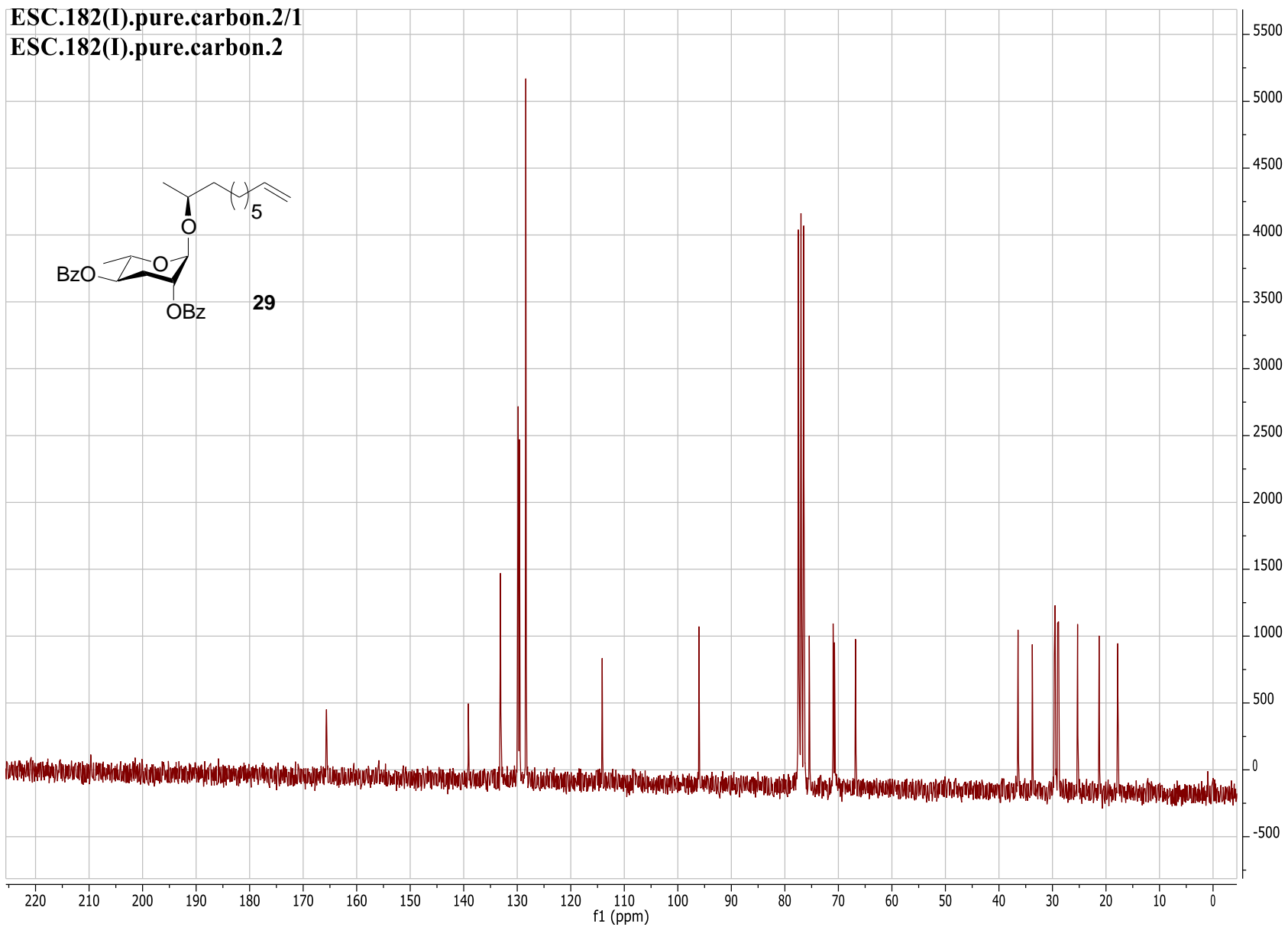
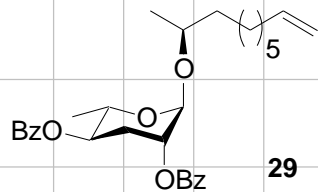


ESC.182(I).pure.proton/1  
ESC.182(I).pure.proton

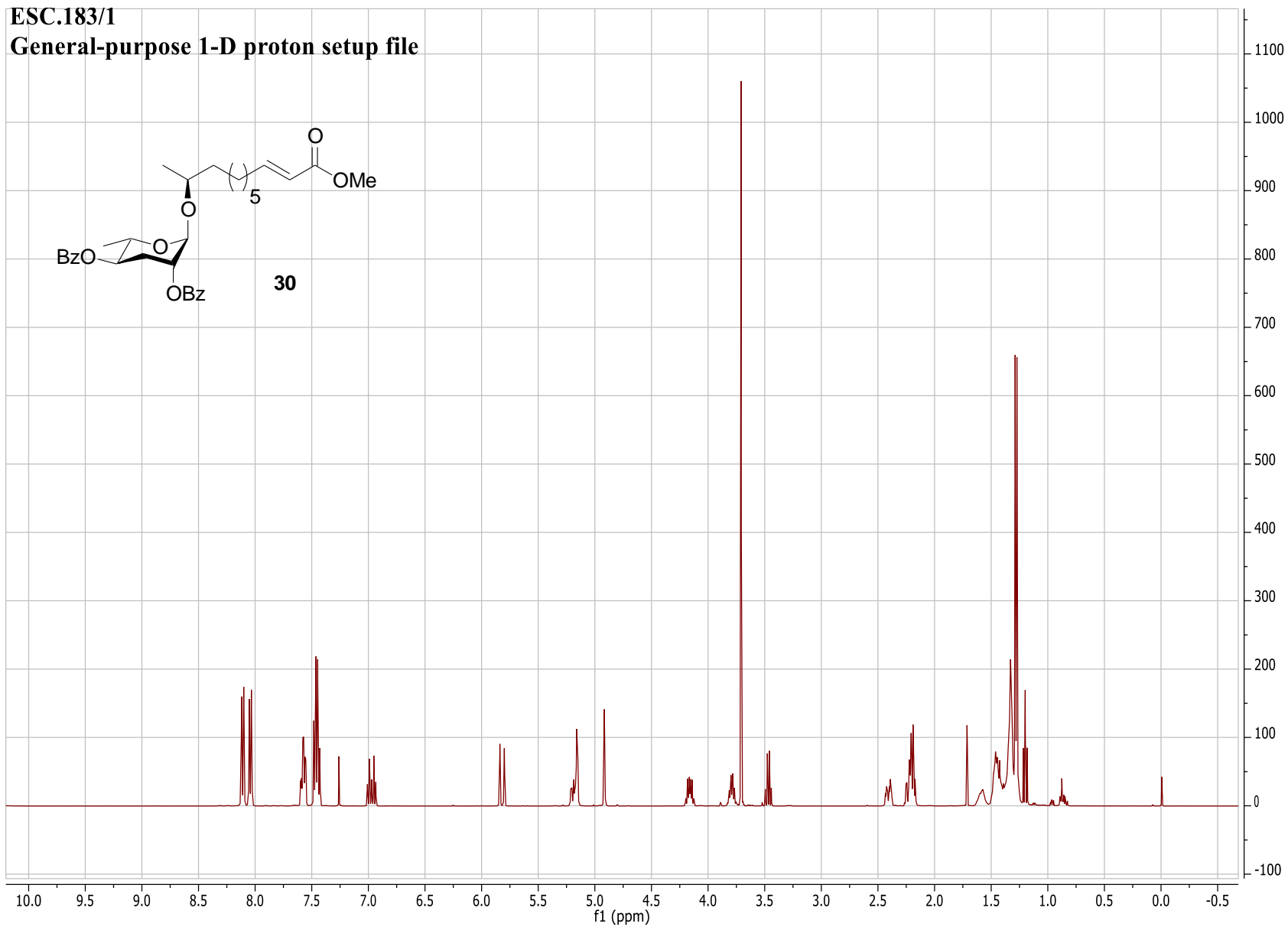
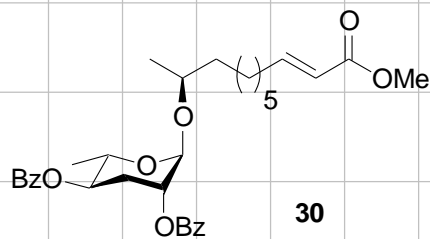


ESC.182(I).pure.carbon.2/1

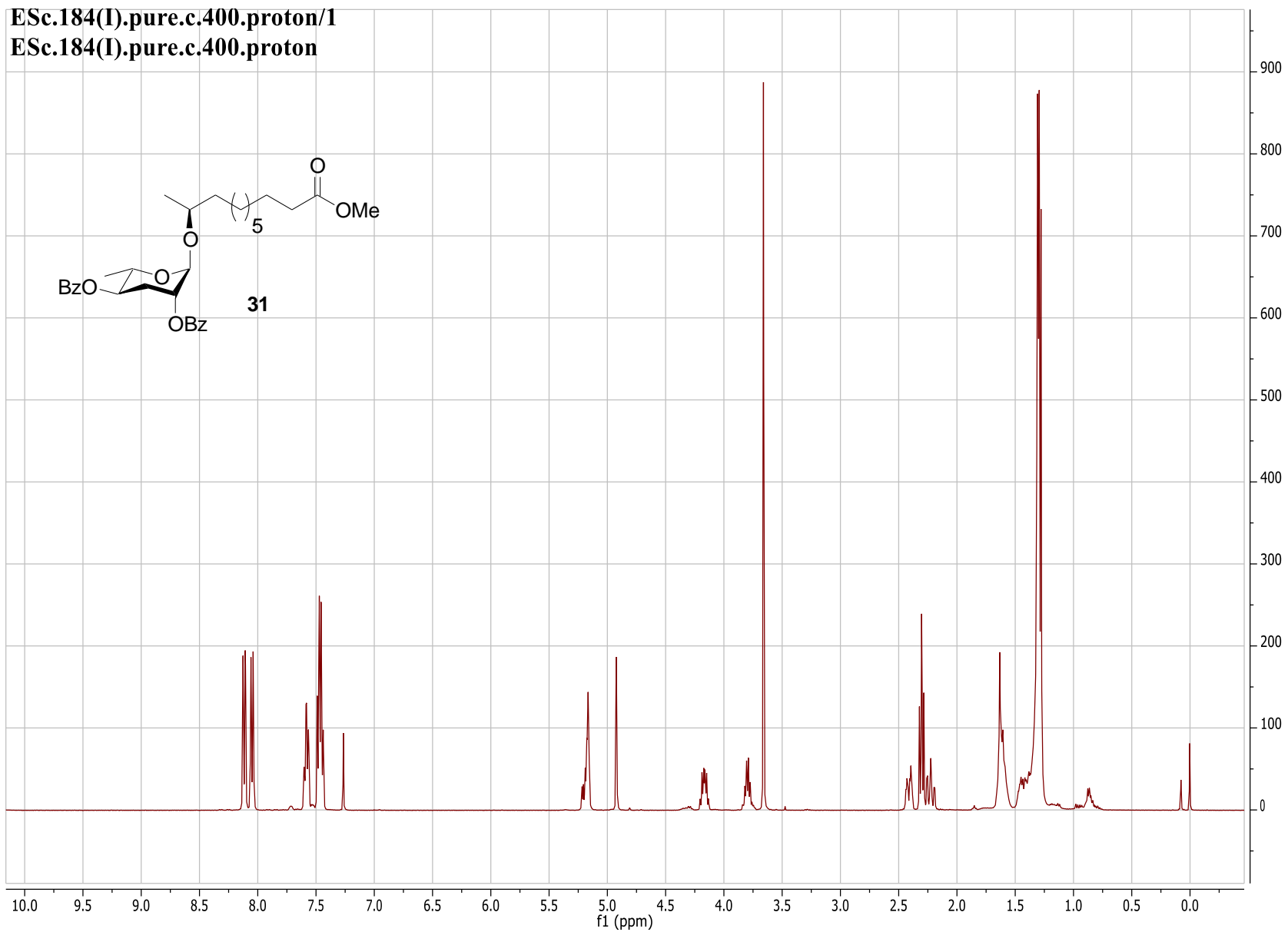
ESC.182(I).pure.carbon.2



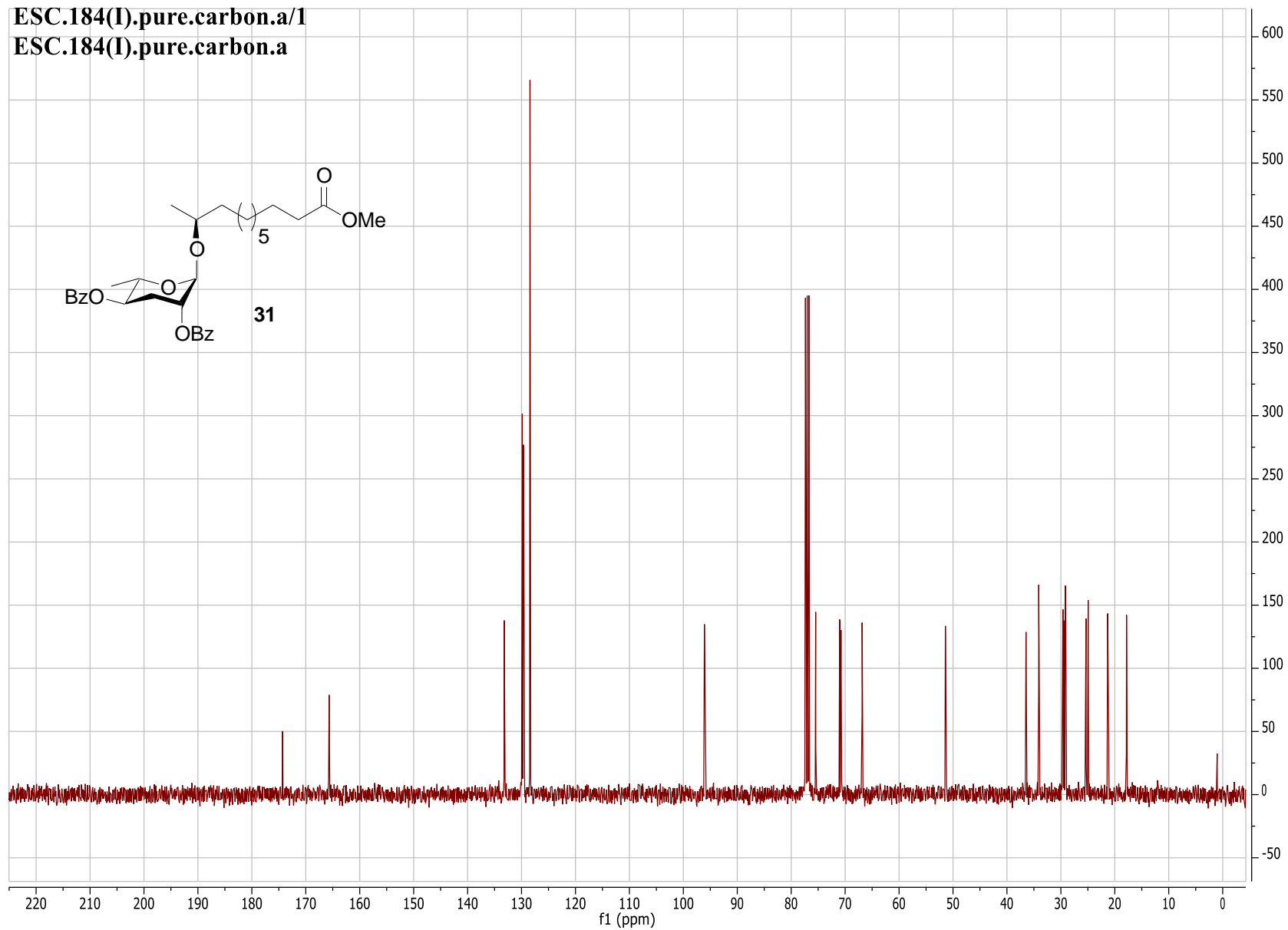
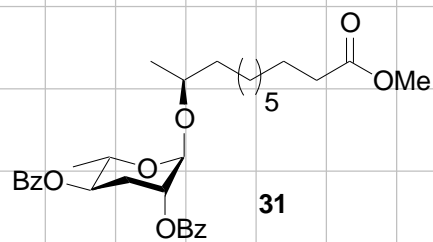
ESC.183/1  
General-purpose 1-D proton setup file



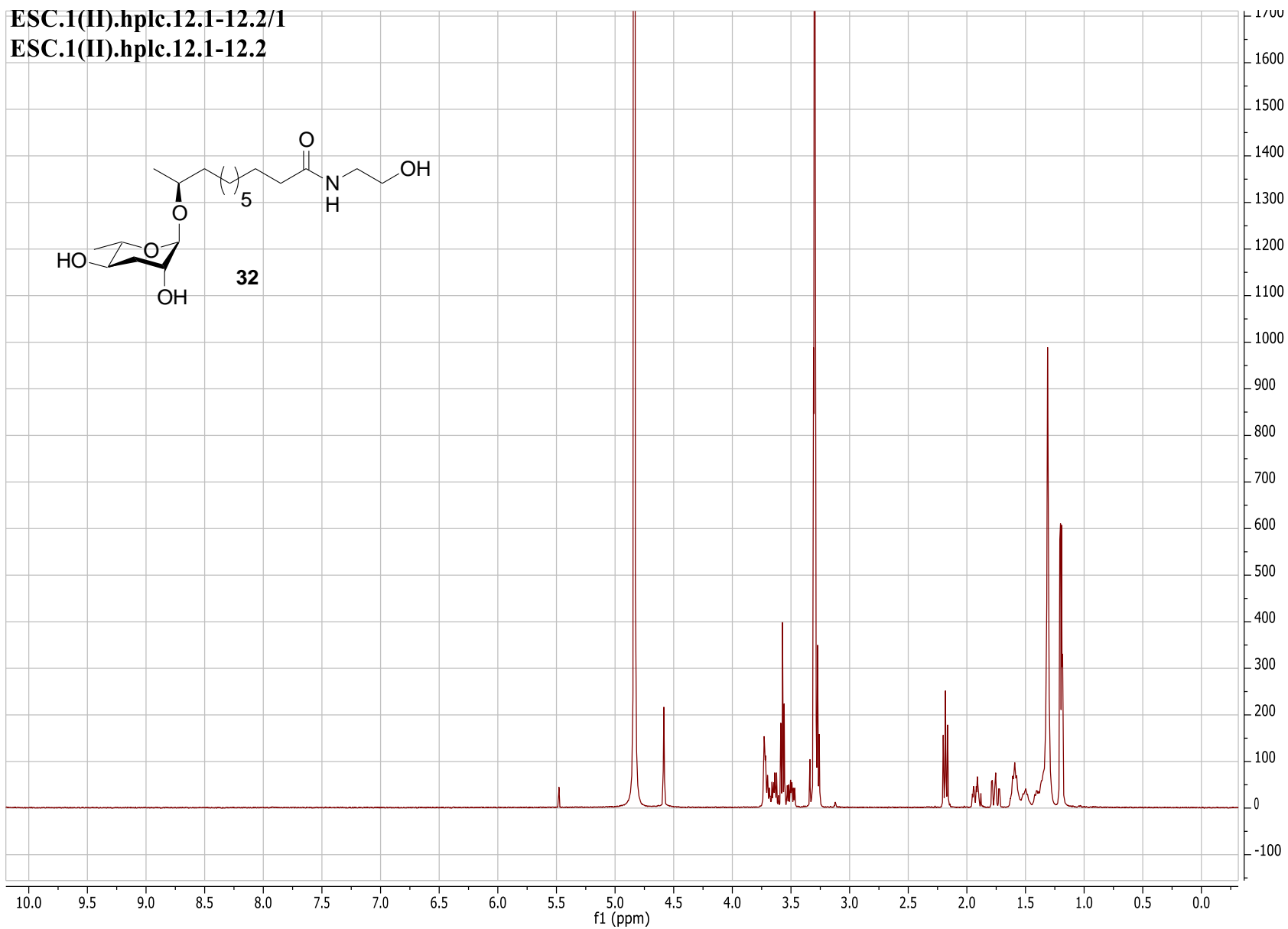
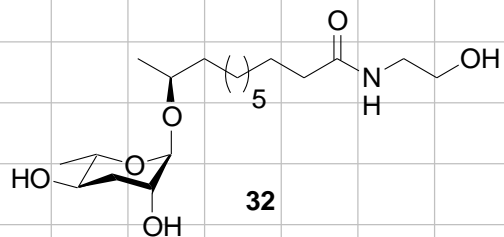
ESc.184(I).pure.c.400.proton/1  
ESc.184(I).pure.c.400.proton



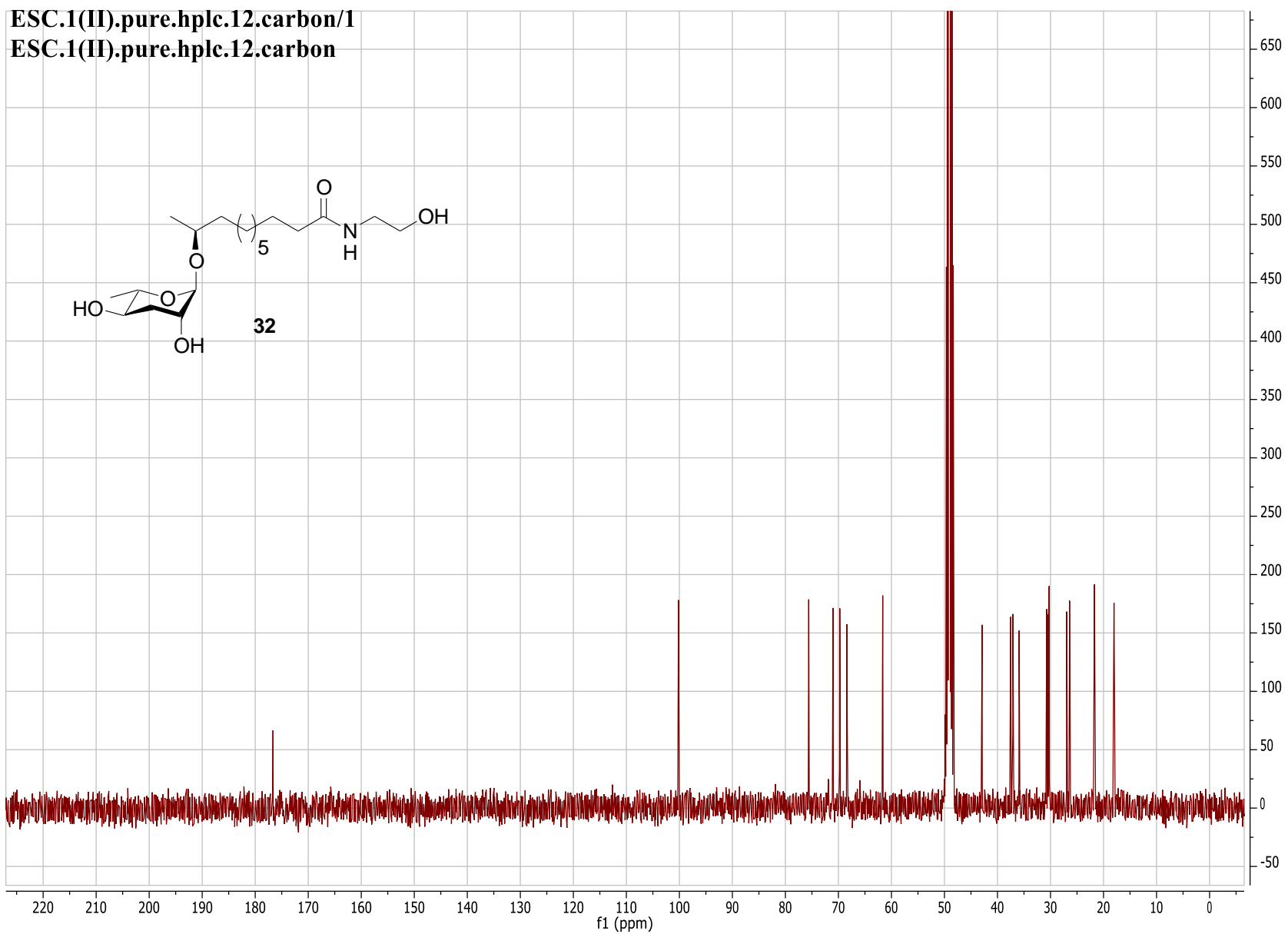
ESC.184(I).pure.carbon.a/1  
ESC.184(I).pure.carbon.a



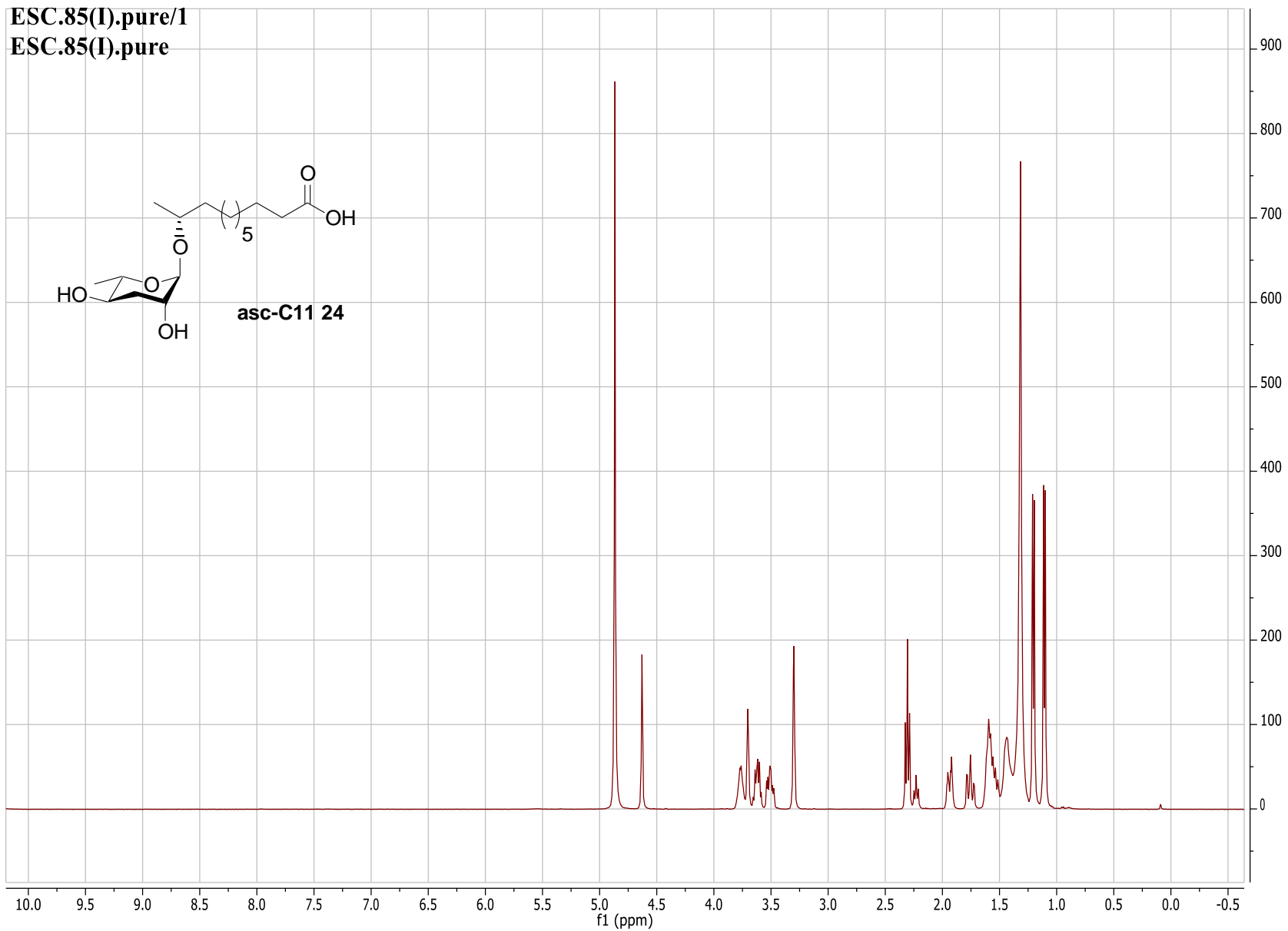
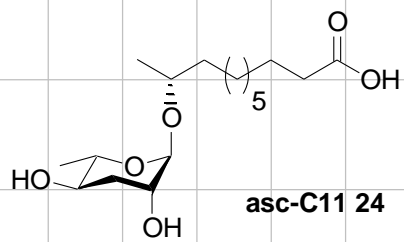
ESC.1(II).hplc.12.1-12.2/1  
ESC.1(II).hplc.12.1-12.2



ESC.1(II).pure.hplc.12.carbon/1  
ESC.1(II).pure.hplc.12.carbon



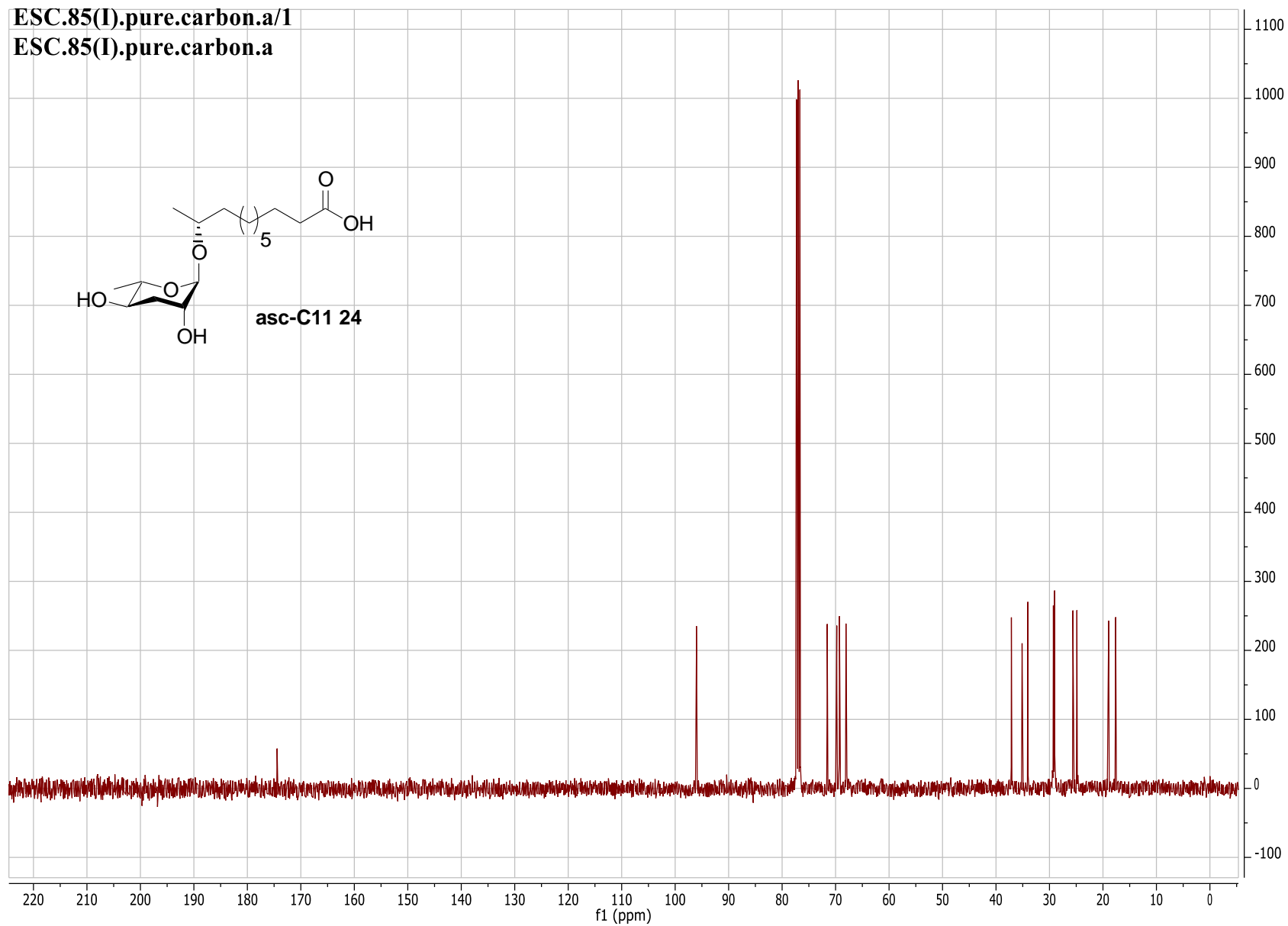
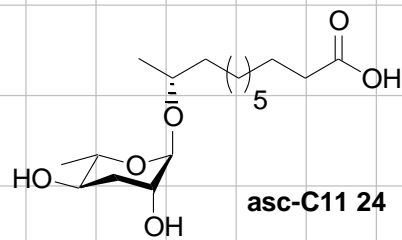
ESC.85(I).pure/1  
ESC.85(I).pure





ESC.85(I).pure.carbon.a/1

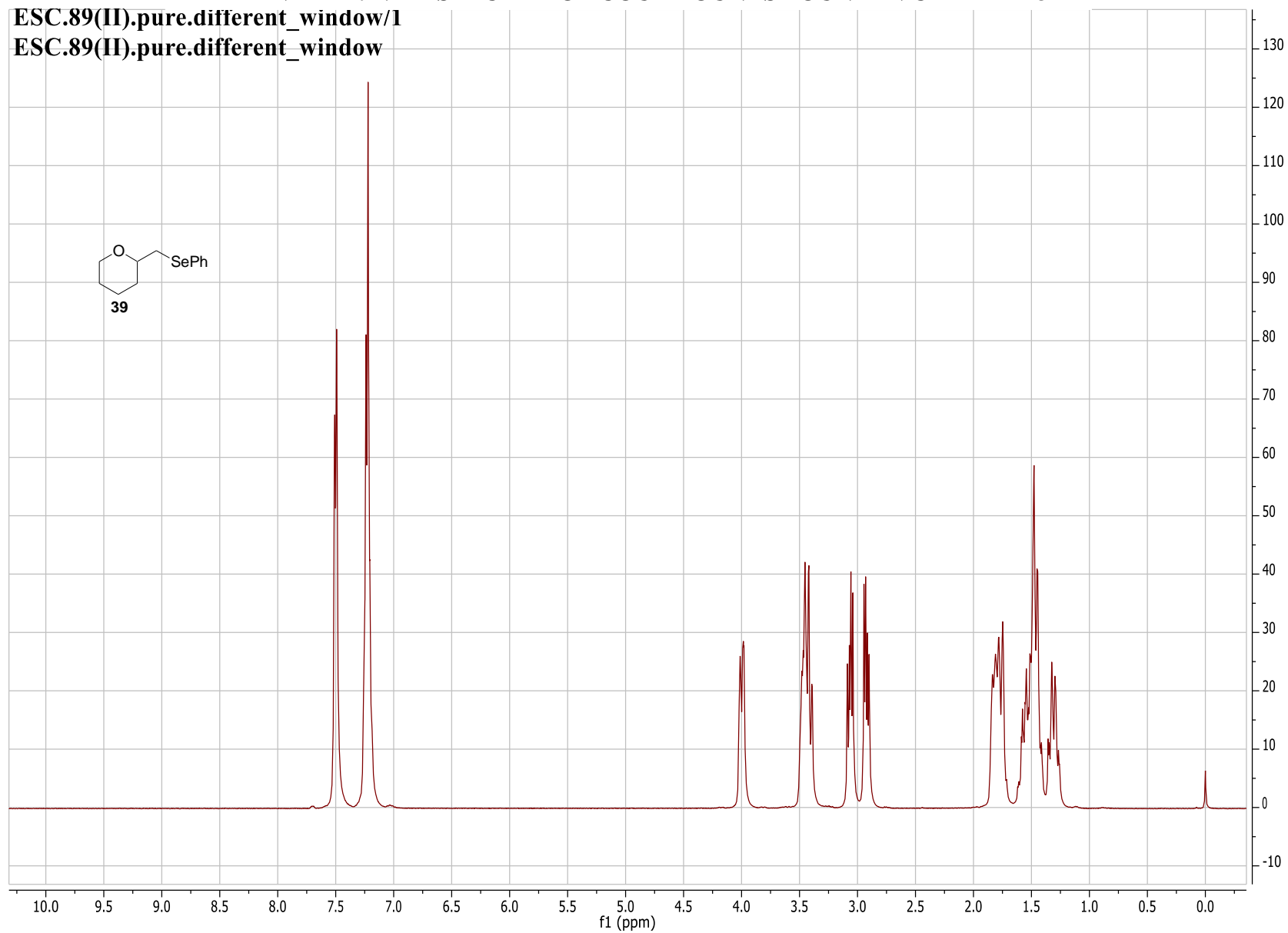
ESC.85(I).pure.carbon.a



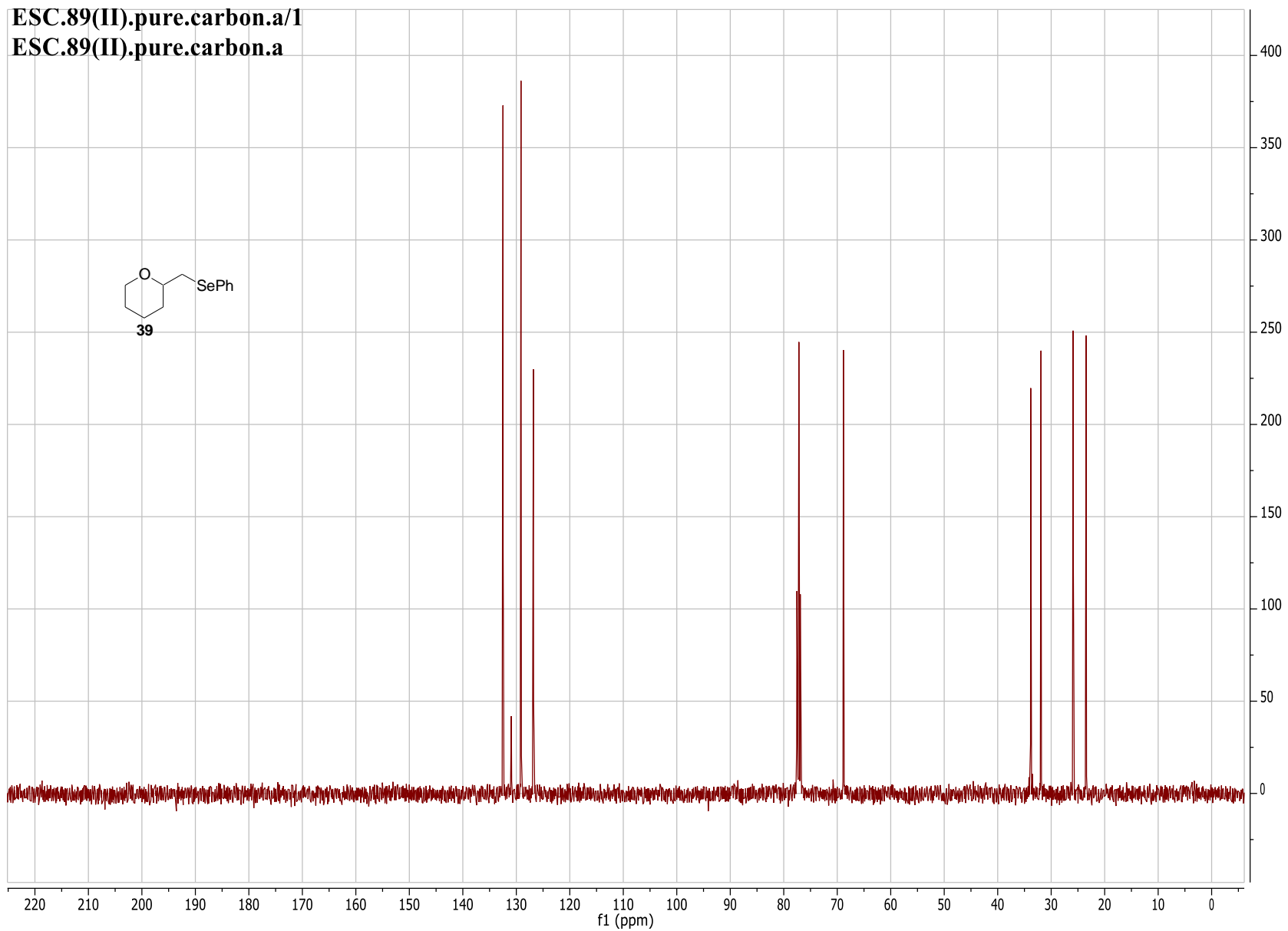
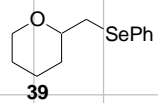
APPENDIX D: NMR SPECTRA OF COUMPOUNDS FOUND IN CHAPTER 3

ESC.89(II).pure.different\_window/1

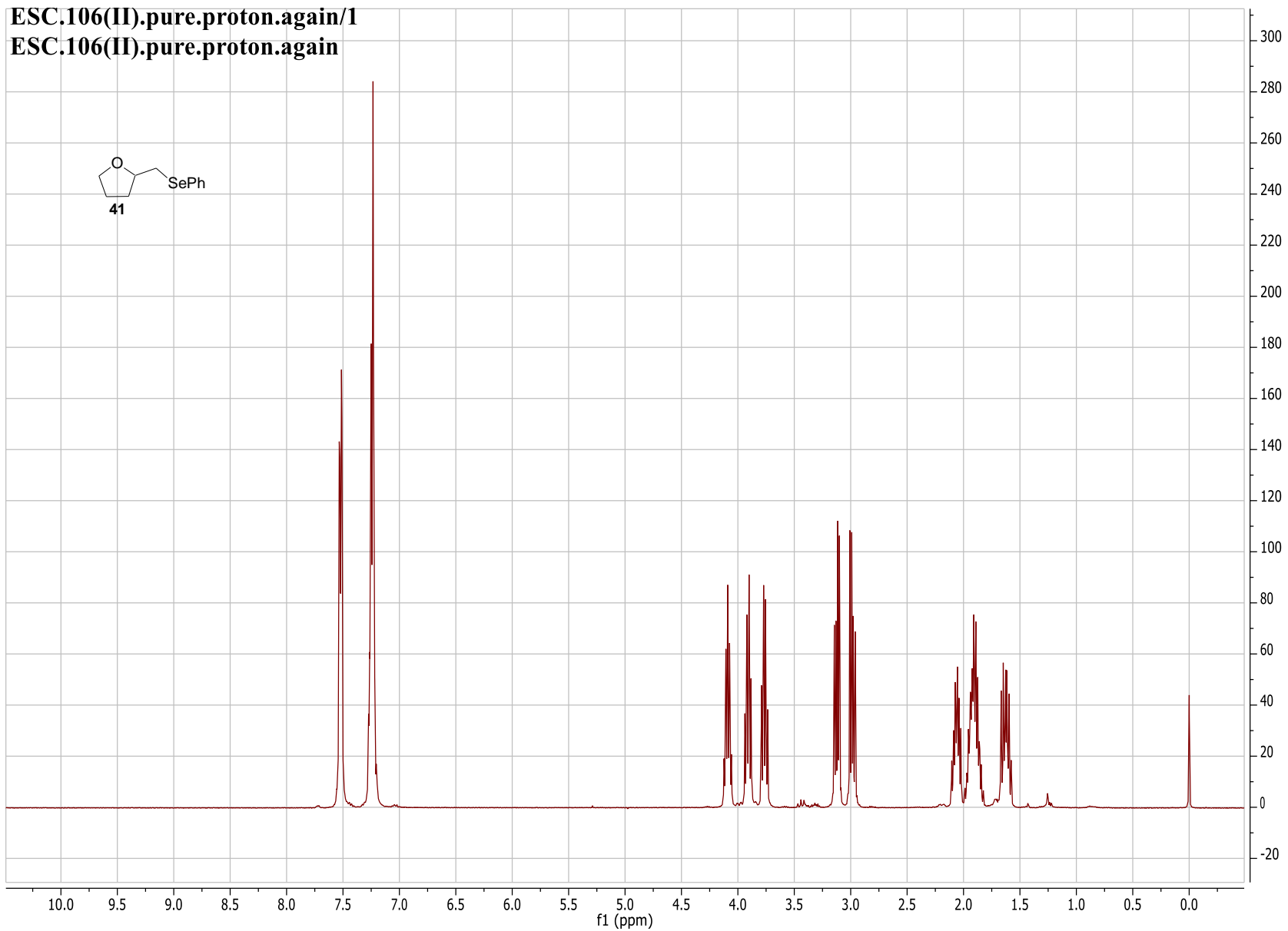
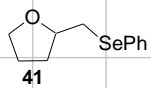
ESC.89(II).pure.different\_window



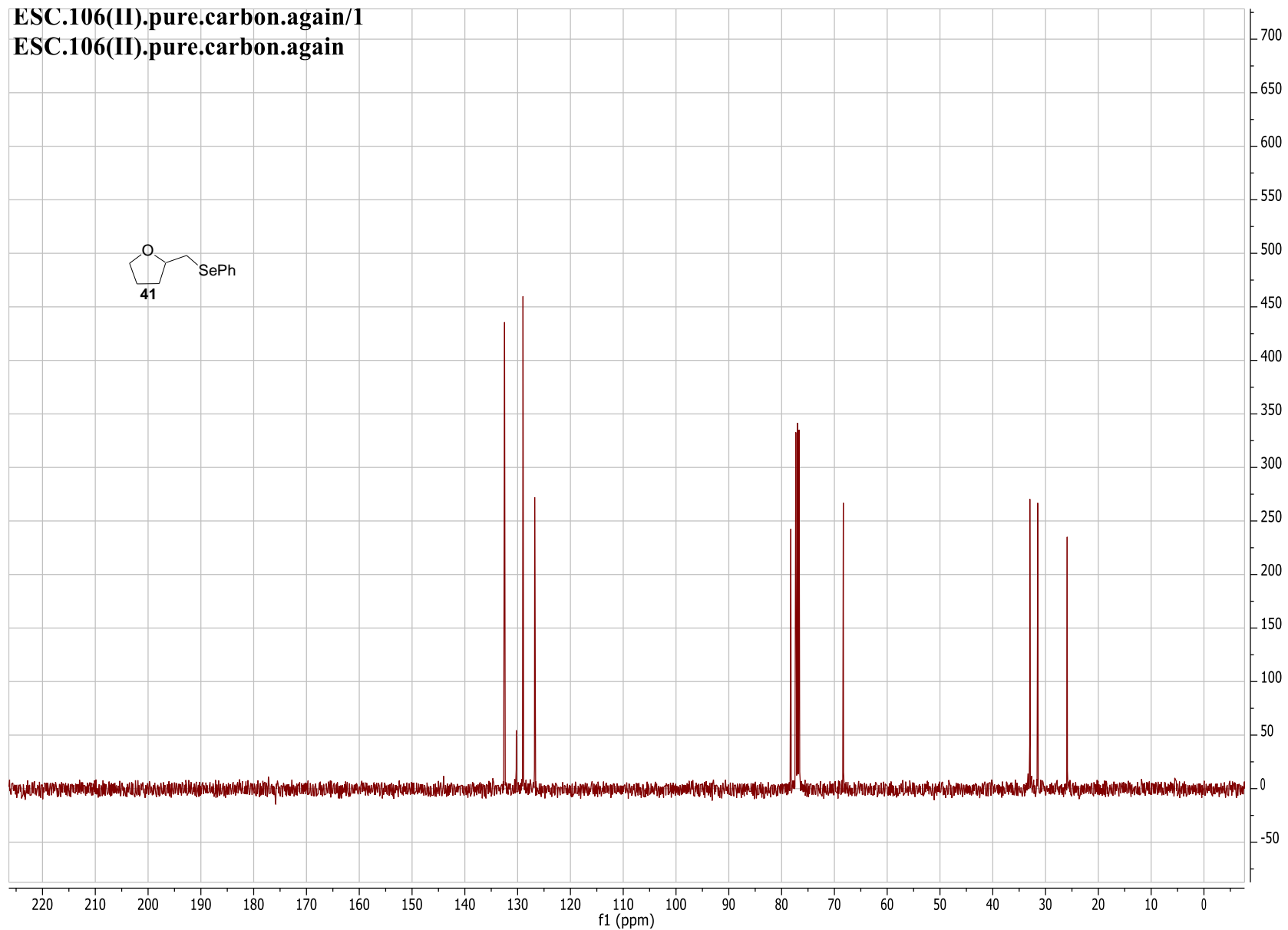
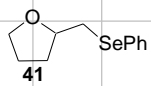
ESC.89(II).pure.carbon.a/1  
ESC.89(II).pure.carbon.a



ESC.106(II).pure.proton.again/1  
ESC.106(II).pure.proton.again

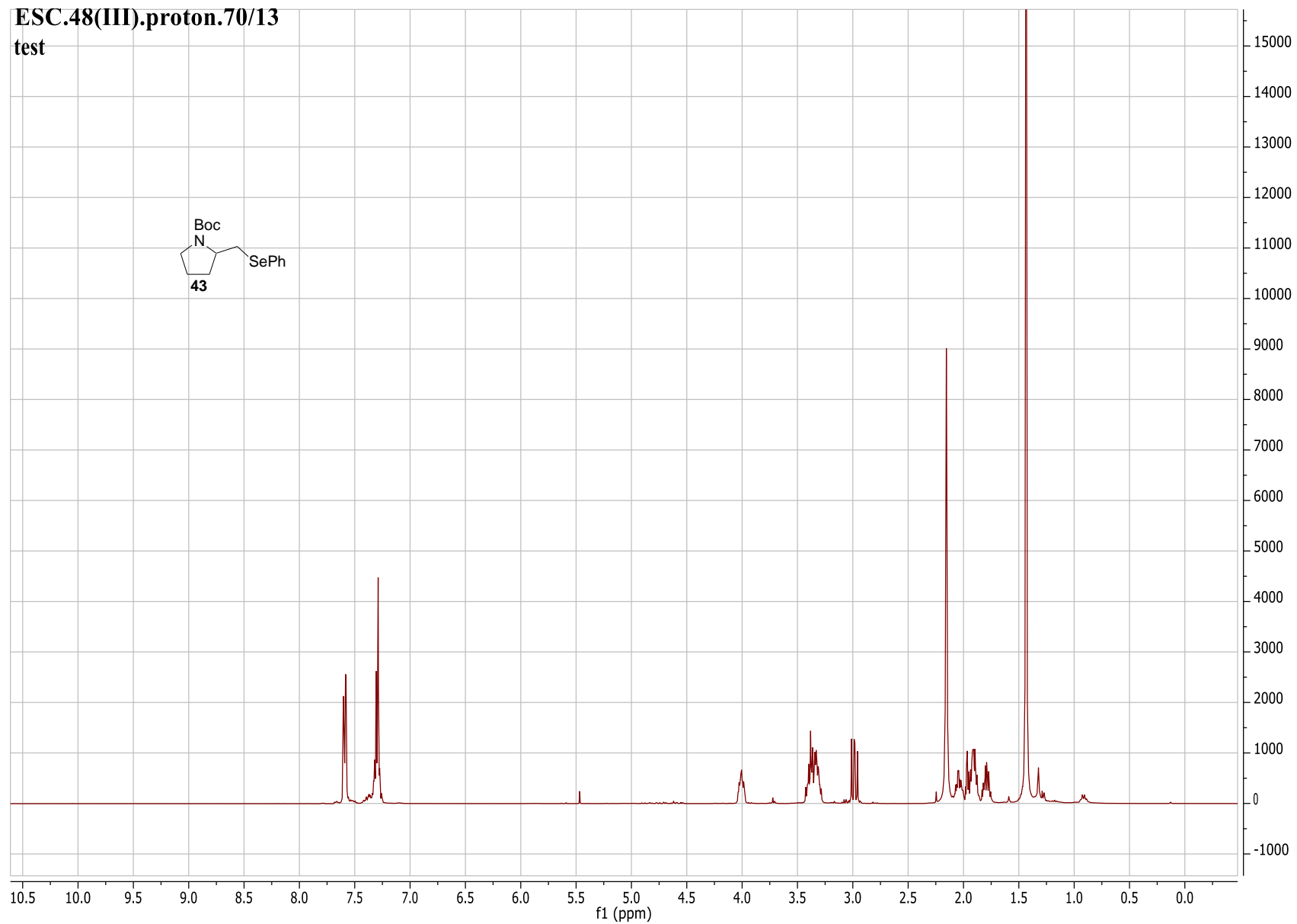
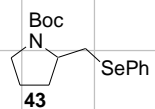


ESC.106(II).pure.carbon.again/1  
ESC.106(II).pure.carbon.again

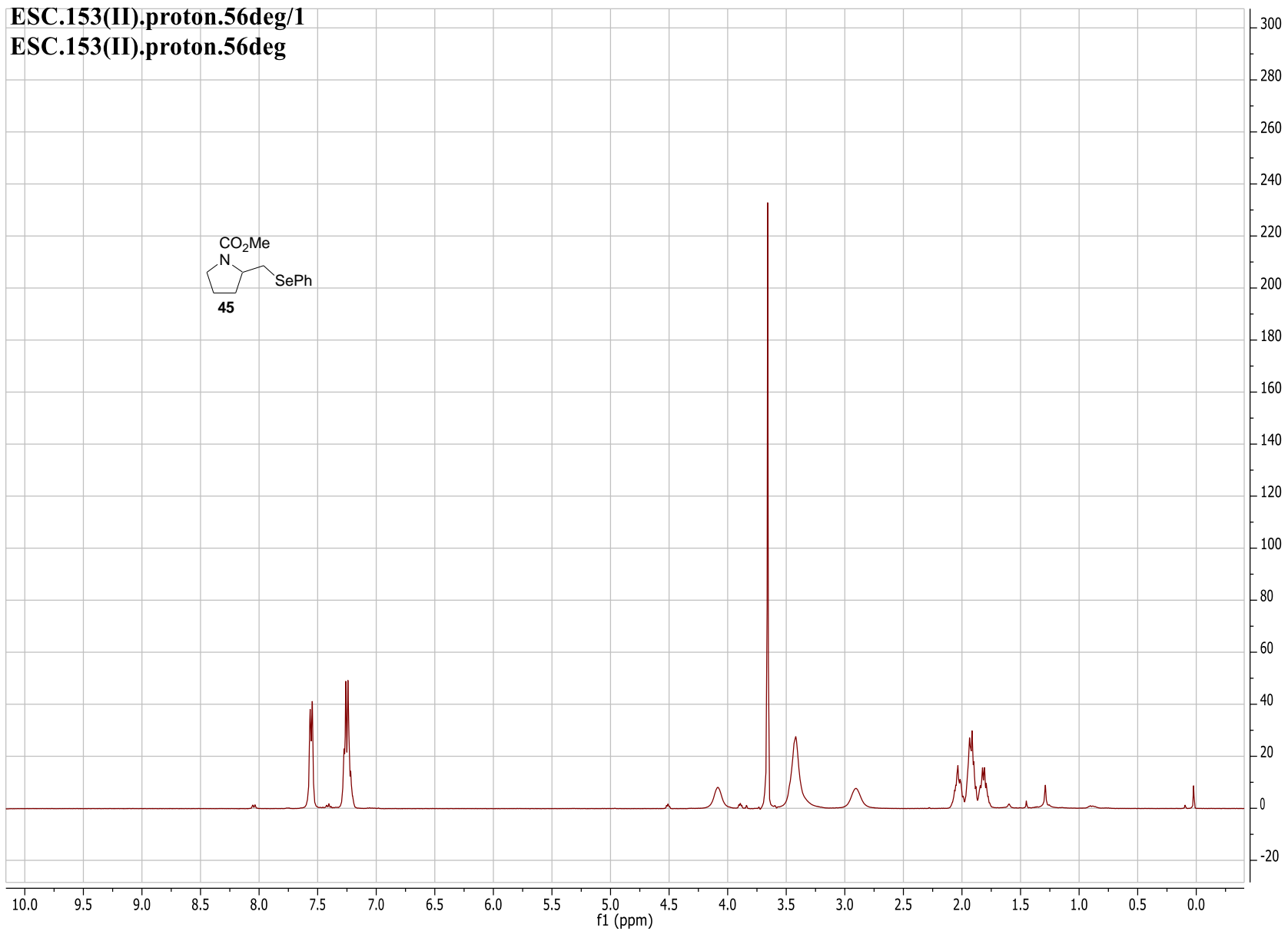
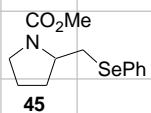


ESC.48(III).proton.70/13

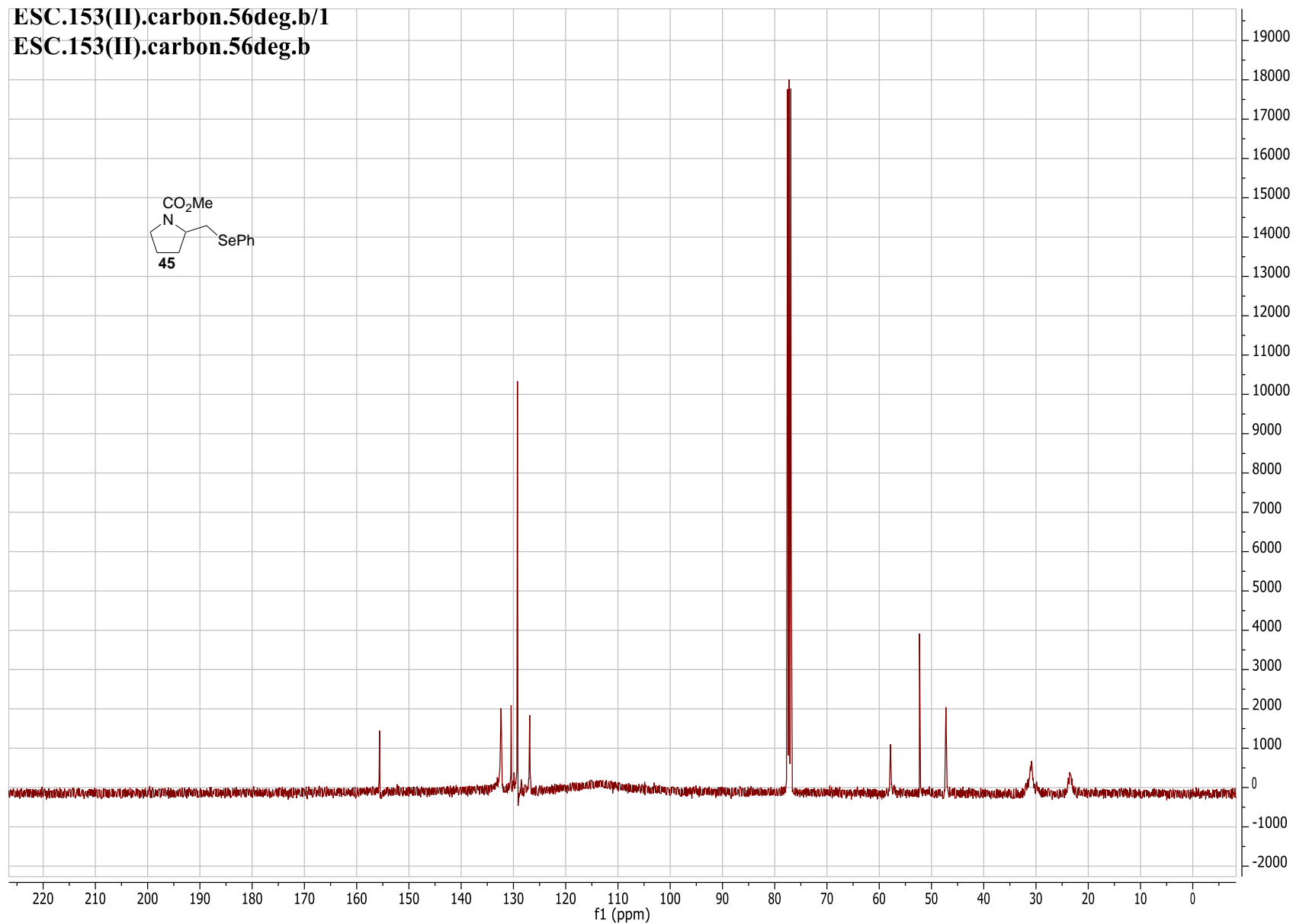
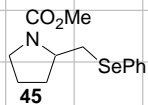
test



ESC.153(II).proton.56deg/1  
ESC.153(II).proton.56deg

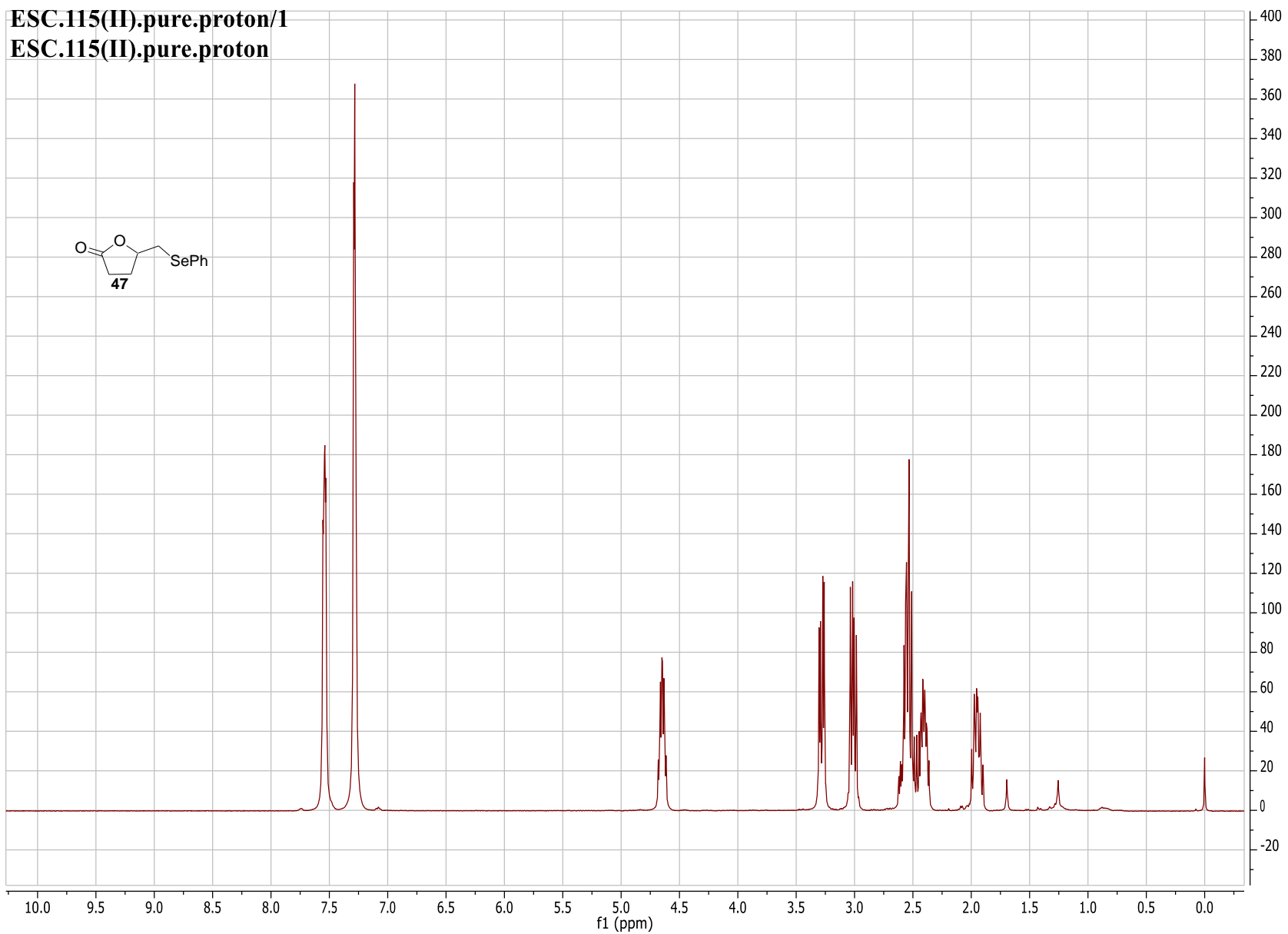
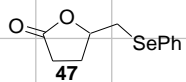


ESC.153(II).carbon.56deg.b/1  
ESC.153(II).carbon.56deg.b

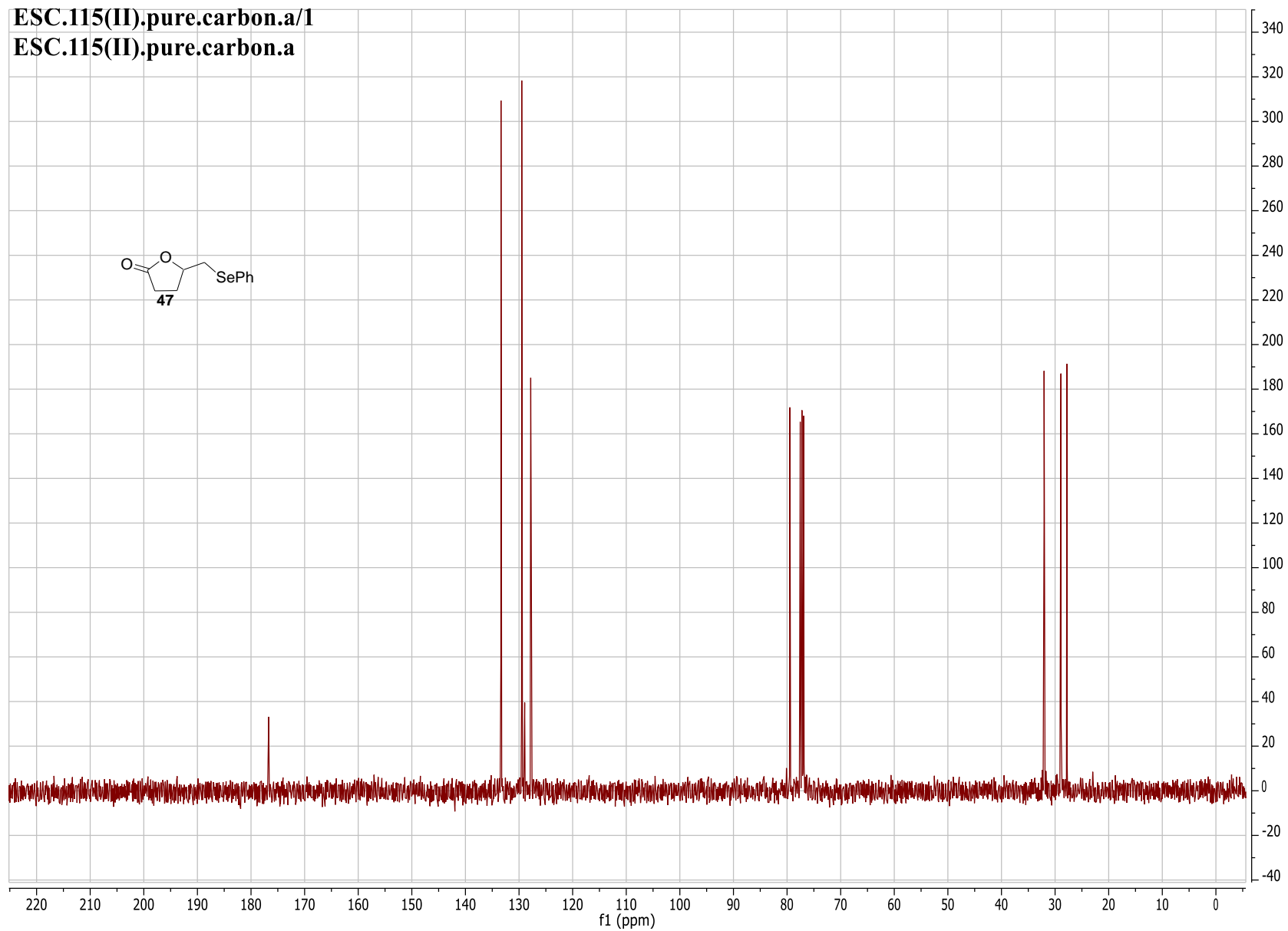
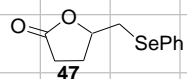




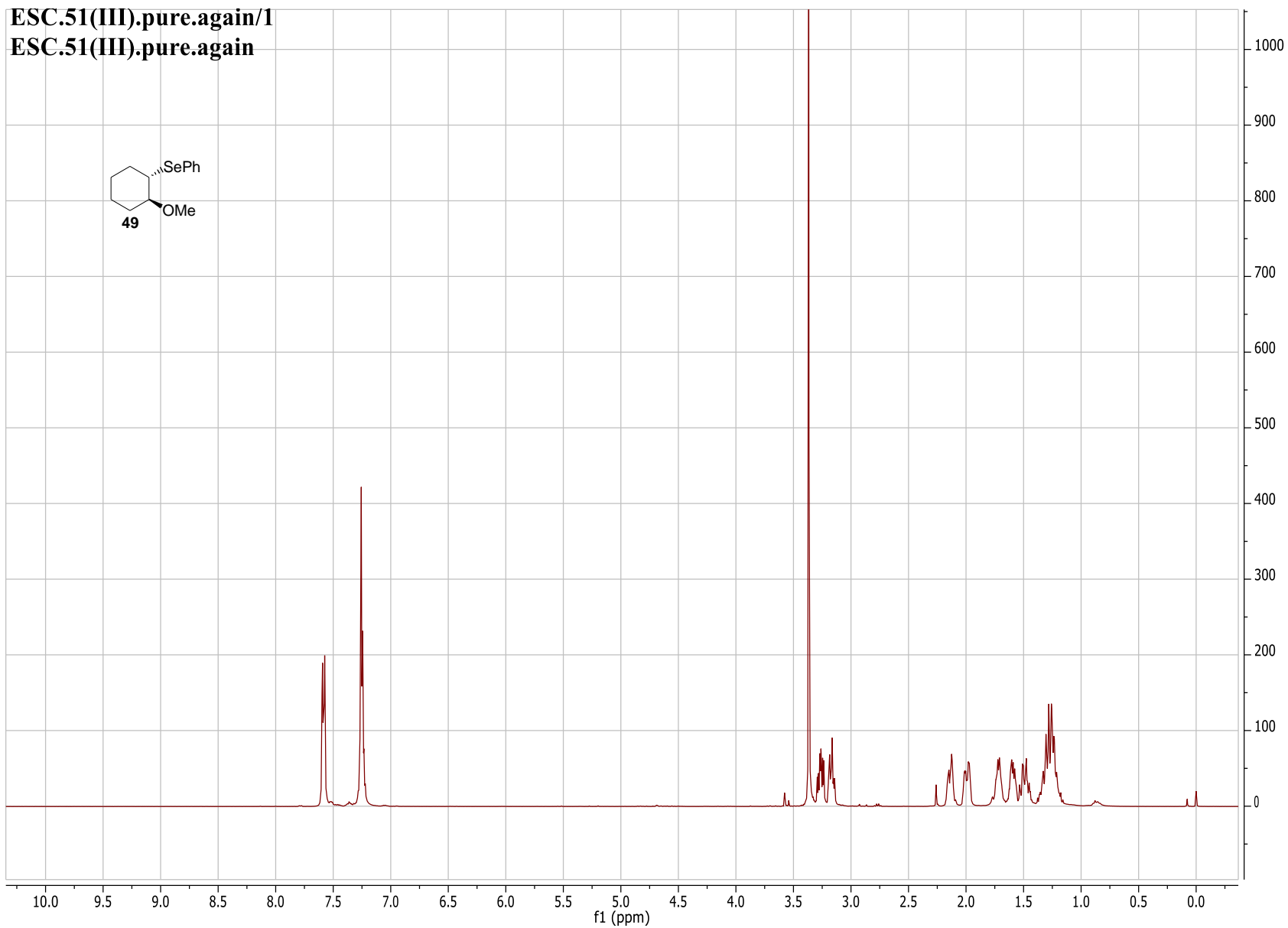
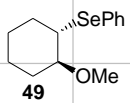
ESC.115(II).pure.proton/1  
ESC.115(II).pure.proton



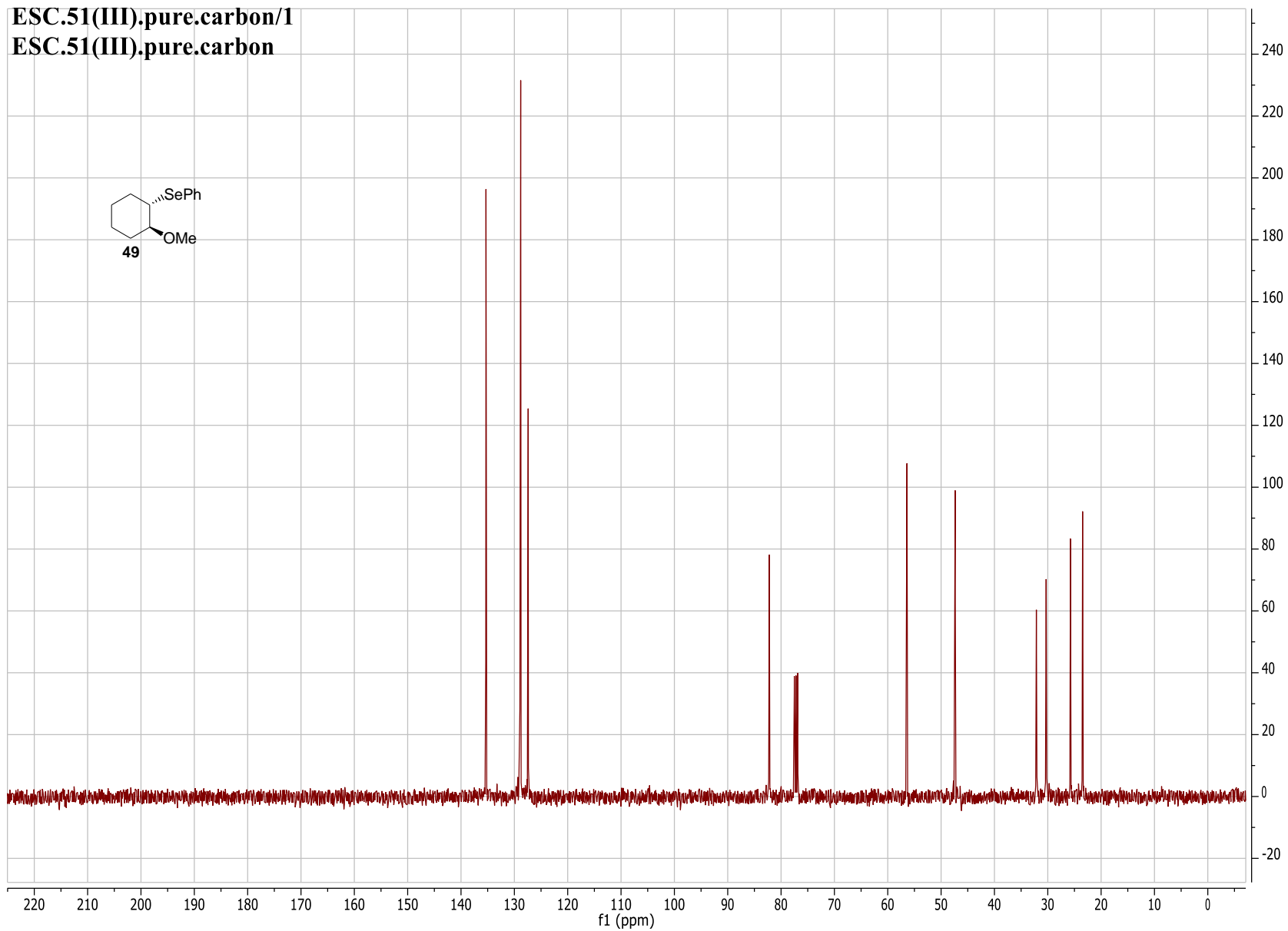
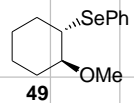
ESC.115(II).pure.carbon.a/1  
ESC.115(II).pure.carbon.a



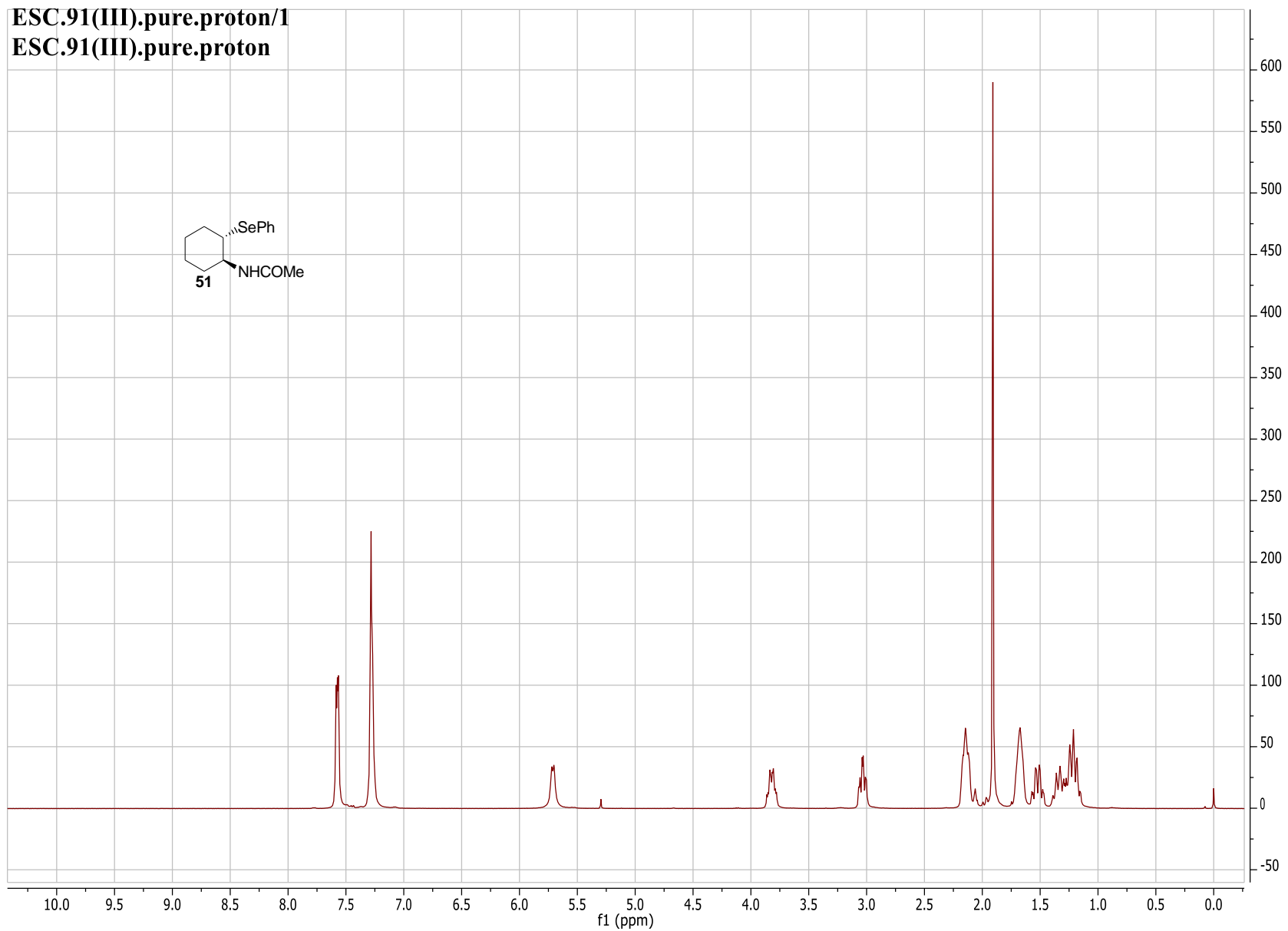
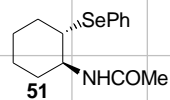
ESC.51(III).pure.again/1  
ESC.51(III).pure.again



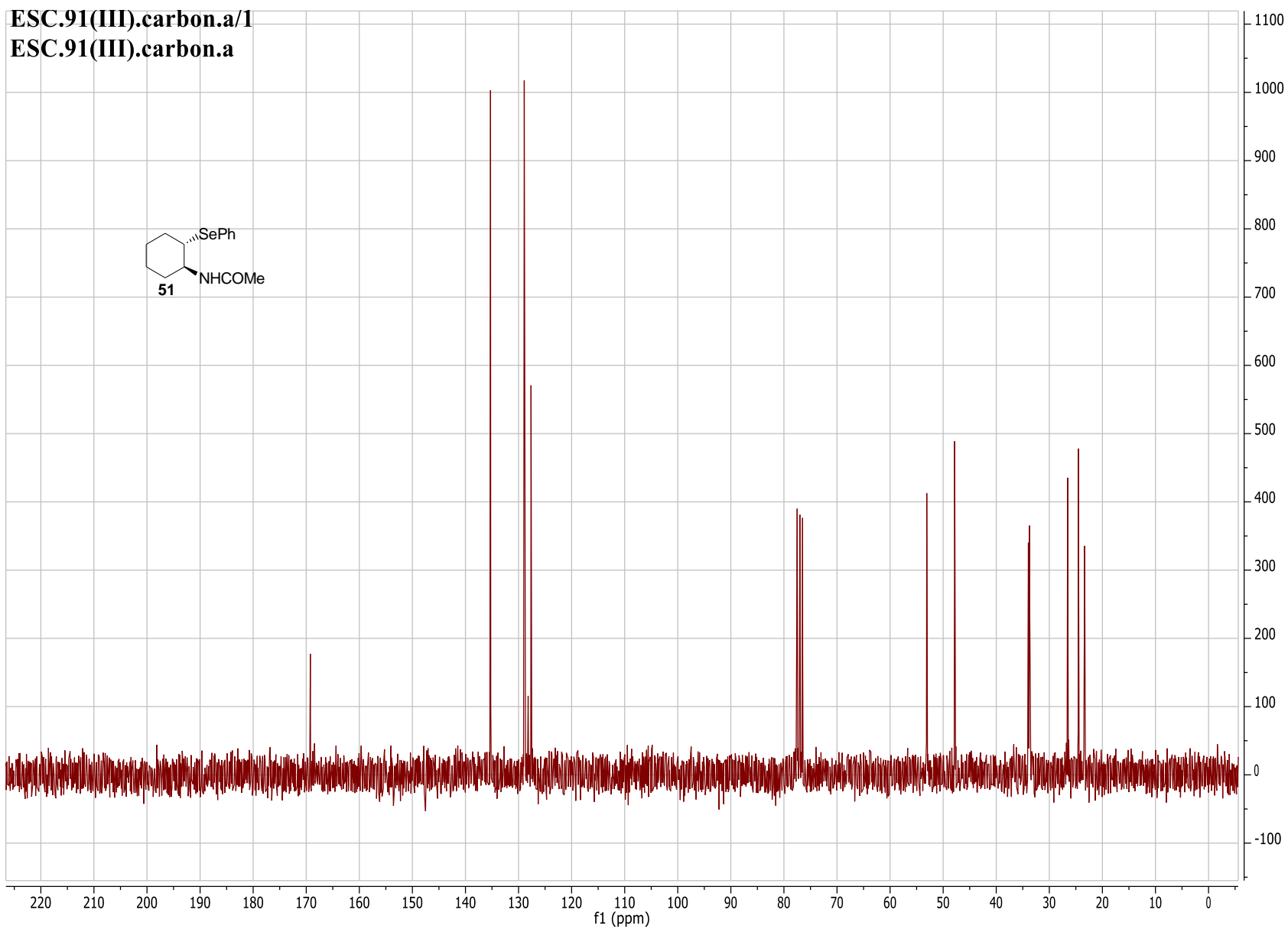
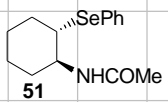
ESC.51(III).pure.carbon/1  
ESC.51(III).pure.carbon



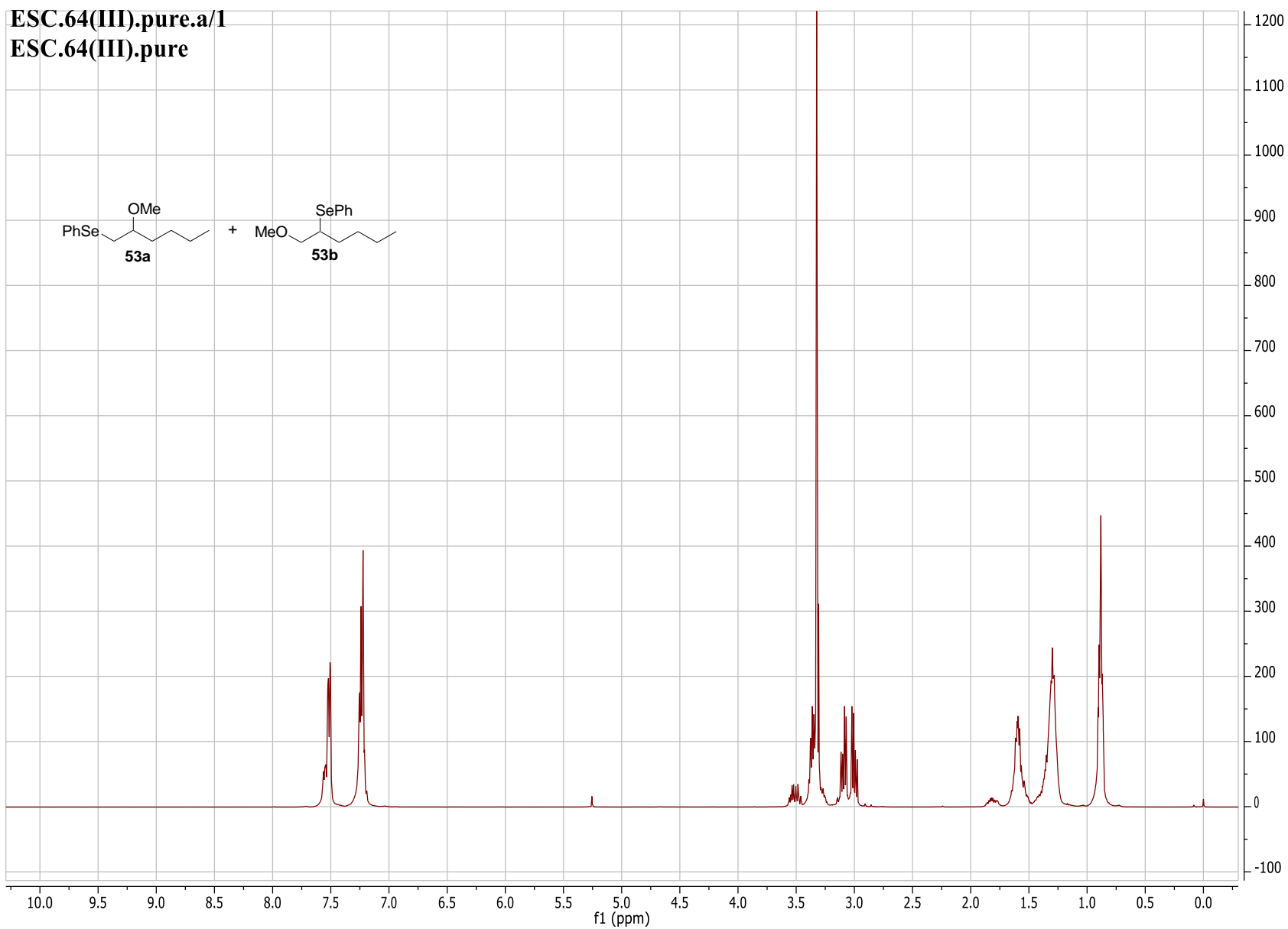
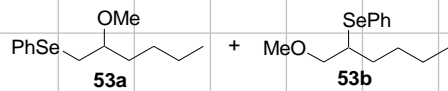
ESC.91(III).pure.proton/1  
ESC.91(III).pure.proton



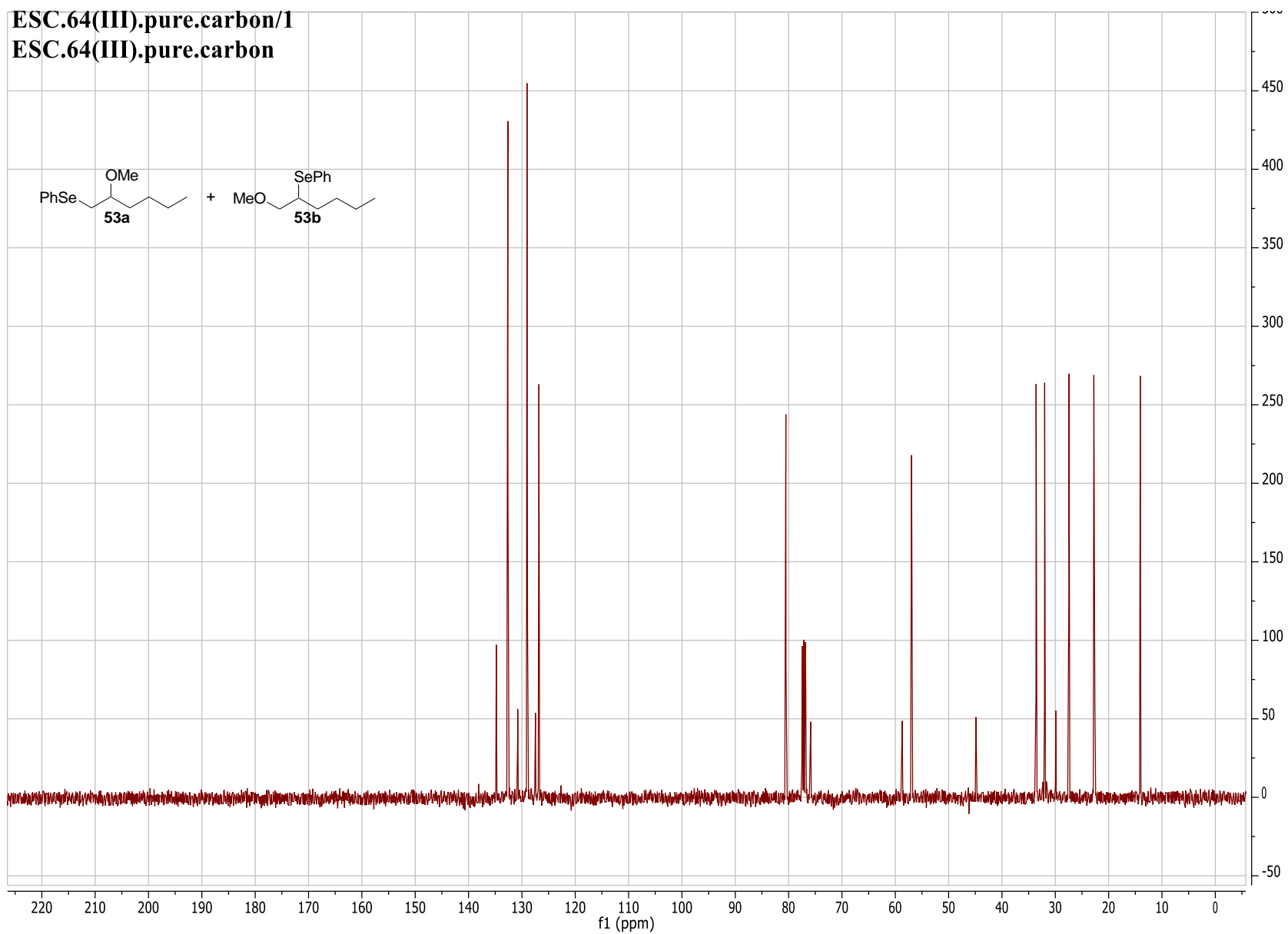
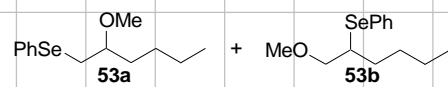
ESC.91(III).carbon.a/1  
ESC.91(III).carbon.a



ESC.64(III).pure.a/1  
ESC.64(III).pure

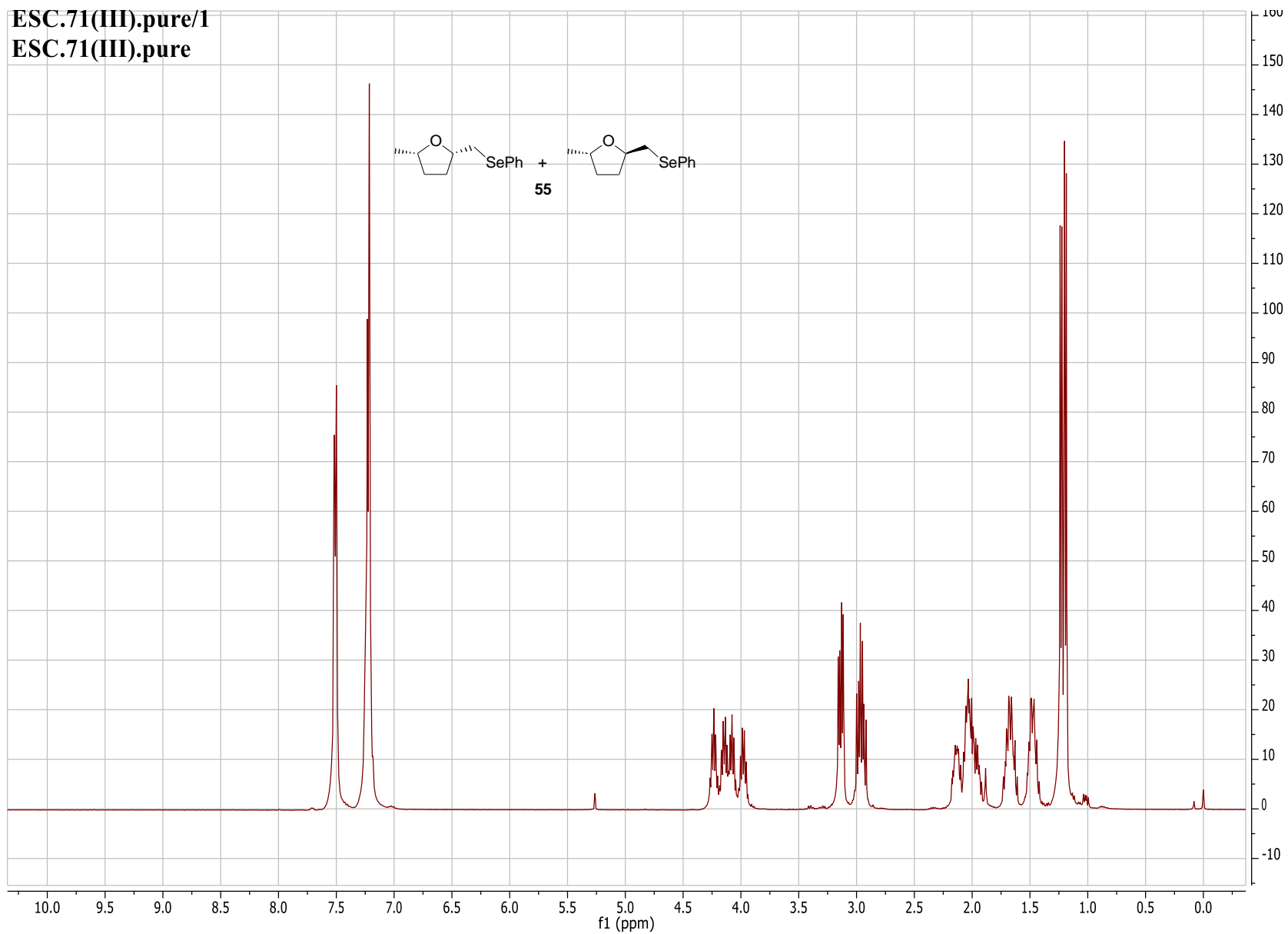


ESC.64(III).pure.carbon/1  
ESC.64(III).pure.carbon



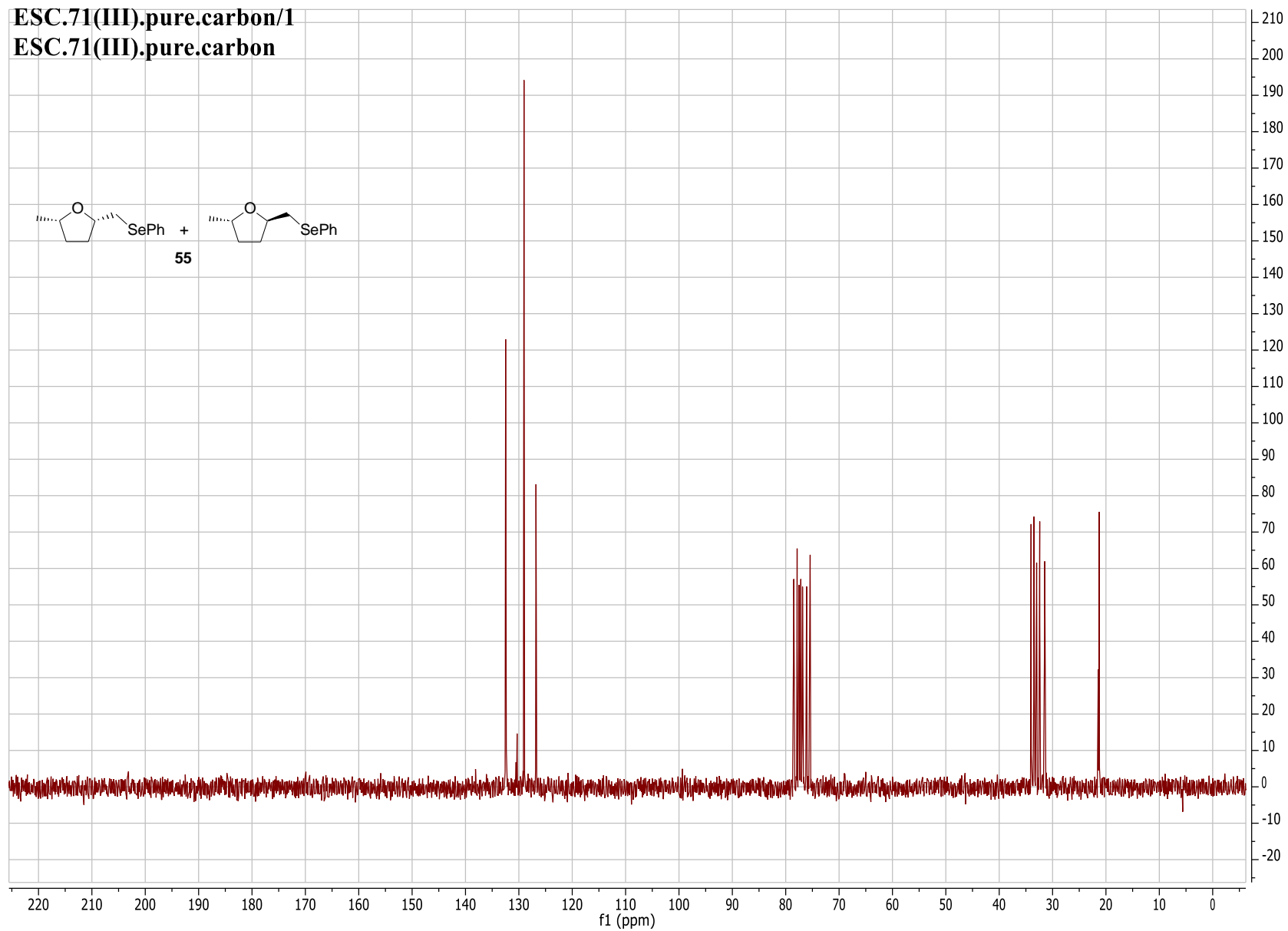


ESC.71(III).pure/1  
ESC.71(III).pure

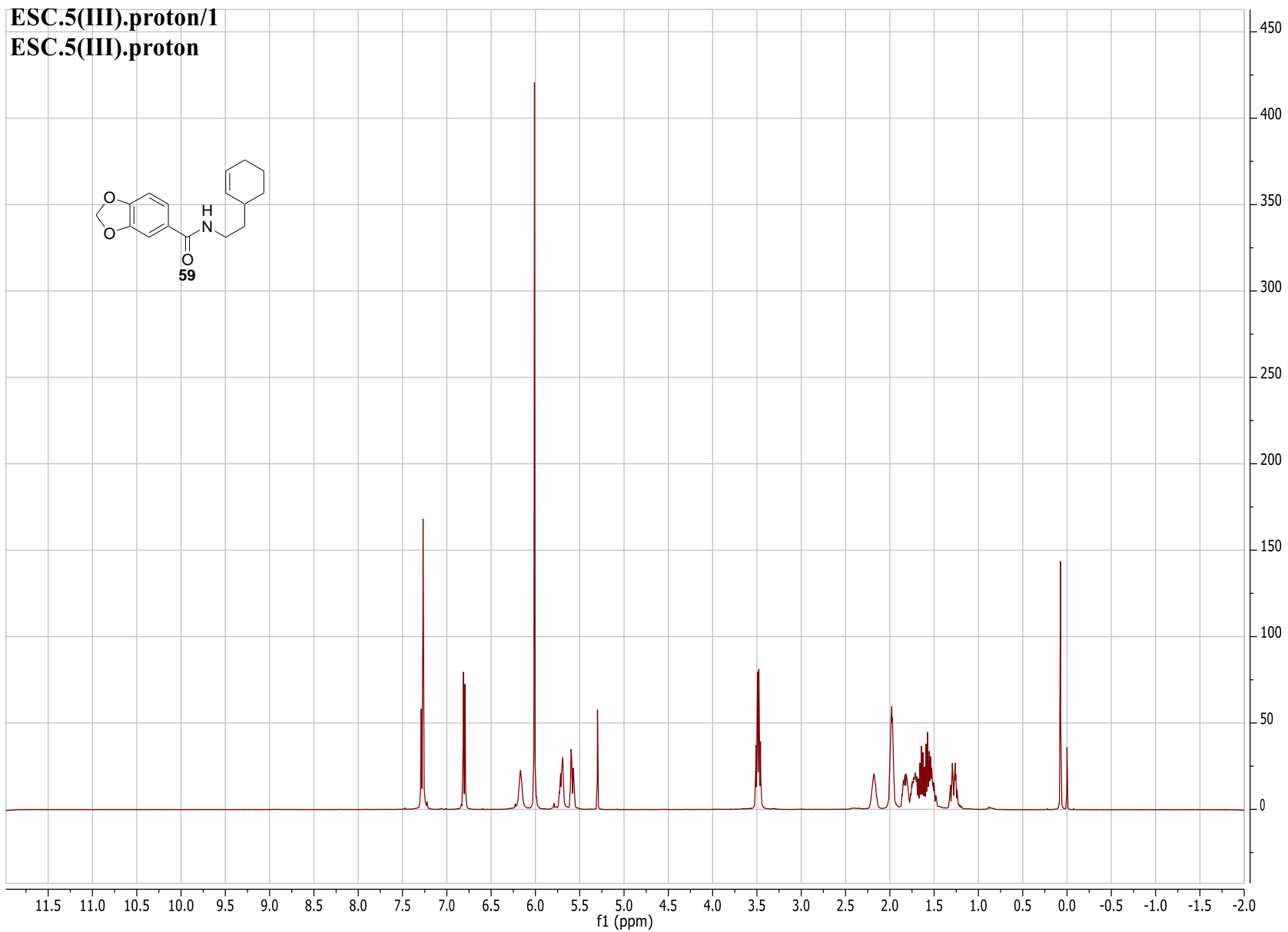
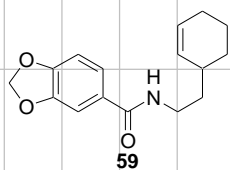


ESC.71(III).pure.carbon/1

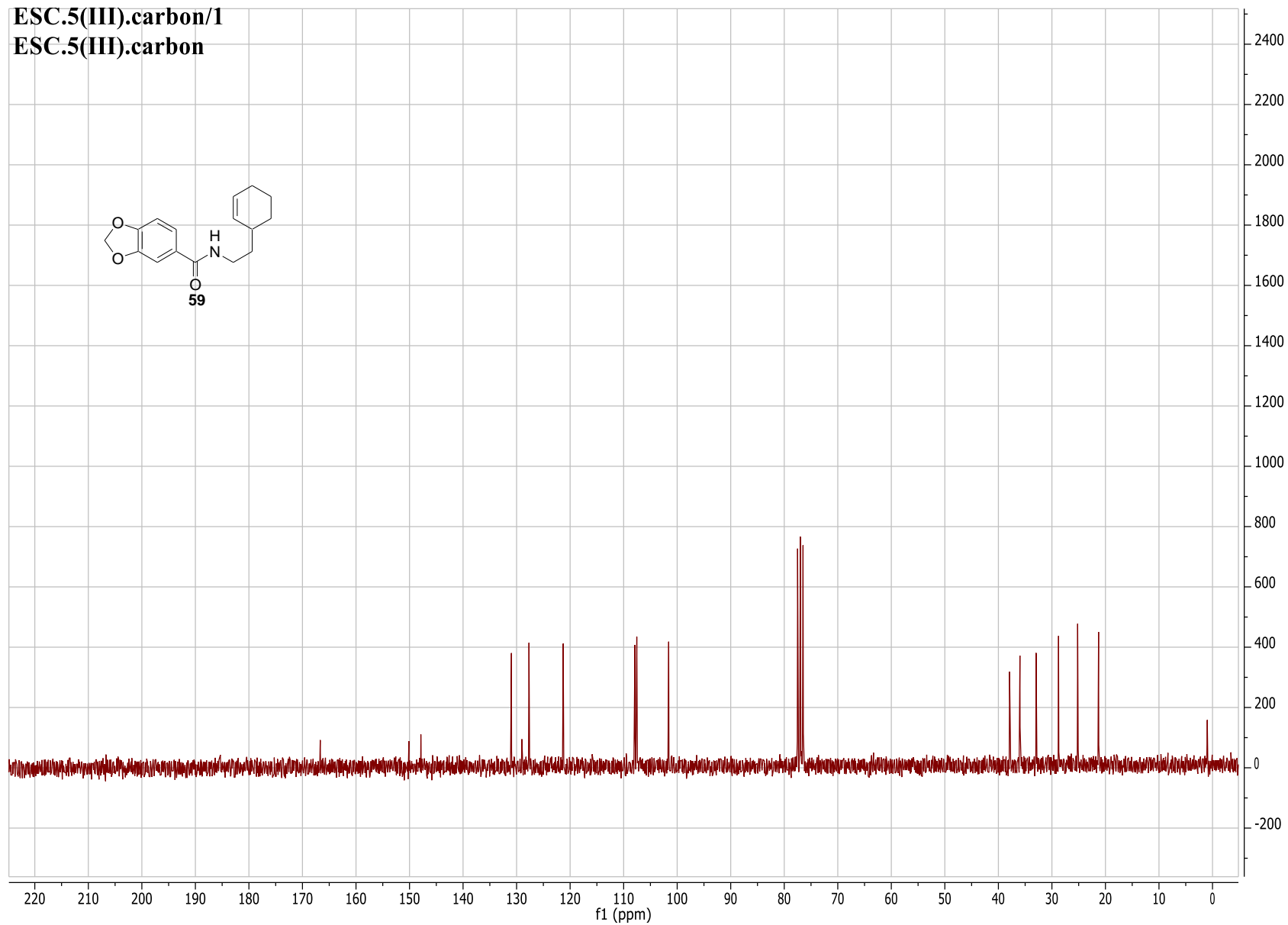
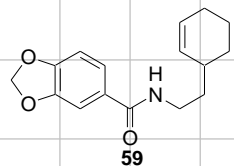
ESC.71(III).pure.carbon



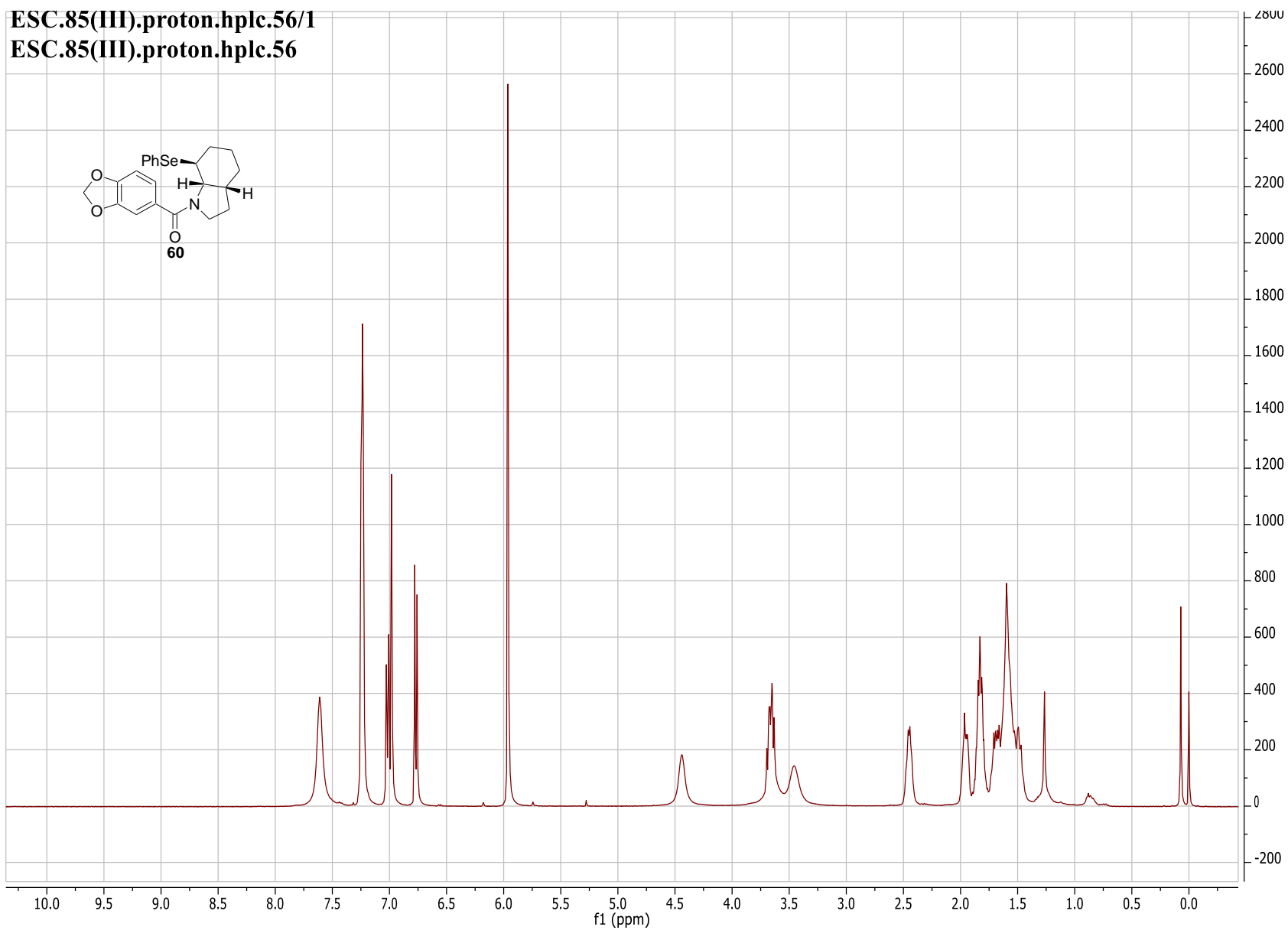
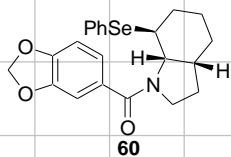
ESC.5(III).proton/1  
ESC.5(III).proton



ESC.5(III).carbon/1  
ESC.5(III).carbon

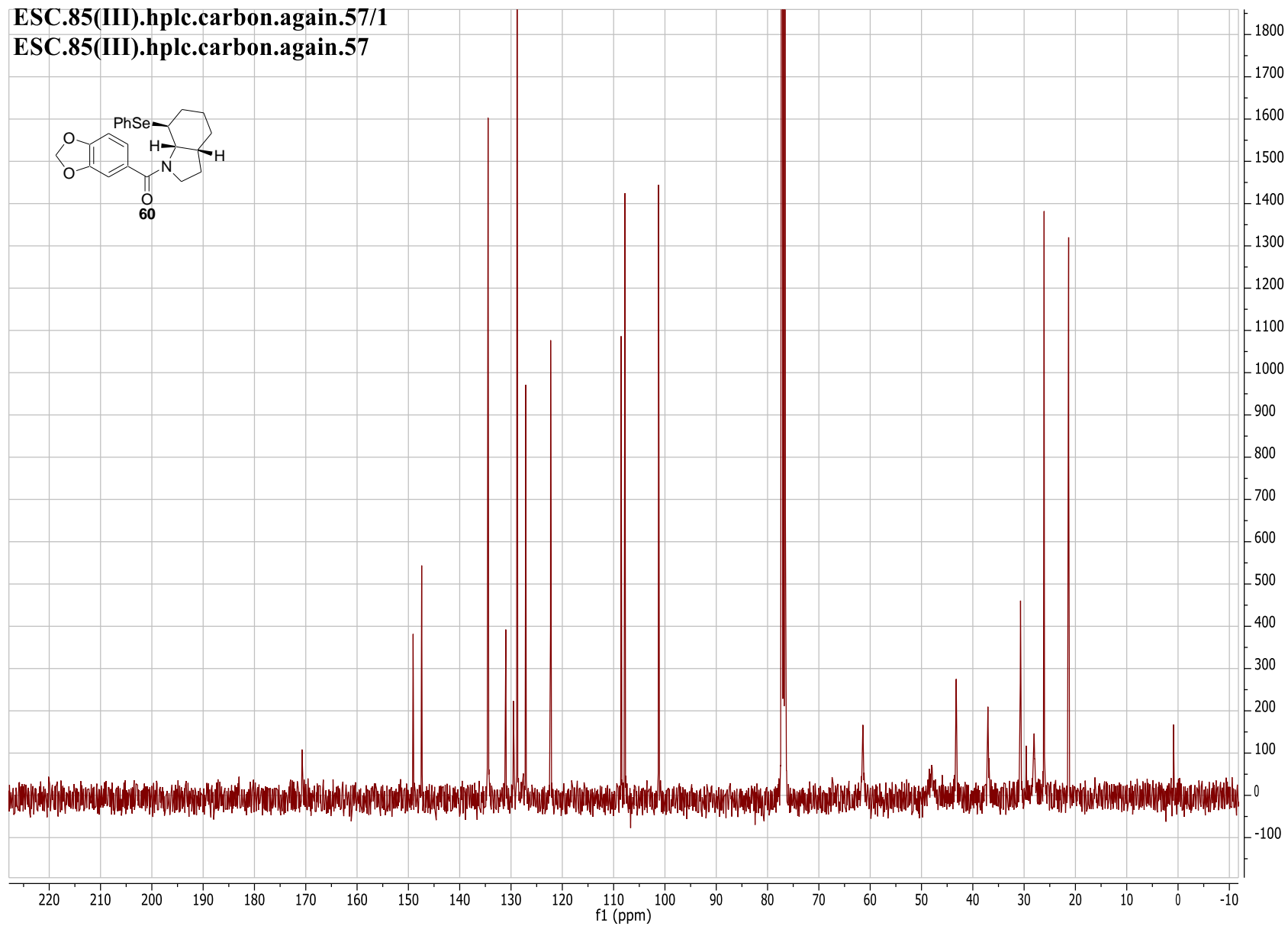
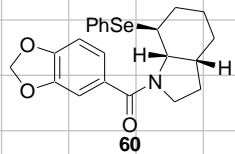


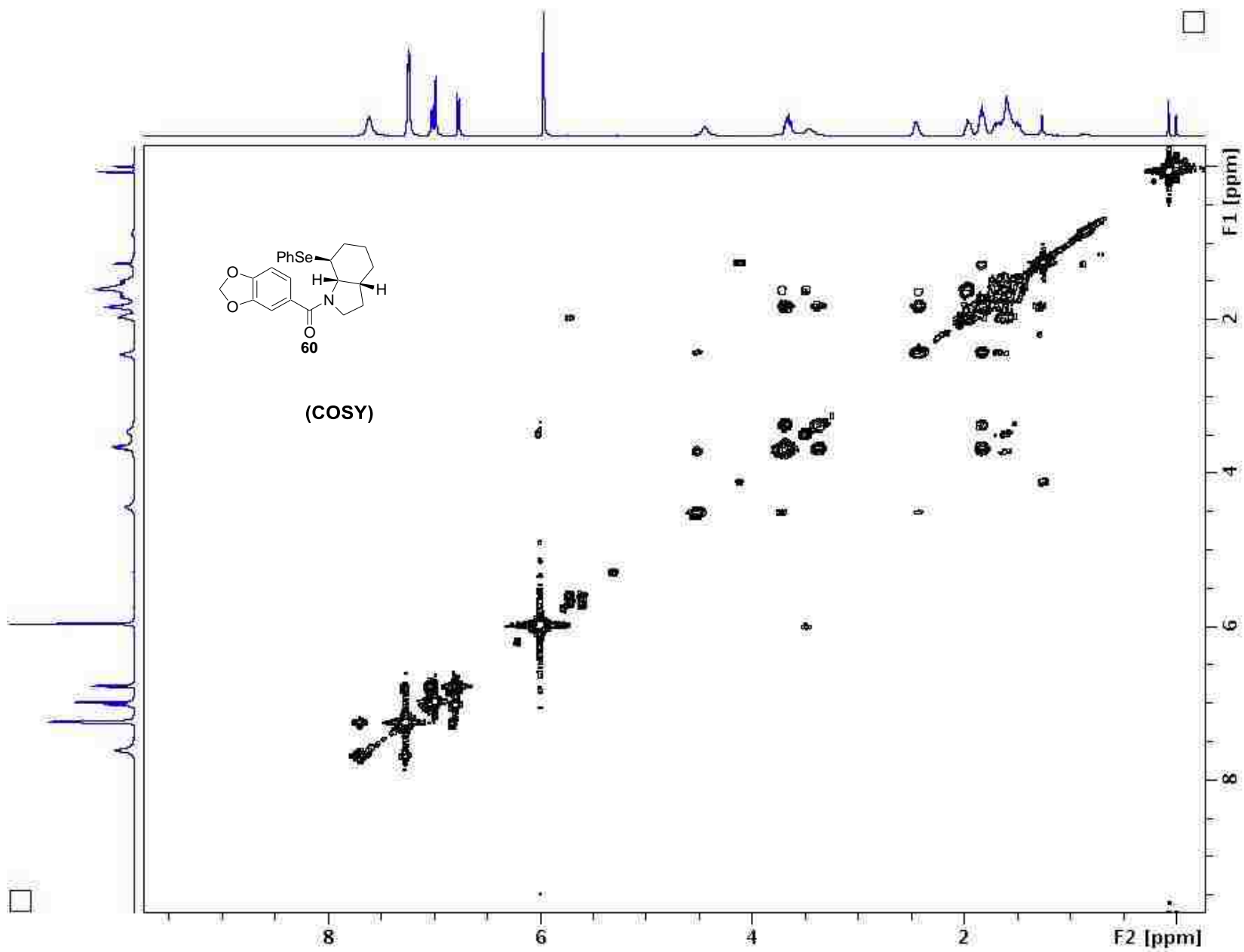
ESC.85(III).proton.hplc.56/1  
ESC.85(III).proton.hplc.56

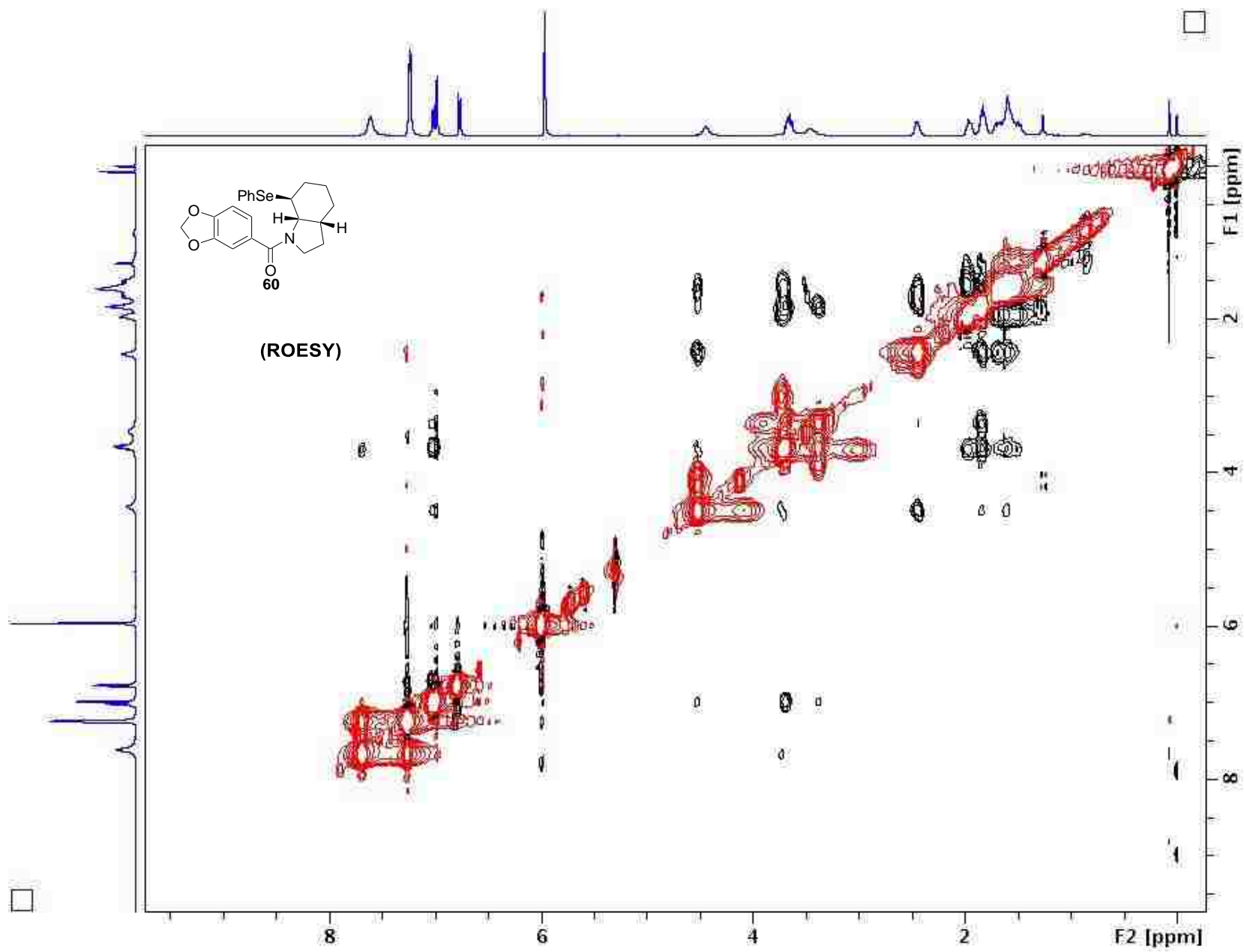


ESC.85(III).hplc.carbon.again.57/1

ESC.85(III).hplc.carbon.again.57

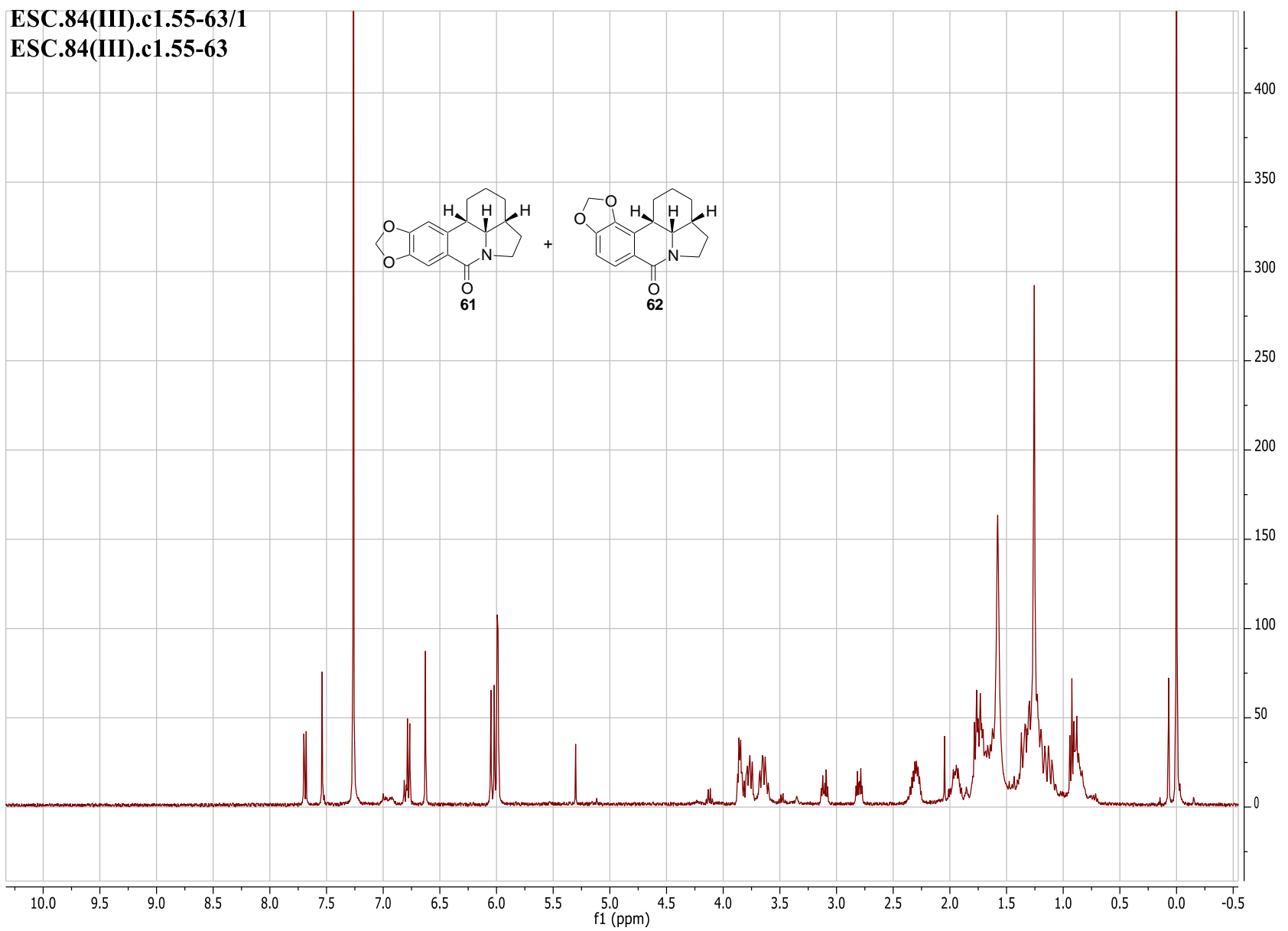




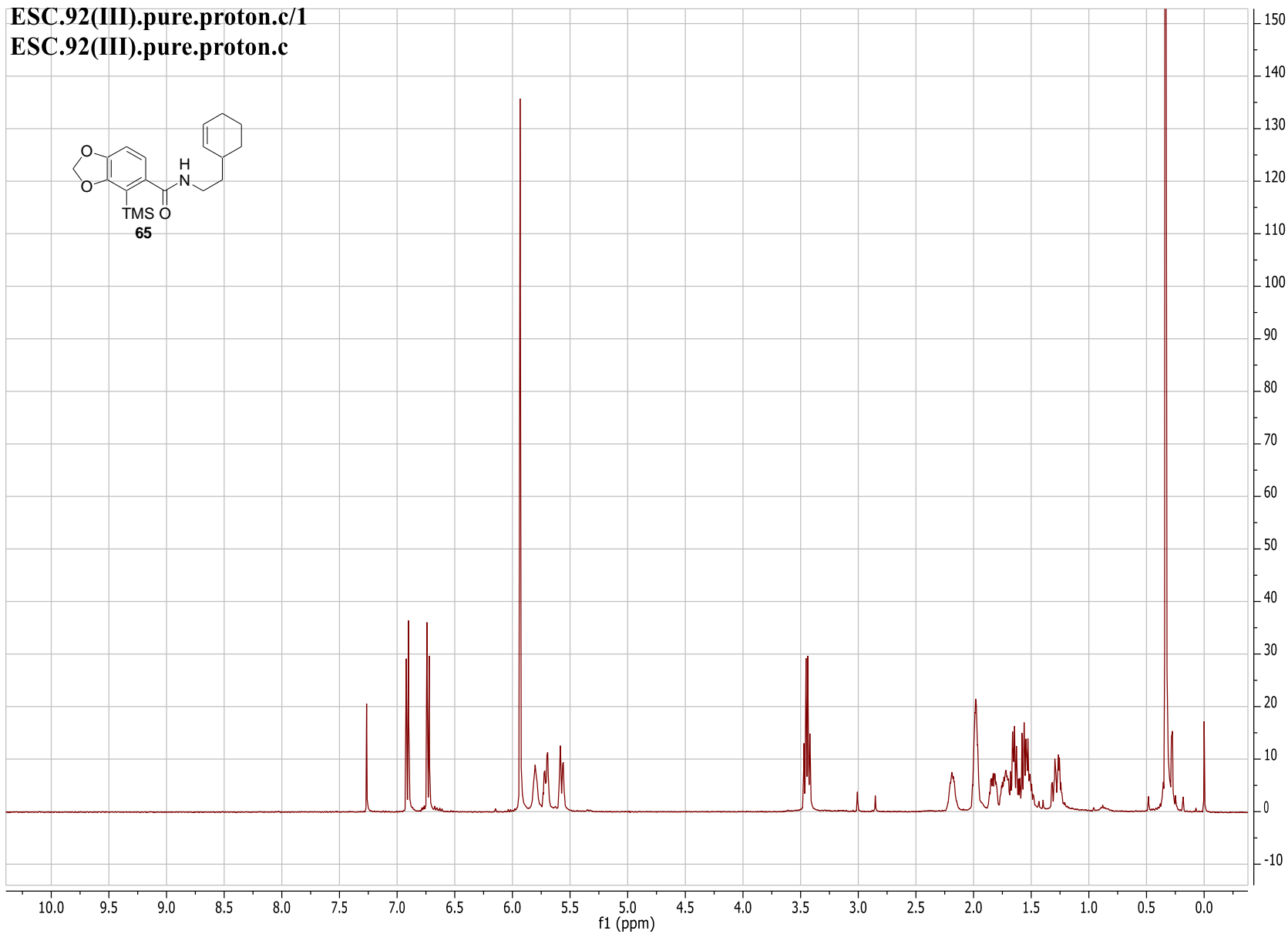
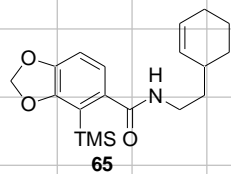




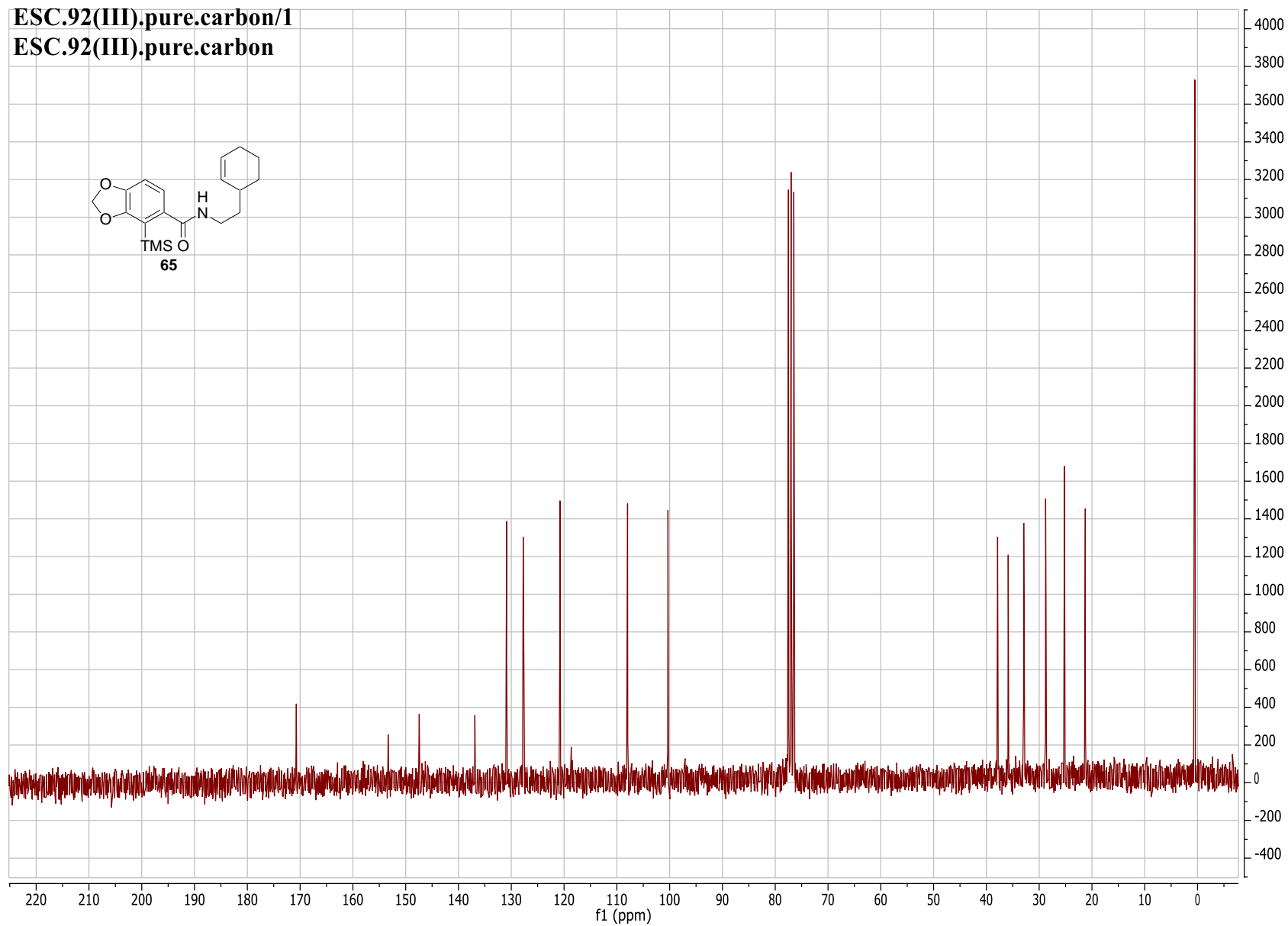
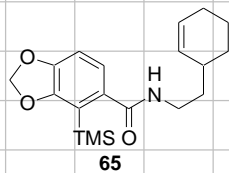
ESC.84(III).c1.55-63/1  
ESC.84(III).c1.55-63



ESC.92(III).pure.proton.c/1  
ESC.92(III).pure.proton.c

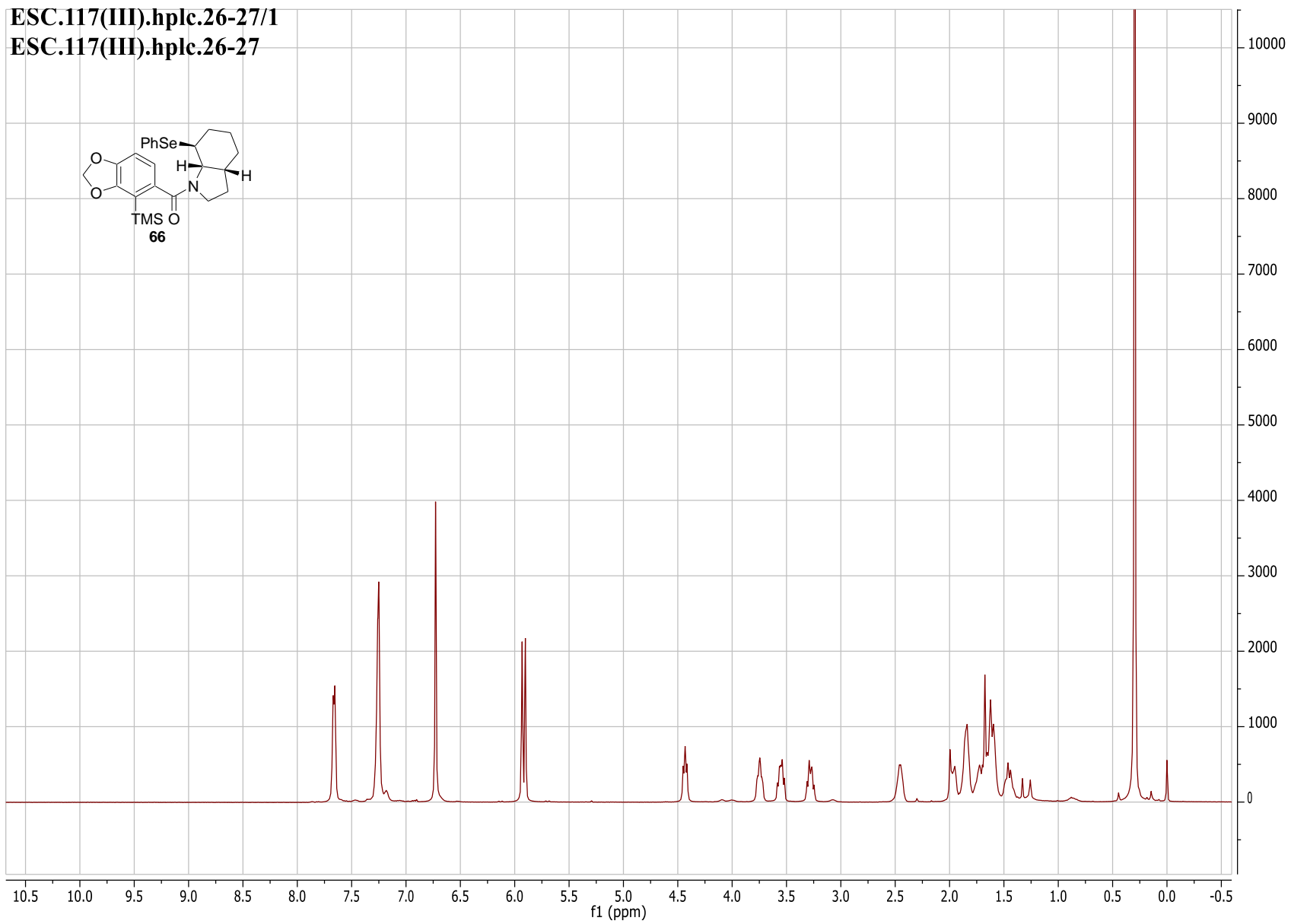
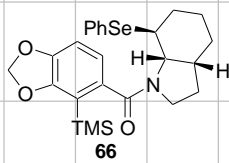


ESC.92(III).pure.carbon/1  
ESC.92(III).pure.carbon

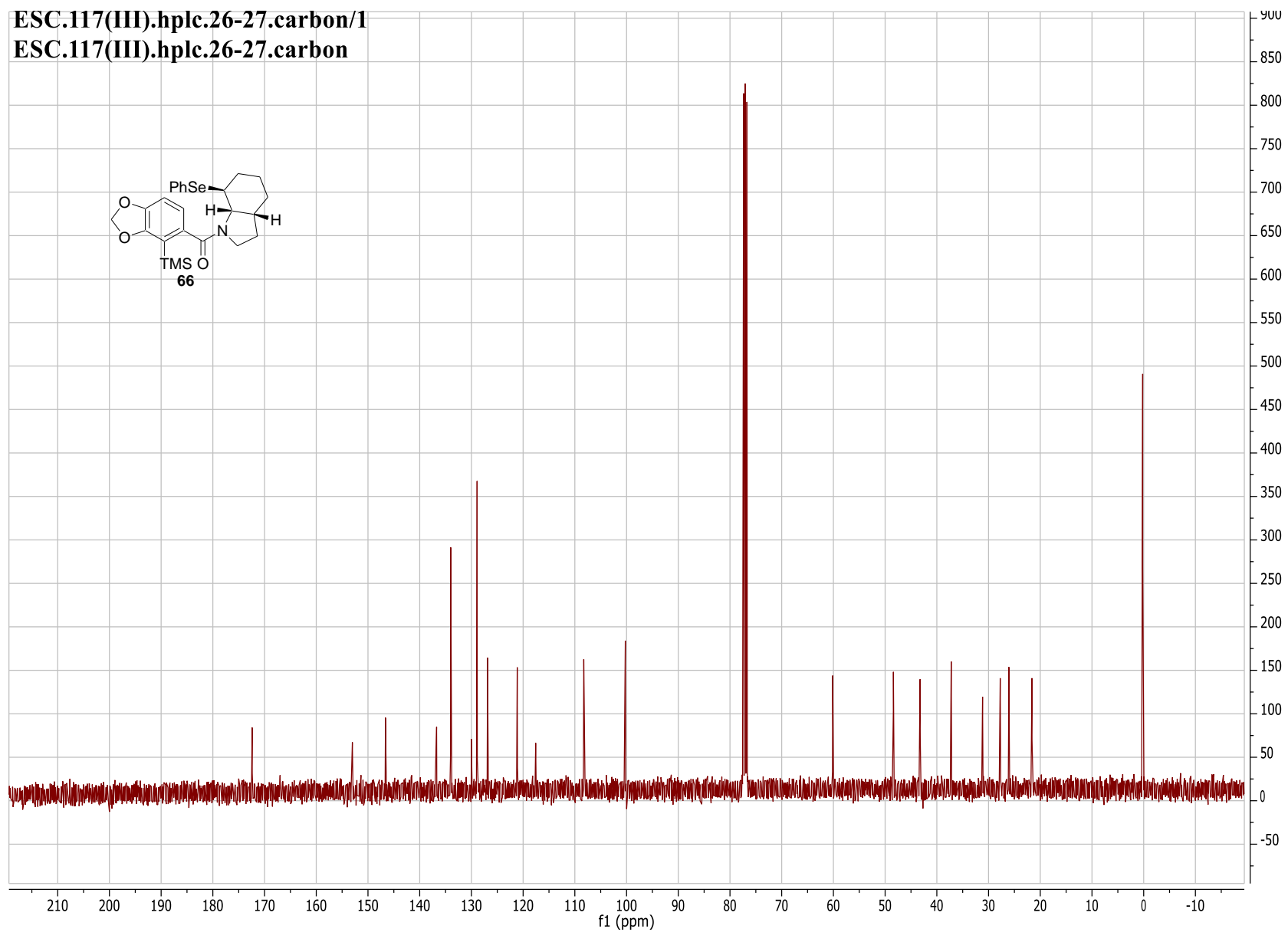


ESC.117(III).hplc.26-27/1

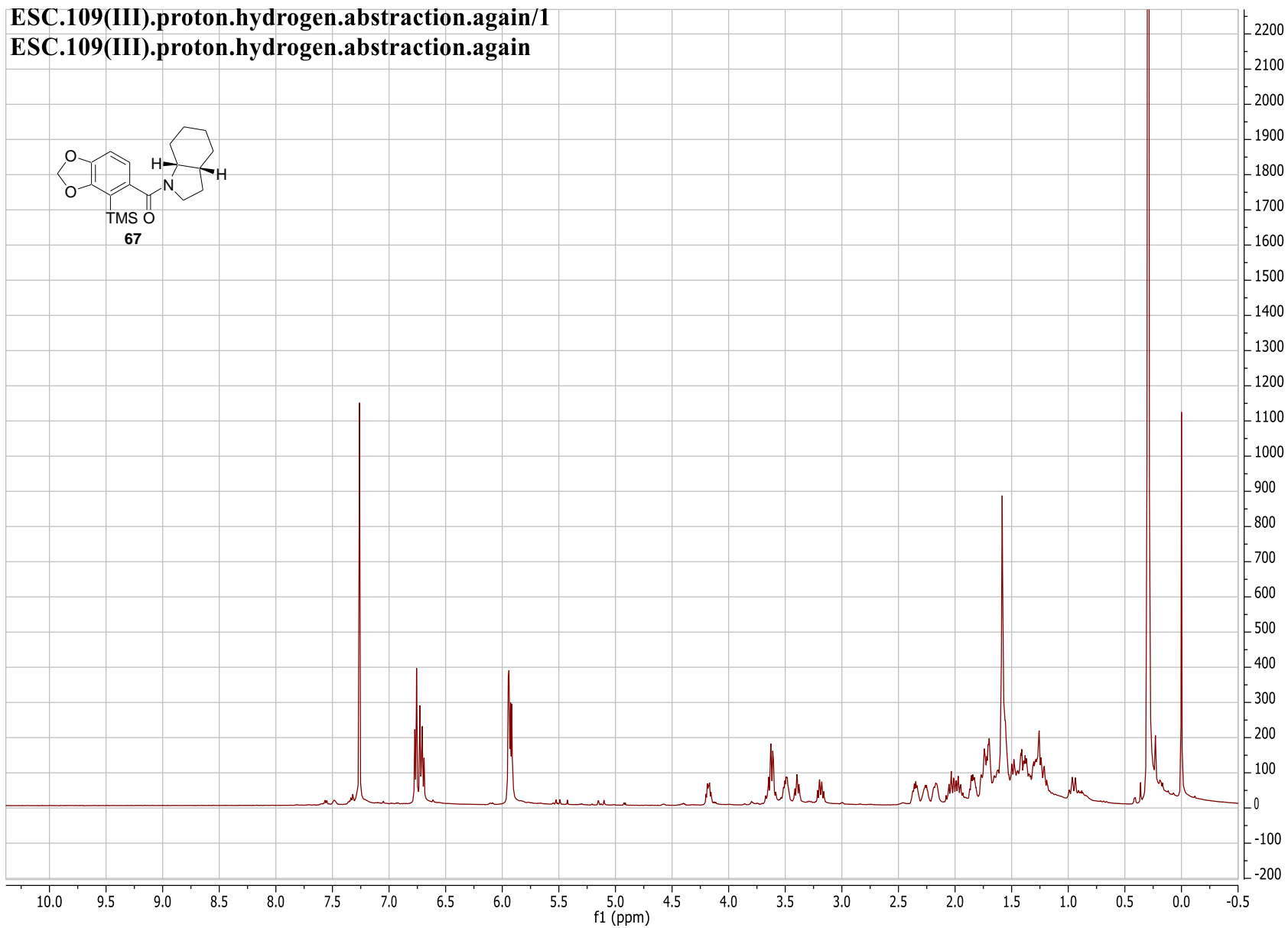
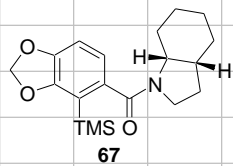
ESC.117(III).hplc.26-27



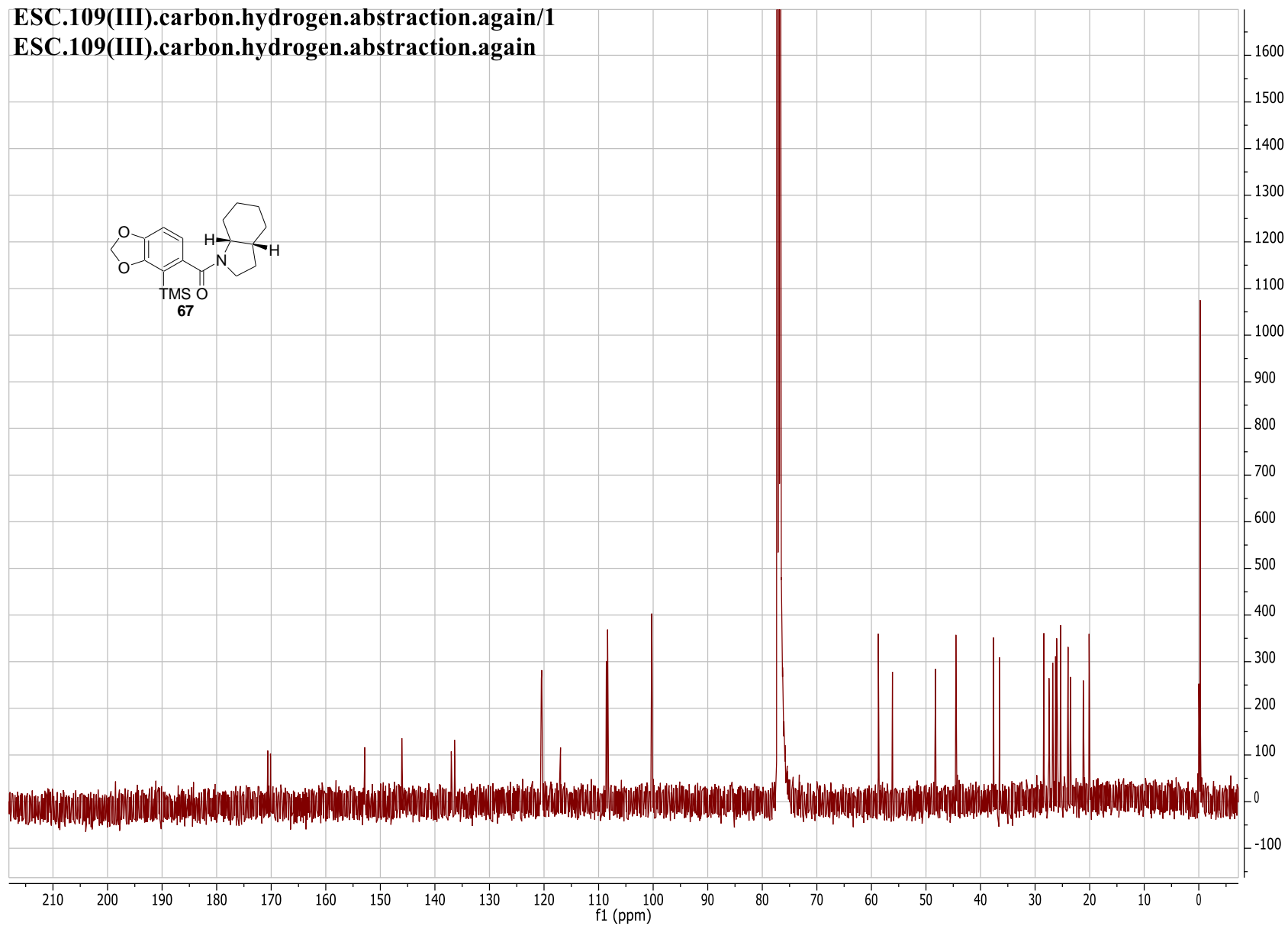
ESC.117(III).hplc.26-27.carbon/1  
ESC.117(III).hplc.26-27.carbon



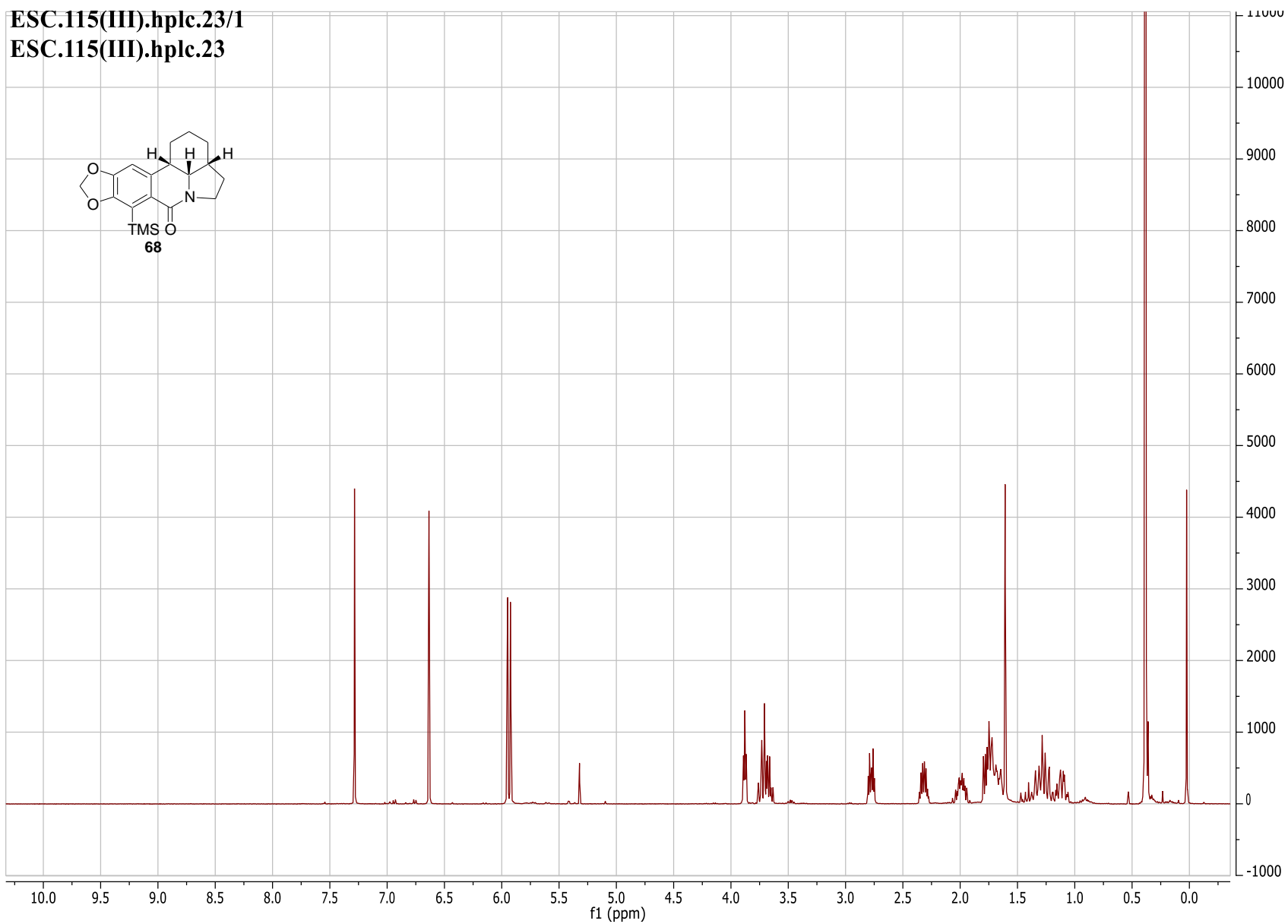
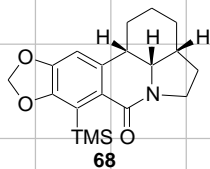
ESC.109(III).proton.hydrogen.abstraction.again/1  
ESC.109(III).proton.hydrogen.abstraction.again



ESC.109(III).carbon.hydrogen.abstraction.again/1  
ESC.109(III).carbon.hydrogen.abstraction.again



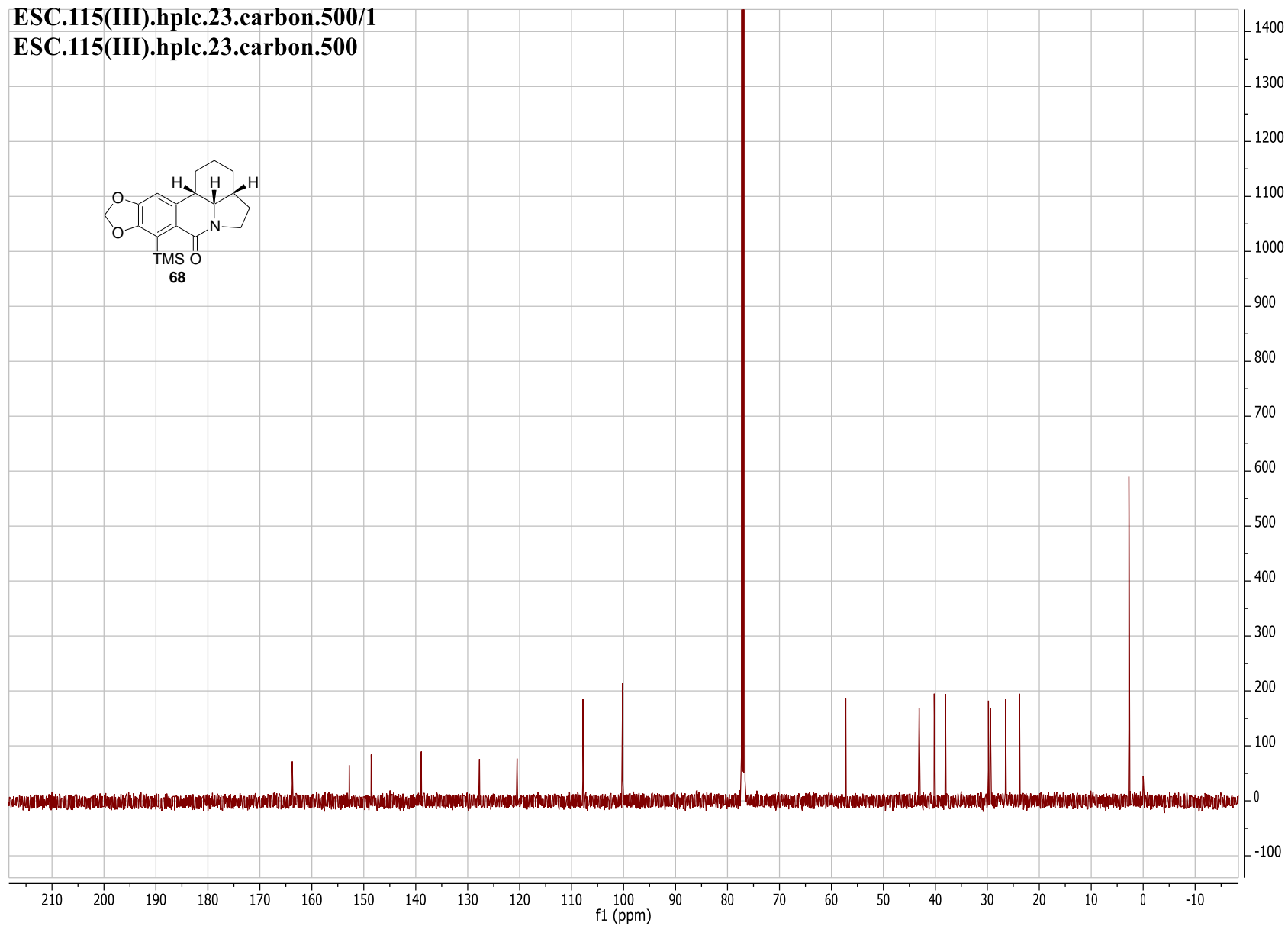
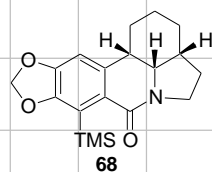
ESC.115(III).hplc.23/1  
ESC.115(III).hplc.23

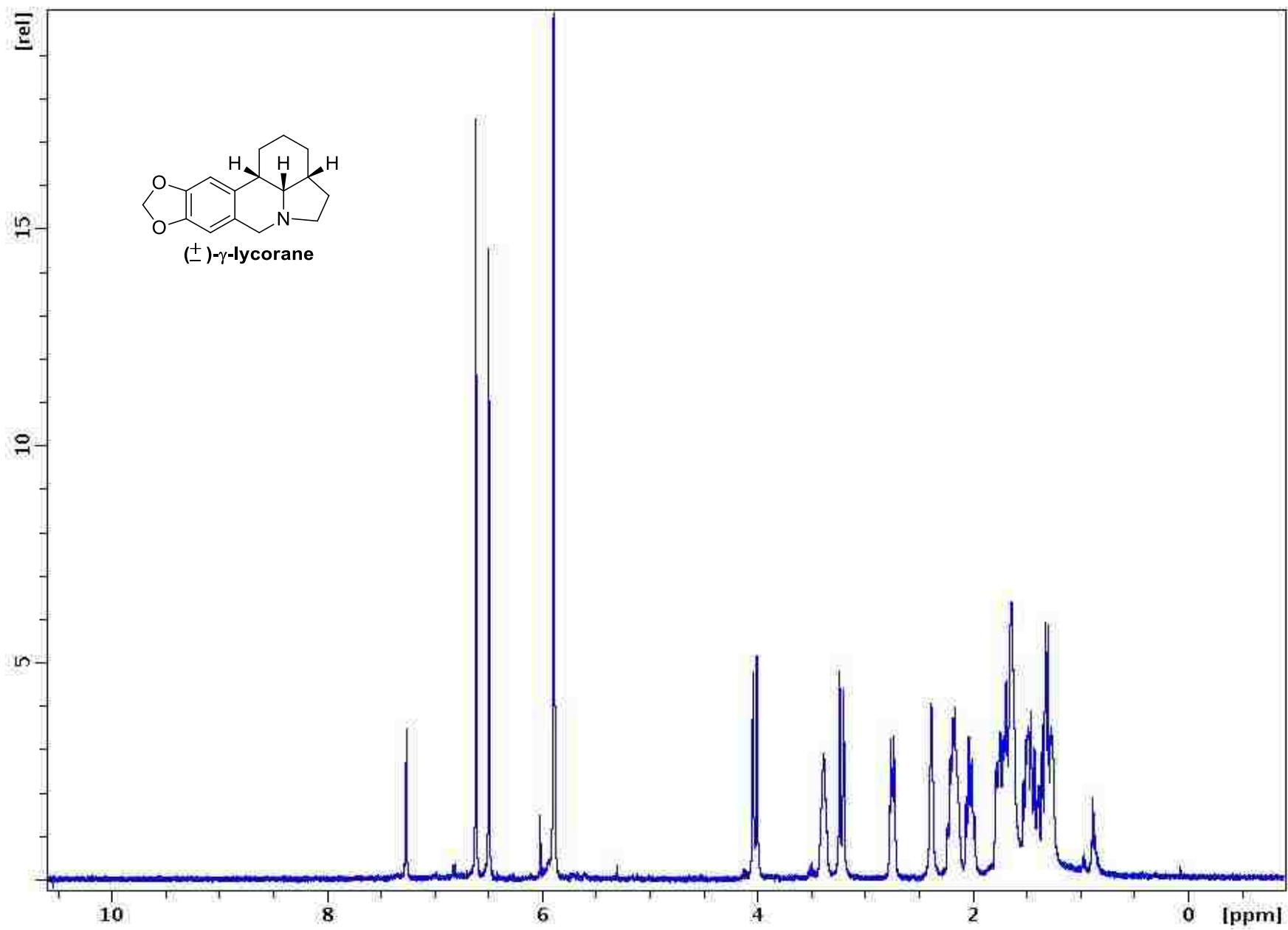




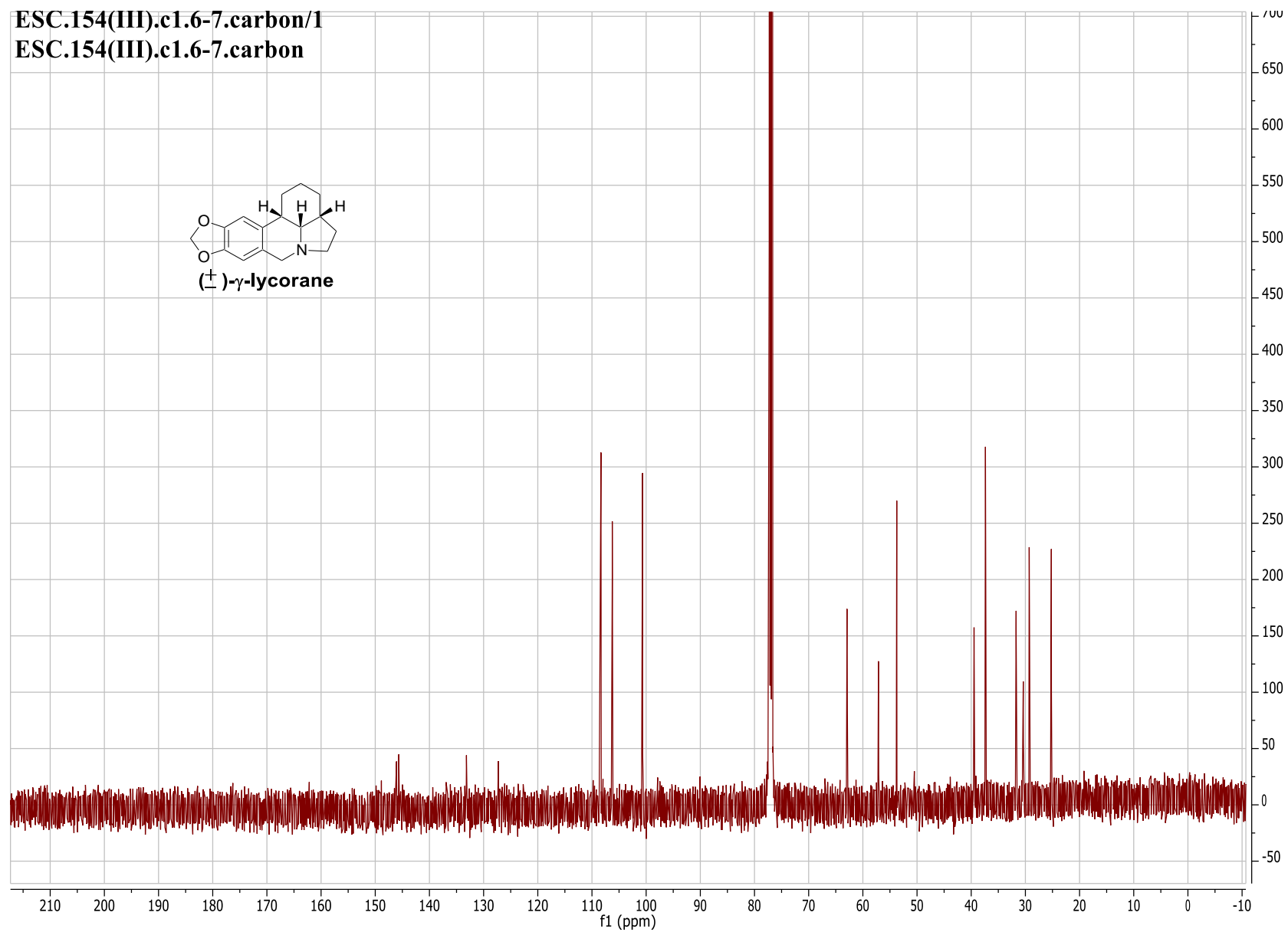
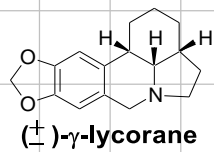
ESC.115(III).hplc.23.carbon.500/1

ESC.115(III).hplc.23.carbon.500



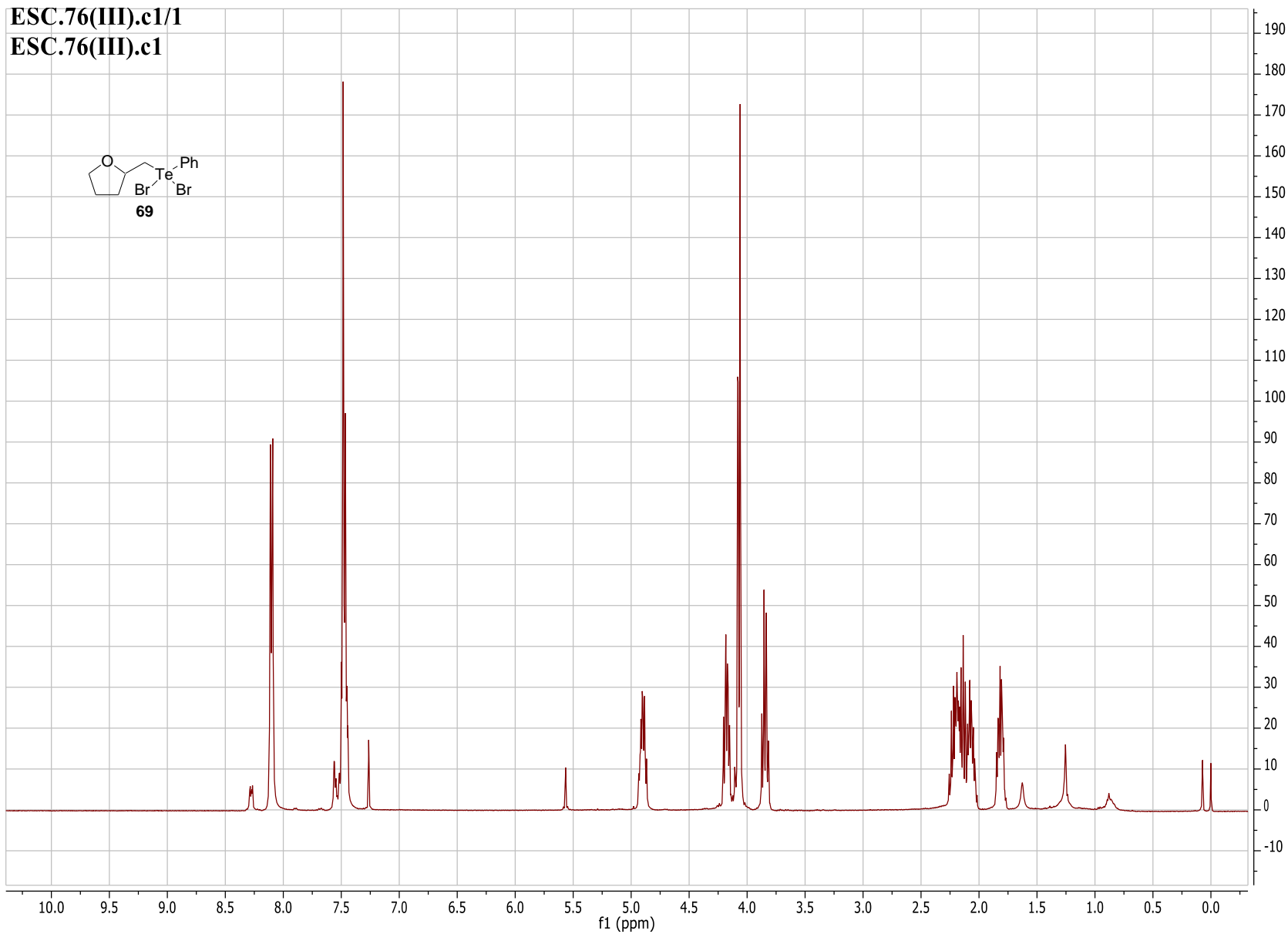
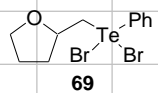


ESC.154(III).c1.6-7.carbon/1  
ESC.154(III).c1.6-7.carbon

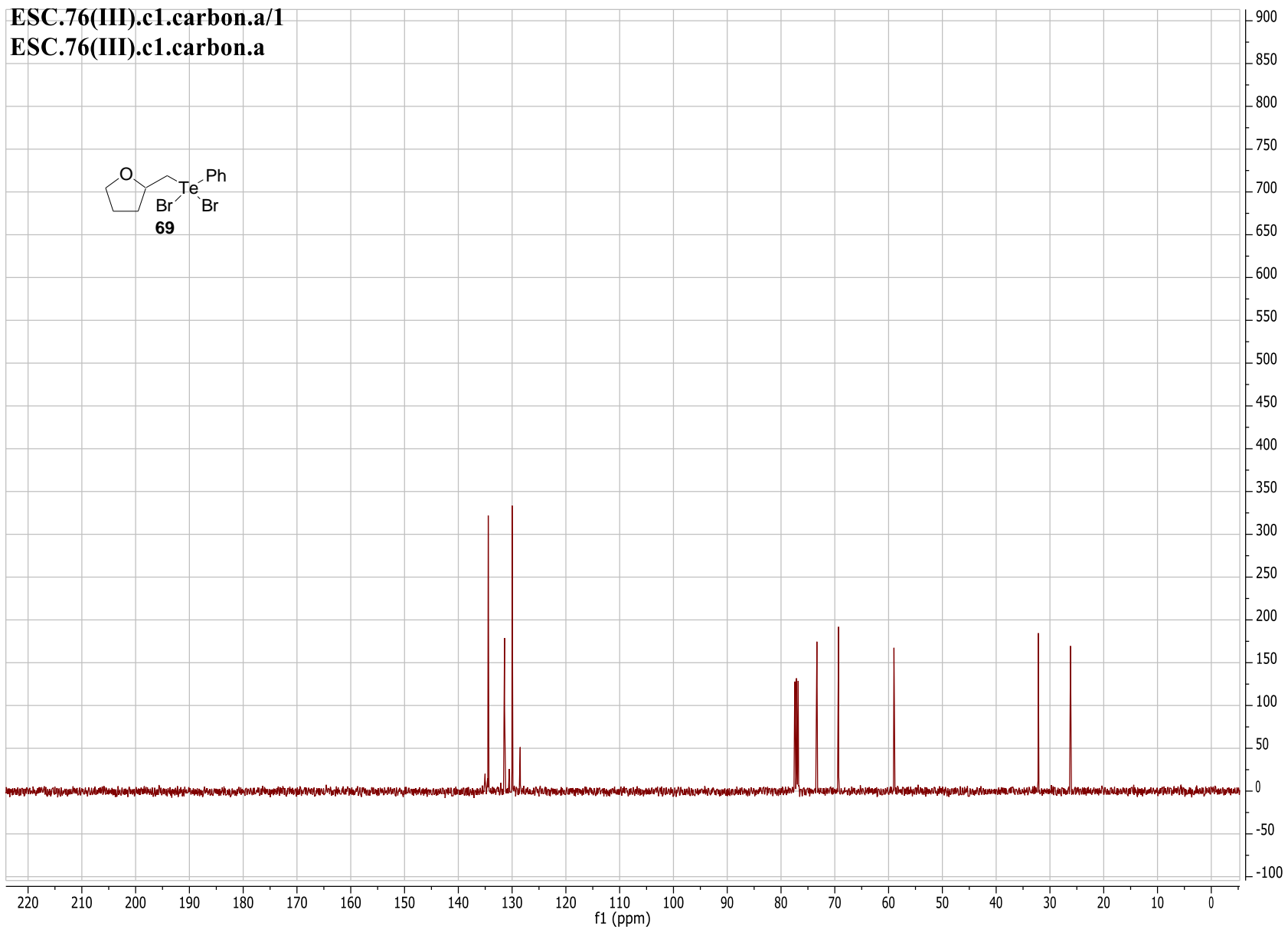
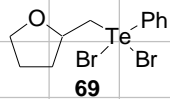


ESC.76(III).c1/1

ESC.76(III).c1

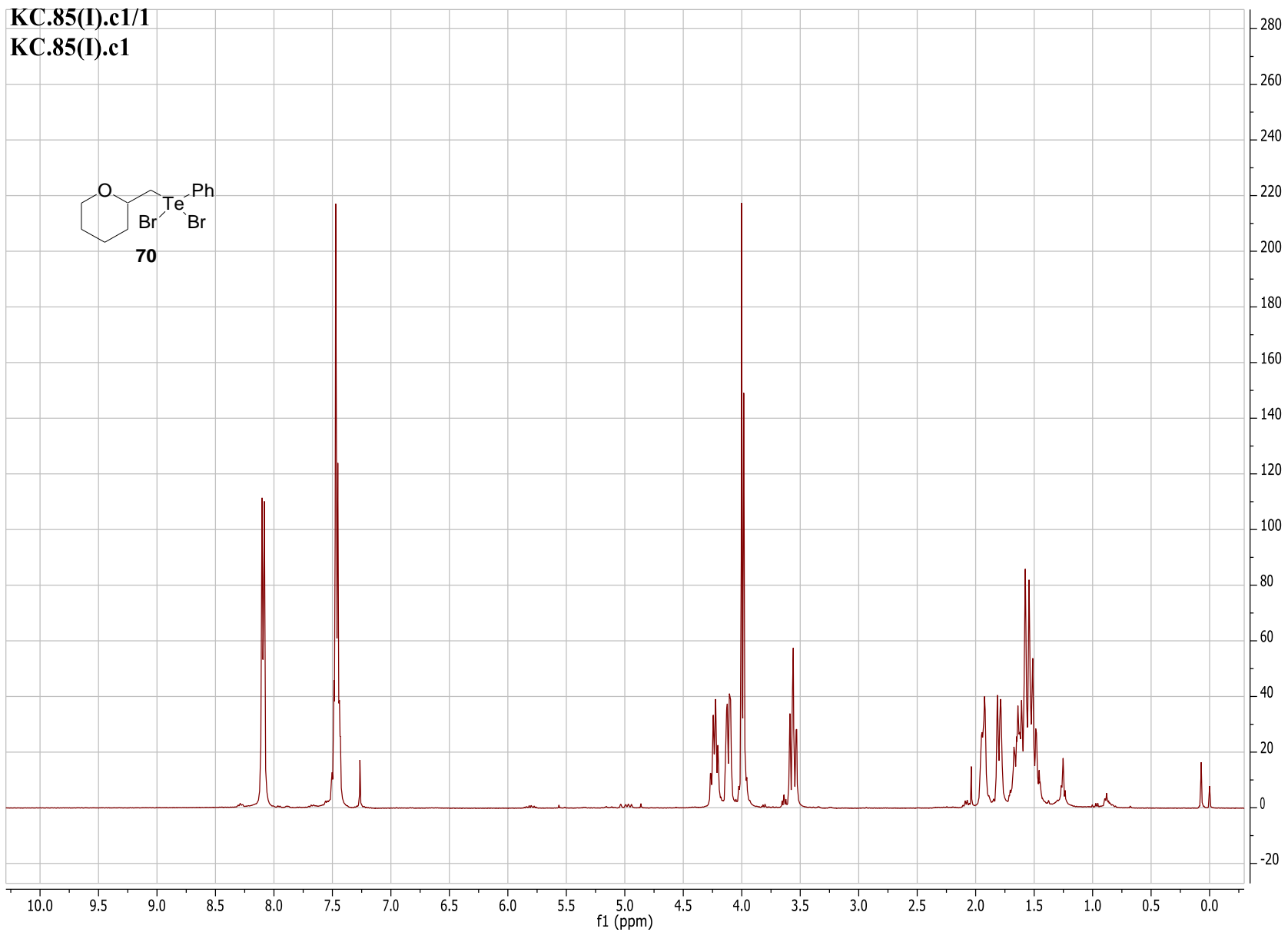
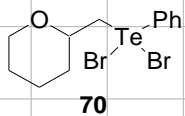


ESC.76(III).c1.carbon.a/1  
ESC.76(III).c1.carbon.a

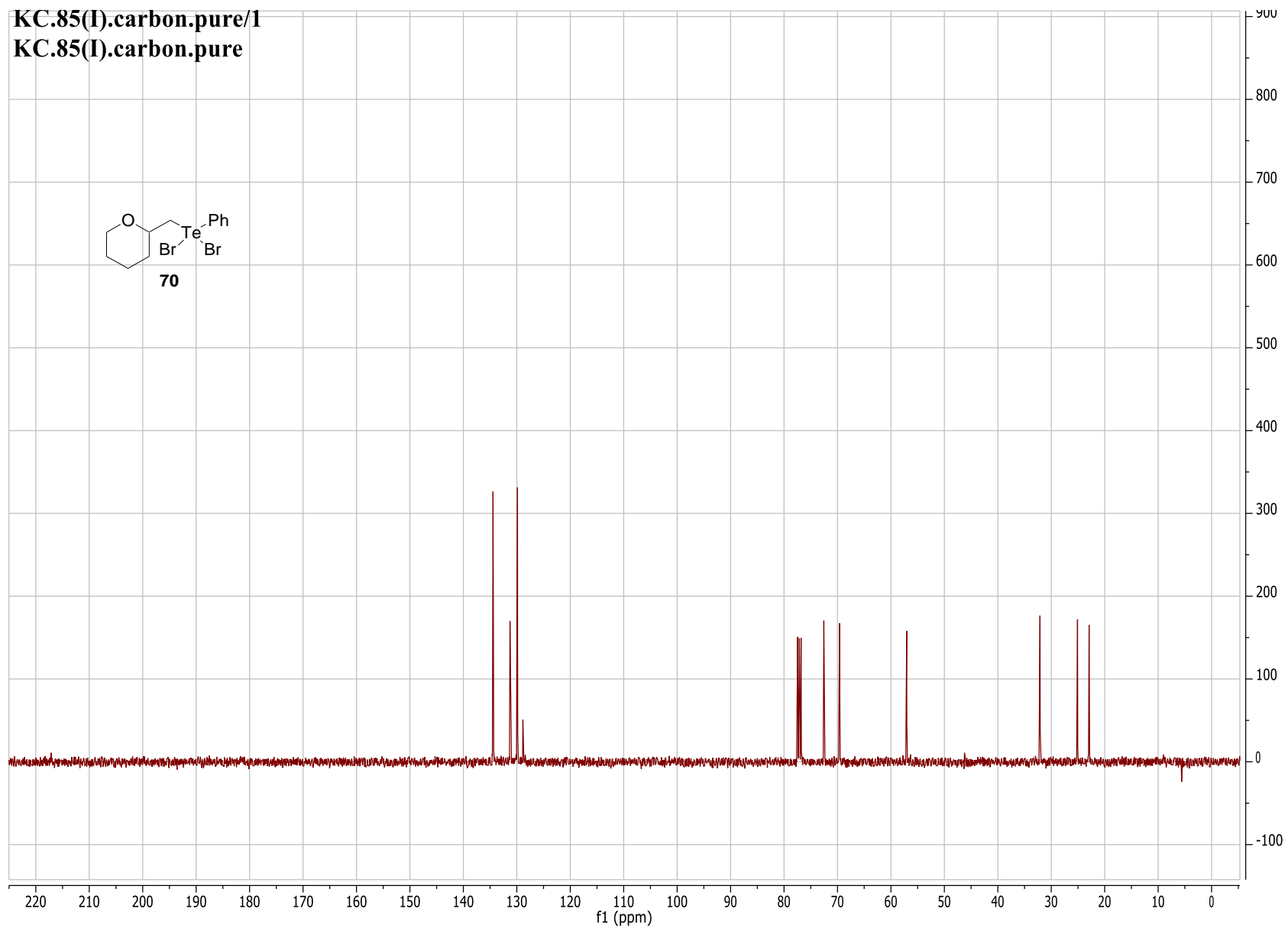
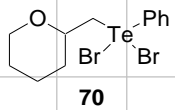


KC.85(I).c1/1

KC.85(I).c1



KC.85(I).carbon.pure/1  
KC.85(I).carbon.pure



## VITA

Elizabeth Susan Conner Balapitiya was born in Lafayette, Louisiana to Timothy C. Conner and Mary B. Conner, and she is married to Nuwan N. Balapitiya. Following completion of her primary studies in 2006, she enrolled at Baylor University in Waco, Texas where she earned her Bachelors degree in May 2010 in the University Scholars program, focusing on Chemistry and Spanish. The following August, she entered the doctoral program in the Department of Chemistry at Louisiana State University in Baton Rouge, Louisiana. She later joined the research group of Dr. Justin R. Ragains in December 2010. Elizabeth is currently a candidate for a doctoral degree in Chemistry, which will be awarded at the May 2015 commencement ceremony.